TUDelft

Delft University of Technology

Mathematical modelling of cellulase production and continuous production of enzymes under carbon-limited conditions by Trichoderma harzianum P49P11

Gelain, Lucas

Important note
To cite this publication, please use the final published version (if applicable).
Please check the document version above.

Mathematical modelling of cellulase production and continuous production of enzymes under carbon-limited conditions by *Trichoderma harzianum* P49P11

Dissertation

for the purpose of obtaining the degree of doctor

at Delft University of Technology,

by the authority of the Rector Magnificus Prof. dr. ir. T. H. J. J. van der Hagen,

chair of the Board for Doctorates

to be defended publicly on

Monday 24 February 2020 at 10:00 o'clock

by

Lucas GELAIN

Master of Science in Chemical Engineering, University of Campinas, Brazil

born in Caxias do Sul, Brazil

This dissertation has been approved by the

Promotors: Prof.dr.ir. L. A. M. van der Wielen and Prof.dr. A. Carvalho da Costa
Copromotors: Dr. W. M. van Gulik and Dr. J. Geraldo da Cruz Pradella

Composition of the doctoral committee:
Rector Magnificus   chairperson
Prof.dr.ir. L. A. M. van der Wielen   Delft University of Technology, promotor
Prof.dr. A. Carvalho da Costa   University of Campinas, promotor, Brazil
Dr. W. M. van Gulik   Delft University of Technology, copromotor

Independent members:
Prof.dr. P. Osseweijer   Delft University of Technology
Dr.ir. A. J. J. Straathof   Delft University of Technology
Prof.dr. A. Riul   University of Campinas, Brazil
Dr. A. Deshmukh   DSM Biotechnology Centre

Reserve member:
Prof.dr. F. Hollmann   Delft University of Technology

Table of contents

Summary

Trichoderma harzianum P49P11 was selected among several other microorganisms at the Biorenewables National Laboratory (LNBR, Brazil) and it was considered a promising strain to produce cellulase. Here in this project, a mathematical model and simulation platforms were developed as potential tools to be used for cellulase maximization using fed-batch mode (**Chapter 2**). Feeding strategies were simulated to maximize cellulase production, at first, only using cellulose as the substrate, and then using glycerol for cell growth and cellulose for cellulase production. Although the mathematical model and simulation platforms were built up for a wild type strain, these tools help to predict data and they can be adapted for optimized strains.

Chapter 3 evaluates the continuous production of enzymes using different carbon sources under carbon-limited conditions. It was found that glucose has a positive influence on the production of enzymes that can catalyse the hydrolysis of p-nitrophenyl-β-D-glucopyranoside (PNPGase). Sucrose and fructose seem to inhibit PNPGase synthesis; however, these substrates could also have a positive influence on the synthesis of other enzymes not evaluated in this project. Cells can uptake glucose without the need to synthesize extracellular enzymes like PNPGase. The increase in the production of PNPGase during the continuous culture using glucose as the carbon source indicates the presence of inducers. It was also discovered in this project that polysaccharides were present in the supernatant of all conditions using glucose, fructose/glucose and sucrose (**Chapter 4** and **Chapter 5**). This suggests that the possible inducers could have come from fragments of the extracellular polysaccharides.

Sugar analysis showed the presence of sugar with the same retention time as gentiobiose in the supernatant of the conditions using glucose as the carbon source, which could be a fragment from polymers released from the cell wall. Gentiobiose could be acting as an inducer of enzymes. In addition, a mechanism was also proposed for continuous PNPGase production under glucose-limited conditions assuming that PNPGase includes beta-glucosidase (**Chapter 4**).

The carbon sources used under carbon-limited conditions influenced the PNPGase productivity and possibly the whole enzymatic cocktail secreted by the fungus. For this reason, shotgun proteomics and SDS-PAGE analysis were performed for the proteins present in the supernatant of the conditions using glucose, fructose/glucose and sucrose (**Chapter 4**). The shotgun proteomics analysis suggested that the different carbon sources used provided the production of different extracellular proteins including several uncharacterized proteins, which can also include different enzymes. This brings the possibility of creating a hypothesis that different carbon sources easily assimilated by the cells could lead to the synthesis of different inducers (fragments of extracellular polysaccharides), which could induce the synthesis of different enzymes under carbon-limited conditions.

Extracellular polysaccharides were the by-products discovered in this project during the production of enzymes under carbon-limited conditions. The behaviour of intracellular metabolites (glycolysis, citric acid cycle, pentose phosphate pathway and nucleotides) was evaluated under four different conditions in duplicate during the production of extracellular

polysaccharides by *Trichoderma harzianum* under carbon-limited conditions (**Chapter 5**). This chapter has provided the first step for the optimization of the production of extracellular polysaccharides and the information about the behaviour of intracellular metabolites using this wild type strain is essential to the development of optimal strains.

Samenvatting

Trichoderma harzianum P49P11 werd geselecteerd uit verschillende andere micro-organismen in het Biorenewables National Laboratory (LNBR, Brazilië) als een veelbelovende stam om cellulase te produceren. Binnen dit project werden een wiskundig model en simulatieplatforms ontwikkeld als potentiële hulpmiddelen voor cellulase-maximalisatie middels van fed-batch cultivatie (**hoofdstuk 2**). Voedingsstrategieën werden gesimuleerd om de productie van cellulase te maximaliseren, eerst met alleen cellulose als substraat en vervolgens glycerol voor celgroei en cellulose voor cellulaseproductie. Hoewel het wiskundige model en de simulatieplatforms werden ontwikkeld voor het wildtype, hebben deze tools, na eventuele aanpassing, tevens voorspellende waarde voor geoptimaliseerde soorten.

In **Hoofdstuk 3** wordt continue productie van enzymen met behulp van verschillende koolstofbronnen onder koolstofbeperkte omstandigheden geëvalueerd. Er werd vastgesteld dat glucose als koolstofbron een positieve invloed heeft op de productie van enzymen die de hydrolyse van p-nitrofenyl-β-D-glucopyranoside (PNPGase) kunnen katalyseren. Sucrose en fructose lijken de synthese van PNPGase te remmen; deze substraten kunnen echter een positieve invloed hebben op de synthese van andere enzymen die niet in dit project zijn geëvalueerd. Cellen kunnen glucose opnemen zonder de noodzaak om extracellulaire enzymen zoals PNPGase te synthetiseren. De toename van de productie van PNPGase tijdens de continue kweek met behulp van glucose als koolstofbron geeft de aanwezigheid van inductoren aan. In dit project werd ook ontdekt dat in het supernatant van de culturen waarbij glucose, fructose/glucose en sucrose werden gebruikt als koolstofbron, polysachariden aanwezig waren (**hoofdstuk 4** en **hoofdstuk 5**). Dit suggereert dat de mogelijke inductoren van enzymproductie afkomstig zouden kunnen zijn van fragmenten van deze extracellulaire polysachariden.

Suikeranalyse van het supernatant van een cultivatie waarbij glucose als koolstofbron werd gebruikt toonde de aanwezigheid aan van een suiker met dezelfde retentietijd als gentiobiose, wat een fragment zou kunnen zijn van polymeren die vrijkomen uit de celwand. Gentiobiose zou kunnen werken als een inductor van enzymen. Bovendien werd ook een mechanisme voorgesteld voor de continue productie van PNPGase onder glucose-beperkte omstandigheden, ervan uitgaande dat PNPGase bèta-glucosidase omvat (**hoofdstuk 4**).

De koolstofbronnen die onder koolstofbeperkte kweek condities werden gebruikt, hadden invloed op de productiviteit van PNPGase en mogelijk op de gehele enzymatische cocktail die door de schimmel werd uitgescheiden. Om deze reden werden shotgun proteomics en SDS-PAGE analyse uitgevoerd om inzicht te krijgen welke eiwitten mogelijk aanwezig zijn in het cultuur supernatant van de cultivaties met glucose, fructose/glucose en sucrose als koolstofbron (**hoofdstuk 4**). De shotgun proteomics-analyse suggereerde dat de verschillende gebruikte koolstofbronnen de productie van verschillende extracellulaire eiwitten opleverden, waaronder verschillende niet-gekarakteriseerde eiwitten, die ook verschillende enzymen kunnen representeren. Dit brengt de mogelijkheid met zich mee om een hypothese te creëren dat verschillende koolstofbronnen die gemakkelijk door de cellen worden geassimileerd, kunnen leiden tot de synthese van verschillende inductoren

(fragmenten van extracellulaire polysacchariden), die de synthese van verschillende enzymen onder koolstofbeperkte omstandigheden kunnen induceren.

Extracellulaire polysachariden waren bijproducten die in dit project werden ontdekt tijdens de productie van enzymen onder koolstofbeperkte cultivatie condities. Het gedrag van intracellulaire metabolieten (intermediairen van glycolyse, citroenzuurcyclus, pentosefosfaatroute en nucleotiden) werd geëvalueerd onder vier verschillende omstandigheden in duplo tijdens de productie van extracellulaire polysacchariden door *Trichoderma harzianum* onder koolstofbeperkte cultivatie condities (**hoofdstuk 5**). Het werk beschreven in dit hoofdstuk is een eerste stap in de richting van de optimalisatie van de productie van extracellulaire polysacchariden en de informatie over intracellulaire metaboliet niveaus in deze wildtype stam is essentieel voor de ontwikkeling van geoptimaliseerde stammen.

Chapter 1

General introduction

This chapter is the introduction of the thesis, concerned with general steps for cellulase and beta-glucosidase production by filamentous fungi as well as mathematical modelling, followed by the scope of the thesis.
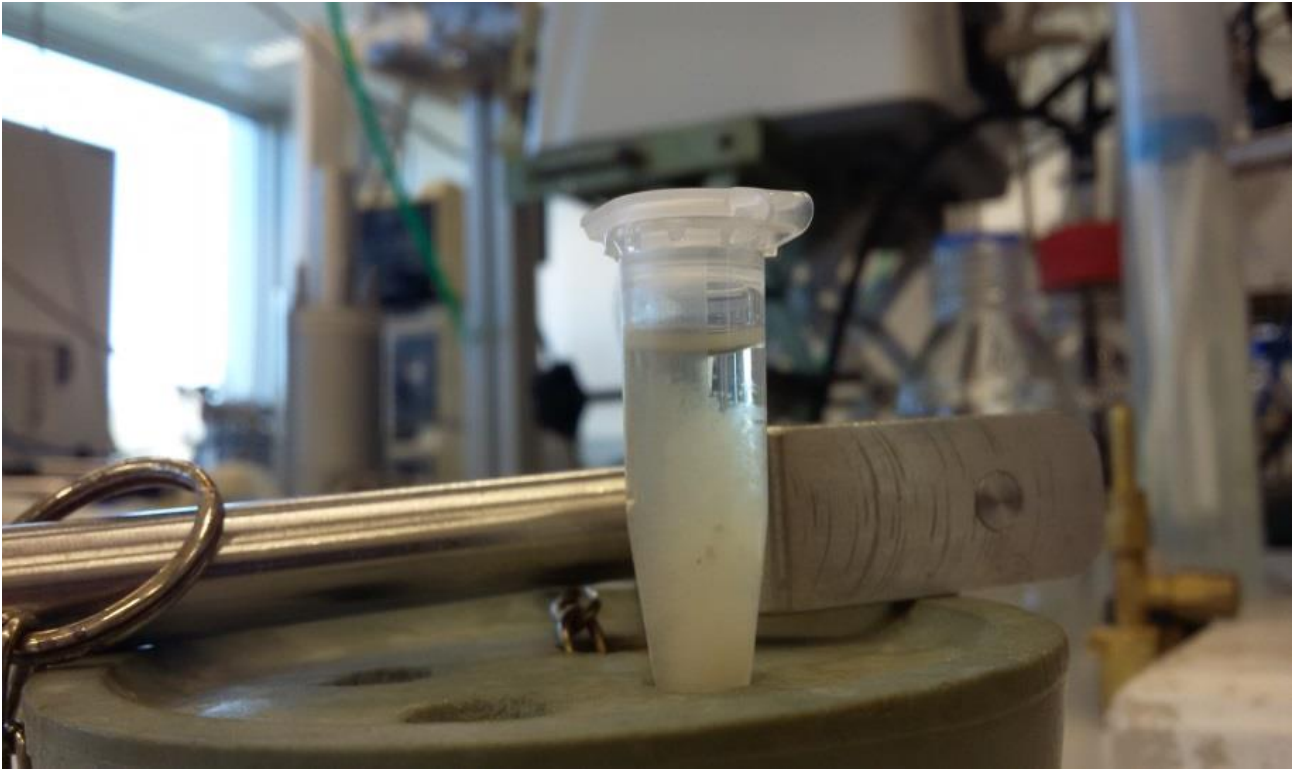
Trichoderma harzianum P49P11☆

1.1 Second-generation ethanol production

Lignocellulosic materials are mainly composed of cellulose, hemicellulose and lignin (Mussatto and Teixeira, 2010). These polymers can be converted into their respective monomers trough acid or enzymatic hydrolysis and then used as the main carbon source to produce chemicals applying fermentation processes. In Brazil, ethanol is generally produced using broth extracted from sugarcane, followed by fermentation. Sugarcane bagasse is a by-product of this process and it is usually converted into energy by combustion (Dias et al., 2012). However, an interesting alternative of exploiting this by-product is the depolymerization of the cellulosic polymers and then, the use of the monomeric sugars to produce ethanol through fermentation. This process is called second-generation ethanol production (Figure 1.1).

The production and use of ethanol as a fuel are beneficial to reduce CO_2 emissions compared with fossil fuels, for the development of attractive activity for the agricultural sector and to decrease the dependence on fossil fuels imported (Lago et al., 2012). Every ton of sugarcane processed to ethanol or sugar generates about 0.3 ton (wet basis) of bagasse (Hofsetz and Silva, 2012). In an ethanol production plant, bagasse is burned to supply energy to the plant; however, due to optimization strategies to minimize energy demand, the excess of bagasse can increase (Dias et al., 2012). This excess of bagasse could also be converted into ethanol providing an increase in the productivity of this fuel without increasing the plantation of the raw material.

Sugarcane bagasse can be chemically or physically pretreated to facilitate the hydrolysis step. The hydrolysis of the sugarcane bagasse pretreated can be performed by enzymes, such as cellulase, or acids. If the enzymatic hydrolysis is the process chosen, the production of enzymes becomes an important step and also needs to be optimized. Thus, monosaccharides and oligosaccharides generated from hydrolysis are available to be converted into chemicals of interest, and ethanol is only one of the possible options.

Enzymatic hydrolysis has some advantages over acid hydrolysis such as mild conditions (avoiding corrosion of process equipment) and lower formation of inhibitory compounds such as furfural and 5-hydroxymethyl-furfural (Verardi et al., 2012). For example, according to Taher et al. (2017), higher ethanol yield and reducing sugars consumption were achieved when the sugars used for the fermentation came from enzymatic hydrolysis when compared to acid hydrolysis of potato peel residues. They suggested that the presence of hydroxymethyl furfural, which came from the breakdown of hexoses during acid hydrolysis, could be inhibiting yeast growth. In addition, the enzymatic hydrolysis shows higher specificity and lower formation of secondary products than conventional acid hydrolysis (Seiboth et al., 2011).

Cellulase is a cocktail of enzymes applied to catalyse the hydrolysis of cellulose materials and is also used for the conversion of lignocellulosic materials into simple sugars. Three types of enzymes are considered as being required for the hydrolysis of cellulose materials into glucose: exo-1,4-beta-glucanase (EC 3.2.1.91 and EC 3.2.1.176); endo-1,4-beta-glucanase (EC 3.2.1.4); and beta-glucosidase (EC 3.2.1.21) (Dyk and Pletschke, 2012). Exo-1,4-beta-glucanase and endo-1,4-beta-glucanase act synergistically to convert cellulose into cello-oligosaccharides and beta-glucosidase convert them into glucose (Shida et al., 2016). The high production cost of these enzymes limits their use for soluble sugar formation (Ahamed and Vermette, 2010) and efforts are needed to maximize the yield and productivity and thereby reduce the production costs (Seiboth et al., 2011).
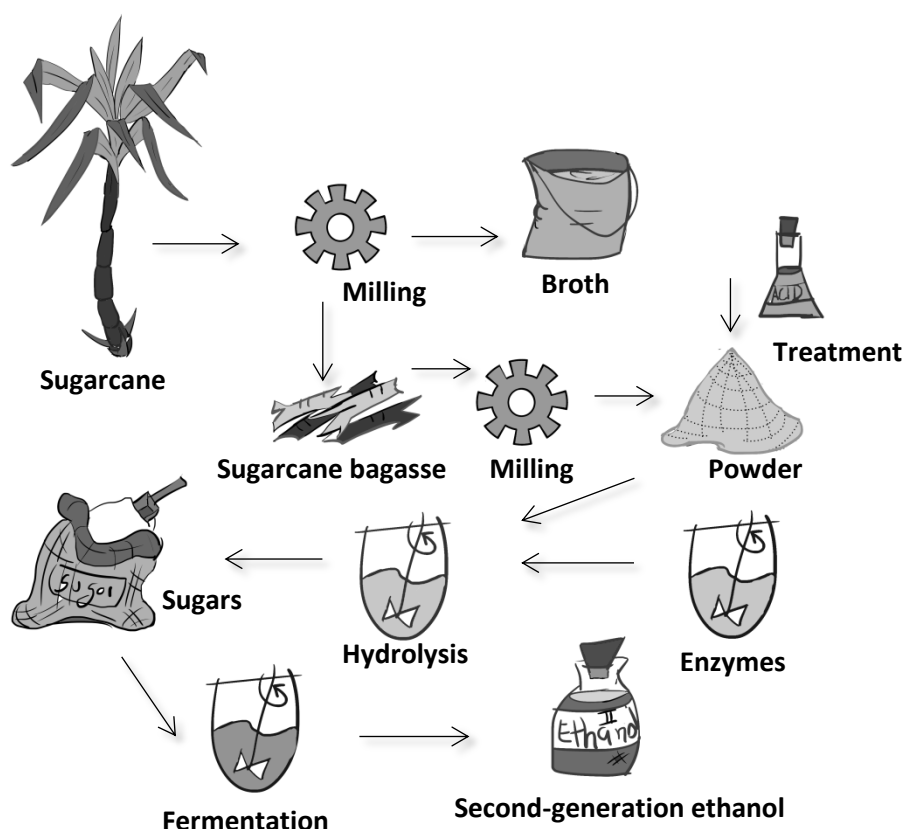
Figure 1.1 – Second-generation ethanol production from sugarcane bagasse at laboratory scale

Beta-glucosidase is a group of enzymes responsible for catalysing the final step of the complete hydrolysis of cellulosic materials into glucose (Sørensen et al., 2013). The yield of glucose obtained from hydrolysis is dependent on the product inhibition and the number of enzymes available. Most of beta-glucosidase of *Trichoderma reesei* is bound to the cell wall and low quantities are secreted to the growth medium (Tiwari et al., 2013; Bischof et al., 2016). For efficient saccharification of lignocellulosic materials by cellulase, high activity of beta-glucosidase is needed to prevent inhibition by cellobiose (Sørensen et al., 2013). Thus, studies to improve beta-glucosidase production become very important for the synthesis of products derived from lignocellulosic materials.

1.2 Microorganisms for the production of lignocellulose-degrading enzymes

The process of production of lignocellulose-degrading enzymes starts with the choice of the microorganism, which could either be a wild type strain that has the potential to produce a large number of these enzymes or an engineered strain producing the enzymes of interest in large quantities. Potential microorganisms to produce enzymes can be isolated from an environment where lignocellulosic materials are supposed to be used as the carbon source. The growth of microorganisms on lignocellulosic materials suggests the production of enzymes that can degrade that material. Several microorganisms can be isolated and tests are performed to define the most promising strain. Once the strain is chosen, a deeper evaluation of the microorganism is performed, followed by optimization of the operating conditions and strain engineering. The basic steps for experiments in bioreactors are illustrated in Figure 1.2. For wild type strains, the production of cellulase requires the presence of an inducer, of which

the chemical and physical properties could have a great influence on the synthesis of those enzymes.
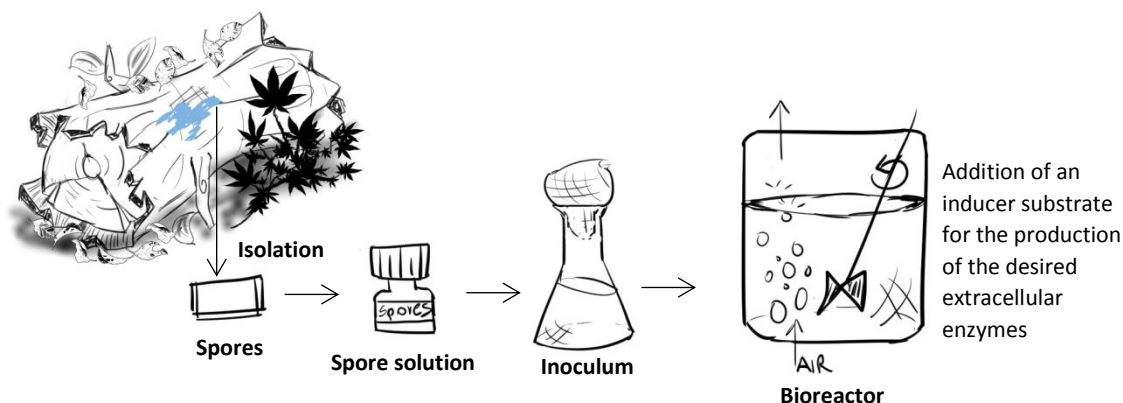
Figure 1.2 – Steps for the production of the lignocellulose-degrading enzymes in the bioreactor

Filamentous fungi of the genera such as *Trichoderma* and *Aspergillus* are recognized for their capability of secreting large amounts of proteins, metabolites and organic acids into the growth medium (Conesa et al., 2001). The genus *Trichoderma* has extensively been studied for cellulase synthesis (Strakowska et al., 2014) and *Trichoderma reesei* became an excellent cellulolytic model organism (Aro, 2003). Figure 1.3 shows the thin and long hyphal structures for the culture of *Trichoderma harzianum* used in this project (400x and 1000x magnification). It was grown in continuous culture (dilution rate of 0.05 h^{-1}) using glucose as the carbon source.
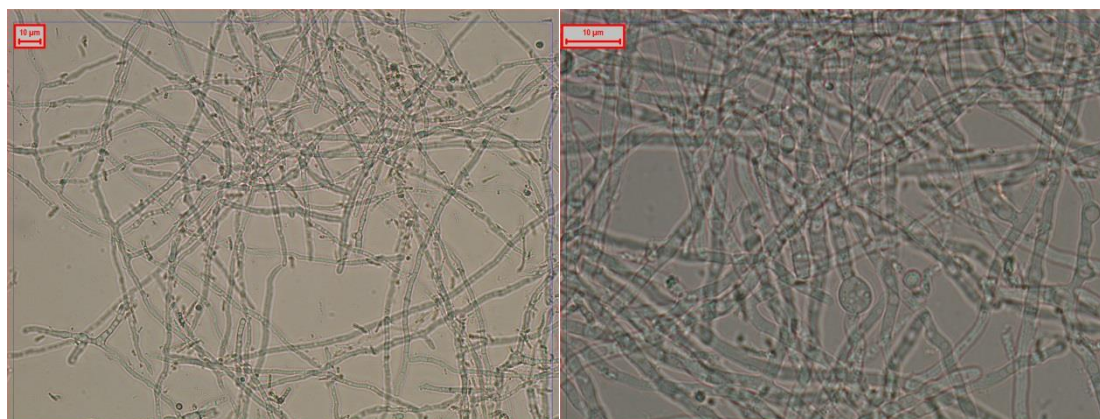
Figure 1.3 – *Trichoderma harzianum* P49P11, 400x magnification (left), 1000x magnification (right)

The submerged cultivation of filamentous fungi basically requires the supply of a simple chemically defined medium containing carbon, nitrogen, sulphur and phosphorus sources, oxygen supply and trace elements (e.g. $Na_2EDTA.2H_2O$, $ZnSO_4.7H_2O$, $MnCl_2.4H_2O$, $CoCl_2.6H_2O$, $CuSO_4.5H_2O$, $Na_2MoO_4.2H_2O$, $CaCl_2.2H_2O$, $FeSO_4.7H_2O$, H_3BO_3 and KI). Furthermore, the proper operating conditions have to be chosen such as optimum temperature, pH and limited shear stress. The growth of filamentous fungi in batch mode and in the submerged condition usually starts with spore swelling and germination, followed by hyphal cell extension and branching, the formation of hyphae networks and the last phase is the cell autolysis (El-Enshasy, 2007). The mycelial growth phenotype of filamentous fungi results from a polar

extension at hyphal tips (Conesa et al., 2001) and calcium ions play a crucial role in the polarized extension of the cell wall (El-Enshasy, 2007). Studies indicate that the secretion of proteins occurs at the apical or subapical hyphal regions, although there has been some controversy (Conesa et al., 2001). The hyphal tips are free from organelles except for a large number of vesicles, which suggests that they are involved in the transport of material to the surface of the plasma membrane, including the transport of enzymes (El-Enshasy, 2007).

1.3 Regulation and production of lignocellulose-degrading enzymes by fungi

The production of cellulase can be directly or indirectly induced by oligosaccharides derived from cellulose and is controlled at the transcriptional level (Aro, 2003). Sophorose is considered as the most potent inducer in *T. reesei* and can be produced by transglycosylation activity of beta-glucosidase in the presence of cellobiose or other cello-oligosaccharides (Aro, 2003). Gentiobiose is another disaccharide that could be produced by transglycosylation and induce cellulase synthesis. Both sophorose and gentiobiose are rare sugars in nature and their synthesis from cellulosic materials has extensively been studied (Suto and Tomita, 2001). It has been reported that basal levels of lignocellulose-degrading enzymes generate inducers from insoluble carbon sources, such as cellulose (when they are present) to initiate full gene expression of cellulase. This expression can subsequently be downregulated, if a high level of glucose is reached, through carbon catabolite repression (Suto and Tomita, 2001).

Usually, the synthesis of lignocellulose-degrading enzymes requires an inducer substrate to stimulate full expression of the genes responsible for their production, although processes have been described in the literature wherein non-inducible substrates have been applied to produce them. Edwards and Munkvold (2014) registered a patent to produce cellulase without using cellulase-inducing carbon sources by the genus *Myceliophthora*. The process starts in batch mode and is switched to fed-batch, followed by continuous culture. The feed solution contains 100 % of non-inducing carbon sources (such as glucose, dextrose, sucrose, molasses, fructose, glycerol, xylose, or a combination thereof), whereby the feed rate is controlled such that the concentration of the non-inducing carbon source in the culture remains below 2 g/L. This cultivation strategy thus avoids the occurrence of catabolite repression.

Karaffa et al. (2006) investigated the expression of cellulase genes for a mutant of *Hypocrea jecorina* CHG1, which carried a fusion between the *cbh2* (cellobiohydrolase 2) promoter region and a glucose oxidase gene of *Aspergillus niger*. The experiments were performed in chemostat mode under carbon-limited conditions. The authors reported that glucose oxidase activity was clearly detectable when using D-galactose as the growth limiting substrate at a low dilution rate of 0.015 h^{-1}, while lactose induced a higher glucose oxidase activity at 0.015, 0.030 and 0.042 h^{-1}. In addition, the *cbh2* promoter activation was not detected when glucose was the carbon source (0.015 – 0.042 h^{-1}). Based on this and further analysis, they concluded that D-galactose can trigger the induction of cellulase at a low growth rate (0.015 h^{-1}). And the expression of cellulase genes for D-galactose condition was not related to a general carbon catabolite derepression since there was no glucose oxidase activity and the *cbh2* promoter activation was not detected at the same dilution rate employing glucose as the carbon source.

Zhang et al. (2017) detected low levels of cellobiose in cultures using *Rhizopus stolonifera* grown on glucose as the substrate in batch mode. They assumed that there might be an enzyme that can synthesize cellobiose from glucose or its intermediate metabolites as

precursors. They provided a new induction model that can describe the synthesis of low levels of cellulase during growth on non-cellulosic substrates. Their results showed that in this organism, uridine diphosphate glucose is formed by a series of metabolic processes from glucose. Then cellobiose is synthesized by a cellobiose synthetase using uridine diphosphate glucose as a glycosyl donor, which turns on the transcription of cellulase genes.

The positive transcription factors XYR1, ACE2 and HAP2/3/5 (upregulates gene expression), and the negative transcription factor CRE1 (downregulates gene expression), which corresponds to the carbon catabolite repression, have been demonstrated to be involved in the regulation of cellulase synthesis (Kubicek et al., 2009). Seiboth et al., (2011) reported that carbon catabolite repression could either act on the expression of cellulase genes directly by repressing individual cellulase genes, repressing the transcription of their activators or by inducer exclusion (inhibition of the uptake of inducers).

Beta-glucosidase seems to play an important role in the regulation of cellulase gene expression through the synthesis or degradation of inducers. Nitta et al. (2012) identified the transcription factor (BglR) that upregulates the initial expression of specific genes encoding beta-glucosidase of *Trichoderma reesei*, with the exception of *bgl1,* which seems to be under the direct control of XYR1. The mutant Δ*bglr* (lacking the expression of specific beta-glucosidase) resulted in significant yields of produced cellulase using cellobiose. This indicates that specific beta-glucosidase can hydrolyse the inducers of cellulase into glucose, thus preventing cellulase synthesis. Chen et al. (2013) investigated the functions of beta-glucosidase in the regulation of lignocellulosic enzyme production by *Penicillium decumbens*. They observed an increase in the production of lignocellulosic enzymes for a mutant with a deletion in the gene *bgl2* that encodes intracellular beta-glucosidase. They suggested that this increase in the production of enzymes was due to the intracellular accumulation of cellobiose.

Figure 1.4 illustrates the cellulase gene expression and secretion pathway based on Portnoy et al. (2011) and Conesa et al. (2001), respectively.
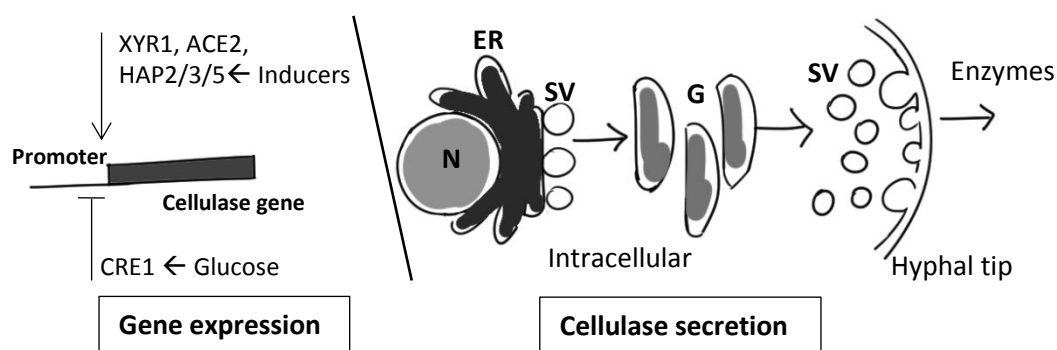
Figure 1.4 – General cellulase gene expression based on Portnoy et al. (2011), positive transcription factors XYR1, ACE2 and HAP2/3/5, negative transcription factor CRE1. Cellulase secretion pathway based on Conesa et al. (2001), N is the nucleus, ER is the endoplasmic reticulum, G is the Golgi apparatus and SV is the secretion vesicles

After having made the choice of a microorganism and having defined the strategies on how to induce cellulase production, the cultivation conditions and medium composition should be tested and optimized. Each fermentation process usually starts in batch mode and can be

transferred to fed-batch mode to further increase the cell density. Figure 1.5 illustrates some steps for the bioreactor setup. In the case of an aerobic process, continuous aeration of the bioreactor is required to maintain the dissolved oxygen concentration at a non-limiting value. Probes to register the values of pH, dissolved oxygen and temperature are essential to have the information for the control of the environmental conditions and to provide uniformity of the production. Acid and base are constantly added to control the pH at a fixed value, and antifoam should be added if it is needed. Base and acid should be placed on a balance to register the addition to the cultivation medium and to observe the dilution effect. To register the loss of water and consequently the increase in the concentrations of the components, the bioreactor should also be placed on a balance. Air condenser with cold water for the outlet of air can decrease water loss. The number and the volume of the samples need to be planned to avoid large variations in the working volume of the bioreactor. The fed-batch mode can be started by adding a constant or periodic feeding and the volume and concentration of the feeding must be known to calculate the productivities.

| Inoculum | Acid | Base | Bioreactor | Medium |
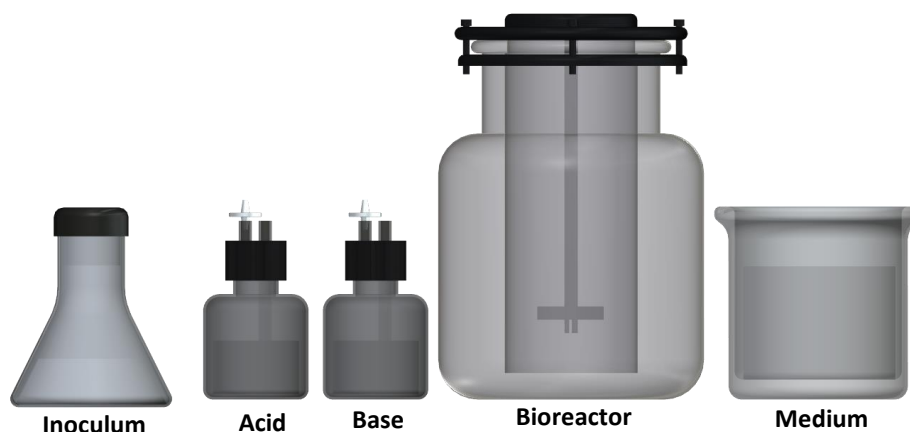
Figure 1.5 – Illustration of some characteristics of batch and fed-batch process

The production of cellulase is usually estimated based on the enzymatic activity using filter paper (cellulose) as a substrate for hydrolysis. The concentration of reducing sugars released per time of reaction is then a measure of the activity of the enzymes. The activity of beta-glucosidase can be estimated using cellobiose or p-nitrophenyl-β-D-glucopyranoside (PNPG).

Although some beta-glucosidase could act on the downregulation of the expression of cellulase genes, this group of enzymes is essential to the saccharification process. Beta-glucosidase can be divided into cellobiase with high cellobiose specificity and aryl-beta-glucosidase with high p-nitrophenyl-β-D-glucopyranoside specificity (Sørensen et al., 2013). Induction of aryl-beta-glucosidase was observed in the presence of gentiobiose, cellobiose, laminaribiose and weakly induced by galactose, amino sugars and aryl-beta-glucosides by *Neurospora crassa* (Eberhart and Beck, 1973). Gao et al. (2012) produced beta-glucosidase using agricultural by-products such as corn stover, wheat bran and corn stover plus wheat bran by *Fusarium proliferatum*. Interestingly, they also produced beta-glucosidase using glucose as the carbon source in the presence of urea.

Beta-glucosidase production under carbon starvation could be related to the presence of extracellular polysaccharides. Rau (1999) observed that prolonged cultivation under carbon-limited conditions leads to the release of beta-glucanase during extracellular polysaccharide

production by *Schizophyllum commune* using glucose as the carbon source. The author mentioned that small fragments of extracellular polysaccharide serve as a carbon source for the fungus. Based on this, it seems that these fragments could have induced the production of beta-glucanase. Thus, in a process using glucose or other easily available carbon sources, carbon starvation conditions could stimulate the production of enzymes for the cells to use the extracellular polysaccharides as a carbon source.

Figure 1.6 illustrates some characteristics of a continuous culture that can be used for enzyme production. The process starts in batch mode and after the end of the batch phase, the process is switched to continuous mode. The batch is finished when the substrate is depleted, which can be observed from a steep decrease in CO_2 production. During chemostat cultivation, a continuous flow of fresh medium enters the bioreactor while the culture broth is removed to keep the volume constant. A peristaltic pump needs to be calibrated and then can be used to supply the medium to the bioreactor. The effluent removed is transferred to a vessel placed on a balance, and the weight as a function of time is used to calculate the exact dilution rate. Base, acid and antifoam, as well as the production of CO_2 and O_2 consumption, must also be considered for the material balance and to calculate the inflow rate of the cultivation medium.
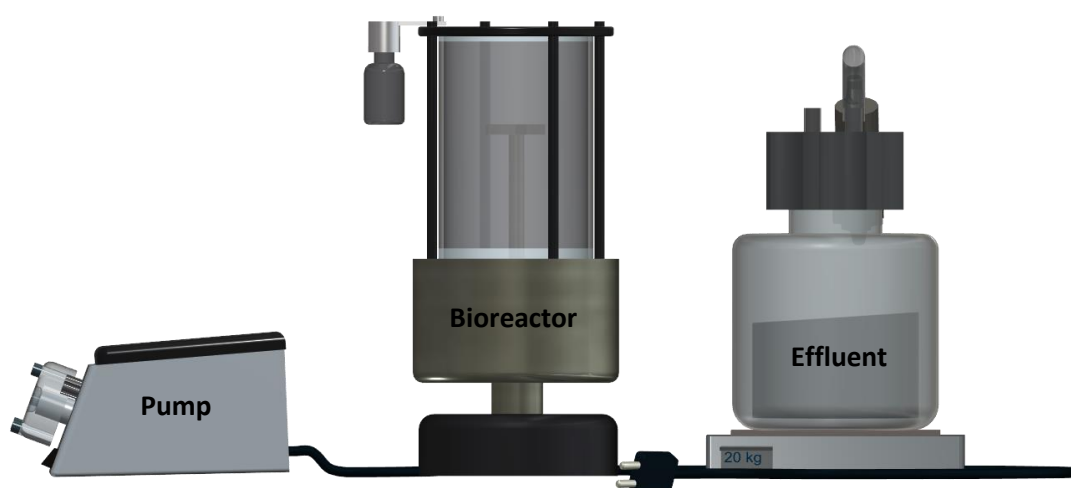
Figure 1.6 – Illustration of some characteristics of a continuous process, feeding pump, bioreactor and control of effluent weight as a function of time

1.4 Analysis of intracellular metabolites

Metabolites are small organic molecules (<1500 Da) acting as intermediates or end products of the cellular regulatory process (Fiehn, 2002; Lamichhane et al., 2018) and the set of metabolites synthesized by a biological system refers to the metabolome (Fiehn, 2002). Metabolomics comprehends the group of techniques applied to detect, identify or quantify the metabolites (Fiehn, 2002; Pinu et al., 2017). The quantitative analysis of metabolites is a prerequisite for metabolic engineering (Buchholz et al., 2001), which can be applied to create optimal strains to produce desired products.

The analysis of the metabolites of a microorganism involves the following steps: the cell growth under specific conditions; sampling and quenching of the cells; extraction and analysis of the metabolites (Pinu et al., 2017). Quenching methods are used to completely stop the cell metabolism, which is required to evaluate the metabolic behaviour of the cells under a specific

condition. Since the intracellular metabolites are inside of compartments, extraction methods are used to disrupt the compartment structures and release the metabolites (Pinu et al., 2017). For the analysis of the metabolites after the extraction, analytical platforms such as gas chromatography, and liquid chromatography coupled to mass spectrometry are employed to estimate the metabolites (Lamichhane et al., 2018; Lameiras et al., 2015).

Koning and van Dam (1992) proposed a quenching method that uses direct sampling into cold methanol solution and this method is considered as the standard protocol in quenching of microbial cells (Pinu et al., 2017). This method allows the washing of the cells to remove extracellular metabolites which could interfere with the analysis of intracellular metabolites (Jonge et al., 2012). However, Bolten et al. (2007) reported potential problems connected to the leakage of intracellular metabolites with cold methanol quenching. Kapoore and Vaidyanathan (2018) investigated the influence of various parameters such as quenching solvents, methanol concentrations and inclusion of buffer additives on intracellular metabolite leakage from *Chlamydomonas reinhardtii*. They reported a significant loss of intracellular metabolites with the use of the conventional 60 % (v/v) methanol, and they recommended the supplementation of 70 mM HEPES to reduce the leakage of metabolites.

According to Pinu et al. (2017), the majority of the quenching methods were developed for bacteria and/or yeast, and a few quenching methods have been reported for filamentous fungi. Jonge et al. (2012) evaluated and optimized a sampling procedure for quantitative metabolomics based on cold aqueous methanol quenching using *Penicillium chrysogenum*, glucose as the limiting substrate and the dilution rate of 0.05 h^{-1}. They optimized the method to reduce leakage and found that metabolite leakage was minimal for a methanol content of the quenching solution of 40 % (v/v) at -20 ^{o}C. They also suggested that it is necessary to validate and optimize the quenching conditions for each microorganism. Lameiras et al. (2015) described a quenching method for quantitative metabolomics aiming to avoid metabolite leakage during sample processing employing *Aspergillus niger* on glucose-limited conditions with dilution rates of 0.043 and 0.089 h^{-1}. They found that the leakage was absent at -20 ^{o}C for 40 % (v/v) methanol solution.

For the extraction of the metabolites, boiling ethanol is one of the most popular methods since the use of buffered boiling ethanol (75% v/v) is a simple and rapid intracellular metabolite extraction protocol (Pinu et al., 2017; Gonzalez et al., 1997). Gonzalez et al. (1997) presented a simple method for the inactivation of metabolism and extraction of intracellular metabolites from yeast cells. The extraction is fast and requires 3 minutes of incubation of yeast cells in the ethanol-buffered mixture at 80 ^{o}C. The extracts are subsequently concentrated by evaporation and the residues are suspended in small volumes of water.

The time between sampling and the actual quench of the cell metabolism is considered the most important factor that influences the efficiency of the quenching method, thus a quick sampling and quenching method is essential to produce an accurate evaluation of the metabolism of the microorganism (Pinu et al., 2017). Lameiras et al. (2015) presented a new rapid sampling device for sampling and quenching that can be used to study the concentrations of intracellular metabolites for filamentous fungi (Figures 1.7). The device was designed to prevent blockage by the cells of filamentous fungi. A peristaltic pump is used to pump the broth via a loop with an internal diameter of 8 mm at 40 mL/s, the residence time of the entire loop is 1.3 s. A pneumatic system pushes down the piston by a pedal control, sterile air or other gas can be used to push the sample from the device to a cold quenching fluid.

Then the piston returns to the initial position. The sample is injected into a quenching solution for further extraction of the metabolites.
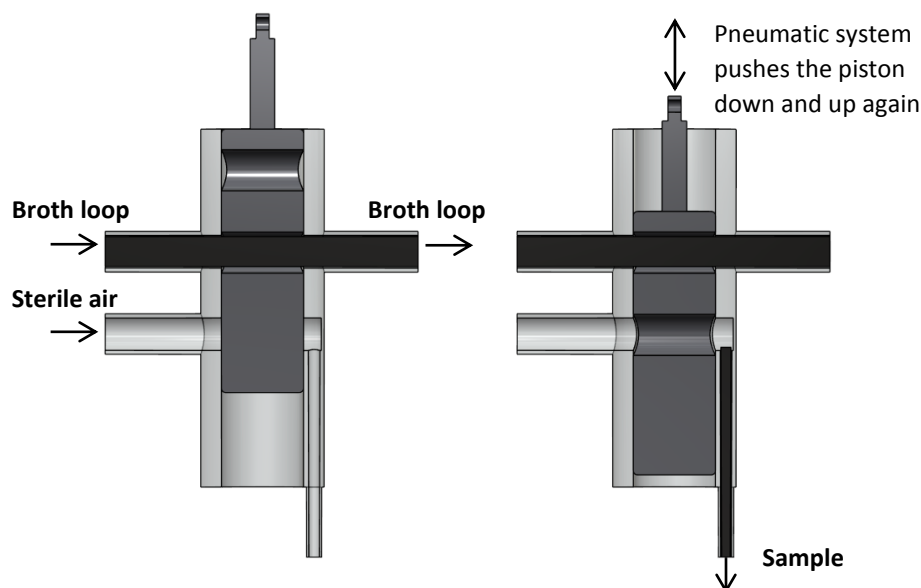
Figure 1.7 – Illustration of the rapid sampling device for the analysis of intracellular metabolites (sectional view)

1.5   Mathematical modelling

Mathematical models are important tools to better understand the relationship among the main components of the system, as well as helping with the control of parameters and on the optimization of a production process. Mathematical models that accurately describe the process can be used to predict the performance of the process under different conditions without the need to perform experiments, thus preventing unnecessary lab work. The complexity of living systems makes their mathematical description complicated (Thilakavathi et al., 2006); therefore, to overcome this complexity, simplification of the description of the cell activities are usually considered during the development of the models.

Several steps are taken to develop the models: material balance; kinetic evaluation of the main components to be described by the equations; parameter estimation; and model validation. In the material balance for the fermentation process, the bioreactor is considered the control volume to be analysed and boundaries surrounding it are applied to verify what enters and leaves this system, as well as the generation and consumption of the components present in the control volume. Each component is usually described by ordinary differential equations. For example, to describe the variation of cell concentration in the system, the equation considers the inflow and outflow of the cells, cell growth and cell death rates. The inflow and outflow of the components are estimated based on the measurements of their concentrations; however, the generation and consumption rate profiles are estimated using kinetic equations. After the development of the models, the parameters are estimated using numerical methods and the experimental data. The numerical methods minimize the difference between the data and the simulations provided by the models through changes in the values of the parameters.

For parameter estimation, an objective function is used to represent the difference between the values of the mathematical models (simulations) and the experimental data. This function is implicitly dependent on the parameters and generates a value correspondent to the sum of the residues between the model prediction and the experimental data. The value of this objective function is minimized to find the best set of parameter values. Several numerical methods can be used to achieve this goal and they can be distinguished by local, global and hybrid methods, which combine both, local and global methods (Almquist et al., 2014).

The local methods require initial values for the parameters, a position in the parameter space to start the optimization, and these values can come from experiments, literature or guessing (Almquist et al., 2014). For local methods, these initial values strongly influence the residue sum of the objective function and several local minimums can be found, which results in different sets of parameters. If the profiles given by the model are very different from the experimental data and they are not representing the phenomena observed, the model structure needs to be changed. However, if the profiles qualitatively describe the experimental data, but the fit to the data is not appropriate, this could just be a matter of adapting the values of some parameters or start with different initial values.

Figure 1.8 shows a simplified diagram for parameter estimation. Initial values are assigned for the parameters, the equations are solved providing the simulation results and an objective function is solved, which shows in how far the simulated results deviate from the experimental data when the initial parameter values are used. This information starts the optimization algorithm until the best set of parameters, which provides a minimum value for the objective function, is found.
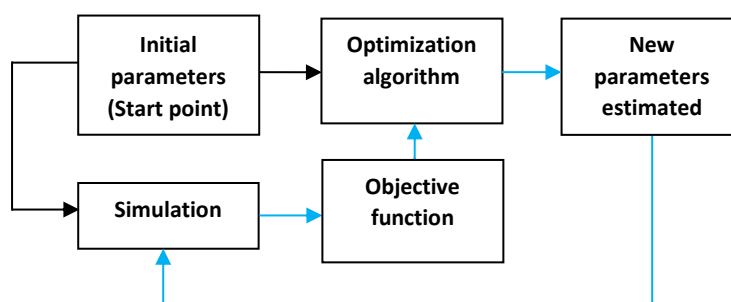
Figure 1.8 – Parameter estimation diagram, blue lines represent the cycle for minimization of the residue from the objective function

1.6 Scope and outline of the thesis

The aim of this thesis is to evaluate the capacity of the wild strain *Trichoderma harzianum* P49P11 to produce extracellular enzymes, such as cellulase and beta-glucosidase, under different conditions. Figure 1.9 illustrates the framework of the thesis. **Chapter 2** describes a study about cell growth and cellulase production in batch culture using glycerol and cellulose as the substrates. The work described in this chapter is based on the strategy proposed by Delabona et al. (2016), where the process of cellulase production starts with a cell growth stage, followed by an induction stage. Mathematical modelling was performed to describe the obtained experimental results using different initial concentrations of cellulose and glycerol. Feeding strategies were simulated to identify possible optimal conditions to maximize cellulase production through fed-batch cultivation.

Carbon-limited chemostat cultivations were exploited using different soluble carbon sources like glucose, sucrose, fructose/glucose mixture, carboxymethyl cellulose, and carboxymethyl cellulose/glucose mixture. These conditions are discussed in **Chapter 3**. Cellulase activity was not measured in these cultures, only PNPGase production was observed based on the methods used. Glucose-limited cultivations had a positive influence on PNPGase synthesis. The presence of extracellular polysaccharides, indicated by ethanol precipitation, was proven by proton NMR, FT-IR and hydrolysis analysis for the experiments using glucose, sucrose and a fructose/glucose mixture as growth limiting carbon sources (**Chapter 4 and 5**). The presence of gentiobiose, a possible fragment from the secreted polysaccharides, was found by sugar analysis for the glucose-limited cultivations. Gentiobiose could be a possible inducer substrate and a hypothetical mechanism for PNPGase production under glucose conditions is presented in **Chapter 4**. Shotgun proteomics and SDS-PAGE analysis were performed for the proteins present in the supernatant of the conditions using glucose, fructose/glucose and sucrose to investigate the production of different enzymes (**Chapter 4**). Samples for quantification of intracellular metabolites were taken from all cultivations described in **Chapter 3** during the steady-state. Metabolites from glycolysis, citric acid cycle, pentose phosphate pathway and nucleotides were analysed to evaluate their behaviour during the production of extracellular polysaccharides, an interesting by-product produced by *T. harzianum* (**Chapter 5**).
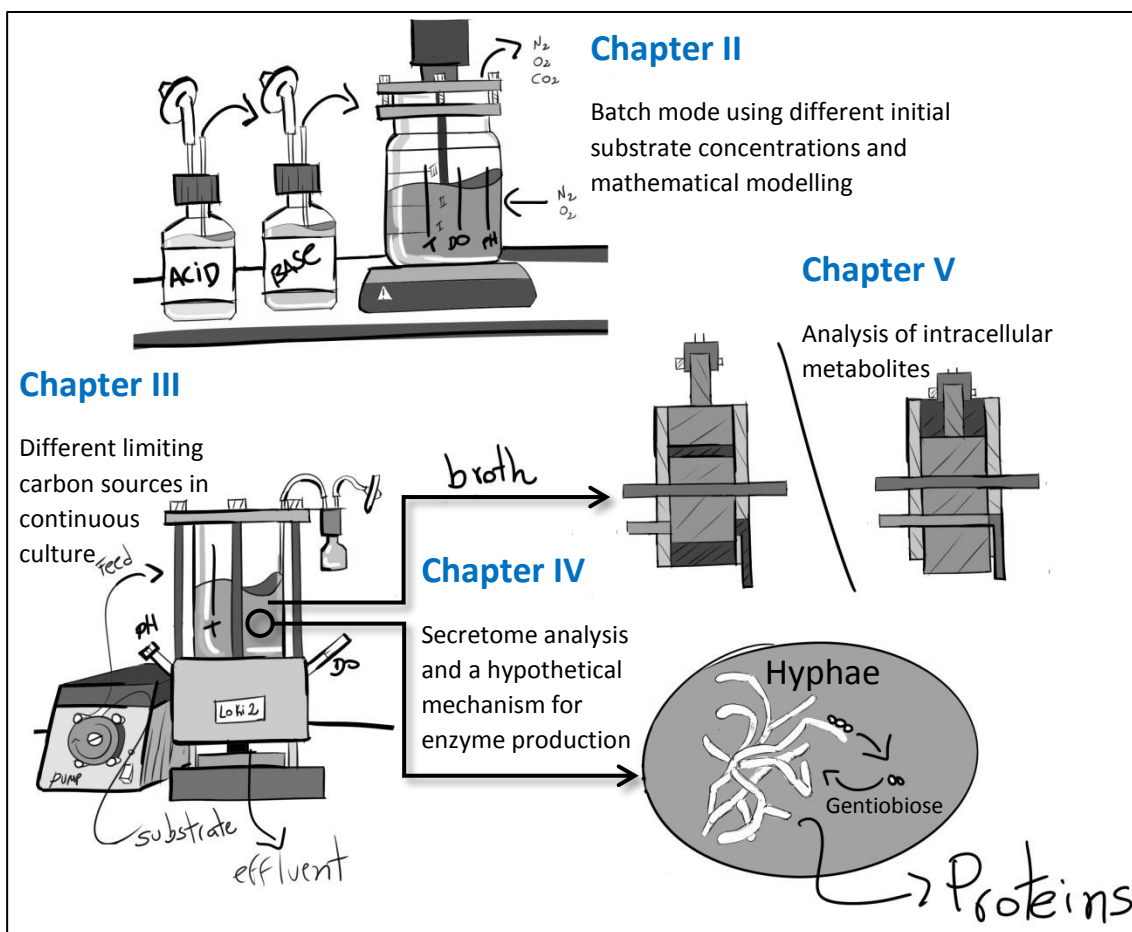
Figure 1.9 – Scope of the thesis

Chapter 2

Mathematical modelling of cell growth using glycerol and cellulase production using cellulose

Cellulase production by *T. harzianum* using cellulose as an inducer substrate is presented in this chapter. A mathematical model was developed to describe cell growth using glycerol as the substrate and to describe cell growth, cellulase and beta-glucosidase production using cellulose as the substrate. In addition, optimization of cellulase production in fed-batch mode was simulated.

Abstract

A cellulase production process can be divided into two steps: a growth stage to achieve the desired cell concentration; followed by an induction stage using an inducer substrate, such as cellulose. In order to evaluate this strategy, two sets of experiments were performed in batch mode. One set of experiments was performed to evaluate the influence of glycerol (initial concentrations of 5, 10, 15 and 20 g/L) regarding cell growth. The other set of experiments considered the induction stage using cellulose as the substrate (initial concentrations of 5, 10, 20, 30 and 40 g/L). A mathematical model was built up to describe cell growth using glycerol, and cellulase production using cellulose. The mathematical model provided a good fit for most of the assays and was also used to simulate a fed-batch experiment. In addition, two feeding strategies were simulated to maximize cellulase production. The first only uses cellulose and the second uses glycerol for cell growth and cellulose for cellulase production. The mathematical model and strategies were developed to maximize enzyme production and they can be adapted for optimized strains.

Keywords

Mathematical modelling, *Trichoderma harzianum*, cellulose, glycerol, fermentation process, and cellulase production

2.1 Introduction

In the biotechnological production of biofuels such as ethanol and other chemicals using lignocellulosic materials, hydrolysis is one of the most important steps of the process. The enzymes used in the hydrolysis step can be commercially produced by filamentous fungi of the genus *Trichoderma,* which is well adapted for fermentation processes (Strakowska et al., 2014). The enzymes used in this step strongly contribute to the manufacturing costs of the final product thus optimizing the hydrolysis step can reduce those costs.

Mathematical modelling allows the development of optimization strategies, thus contributing to decreasing the manufacturing costs, and also allows operation control to maintain a uniform production. Mathematical modelling of *Trichoderma reesei* for cellulase production has been proposed in the past years (Bader et al., 1993; Velkovska et al., 1997; Ma et al., 2013). A mathematical model to describe cellulase production by *Trichoderma harzianum* using sugarcane bagasse pretreated as the carbon source was also proposed (Gelain et al., 2015).

Delabona et al. (2016) claimed that in a two-stage process consisting of growth of *T. harzianum* on glycerol, followed by the induction with sugarcane bagasse pretreated, an important increase in the enzymatic activity and productivity of cellulase was achieved in comparison to a similar process wherein glucose was used as the substrate during the growth stage. The authors suggested that the increase in the production was due to a greater number of active tips of the mycelia, as well as long hyphae, which increased the protein secretion capacity. In addition to this, glycerol is reported as being a neutral carbon source (Ilmén et al., 1997), thus preventing catabolite repression to occur.

Previous experiments in this project, first using glycerol for cell growth, followed by an induction stage using cellulose provided a higher cellulase activity than the experiments only using cellulose (data not shown). Based on the work of Delabona et al. (2016) and these previous experiments, this production approach has the potential to improve cellulase productivity. Mathematical modelling of the microorganism *T. harzianum* P49P11 using sugarcane bagasse pretreated in batch mode was already performed (Gelain et al., 2015). However, due to the complexity and heterogeneity of the sugarcane bagasse, a simpler substrate, such as cellulose, would be more suitable for evaluating the kinetics of the first experiments for the development of the mathematical model for the two-stage process. After the development of the models, they can be adapted for the fed-batch process and strategies based on simulations could be used to increase cellulase productivity.

The present work has as the main objective to obtain more quantitative information on the kinetics of growth and enzyme production of *Trichoderma harzianum* for the construction of a mathematical model to be used in the optimization of cellulase production. For the study of the cell growth stage, experiments were performed using glycerol as the substrate, while cellulose was used as the inducer for cellulase production. A mathematical model was developed to describe cell growth on glycerol and also to describe cellulase production induced by cellulose in batch mode. Subsequently, the model was adapted for fed-batch mode and simulations were performed for the maximization of cellulase production.

2.2 Materials and Methods

2.2.1 Microorganism

The wild strain *Trichoderma harzianum* P49P11 was used in this study. The strain was isolated from the Amazon forest (Delabona et al., 2013). It was grown on potato dextrose agar at 29 ^{o}C for 5 days and then used for inoculum preparation.

2.2.2 Culture conditions

The culture conditions were prepared according to Gelain et al. (2015). The spore suspension of *T. harzianum* was transferred to a 2 L Erlenmeyer flask containing, per litre: glucose, 10 g; peptone, 1 g; Tween 80, 1 mL; saline solution, 50 mL. After 60 h of cultivation at 29 ^{o}C and 200 rpm in a shaker (New Brunswick Scientific innova44), 10 % (v/v) was transferred to a 3 L bioreactor (New Brunswick Scientific BioFlo 115) containing per litre: glycerol, 5, 10, 15, or 20 g; or cellulose, 5, 10, 20, 30 or 40 g; peptone, 1 g; Tween 80, 1 mL; saline solution, 50 mL. The solution of Mandels was used (Mandels and Reese, 1957), in g/L: KH_2PO_4, 20; $(NH_4)_2SO_4$, 14; urea, 3; $MgSO_4.7H_2O$, 3; $CaCl_2$, 3; $FeSO_4.7H_2O$, 0.05; $ZnSO_4.7H_2O$, 0.014; $MnSO_4.H_2O$, 0.016; $CoCl_2$, 0.02. The batch mode experiments were performed in duplicate with a volume of 1.9 L. The temperature was controlled at 29 ^{o}C and the pH was controlled at 5.0 ±0.5 by the addition of an aqueous NH_4OH solution (1:3) and 0.4 M H_2SO_4. The stirring speed was kept between 200 and 300 rpm, and the airflow between 0.48 and 0.7 vvm to prevent dissolved oxygen to drop below 30 %. Furthermore, 1 mL/L of polypropylene glycol antifoaming agent (P2000, Dow Chemical, Brazil) was added. The media were sterilized at 121 ^{o}C for 30 min.

One fed-batch experiment was performed. First starting in batch mode with 15 g/L of glycerol, after 24 h, one pulse of cellulose was added resulting in 20 g/L of cellulose inside the bioreactor. The operating conditions were the same as those used for batch mode. The system used to perform the feeding of the dry cellulose is shown in Figure 2.1. The system is basically composed of an internal and an external hose connected to a flask containing the dry cellulose to be fed. The liquid of the cultivation medium was forced to enter in this flask by pressure difference and when a certain volume was reached, the flask was manually mixed and turned down. The pressure was released making the content inside the flask enter the bioreactor.

Figure 2.1 – Cellulose feeding method

2.2.3   Analytical procedures

The analytical procedures were performed according to Gelain et al. (2015). Cellulase activity was determined using the filter paper activity (FPA) assay (Ghose, 1987). The scale was 10 times reduced to minimize time and reagents. The filter paper activity was assayed by incubating the diluted enzymes (50 µL) with 100 µL of 50 mM sodium citrate buffer (pH 4.8) containing the filter paper Whatman No. 1 (5 mg). The reaction mixture was incubated at 50 ^{o}C for 60 min and stopped by adding 300 µL of the DNS reagent. Reducing sugars were measured by the DNS method (Miller, 1959). The solution was placed in a water bath at 95 ^{o}C for 5 min and, after cooling, 2 mL of water was added. The measurement was made at 540 nm.

Xylanase activity was determined by the method described by Bailey and Poutanen (1989). The activity was measured using beechwood xylan as the substrate. 50 µL of 0.5 % (w/v) substrate, 40 µL of 50 mM sodium citrate buffer (pH 4.8), and 10 µL of the diluted enzyme extract were used. After 10 min of incubation at 50 ^{o}C, the reaction was stopped by adding 100 µL of the DNS reagent and the measurement was made at 540 nm by the DNS method. The activity of beta-glucosidase was estimated according to Zhang et al. (2009). The activity was measured using p-nitrophenyl-β-D-glucopyranoside (PNPG) as the substrate. The reaction mixture was composed of 80 µL of 1 mM substrate diluted in 50 mM citrate buffer (pH 4.8), and 20 µL of the diluted enzyme extract. After 10 min at 50 ^{o}C, the reaction was stopped by adding 100 µL of 1 M sodium carbonate. The measurement was made at 400 nm.

Total protein was measured using microplates with the Bio-Rad protein assay reagent and bovine serum albumin as the standard (Bradford, 1976).

The cellulose and mycelium concentrations for the experiments using cellulose were determined according to the method of Ahamed and Vermette (2009). 10 mL of culture broth was centrifuged (3000x g for 20 min), the sample was washed with distilled water and dried at 70 ^{o}C until constant weight to determine the total dry mass. The dried sample was suspended in 3 mL of acetic acid–nitric acid reagent (ratio of 80 % acetic acid to nitric acid of 10:1) and boiled for 30 minutes in a water bath. After cooling and centrifuging, the sample was washed again, and the resulting solid, mainly composed of cellulose, was dried at 70 ^{o}C until constant weight.

For glycerol assays, 10 mL of culture broth was withdrawn and centrifuged (3000x g for 20 min). The supernatant was used to measure glycerol concentrations and the pellet was dried (70 ^{o}C) until constant weight for the determination of cell concentration. Glycerol was measured using the column Aminex HPX-87H 300x7.8mm (BIO-RAD), a flow rate of 0.6 mL/min, isocratic conditions, and H_2SO_4 as the eluent for 30 min. The equipment was the Agilent 1260 Infinity with an infrared detector.

2.2.4   Mathematical methods

Parameter estimation and simulations were performed using Matlab R2013b. The differential equations were solved by the *ode45* function, the objective function was minimized by the *fmincon* function using the interior-point algorithm, and the *interp1* was used for interpolation. The simulations of the equations were performed using Simulink (Matlab). The optimizations were performed according to Becerra (2004), where optimal profiles are obtained considering the manipulated variable as parameters and performing parameter estimation. The experiments with initial glycerol concentrations of 5, 10 and 20 g/L and initial cellulose concentrations of 10, 20 and 30 g/L were employed for parameter estimation. The experiment with 15 g/L of glycerol was used for validation of the mathematical model using glycerol as the substrate and the experiments with 5 and 40 g/L of cellulose were used for extrapolation analysis of the mathematical model using cellulose as the substrate. The fed-batch experiment was used to test the prediction capacity of the model using cellulose as the substrate. The objective function is described elsewhere (Andrade et al., 2013).

2.3   Results and Discussion

2.3.1   Study of growth stage using glycerol

The growth during batch cultivation was evaluated using different initial concentrations of glycerol. Experimental results for four different conditions are shown below (5, 10, 15 and 20 g/L), Figures 2.2 and 2.3. It can be observed that glycerol consumption for all conditions was fast, for the conditions at 5 and 10 g/L, there was no glycerol after 24 h and for the conditions at 15 and 20 g/L, after 32 h. The maximum concentration of mycelium was observed at 24 h for all the experiments.

The highest mycelium concentration, around 8 g/L, was achieved using 20 g/L of glycerol. However, according to the Tukey test at 95 % confidence interval, the obtained maximum mycelium concentrations at 24h for the conditions using 10, 15 and 20 g/L of glycerol were not significantly different. For the conditions using 15 and 20 g/L, there was still

glycerol at 24 h, indicating that the cell concentration probably increased after this time until the depletion of glycerol. Enzyme activities (secreted enzymes) were not measured because of the expected low induction by glycerol.

Figure 2.2 – Glycerol concentrations vs time during batch cultivation using different initial concentrations of glycerol

Figure 2.3 – Cell concentrations vs time during batch cultivation using different initial concentrations of glycerol

Table 2.1 compares the cell yield on glycerol ($\Delta X/\Delta G$), cell growth rate ($\Delta X/\Delta t$), glycerol consumption rate ($\Delta G/\Delta t$) and the specific cell growth rate ($\Delta X/\Delta t\, X_{24h}$) for the interval of time between 8 and 24 h. The condition using 10 and 15 g/L provided similar yields of cell on glycerol and the condition at 5 g/L provided the highest yield. The condition at 20 g/L resulted in the lowest yield, although the high experimental error interfered with the analysis. The cell growth rate and substrate consumption rate increased with the increase in the initial

concentrations of glycerol. The specific cell growth rate considering the cell concentration at 24 h (X_{24h}) was similar to all the conditions.

Table 2.1 – Cell yield on glycerol ($\Delta X/\Delta G$), cell growth rate ($\Delta X/\Delta t$), glycerol consumption rate ($\Delta G/\Delta t$) and the specific cell growth rate ($\Delta X/\Delta t\, X_{24h}$) from 8 to 24 h (Figures 2.2 and 2.3)

Condition (g/L)	5	10	15	20
$\Delta X/\Delta G$ (g/g)	0.5 ±0.04	0.41 ±0.038	0.42 ±0.032	0.35 ±0.092
$\Delta X/\Delta t$ (g/L h)	0.17 ±0.0135	0.27 ±0.025	0.30 ±0.011	0.38 ±0.1
$\Delta G/\Delta t$ (g/L h)	0.34 ±0.0003	0.66 ±0.005	0.72 ±0.146	1.08 ±0.0203
$\Delta X/\Delta t\, X_{24h}$ (h^{-1})	0.04 ±0.003	0.044 ±0.004	0.046 ±0.002	0.047 ±0.014

2.3.2 Study of induction stage using cellulose

The induction of cellulase synthesis was evaluated in this work by performing five batch conditions with different initial concentrations of cellulose (5, 10, 20, 30 and 40 g/L). For these experiments, cellulose was used as the substrate during both, growth and the induction stage. The measured cellulase activities vs time are shown below (Figures 2.4 – 2.9).

Virtually, all cellulose was consumed before 60 h (Figure 2.4). In the beginning, it seems that there was a small or no reduction in substrate concentration, this probably occurs due to the presence of nutrients coming from the inoculum and medium solution (peptone). Cell concentration (Figure 2.5) increased with the increase in the initial substrate concentration from 5 to 30 g/L of cellulose, achieving around 9 g/L of cells. The highest cell concentration was observed at 24 h. The condition using 40 g/L of cellulose led to the same cell concentration as the condition using 30 g/L at 24 h and this could have happened due to possible interference from the method used for the analysis. For the estimation of cell concentration, an acid solution is added to a dried sample containing cellulose and cell to digest the cell mass. Then, the sample treated with acid is washed and dried. The difference between the total mass (cellulose mass plus cell mass) and the mass after the digestion (cellulose mass) is the cell mass present in the sample. For the condition at 40 g/L, the cellulose concentration was 28 ±3 g/L at 24 h and this concentration could have prevented the complete digestion of the cell mass at the conditions used, which could have resulted in a lower cell concentration. Perhaps, longer reaction time and/or a higher acid concentration can improve cell concentration analysis when high concentrations of cellulose remain in the samples. Another explanation is that the initial concentration of 40 g/L of cellulose inhibited cell growth.

The Tukey test with 95 % confidence interval was applied to analyse whether there were significant differences in the average values for proteins, cellulase and beta-glucosidase activities at 72 h. According to the test, the measured protein concentrations, as well as the cellulase and beta-glucosidase activities at 72 h for the initial cellulose concentrations of 10, 20, 30 and 40 g/L were not significantly different. The conditions using 20 and 30 g/L provided the highest activities of xylanases and these conditions were not significantly different from each other. The microorganism used was a wild type strain and the increase in the substrate above 10 g/L could have provoked inhibition of the production of proteins, including cellulase and beta-glucosidase. Another explanation is that the concentration of enzymes produced in the condition at 10 g/L is considered by the microorganism already enough to degrade the substrate at conditions using higher initial concentrations of cellulose (20, 30 and 40 g/L). Considering the Tukey test, the conditions at 10, 20 and 30 g/L provided similar activities for

cellulase and beta-glucosidase. Thus, 10 g/L is the preferable condition for cellulase production since it reduces substrate usage.
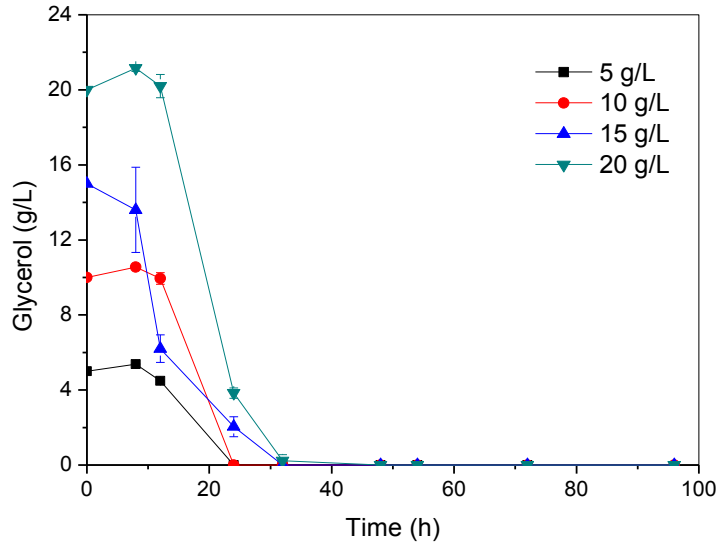

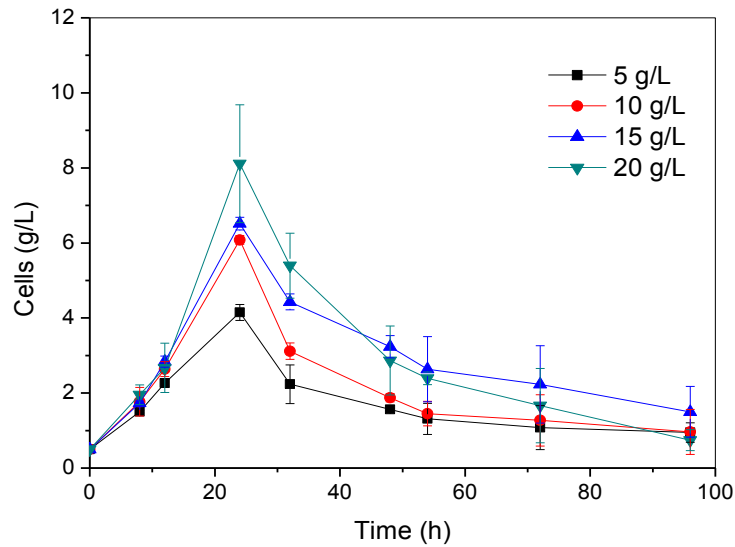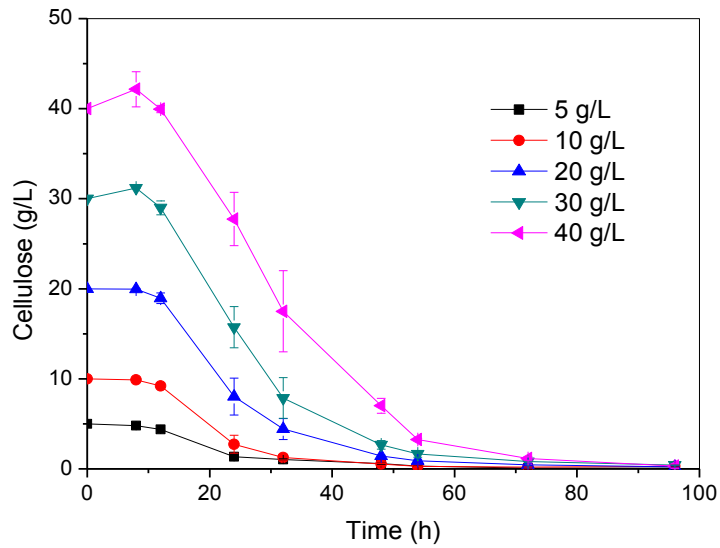Figure 2.4 – Cellulose concentrations vs time during batch cultivation using different initial concentrations of cellulose
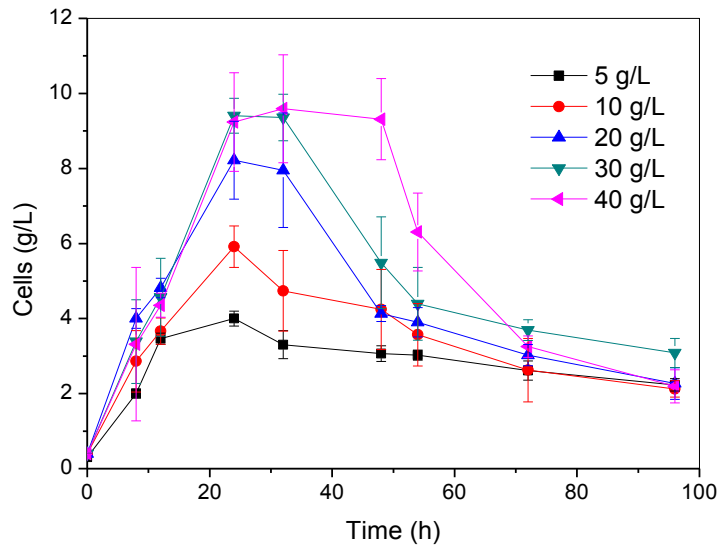
Figure 2.5 – Cell concentrations vs time during batch cultivation using different initial concentrations of cellulose

28
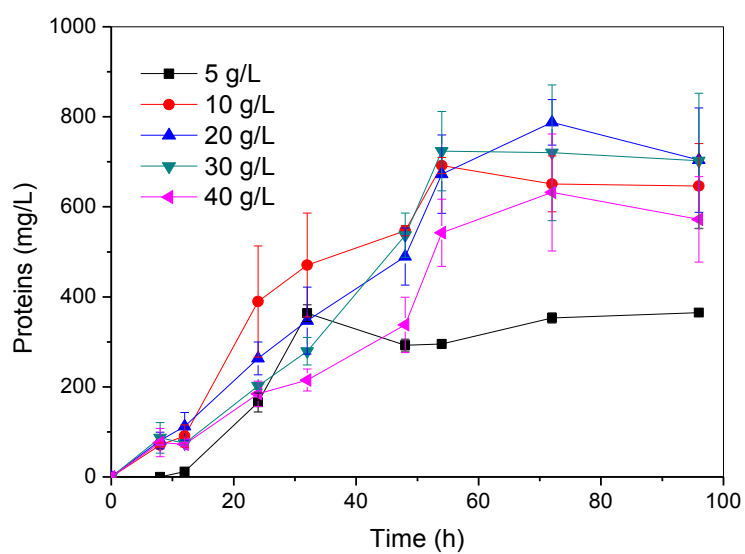
Figure 2.6 – Protein concentrations vs time during batch cultivation using different initial concentrations of cellulose
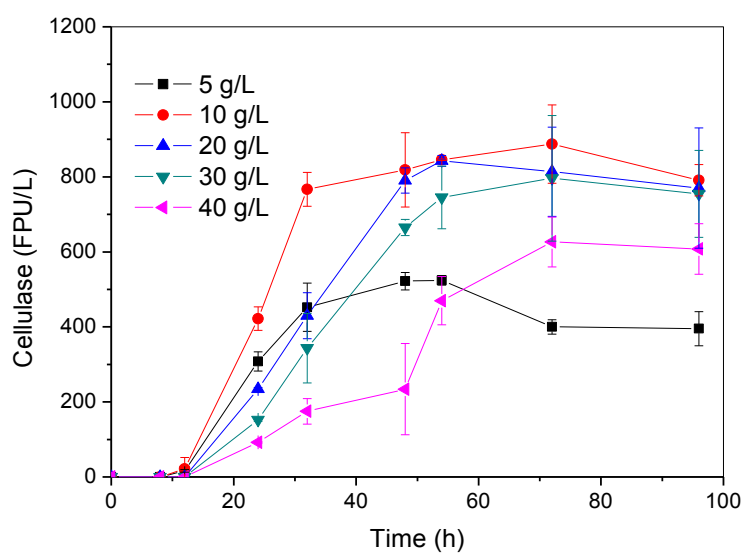
Figure 2.7 – Cellulase activity vs time during batch cultivation using different initial concentrations of cellulose
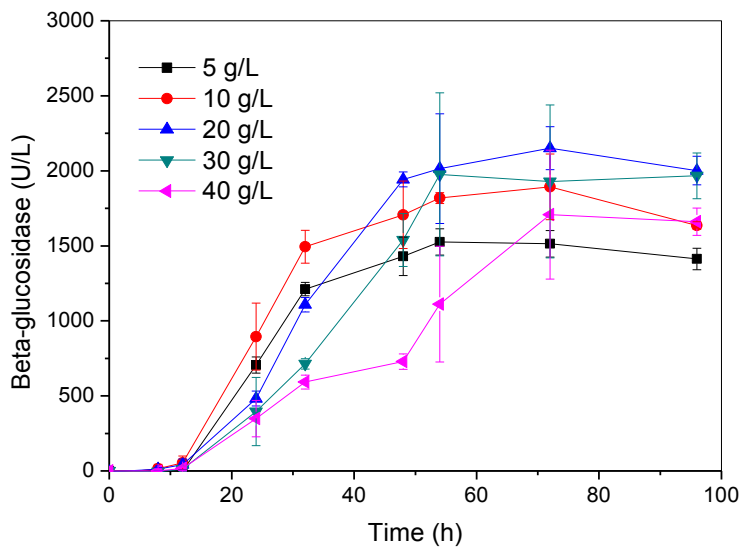
Figure 2.8 – Beta-glucosidase activity vs time during batch cultivation using different initial concentrations of cellulose
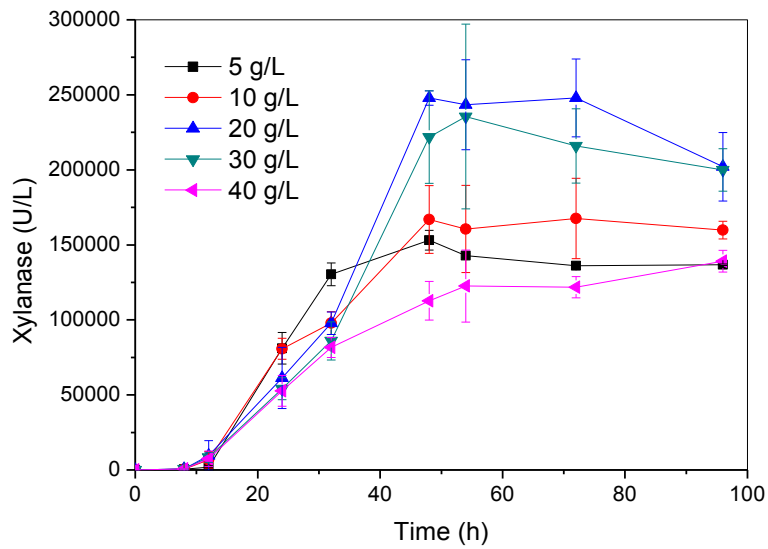
Figure 2.9 – Xylanase activity vs time during batch cultivation using different initial concentrations of cellulose

Table 2.2 compares the cell yield on cellulose ($\Delta X/\Delta C$), cell growth rate ($\Delta X/\Delta t$), cellulose consumption rate ($\Delta C/\Delta t$) and the specific cell growth rate ($\Delta X/\Delta t\, X_{24h}$) for the interval of time between 8 and 24 h. It also compares the specific cellulase production rate ($\Delta F/\Delta t\, X_{72h}$), specific beta-glucosidase production rate ($\Delta B/\Delta t\, X_{72h}$) and specific xylanase production rate ($\Delta Xy/\Delta t\, X_{72h}$) between 8 and 72 h.

The condition using 10, 20, 30 and 40 g/L provided similar yields of cell on cellulose and the condition at 5 g/L provided the highest yield. The cell growth rate and substrate consumption rate increased with the increase in the initial concentrations of cellulose from 5 to 30 g/L. The value of cell growth rate for the condition at 40 g/L was similar to the condition

at 30 g/L, this indicates inhibition of cell growth rate for the 40 g/L condition due to the higher initial concentration of cellulose. The specific cell growth rate considering the cell concentration at 24 h (X_{24h}) was similar to all the conditions. The lower specific enzyme production rate for the conditions at 30 and 40 g/L in comparison with the conditions at 10 and 20 g/L indicates inhibition due to the higher initial concentrations of the substrate.

Table 2.2 – Cell yield on cellulose ($\Delta X/\Delta C$), cell growth rate ($\Delta X/\Delta t$), cellulose consumption rate ($\Delta C/\Delta t$), and the specific cell growth rate ($\Delta X/\Delta t\, X_{24h}$) from 8 to 24 h. The specific cellulase production rate ($\Delta F/\Delta t\, X_{72h}$), the specific beta-glucosidase production rate ($\Delta B/\Delta t\, X_{72h}$) and the specific xylanase production rate ($\Delta Xy/\Delta t\, X_{72h}$) from 8 to 72 h (Figures 2.4 – 2.9)

Condition (g/L)	5	10	20	30	40
$\Delta X/\Delta C$ (g/g)	0.59 ±0.07	0.42 ±0.15	0.35 ±0.1	0.39 ±0.09	0.41 ±0.19
$\Delta X/\Delta t$ (g/L h)	0.13 ±0.015	0.19 ±0.06	0.26 ±0.07	0.38 ±0.076	0.37 ±0.15
$\Delta C/\Delta t$ (g/L h)	0.22 ±0.02	0.45 ±0.06	0.75 ±0.13	0.97 ±0.1424	0.90 ±0.22
$\Delta X/\Delta t\, X_{24h}$ (h^{-1})	0.031 ±0.004	0.032 ±0.011	0.032 ±0.009	0.04 ±0.008	0.04 ±0.017
$\Delta F/\Delta t\, X_{72h}$ (FPU/g h)	2.4 ±0.14	5.28 ±1.17	4.2 ±0.65	3.37 ±0.73	3 ±0.34
$\Delta B/\Delta t\, X_{72h}$ (U/g h)	9 ±0.61	11.2 ±2.5	11 ±0.52	8.2 ±2.2	8.2 ±2.13
$\Delta Xy/\Delta t\, X_{72h}$ (U/g h)	809 ±21	993 ±261	1277 ±145	910 ±110	581 ±39

2.3.3 Mathematical modelling for batch mode

The material balance of the components for a batch process can be described by Equation 2.1. In the batch process, the volume is constant and there are no inflow and outflow rates.

$$R_i = M_l \frac{d(C_i)}{dt} \tag{2.1}$$

Where, i is the component analysed, R_i is the component production/consumption rate, M_l is the mass of liquid and C_i is the component concentration in the liquid. The production rate of cells (R_X), substrate consumption rate (R_S) and production rate of enzymes (R_E) are described by Equations 2.2, 2.3 and 2.4 respectively.

$$R_X = \mu_X C_X M_l \tag{2.2}$$

$$R_S = -q_S C_X M_l \tag{2.3}$$

$$R_E = q_E C_X M_l \tag{2.4}$$

Where, μ_X is the specific cell growth rate, q_S is the specific substrate consumption rate, q_E is the specific enzyme production rate and C_X is the cell concentration. Then, Equations 2.2, 2.3 and 2.4 can be reorganized in combination with Equation 2.1:

$$\frac{dC_X}{dt} = \mu_X C_X \tag{2.5}$$

$$\frac{dC_S}{dt} = -q_S C_X \tag{2.6}$$

$$\frac{dC_E}{dt} = q_E C_X \tag{2.7}$$

Where, C_S is the substrate concentration and C_E is the enzymatic activity in the medium. Furthermore, kinetic equations are required to describe the mentioned specific rates (μ_X, q_S, q_E) as a function of external concentrations of substrates and products and in some cases, the specific growth rate. The mathematical model developed for the batch process is based on Equations 2.5, 2.6 and 2.7.

Glycerol and cellulose were used as substrates in this chapter and were proposed equations for the specific glycerol consumption rate (q_G) and for the specific cellulose consumption rate (q_C). The substrate consumption rate was considered dependent on cell growth rate and proportional to mycelium concentration (C_X) (Equation 2.8 and 2.9). Equation 2.8 describes the consumption of glycerol (C_G) for cell growth and Equation 2.9 describes the consumption of cellulose (C_C) for cell growth and has also a second term that describes the consumption of cellulose by active cells (C_{Xact}). Active cells are an attempt at cell segregation, wherein this case, they are considered as being the part of cells responsible for synthesizing the enzymes. This term considers that part of cells is being activated due to the presence of an inducer (cellulose). Parameters are displayed in Table 2.3 and Table 2.4.

$$\frac{dC_G}{dt} = -q_G C_X \tag{2.8}$$

$$q_G = \alpha' \left(\frac{dC_X}{dt} \right)_g$$

$$\frac{dC_C}{dt} = -q_C C_X \tag{2.9}$$

$$q_C = \alpha \left(\frac{dC_X}{dt} \right)_g + \beta \left(\frac{dC_{Xact}}{dt} \right)_g \frac{C_{Xact}}{C_X}$$

Where, α' is the constant of glycerol consumption, α is the constant of cellulose consumption for cells and β is the constant of cellulose consumption for active cells.

The cell growth model is divided into two rates considering a specific cell growth rate (μ_X) and a specific cell death rate (μ_{Xd}). Equation 2.10 describes the cell growth rate and Equation 2.11 describes the cell death rate. Both rates are dependent on the substrate C_S (C_S = cellulose (C_C) or glycerol (C_G)) according to the *Monod* equation. The cell growth rate has an inhibition term dependent on cell concentration according to the logistic equation for population growth (Fujikawa et al., 2004). It was assumed that there was a control of cell growth based on cell concentration where $C_{X_{mS}}$ is considered the maximum cell concentration allowed by the environment.

$$\left(\frac{dC_X}{dt} \right)_g = \mu_X C_X \tag{2.10}$$

$$\mu_X = \mu_{XmS} \left(\frac{C_S}{C_S + k_S} \right) \left(1 - \frac{C_X}{C_{X_{mS}}} \right)$$

$$\left(\frac{dC_X}{dt} \right)_d = \mu_{Xd} C_X \tag{2.11}$$

$$\mu_{Xd} = \mu_{XmdS} \left(\frac{C_S}{C_S + k_{Sd}} \right)$$

$$\frac{dC_X}{dt} = \left(\frac{dC_X}{dt}\right)_g - \left(\frac{dC_X}{dt}\right)_d \tag{2.12}$$

Where, μ_{XmS} is the maximum specific cell growth rate, k_S is the *Monod* constant for cell growth, C_{XmS} is the maximum cell concentration, μ_{XmdS} is the maximum specific rate for cell death and k_{Sd} is the *Monod* constant for cell death.

Velkovska et al. (1997) proposed that the cellulase production by *Trichoderma reesei* Rut C30 using cellulose was not associated with cell growth. They developed a mathematical model with cell segregation where first the formation of a primary mycelium responsible for a high substrate consumption rate occurs, followed by the formation of a secondary mycelium. This secondary mycelium was considered responsible for cellulase synthesis. This segregation was also considered in this project and the cells responsible for enzyme production were named active cells. This model considers a specific active cell growth rate (μ_e) and a specific deactivation rate of active cells (μ_{ed}). Equation 2.13 describes the active cell growth rate and Equation 2.14 describes the deactivation rate.

$$\left(\frac{dC_{Xact}}{dt}\right)_g = \mu_e C_X \tag{2.13}$$

$$\mu_e = \mu_{em}\left(\frac{C_C}{C_C + k_{Ce}}\right)\left(1 - \frac{C_{Xact}}{C_{Xact_m}}\right)$$

$$\left(\frac{dC_{Xact}}{dt}\right)_d = \mu_{ed} C_{Xact} \tag{2.14}$$

$$\mu_{ed} = k_{da}$$

$$\frac{dC_{Xact}}{dt} = \left(\frac{dC_{Xact}}{dt}\right)_g - \left(\frac{dC_{Xact}}{dt}\right)_d \tag{2.15}$$

Where, μ_{em} is the maximum specific growth rate for active cells, k_{Ce} is the *Monod* constant for active cell growth, C_{Xact_m} is the maximum active cell concentration and k_{da} is the deactivation constant for active cells.

The enzyme production rates consider a specific cellulase production rate (q_F) and a specific beta-glucosidase production rate (q_B). The cellulase (C_F) and beta-glucosidase (C_B) production rates have an inhibition term dependent on enzymatic activity, and a second, dependent on cellulose concentration (C_C) (Equations 2.16 and 2.17). The enzyme production rates are proportional to active cell concentration. The parameters a and b represent controls regarding the inhibition influence of cellulose according to another parameter, S_{iF} and S_{iB}, respectively, and when cellulose concentration is above these values (S_{iF} and S_{iB}), a and/or b are equal to 0.15, adding an inhibition effect on enzyme production rate. Otherwise, a and/or b are equal to zero. S_{iF} and S_{iB} are cellulose concentrations that inhibit the production of cellulase and beta-glucosidase, respectively. The values of a and b were manually adjusted according to the residual value of the objective function.

$$\frac{dC_F}{dt} = q_F C_{Xact} - k_{dF} C_F \tag{2.16}$$

$$q_F = q_{Fm}\left(1 - \frac{C_F}{C_{Fm}}\right)\left(\frac{1}{aC_C{}^2/k_{iF} + 1}\right)$$

$$\frac{dC_B}{dt} = q_B C_{Xact} - k_{dB} C_B \tag{2.17}$$

$$q_B = q_{Bm} \left(1 - \frac{C_B}{C_{Bm}}\right) \left(\frac{1}{bC_C{}^2/k_{iB} + 1}\right)$$

Where, q_{Fm} is the maximum specific rate for cellulase production, C_{Fm} is the maximum cellulase activity, k_{iF} is the inhibition constant for cellulase production, k_{dF} is the deactivation constant for cellulase, q_{Bm} is the maximum specific rate for beta-glucosidase production, C_{Bm} is the maximum beta-glucosidase activity, k_{iB} is the inhibition constant for beta-glucosidase production and k_{dB} is the deactivation constant for beta-glucosidase.

2.3.4 Mathematical modelling for fed-batch mode

The material balance for a fed-batch process can be described by Equation 2.18. In the fed-batch process, the mass of liquid (M_l) is a function of time and there are only inflow rates.

$$C_i \frac{d(M_l)}{dt} + M_l \frac{d(C_i)}{dt} = F_l^{in} C_i^{in} + R_i \tag{2.18}$$

Where, F_l^{in} is the inflow rate of liquid and C_i^{in} is the concentration of the component from the inflow of liquid. Equation 2.18 can be reorganized according to the definition of dilution rate (D):

$$D = \frac{1}{M_l} \frac{d(M_l)}{dt} = \frac{F_l^{in}}{M_l}$$

$$\frac{d(C_i)}{dt} = \frac{R_i}{M_l} + D(C_i^{in} - C_i) \tag{2.19}$$

The mathematical model developed for the batch process was adapted to representing the fed-batch process using Equation 2.19. The dilution rate (D) considers a feeding of glycerol. It was considered that there was no dilution effect inside the bioreactor when cellulose (solid material) was added. Equation 2.20 represents the cell growth rate based on glycerol consumption.

$$\left(\frac{dC_X}{dt}\right)_g = \mu_{XmG} \left(\frac{C_G}{C_G + k_G}\right) \left(1 - \frac{C_X}{C_{XmG}}\right) C_X - DC_X \tag{2.20}$$

Equation 2.21 considers the cell death rate (Equation 2.11). Parameter estimation for the conditions using glycerol concluded that the *Monod* constant for cell death rate (k_{Gd}) is equal to zero:

$$\frac{dC_X}{dt} = \mu_{XmG} \left(\frac{C_G}{C_G + k_G}\right) \left(1 - \frac{C_X}{C_{XmG}}\right) C_X - C_X(\mu_{XmdG} + D) \tag{2.21}$$

Equation 2.22 describes glycerol consumption where $C_{G,f}$ is the glycerol from the feed.

$$\frac{dC_G}{dt} = -\alpha' \left(\frac{dC_X}{dt}\right)_g C_X + D\left(C_{G,f} - C_G\right) \tag{2.22}$$

Equation 2.23 describes cellulose consumption only dependent on active cells. In this equation, cellulose consumed only goes for active cells and the consumption rate for cell growth is considered equal to zero (Equation 2.23 is derived from Equation 2.9). Equation 2.24

describes the cell growth rate for active cells and Equation 2.25 considers the deactivation rate of active cells (Equation 2.14).

$$\frac{dC_C}{dt} = -\beta \left(\frac{dC_{Xact}}{dt}\right)_g C_{Xact} - DC_C \tag{2.23}$$

$$\left(\frac{dC_{Xact}}{dt}\right)_g = \mu_{em} \left(\frac{C_C}{C_C + k_{Ce}}\right)\left(1 - \frac{C_{Xact}}{C_{Xact\,m}}\right)C_X - DC_{Xact} \tag{2.24}$$

$$\frac{dC_{Xact}}{dt} = \mu_{em} \left(\frac{C_C}{C_C + k_{Ce}}\right)\left(1 - \frac{C_{Xact}}{C_{Xact\,m}}\right)C_X - C_{Xact}(k_{da} + D) \tag{2.25}$$

The feed of cellulose was discretized since it was considered to be added by pulses. As the simulated feeding was not continuously added, it was not incorporated in the model as an inflow rate. Figure 2.10 shows how this was considered in the simulation. The integrator block had the "External reset: rising" option active, which enables the reset of the integrator when the feed increases due to a simulated pulse of cellulose. In every feed, the integrator block considers the cellulose inside the bioreactor plus the pulse of cellulose and uses this value as an initial substrate concentration to initiate the integration again.
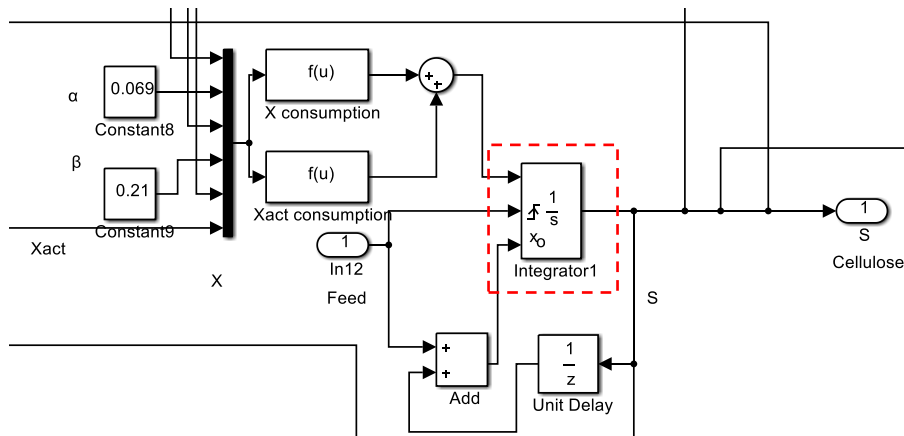
Figure 2.10 – Discretization of the feed of cellulose, Simulink (Matlab)

Cellulose feeding was optimized following an adapted algorithm from Becerra (2004), where is this case, the optimization occurs at one value of the manipulated variable at a time, keeping the remaining values static in the matrix. Once this first value of the manipulated variable is optimized based on the objective function, the algorithm moves to the next one, and after building up the optimal profile, the algorithm repeats the single optimization at a time until satisfying a condition. This alteration was done to be able to only optimize a range of values of the manipulated variable instead of optimizing all of them for every integration step. For example, optimization of the manipulated variable every 8h (pulse of cellulose), not every integration step (integration step = 1 h).

Equation 2.26 and 2.27 represent the cellulase and beta-glucosidase production rates considering a dilution rate.

$$\frac{dC_F}{dt} = q_{Fm} \left(1 - \frac{C_F}{C_{F\,m}}\right)\left(\frac{1}{aC_C{}^2/k_{iF} + 1}\right)C_{Xact} - C_F(k_{dF} + D) \tag{2.26}$$

$$\frac{dC_B}{dt} = q_{Bm}\left(1 - \frac{C_B}{C_{Bm}}\right)\left(\frac{1}{bC_C{}^2/k_{iB} + 1}\right)C_{Xact} - C_B(k_{dB} + D) \tag{2.27}$$

The model was used to simulate one condition where there is a continuous feeding of glycerol and a discrete feeding of cellulose (simulation platform Figure 2.11A). The feed of glycerol is to keep the cell at the desired concentration, and cellulose consumption is only for enzyme production. In this simulation, cellulose consumption does not influence cell growth rate because glycerol was considered as the carbon source more easily available for cell growth. Cellulose was only considered to be used to produce active cells. In addition, one condition starting in batch mode using cellulose as the substrate and a discrete cellulose feeding was also simulated (simulation platform Figure 2.11B). This simulation considers that cellulose is for both, growth and enzyme production.
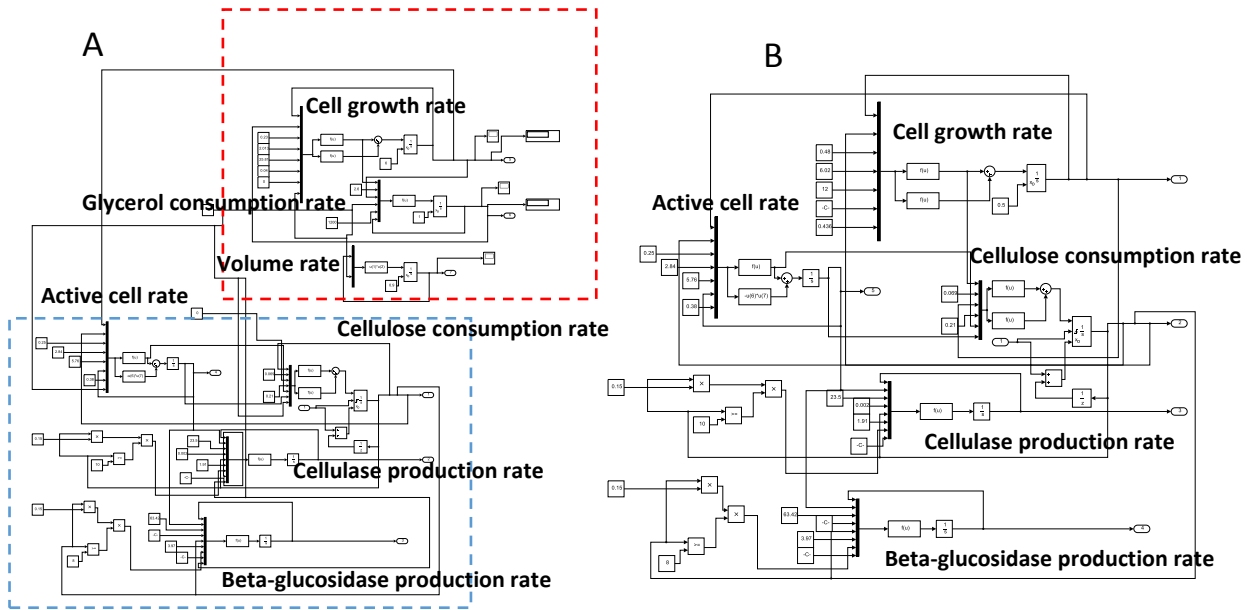
Figure 2.11 – (A) simulation platform for fed-batch using glycerol for cell growth (red) and cellulose for cellulase synthesis (blue) and (B) simulation platform for fed-batch only using cellulose in Simulink (Matlab)

2.3.5   Results for mathematical modelling using glycerol in batch mode

The experiments varying the initial concentrations of glycerol presented in Figures 2.2 and 2.3 were employed for parameter estimation for the growth stage. Equations 2.8 and 2.12 were used. The initial conditions for parameter estimation were 0.5 g/L of cell and 5, 10 and 20 g/L of glycerol. The experiment using 15 g/L of glycerol was used to validate the model. The results of the fit (continuous lines) and the experimental data are shown in Figures 2.12 and 2.13. The good fit allows the use of the model to perform fed-batch simulations towards the maximization of cell concentration or until the achievement of the desired value. Parameters are shown in Table 2.3.

Table 2.3 – Parameters for the mathematical model using glycerol as the substrate

μ_{XmG}	Maximum specific cell growth rate (h⁻¹)	0.23
k_G	Monod constant for cell growth (g/L)	2
C_{X_mG}	Maximum cell concentration (g/L)	25.8
μ_{XmdG}	Maximum specific rate for cell death (h⁻¹)	0.04
k_{Gd}	Monod constant for cell death (g/L)	0
α'	Constant of glycerol consumption (g (of C_G) L g⁻² (of C_X))	0.38
D	Dilution rate (h⁻¹)	0.0042
C_X	Cell concentration (g/L)	
C_G	Glycerol concentration (g/L)	
$C_{G,f}$	Glycerol concentration in the feed (g/L)	1200
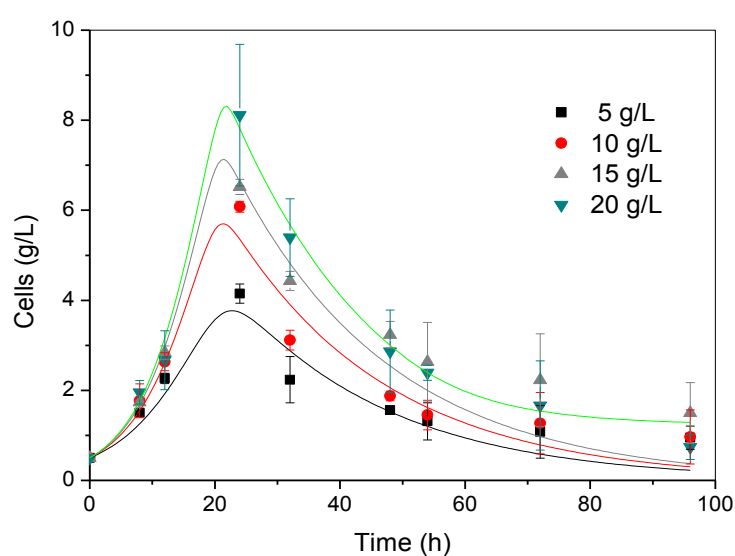
Figure 2.12 – Fit of the model for cell concentration (continuous lines)
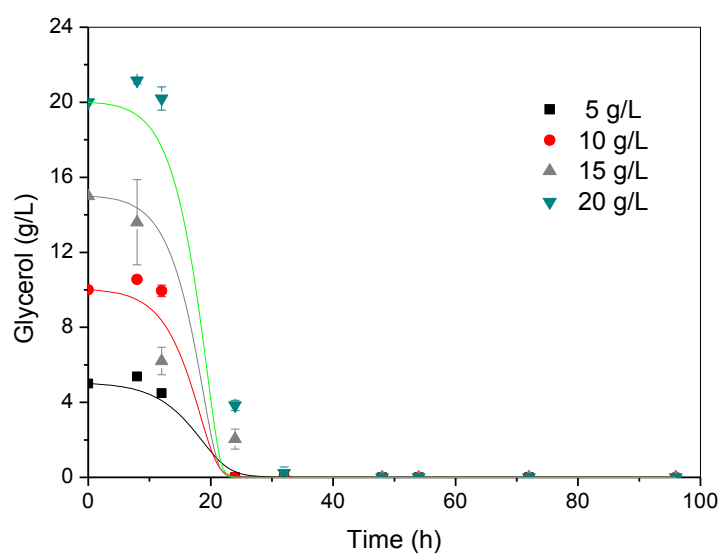
Figure 2.13 – Fit of the model for glycerol concentration (continuous lines)

2.3.6 Results for mathematical modelling using cellulose in batch mode

Assays with initial concentrations of cellulose of 10, 20 and 30 g/L were used for parameter estimation. Equation 2.9 was used for cellulose consumption, Equation 2.12 for cell growth, Equation 2.15 for active cell concentration and Equations 2.16 and 2.17 for enzyme production. The initial conditions for parameter estimation were 0.4 g/L of cell, 10, 20 and 30 g/L of cellulose and the enzymatic activities of cellulase and beta-glucosidase were considered zero. The inclusion of the assays at 5 and 40 g/L in parameter estimation resulted in a poor fit (data not shown). However, these data were used to verify the capacity of the model to predict data out of the range of concentrations used for parameter estimation (see next section). Figures 2.14, 2.15 and 2.16 show the fit of the model for cell growth, substrate consumption and cellulase production using 10, 20 and 30 g/L of cellulose, respectively, and Figure 2.17 shows the fit of beta-glucosidase activity for those three conditions. The model could describe well the data. Parameters are shown in Table 2.4.

Table 2.4 – Parameters for the mathematical model using cellulose as the substrate

μ_{XmC}	Maximum specific cell growth rate (h^{-1})	0.48
k_C	Monod constant for cell growth (g/L)	6
$C_{X_{mC}}$	Maximum cell concentration (g/L)	12
μ_{XmdC}	Maximum specific rate for cell death (h^{-1})	0.095
k_{Cd}	Monod constant for cell death (g/L)	0.44
q_{Fm}	Maximum specific rate for cellulase production (FPU/g h)	23.5
C_{F_m}	Maximum cellulase activity (FPU/L)	2513
k_{iF}	Inhibition constant for cellulase production $(g/L)^2$	1.91
k_{dF}	Deactivation constant for cellulase (h^{-1})	0.002
q_{Bm}	Maximum specific rate for beta-glucosidase production (U/g h)	63.42
C_{B_m}	Maximum beta-glucosidase activity (U/L)	5013
k_{iB}	Inhibition constant for beta-glucosidase production $(g/L)^2$	3.97
k_{dB}	Deactivation constant for beta-glucosidase (h^{-1})	0.0011
μ_{em}	Maximum specific growth rate for active cells (g (of C_{Xact}) /g h)	0.25
k_{Ce}	Monod constant for active cell growth (g/L)	2.84
C_{Xact_m}	Maximum active cell concentration (g/L)	5.76
S_{iF}	Concentration of cellulose that inhibits cellulase production (g/L)	10
S_{iB}	Concentration of cellulose that inhibits beta-glucosidase production (g/L)	8
k_{da}	Deactivation constant for active cells (h^{-1})	0.38
a	Inhibition control for cellulase	0/0.15
b	Inhibition control for beta-glucosidase	0/0.15
α	Constant of cellulose consumption for cells (g (of C_C) L g^{-2} (of C_X))	0.069
β	Constant of cellulose consumption for active cells (g (of C_C) L g^{-2} (of C_{Xact}))	0.21
C_X	Cell concentration (g/L)	
C_{Xact}	Active cell concentration (g/L)	
C_C	Cellulose concentration (g/L)	
C_F	Cellulase activity (FPU/L)	
C_B	Beta-glucosidase activity (U/L)	

According to the parameter estimation using cellulose, the maximum concentration of cells and active cells allowed in the bioreactor are 12 g/L and 5.76 g/L, respectively. The maximum cellulase and beta-glucosidase activities are 2513 FPU/L and 5013 U/L, respectively. According to the parameters for glycerol condition (Table 2.3), the maximum concentration of cells allowed in the bioreactor is 25.8 g/L. The use of glycerol with cellulose could allow the increase in cell concentration compared to experiments only using cellulose, creating the

possibility of also increasing the concentration of active cells, which could provide an increase in enzyme synthesis.
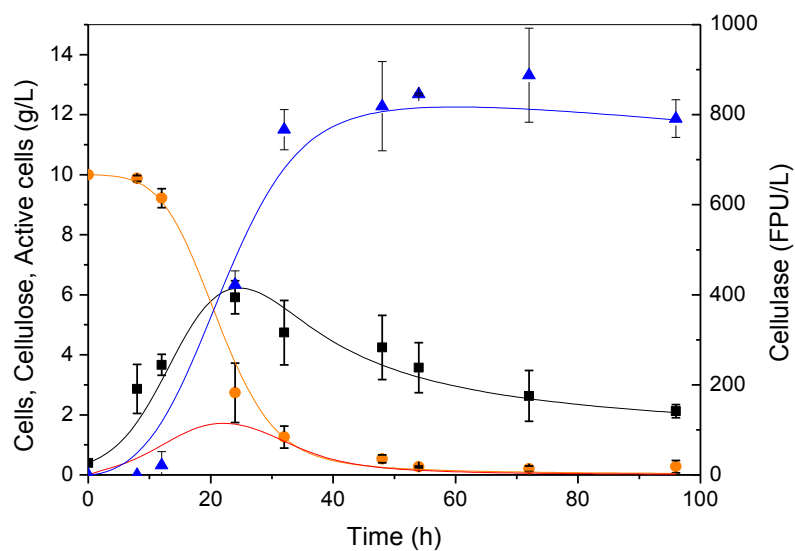
Figure 2.14 – Fit of the model for the assay using 10 g/L of cellulose, (●) cellulose, (■) cells, (▲) cellulase activity, (-) active cell simulation
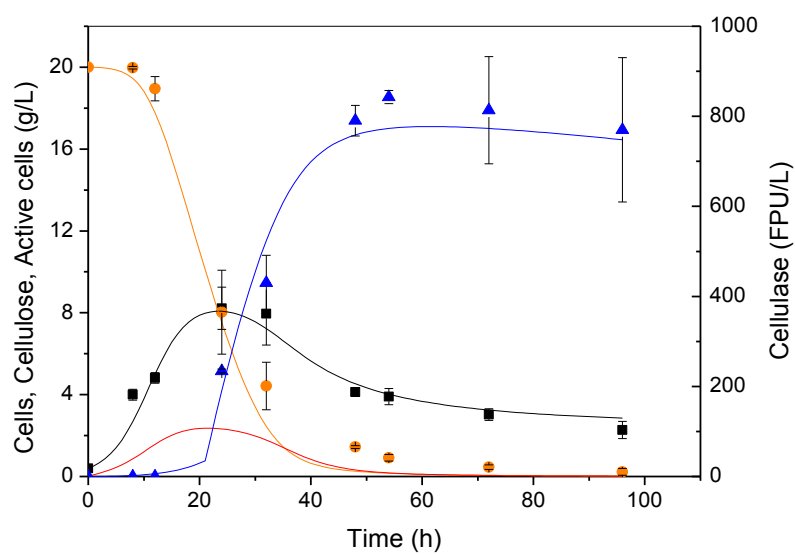
Figure 2.15 – Fit of the model for the assay using 20 g/L of cellulose, (●) cellulose, (■) cells, (▲) cellulase activity, (-) active cell simulation
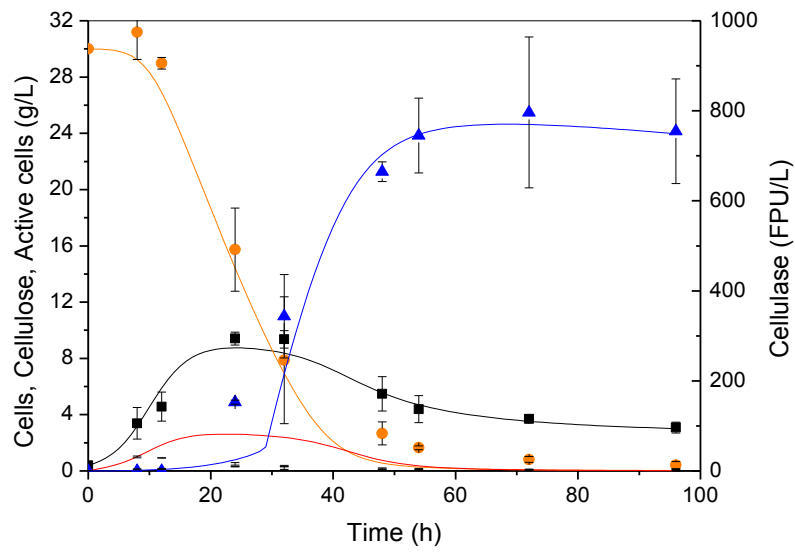
Figure 2.16 – Fit of the model for the assay using 30 g/L of cellulose, (●) cellulose, (■) cells, (▲) cellulase activity, (-) active cell simulation
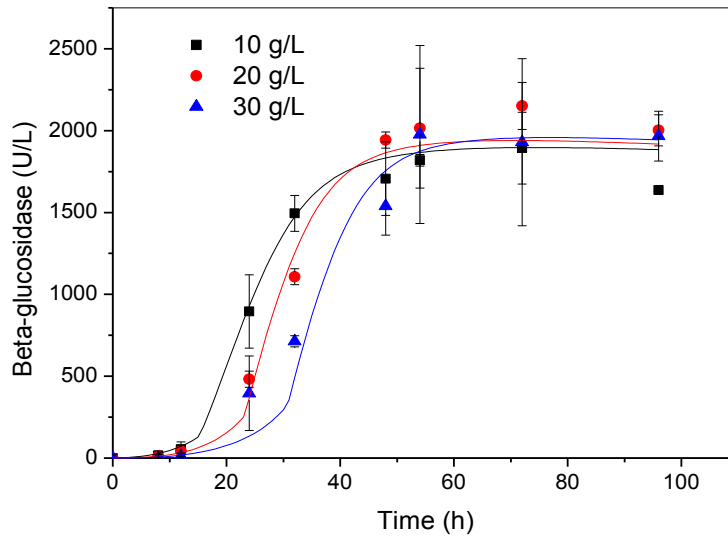
Figure 2.17 – Fit of the model for the assays using 10, 20 and 30 g/L of cellulose for beta-glucosidase activity

2.3.7   Prediction capacity of the mathematical model using cellulose as the substrate

For extrapolation of the mathematical model using cellulose as the substrate, the 5 and 40 g/L conditions were used. The simulations are shown in Figures 2.18 and 2.19 for cell growth, cellulose consumption, and cellulase production. Figure 2.20 shows beta-glucosidase simulation. Simulation for 40 g/L condition indicates a good fit for cell concentration, substrate

consumption and beta-glucosidase production. For the 5 g/L condition, the model could only predict well the substrate consumption and beta-glucosidase activity. Cellulase production was overestimated, but follows the same profile of the experimental data. The overestimation of cellulase production in both conditions suggests that the model is not representing well the inhibition influence on the 40 g/L condition and the enzyme denaturation effect on the 5 g/L condition.
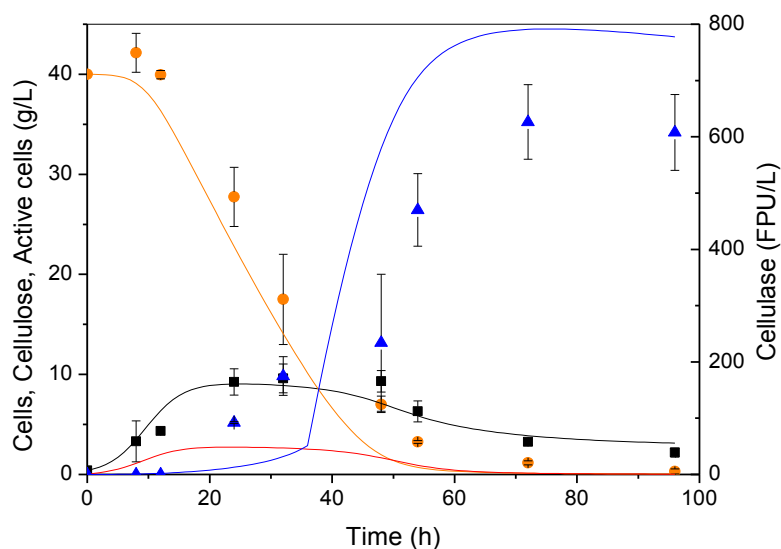
Figure 2.18 – Extrapolation of the mathematical model for the assay using 40 g/L of cellulose, (●) cellulose, (■) cells, (▲) cellulase activity, (-) active cell simulation
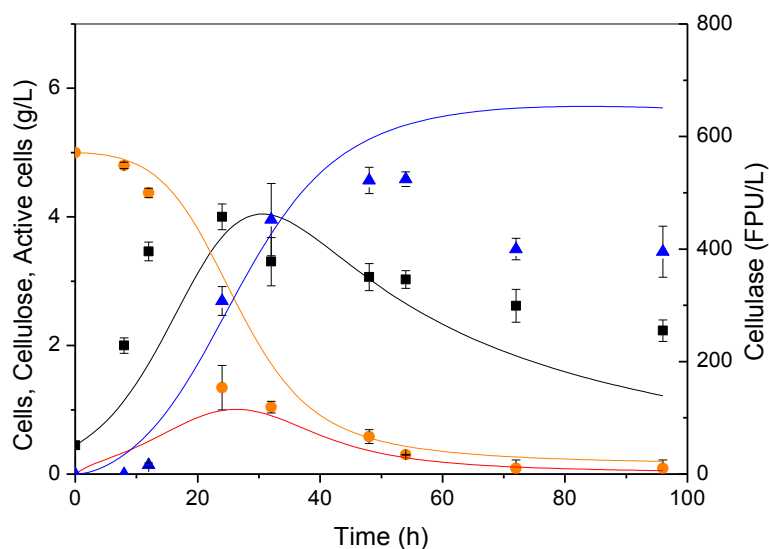
Figure 2.19 – Extrapolation of the mathematical model for the assay using 5 g/L of cellulose, (●) cellulose, (■) cells, (▲) cellulase activity, (-) active cell simulation
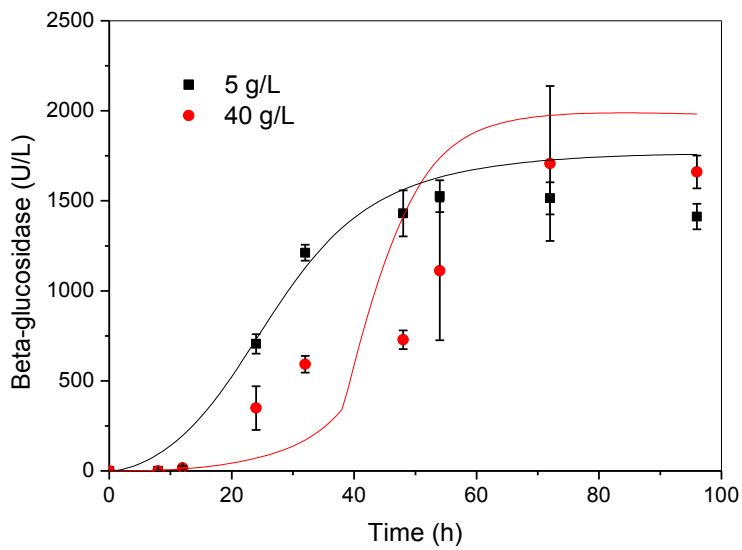
Figure 2.20 – Extrapolation of the mathematical model for the assays using 5 and 40 g/L of cellulose for beta-glucosidase activity

It was also performed a simulation to predict the production of the enzymes in a fed-batch process that started with glycerol for the batch phase, followed by one feeding of cellulose after 24 h. The feed of cellulose resulted in a concentration of 20 g/L inside the bioreactor. Only cellulose consumption was considered for the simulation. Assuming that the cellulose consumed was mainly for cellulase synthesis, Equation 2.23 was used (with the dilution rate equal to zero) to represent substrate consumption rate, where the influence of cell growth is not present. The results of the simulations are presented in Figures 2.21 and 2.22 only after the feeding of cellulose. The batch phase using glycerol is not presented. It can be seen that the model could represent well the production of cellulase, cell growth and cellulose consumption; however, beta-glucosidase production was overestimated, indicating that the parameters that describe the inhibition mechanism are not suitable for representing this group of enzymes at this condition (b = 0.15 and S_{iB} = 8). For this reason, a simulation was done with other parameter values: b = 0.3; and S_{iB} = 3.

The simulation suggests that the mathematical model developed is suitable for predicting cellulase production in fed-batch using glycerol for cell growth at first and then cellulose for cellulase production. However, more experiments in fed-batch mode are needed to confirm the capacity of the model.
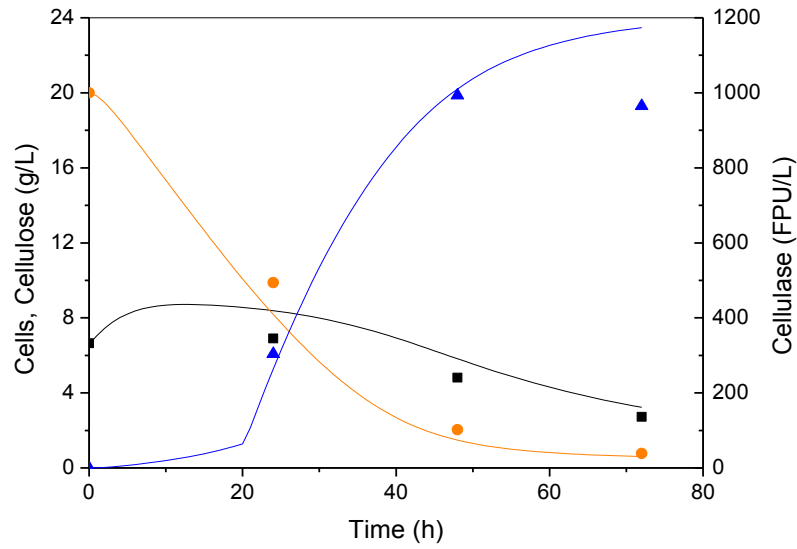
Figure 2.21 – Fit of the model for the assay using glycerol at first (15 g/L) for cell growth then cellulose for cellulase induction (20 g/L), (●) cellulose, (■) cells, (▲) cellulase activity
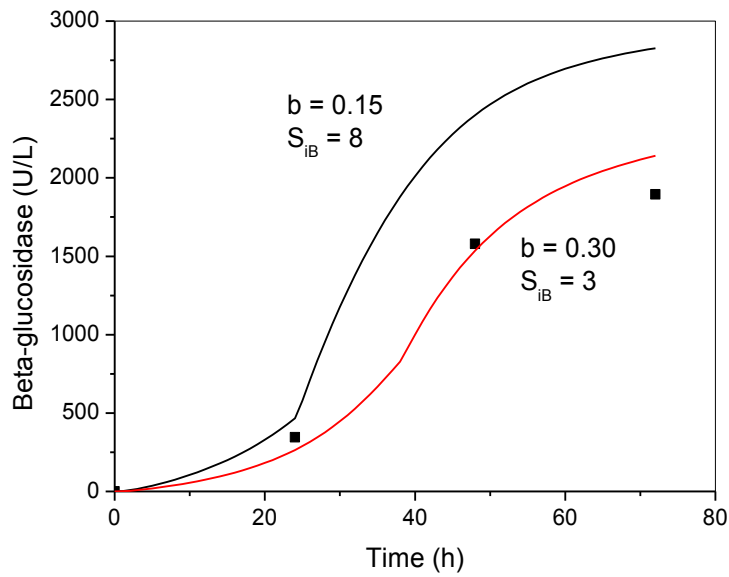
Figure 2.22 – Fit of the model for the assay using glycerol at first (15 g/L) for cell growth then cellulose for beta-glucosidase induction (20 g/L)

2.3.8 Correlation coefficients

Equation 2.28 describes the correlation coefficient (Neto et al., 2013). This equation was used to evaluate the fit of the model for cellulose and glycerol conditions. Values close to 100 % indicate a good fit of the mathematical model.

$$COR(\%) = \left(1 - \frac{\sum_{i=1}^{n}(y_i - y_{pi})^2}{\sum_{i=1}^{n}(y_i - \bar{y_i})^2}\right)100 \tag{2.28}$$

Where y_i and y_{pi} are the experimental data and predicted values of the model, respectively, n is the number of experimental data and $\bar{y_i}$ is the average of the experimental data. Table 2.5 shows the COR values for glycerol conditions including the validation test (15 g/L of glycerol). Table 2.6 presents the results for cellulose conditions including the extrapolation analysis (5 and 40 g/L of cellulose) and the fed-batch condition. For the fed-batch, the parameters describing the inhibition effect on beta-glucosidase production was modified (Table 2.6). As it was visually observed, the mathematical model using glycerol as the substrate described well the experimental data. On the other hand, the mathematical model using cellulose as the substrate was not good at predicting the cellulase production for the conditions out of the range used for parameter estimation (5 and 40 g/L of cellulose). However, they could predict well the cellulase production for the fed-batch experiment.

Table 2.5 - Correlation coefficient (%) for glycerol conditions

	Condition (g/L)	Cells	Glycerol
	5	83.19	98.45
	10	91.30	98.22
Validation	15	84.42	83.59
	20	98.32	96.89

Table 2.6 - Correlation coefficient (%) for cellulose conditions

	Condition (g/L)	Cells	Cellulose	Cellulase	Beta-glucosidase
	5	82.62	89.69	62.94	93.58
Parameter estimation	10	86.72	99.26	97.68	98.51
	20	99.54	98.74	98.37	91.89
	30	95.13	98.78	96.56	97.26
	40	88.30	96.40	51.93	64.98
	20 (Fed-batch)[a]	69.10	98.64	93.80	96.64[b]

a – Fed-batch starting with glycerol. b – Parameters, b = 0.30, S_{iB} = 3.

2.3.9 Simulation of strategies for cellulase maximization

The mathematical model employing the simulation platforms (Figure 2.11) with the parameters presented in Table 2.3 and 2.4 were used to simulate two strategies to maximize cellulase production in fed-batch mode. The use of fed-batch allows the achievement of higher productivity of cellulase than the process in batch mode (Reis et al., 2013). The parameters that represent the inhibition effect on beta-glucosidase production was not modified since more fed-batch experiments are needed to better understand the feeding influence on beta-glucosidase production. The first simulation (Figures 2.23 and 2.25) starts with 20 g/L of cellulose and 0.5 g/L of cells. A discrete feeding of cellulose is optimized (maximum of 10 g/L inside the bioreactor) considering a fixed time (96 h) and 12 feeds, where the first feeding is the initial cellulose concentration (grey bars). Equation 2.9 was used for the prediction of cellulose consumption, Equation 2.12 for cell growth, Equation 2.15 for active cell growth and Equations 2.16 and 2.17 for enzyme production. The feeding was discretized because of the method presented in Figure 2.1, cellulose was added by a pulse and there was not a continuous feeding system to be adapted. The cellulose consumption rate considers the amount of cellulose inside the bioreactor plus the cellulose added through the pulse. The

optimization algorithm searches the highest cellulase activity at 96 h using as the restriction the maximum concentration of cellulose allowed inside the bioreactor, 30 g/L.

Based on the results of the mathematical model in batch mode, the use of only cellulose allows a maximum cell concentration of 12 g/L. On the other hand, glycerol can provide a maximum cell concentration of 25.8 g/L. Since enzyme production is considered proportional to the concentration of cells (Delabona et al., 2016), the increase in cell concentration could provide an increase in cellulase and beta-glucosidase production. Thus combining cellulose with glycerol could be favourable for enzyme synthesis since glycerol could be used to keep a high cell concentration without repression consequences, and cellulose could only be used to induce cellulase and beta-glucosidase synthesis. For this reason, a second simulation was performed.

The second simulation (Figures 2.24 and 2.25) starts with 10 g/L of cellulose, 1 g/L of glycerol and 6 g/L of cells. It considers a constant feed of glycerol of 0.0042 h^{-1} from a 1200 g/L solution to keep the cell concentration close to 18 g/L, a discrete feed of cellulose (12 feeds) and a fixed time of 96 h. Equation 2.21 was used for cell growth, Equation 2.22 for glycerol consumption, Equation 2.23 for cellulose consumption, Equation 2.25 for active cell growth and Equations 2.26 and 2.27 for enzyme production. Glycerol consumption was considered for cell growth rate, and cellulose consumption was only considered for enzyme production (Equation 2.23). The maximum concentration of cellulose allowed inside the bioreactor was 10 g/L. The volume increased from 0.9 to 1.35 L. Figure 2.25 shows cellulase and beta-glucosidase productions for both simulations.

The simulations indicate that higher cell concentrations can lead to higher enzymatic activities and productivities. The cellulase produced by the wild strain used in this study (*Trichoderma harzianum* P49P11) might be tightly controlled by the microorganism, which restricts the maximization of productivity. The strategies proposed here are examples of possibilities that can be used for optimized strains.
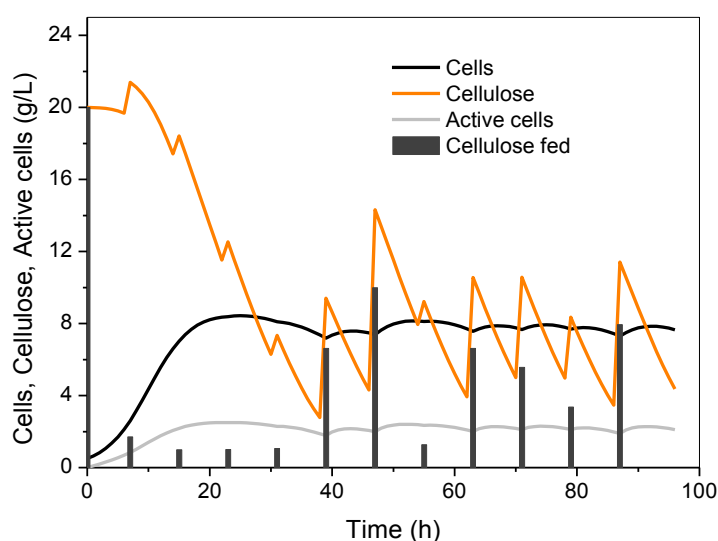
Figure 2.23 – Simulated strategy only using cellulose in the feed
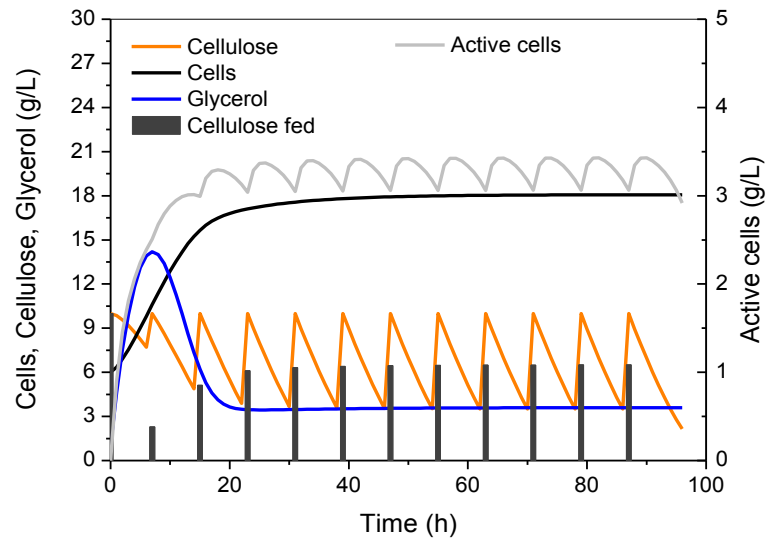
Figure 2.24 – Simulated strategy using cellulose and glycerol in the feed
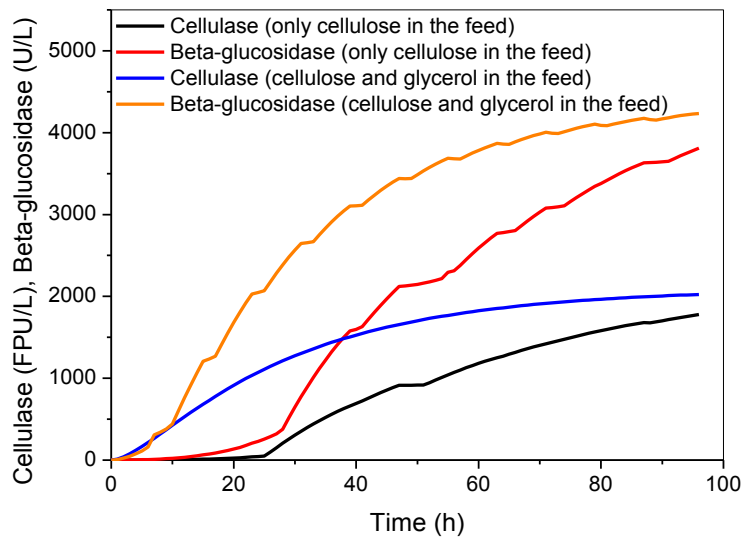
Figure 2.25 – Simulated strategy, enzymatic activities

The complete Matlab code used for parameter estimation and to solve the optimal control problem is presented in the supplementary material. Simulink (Matlab) was used to perform the simulations for parameter estimation. This configuration allows the use of all the mathematical and logical structures available in the library of this toolbox to be easily incorporated in the mathematical model. In this project, it was used a logic control to represent the inhibition influence on enzyme synthesis.

2.4 Conclusions

A two-stage approach to cellulase production was evaluated with the purpose of constructing a mathematical model for the system. A mathematical model for glycerol and cellulose conditions was developed and presented a good fit for the majority of the

experimental data. Fed-batch analysis has indicated that the mathematical model can predict the profiles of the experimental data; however, more experiments are needed to find the best set of parameters to better describe the inhibition influence. Simulations of strategies were presented as possibilities that can be exploited in future works. The model and strategies were developed as tools to be used for cellulase maximization. Since this project presented a process using a wild strain, these tools can be adapted for the maximization of cellulase employing strains less repressed.

Chapter 3

Enzyme production under carbon-limited conditions

Continuous cultures were performed under carbon-limited conditions using different carbon sources (glucose, sucrose, fructose/glucose and carboxymethyl cellulose). Glucose was found to induce the production of enzymes that can catalyse the hydrolysis of p-nitrophenyl-β-D-glucopyranoside (PNPGase).
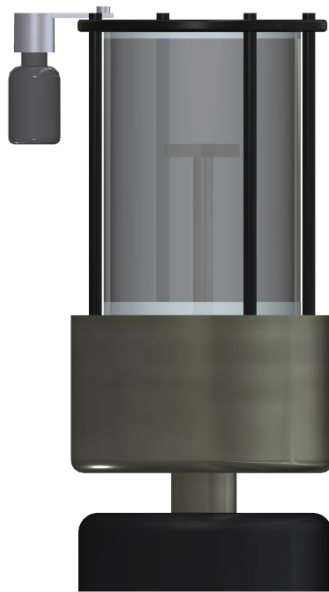
Abstract

Carbon-limited chemostat cultures were performed using different carbon sources (glucose, 10 and 20 g/L; sucrose, 10 g/L; fructose/glucose, 5.26/5.26 g/L; carboxymethyl cellulose, 10 g/L; and carboxymethyl cellulose/glucose, 5/5 g/L) to verify the capability of the wild type strain *Trichoderma harzianum* to produce extracellular enzymes (cellulase and PNPGase). All chemostat cultures were carried out at a fixed dilution rate of 0.05 h^{-1}. Experiments using glucose, fructose/glucose and sucrose were performed in duplicate. PNPGase was the only group of enzymes found by the methods employed. When sucrose was used as the substrate, the lowest PNPGase productivity was obtained. A concentration of 20 g/L of glucose in the feed provided the highest productivity (1048 ±16 U/mol h), followed by 10 g/L of glucose, carboxymethyl cellulose/glucose, fructose/glucose and carboxymethyl cellulose. The use of carboxymethyl cellulose as the sole carbon source resulted in a very low cell concentration (0.82 ±0.3 g/L) and did not induce the production of cellulase. Based on the obtained results, a PNPGase production process was developed mainly using glucose.

Keywords

3.1 Introduction

In second-generation ethanol production processes using lignocellulosic materials as feedstock, enzymatic hydrolysis can be used to release the sugars. In this case, the production of suitable enzymes is an important step and the presence of efficient beta-glucosidase could lead to high conversion yields thus contributing to decreasing process costs. Beta-glucosidase hydrolyses the *O*-glycosyl linkage of terminal non-reducing beta-D-glycosyl residues releasing beta-D-glucose and can be divided into cellobiase, with a high cellobiose specificity, and aryl-beta-glucosidase, with a high p-nitrophenyl-β-D-glucopyranoside (PNPG) specificity (Sørensen et al., 2013). Thus, the estimation of enzymatic activity using the substrate PNPG indicates the presence of enzymes that can catalyse the hydrolysis of glycosidic bonds like beta-glucosidase.

According to Allen and Andreotti (1982), beta-glucosidase is an important group of enzymes and an increase in its level enhances the rate of saccharification of cellulose by reducing the level of cellobiose, which is an inhibitor of cellulose hydrolysis. In addition, they also reported that for the *in vitro* saccharification of cellulose with *Trichoderma reesei* cellulase, 50 % of the cellulase can be replaced with equivalent units of beta-glucosidase with no loss of the rate of saccharification. This suggests that in an optimized process, beta-glucosidase could work as a supplement of cellulase cocktails, contributing to reducing the costs of enzymatic hydrolysis.

Glucose, usually reported as a repressor of the synthesis of cellulase, can be used as the substrate for beta-glucosidase production in batch cultivation (Jäger et al., 2001), as well as in carbon-limited continuous culture (Strobel and Russell, 1987). Allen and Andreotti (1982) discussed the production of beta-glucosidase in continuous cultures of *Aspergillus phoenicis* using corn dextrin as the inducer at different dilution rates. Although this strain can also produce beta-glucosidase when glucose is the sole carbon source, corn dextrin was used, as its presence resulted in higher levels of these enzymes. Beta-glucosidase production in the presence of glucose seems unnecessary because glucose can be taken up as such. However, glucose could act as an indicator of the presence of cellulose and the microorganism might produce beta-glucosidase to be ready to perform efficient hydrolysis (Strobel and Russell, 1987).

Another possibility could be the presence of extracellular polysaccharides, whose fragments, under carbon-limited conditions, could stimulate the production of enzymes, thus the cells could use the polysaccharides as another carbon source. Pessoni et al., (2015) demonstrated that fructose could induce β-fructofuranosidase activity in *Penicillium janczewskii*, which could be related to structural changes in the cell wall (a decrease in the cell wall thickness) when the carbon was depleted, indicating that polysaccharides released from the cell wall could be inducing glucanase.

In this work, the production of cellulase and PNPGase were measured in carbon-limited chemostat cultures employing the wild strain *Trichoderma harzianum* and using different carbon sources. This study shows the potential of this microorganism to produce PNPGase continuously and suggests that the optimization of the operating conditions as well as the strain could lead to a promising enzyme production process mainly using glucose.

3.2 Materials and Methods

3.2.1 Microorganism

A wild type strain, *Trichoderma harzianum* P49P11, was used in this study. The strain was isolated from the Amazon forest (Delabona et al., 2013). It was grown on potato dextrose agar at 29 ^{o}C and the spores were harvested after 5-7 days with sterilized water. The spore solutions were kept in stock at -80 ^{o}C.

3.2.2 Culture conditions

Spores from *T. harzianum* were used to inoculate 500 mL shake flasks containing 250 mL of the medium: 10 g/L of glucose (carbon source), 2 g/L of KH_2PO_4, 5 g/L of $(NH_4)_2SO_4$, 0.3 g/L of $MgSO_4.7H_2O$, 0.3 g/L of $CaCl_2.2H_2O$, 1 mL/L of trace elements solution, and 1 g/L of peptone. Trace elements solution: 15 g/L of $Na_2EDTA.2H_2O$, 4.5 g/L of $ZnSO_4.7H_2O$, 1 g/L of $MnCl_2.4H_2O$, 0.3 g/L of $CoCl_2.6H_2O$, 0.3 g/L of $CuSO_4.5H_2O$, 0.4 g/L of $Na_2MoO_4.2H_2O$, 4.5 g/L of $CaCl_2.2H_2O$, 3 g/L of $FeSO_4.7H_2O$, 1 g/L of H_3BO_3, 0.1 g/L of KI. The medium was sterilized at 121°C for 20 min. The shake flasks were incubated in an orbital shaker for 24 - 48 h at 29 ^{o}C and 200 rpm before inoculating the bioreactor (10 % v/v).

Different limiting carbon sources were applied to evaluate the production of enzymes in continuous culture: 10 g/L of glucose (G101 and G102), 10 g/L of sucrose (S1 and S2), 5.26 and 5.26 g/L of fructose and glucose (FG1 and FG2), 10 g/L of carboxymethyl cellulose (CMC), 5 and 5 g/L of carboxymethyl cellulose and glucose (CMCG). The medium composition was the same as described for shake flasks, only peptone was not added to the feed medium. In addition, 20 g/L of glucose was also tested in the feed (G201 and G202) with the following modifications to the medium composition: 3 g/L of KH_2PO_4; and 6 g/L of $(NH_4)_2SO_4$. These alterations were made to keep the same residual concentrations of these compounds in the effluent as for the condition using 10 g/L of glucose. The chemostat cultivation with glucose, sucrose and fructose/glucose as carbon sources was performed in duplicate. The medium was sterilized by filtration using a filter 0.2 μm (Sartorius stedim, Sartopore 2). The medium composition used for the batch phase, preceding the chemostat phase, was the same as used for the shake flask cultivation, except for the first batch experiment in which 20 g/L of sucrose was used as the carbon source. Glucose provided a faster batch phase, thus sucrose was replaced by glucose (10 g/L) for the next experiments. The medium for the batch phase was sterilized by filtration using a filter 0.2 μm (AcroPak™ 20).

3.2.3 Chemostat system

The experiments were performed using a 7 L bioreactor (Applikon, Delft, the Netherlands). The mass of the cultivation medium was controlled through a pneumatic system connected to a control unit, which opened a valve at the bottom of the bioreactor and started an effluent pump when it was needed to maintain a constant broth mass of 4 kg.

The temperature was controlled by a water bath at 29 ^{o}C, and pH 5 was controlled by the addition of 2 M KOH and 2 M H_2SO_4. Sterile air was supplied via a mass flow controller (Brooks 58505, calibration at 0 ^{o}C and 1 bar). The gas outflow was passed through a condenser at 4 ^{o}C and a Nafion dryer before the volume fraction of oxygen and carbon dioxide were measured by the NGA 2000 off-gas analyser. An overpressure of 0.2-0.3 bar was applied.

3.2.4 Operating conditions

All chemostat experiments were started in batch mode and after a sharp drop of the CO_2 production observed after 22-24 h, the process was switched to carbon-limited continuous cultures with a dilution rate of 0.05 h^{-1} ±0.003 h^{-1}.

For the batch phase, the stirring speed was kept between 200 and 400 rpm; however, for the continuous culture, it was changed to a constant stirring speed of 600 rpm. The airflow of 1 L/min was used, and only for the condition using 20 g/L of glucose, the airflow was 1.5 L/min. A constant antifoam addition (Basildon BC antifoam 86/013) of approximately 7 µL/min was used. The achievement of the steady-state was assumed when the CO_2 production and mycelium concentration were constant for at least 6 residence times as well as a constant PNPGase activity for at least 4 residence times.

Samples for quantification of the mycelium concentration and enzyme activities were taken before the steady-state for some conditions to observe the profiles, and at steady-state for all the conditions to also estimate the concentration of residual sugars, total organic carbon (TOC) and total nitrogen (TN). For sugar analysis, the samples were frozen in liquid nitrogen right after the filtration by 0.45 µm filter (Millex-HV durapore PVDF membrane) and stored at - 80 °C.

3.2.5 Enzymatic activity

The enzymatic activity was performed according to Gelain et al. (2015). The enzymatic activity of cellulase was determined using the filter paper activity (FPA) assay (Ghose, 1987). The scale was 10 times reduced to minimize time and reagents. The filter paper activity was assayed by incubating the diluted enzymes (50 µL) with 100 µL of 50 mM sodium citrate buffer (pH 4.8) containing the filter paper Whatman No. 1 (5 mg). The reaction mixture was incubated at 50 °C for 60 min and stopped by adding 300 µL of DNS reagent. Reducing sugars were measured by the DNS method (Miller, 1959). The solution was placed in a water bath at 95 °C for 5 min and, after cooling, 2 mL of water was added and the measurement was made at 540 nm in the spectrophotometer.

The activity of PNPGase was determined according to Zhang et al. (2009). The activity was measured using p-nitrophenyl-β-D-glucopyranoside (PNPG) as the substrate. The reaction mixture was composed of 80 µL of 1 mM substrate diluted in 50 mM citrate buffer (pH 4.8), and 20 µL of the diluted enzyme extract. After 10 min at 50 °C, the reaction was stopped by adding 100 µL of 1 M sodium carbonate. The measurement was made at 400 nm.

3.2.6 Sugar analysis

Glucose, sucrose and fructose were measured. For this analysis, the samples were diluted with 1 M NaOH to precipitate the proteins that could interfere with the analysis. Subsequently, the precipitate was removed by centrifugation (2000x g, 10 min). The samples were analysed using high-performance anion exchange (HPAE) Dionex ICS-5000 with PAD detector (Rohrer et al., 2013).

3.2.7 Total organic carbon (TOC) and total nitrogen (TN)

For the determination of the TOC and TN, 3 mL of supernatant was filtered by 0.45 µm membrane (Millex-HV durapore PVDF membrane) and analysed with a Shimadzu TOC-L

analyser using the difference method for the TOC estimation and the total nitrogen unit (TNM-L) for TN estimation.

3.2.8 Dry cell weight concentration

For the estimation of dry cell weight, 5 mL of sample was withdrawn from the bioreactor. The weight of the samples was measured and then they were poured on a 0.45 μm filter of known mass (Pall membrane filter, Supor). Subsequently, the cells were filtered and washed with Milli-Q water. The filter was placed in an oven at 70 °C for one day and cooled down in a desiccator before the measurement of the weight.

3.2.9 Carbon recovery, by-products and specific rates

For all chemostat experiments, the carbon balances were calculated to verify the production of by-products. Carbon recovery (C_r, %) is described by Equation 3.1 considering the carbon dioxide production rate (R_{CO_2}, Cmol/h), cell production rate (R_X, Cmol/h), carbon from by-product formation (R_{byp}, Cmol/h) and carbon consumption rate (R_C, Cmol/h).

$$C_r(\%) = \left(\frac{R_{CO_2} + R_X + R_{byp}}{R_C}\right) 100 \tag{3.1}$$

By-products were estimated using the total organic carbon analysis (C_{TOC}, Cmol/kg) by Equation 3.2. For the carbon balance, all the carbon from the feed was considered to be consumed due to the low concentration of residual sugars ($C_{sugars,l}$ Cmol/kg) in the liquid outflow (F_l^{out}, kg/h). Carbon present in the proteins was not considered due to the low concentration of proteins (30-200 mg/L) and unknown composition.

$$R_{byp} = F_l^{out}(C_{TOC} - C_{sugars,l}) \tag{3.2}$$

Because no elemental composition analysis of this microorganism was performed, the carbon fraction in the cells was assumed as being the same as *T. reesei* QM9414 (Ross et al., 1983): $CH_{1.8}O_{0.71}N_{0.143}$ + 9.4 % of ashes.

Specific production and consumption rates (q_i, mol/mol h) were defined as described by Equation 3.3, where i is the component analysed, R_i (mol/h) is the production or consumption rate, C_X (mol/kg) is the cell concentration and M_l (kg) is the mass of liquid. The complete material balance for the system is presented in the supplementary material.

$$q_i = \frac{R_i}{C_X M_l} \tag{3.3}$$

3.3 Results and Discussion

3.3.1 Enzyme production using different carbon sources

Previous experiments in batch mode with different initial concentrations of sucrose (Figure 3.1) demonstrated that *T. harzianum* was able to synthesize PNPGase. The culture and operating conditions used were similar as reported in section 3.2.2 for batch mode, with the addition of 0.15 g/L of urea. For this reason, sucrose was used as the carbon source in carbon-limited chemostat cultures to verify whether the synthesis of PNPGase would also occur in these conditions. Cellulase activity was also analysed for all the conditions studied in this

chapter; however, this group of enzymes was not present in the supernatant according to the analytical methods employed.
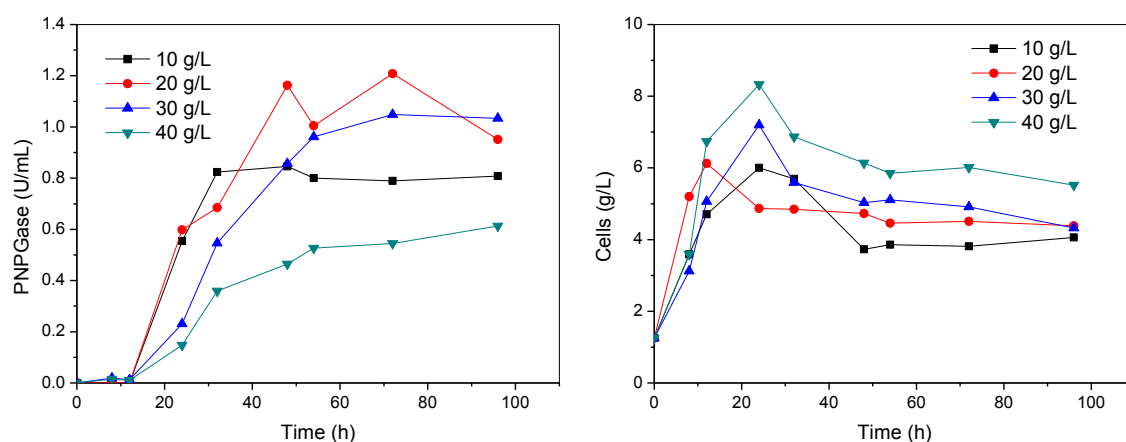
Figure 3.1 – PNPGase activity and cell concentration during batch cultivation using different initial concentrations of sucrose

The chemostat cultivation of *T. harzianum* was initiated by first performing batch cultivation using 20 g/L of sucrose as the sole carbon source. After the batch phase was finished, the culture was switched to chemostat mode, using 10 g/L of sucrose in the feeding medium (S1) (Figure 3.2). During the first six days of chemostat cultivation, corresponding to approximately seven volume changes, the dry cell weight concentration decreased from close to 10 g/L to a steady-state concentration of 4.5 ±0.2 g/L. Thereafter, there was a decrease in the measured PNPGase activity in the supernatant until achieving a steady-state value of around 0.1 U/mL, which corresponded to the specific productivity of about 1 U/(g (cells) h). This value was significantly lower than the specific productivity calculated from the batch culture data (Figure 3.1), which was approximately 6.7 U/(g (cells) h) during the carbon excess phase with an initial sucrose concentration of 20 g/L. This shows that the sucrose-limited condition was not beneficial for PNPGase production.

After maintaining the steady-state on sucrose for another ten volume changes, the chemostat feed medium was replaced by a medium containing an equimolar mixture of fructose and glucose (FG1), whereby the amounts of glucose and fructose were the same as for the condition only using sucrose, but in this case, the sugars were available as the monomers of the disaccharide. As can be observed in Figure 3.2, the cell concentration remained the same, as was expected; however, the enzymatic activity roughly increased by a factor of two. After 15 days (18 volume changes) the feed was switched to 10 g/L of glucose as the sole carbon source (G101). Again, the cell concentration remained the same but a sharp increase in PNPGase activity was observed. The activity achieved an increase of around 17 and 5 times when compared to the sucrose and fructose/glucose conditions, respectively.

This first continuous culture in sequence indicated that under carbon-limited conditions, the presence of sucrose and fructose might have inhibited PNPGase synthesis; however, glucose fed as monomer could stimulate the production.
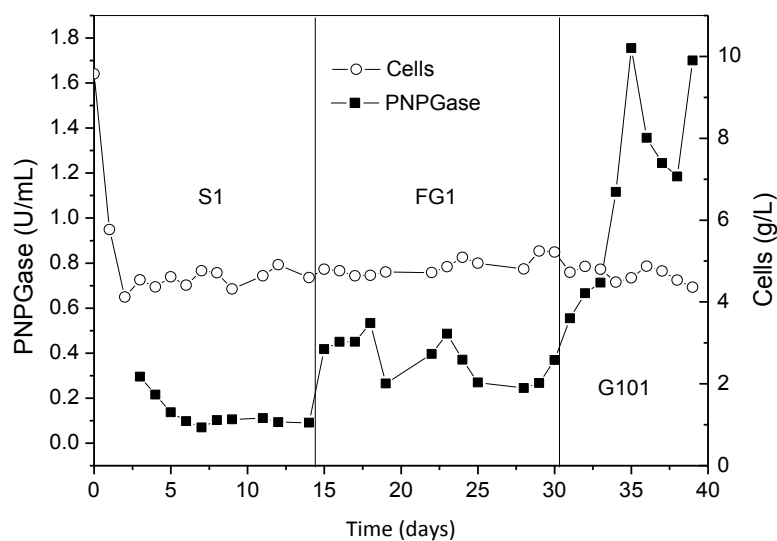
Figure 3.2 – Continuous PNPGase production using sucrose (S1), fructose/glucose (FG1) and glucose (G101) in sequence

Although glucose as the sole carbon source provided the highest activity, this was achieved after 36 volume changes in the carbon-limited chemostat cultivation. Therefore, a second chemostat experiment was carried out starting with glucose at 10 g/L (G102) to verify the reproducibility of the measured enzyme activity during the glucose-limited condition. After the steady-state was obtained, the glucose concentration in the feed medium was increased to 20 g/L (G201) to verify whether an increase in cell concentration at steady-state would result in a proportional increase in PNPGase production.

Figure 3.3 shows the result of this sequential chemostat experiment. The batch phase was performed with an initial glucose concentration of 10 g/L. The PNPGase activity after the batch phase was comparable to what was observed in the previous experiment (Figure 3.2). After the start of the chemostat phase with 10 g/L of glucose in the feed, the activity of the enzymes remained at a low level and increased after the 5th day (Figure 3.3), to reach a more or less stable value of 1 U/mL. On the 14th day, after 17 volume changes, the feed was switched to 20 g/L of glucose. After another 4 volume changes, the enzymatic activity sharply increased to 6 U/mL, 6 times higher than the condition using 10 g/L of glucose, while a doubling was expected if the specific productivity (U/(g (cells) h)) would have remained the same. These data indicate that an increase in cell concentration leads to a significant increase in specific PNPGase productivity. Another explanation could be that long term cultivation under carbon-limited conditions leads to adaptation of the fungus to produce increased amounts of enzymes.
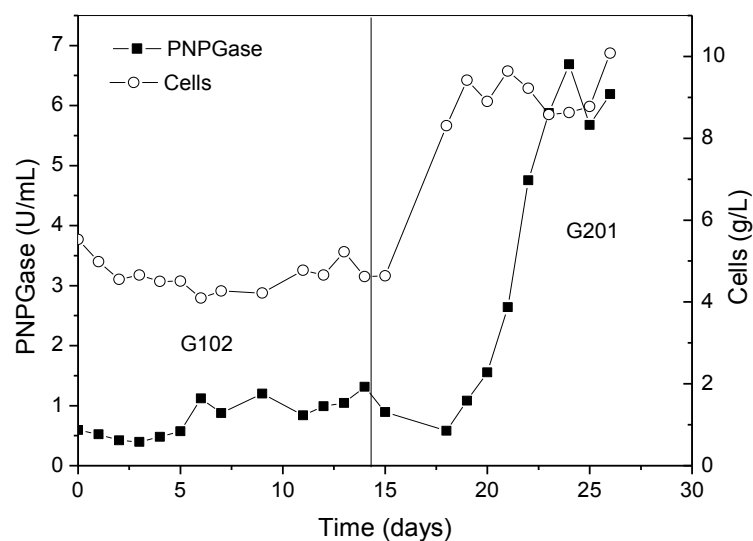
Figure 3.3 – Continuous PNPGase production using glucose at 10 (G102) and 20 g/L (G201) in sequence

A third glucose-limited chemostat experiment was carried out with a glucose concentration of 20 g/L in the feed medium (G202). Initially, the measured PNPGase activity in the supernatant was low but sharply increased to a value of 7 U/mL, after 7 days of chemostat cultivation (Figure 3.4), thus reaching a similar value as in the first 20 g/L of glucose chemostat (G201).
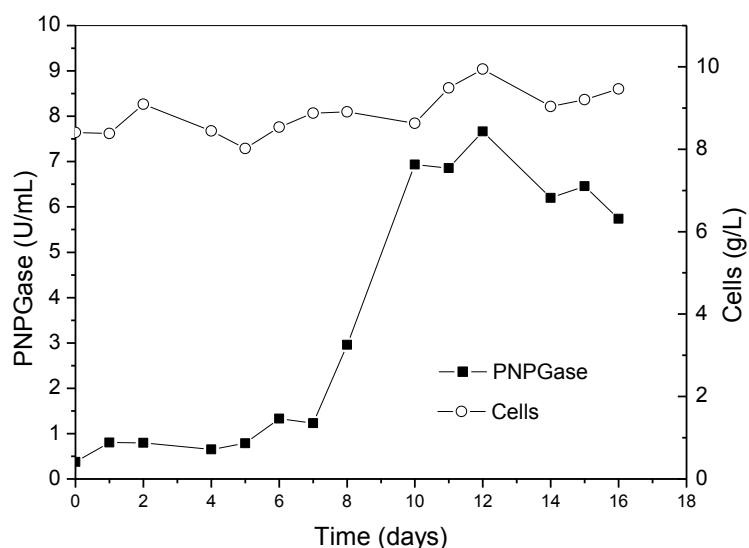
Figure 3.4 – Continuous PNPGase production using glucose at 20 g/L (G202)

Table 3.1 summarizes the results for the duplicate of sucrose (S2) and fructose/glucose (FG2) conditions. It also shows the conditions using carboxymethyl cellulose without and with an equimolar amount of glucose (CMC and CMCG). The glucose polysaccharide carboxymethyl cellulose (CMC) was used as the sole carbon source (10 g/L) and in combination with glucose (5

g/L CMC + 5 g/L glucose) to verify whether CMC would induce cellulase production. However, from the filter paper activity test, it was observed that cellulase activity was not present under those conditions. The combination of CMC with glucose (CMCG) resulted in a steady-state of cell concentration of around 2 g/L, indicating that CMC was not fully consumed. CMC alone provided the lowest cell concentration and consequently a low enzymatic activity. Even though *T. harzianum* is able to consume complex substrates such as sugarcane bagasse pretreated in batch mode (Gelain et al., 2015), it was not able to consume a soluble glucose polymer in chemostat culture confirming that cellulase activity was not induced by CMC. The chemostat cultivation on CMC as the sole carbon source was the only experiment where the cell concentration was not very stable after 6 residence times, probably due to the low concentration.

Duplicates of the sucrose and fructose/glucose chemostat cultivations showed similar cell concentrations compared to the previous experiments (Figure 3.2). The PNPGase activity for the duplicate of the sucrose cultivation (S2) was again very low. In the fructose/glucose duplicate chemostat (FG2), the activity was higher than for FG1, and this could have been caused by the fact that the experiment FG2 was preceded by a glucose-limited chemostat in the same bioreactor (feed concentration of 20 g/L). Therefore, cells from the previous experiment had accumulated on the walls of the bioreactor, and when part of these cells fell back into the liquid phase, this could have influenced PNPGase production. FG2 was the only experiment for which the cells on the walls of the bioreactor could have influenced the enzymatic activity since other conditions were very stable. Nevertheless, this could indicate that components from the cell wall when experiments are performed with glucose could act as inducers of PNPGase and this should be better exploited in future works.

Table 3.1 – Results for the conditions using sucrose (S2), fructose/glucose (FG2), carboxymethyl cellulose (CMC) and carboxymethyl cellulose/glucose (CMCG) at steady-state

Condition	PNPGase (U/mL)			Cells (g/L)		
S2	0.0544	±	0.0072	4.40	±	0.24
FG2	0.927	±	0.178	4.90	±	0.284
CMCG	0.526	±	0.0511	2.16	±	0.322
CMC	0.0766	±	0.00313	0.82	±	0.277

3.3.2   General behaviour of *T. harzianum* during carbon-limited chemostat cultivations

All chemostat experiments were started after an initial batch phase and were switched to chemostat mode when the carbon source was depleted. For the condition G202, for example, the batch phase started with 10 g/L of glucose and, after 23 h, it was switched to continuous culture using 20 g/L of glucose in the feed. Before reaching the steady-state, a transition phase was observed (phase preceding the steady-state of CO_2 and cells). This behaviour was observed in all experiments after the batch phase. Different colours of the cells were observed for the different stages: batch, transition phase and steady-state of cells and CO_2. Figure 3.5 shows that the colour changed from brown-yellow to white-yellow. Although viscosity was not measured, the observed viscosity of the medium also changed, it was higher during the steady-state (C) than during the batch (A) and transition phase (B). However, the supernatant was not viscous, only with the presence of the cells the medium appeared to be more viscous.

The main problem observed when working with this strain was the foam formation during the batch and transition phase. During steady-state with respect to cell concentration and CO_2 concentration in the off-gas, foam formation was much less and was easily controlled by periodic addition of a small amount of antifoam (approximately 7 μL/min).
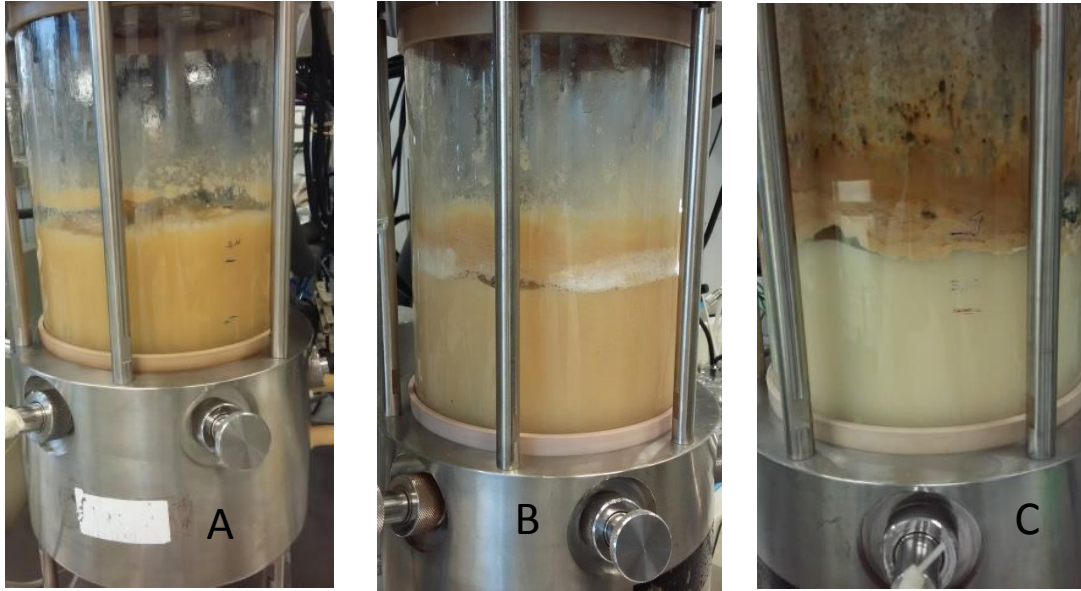
Figure 3.5 – Different colours between the batch (A), transition phase (B), and steady-state of cells and CO_2 (C) for the experiment G202

3.3.3 Quantitative physiology of *T. harzianum*

During batch cultivation, the maximum specific growth rate of the cells can be estimated from the carbon dioxide measurement in the off-gas. Figure 3.6 shows the carbon dioxide production during the exponential growth stage using glucose as the carbon source for three experiments named A, B and C. Equation 3.4 describes the average parameters of the exponential fit presented in Figure 3.6. The maximum specific cell growth rate based on the exponential fit is 0.20 ±0.007 h^{-1}.

$$x^{out}_{CO_2} = 0.0008(e^{0.20t})$$
(3.4)
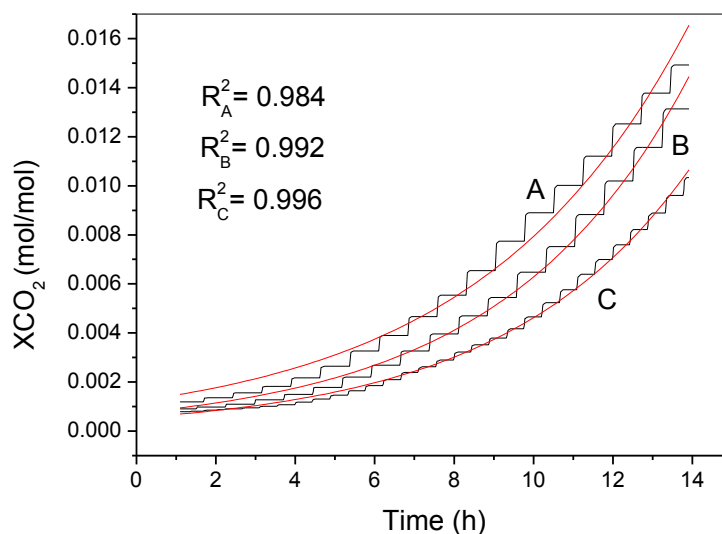
Figure 3.6 – Carbon dioxide production at the exponential growth phase (black) and exponential fit (red) using glucose as the carbon source for three experiments named A, B and C at the same conditions

Using the material balance equations with the data from each steady-state chemostat, the specific rates can be calculated from the measured gas and liquid in- and outflows and the concentrations of compounds in the gas and liquid phases. The thus obtained specific rates provide quantitative information and can be used to compare conditions aiming at the increase in the productivity and product yield, verify the presence of by-products and also to detect possible problems during the chemostat cultivation. If the specific rates are similar among different conditions, this indicates that there is low or no influence of the cultivation conditions on the culture behaviour. Table 3.2 shows the calculated average for specific rates during steady-state for all the conditions applied, except for the chemostat cultivations on CMCG and CMC as carbon sources. The table shows the specific cell growth rate (μ_X), specific carbon consumption rate (q_C), specific PNPGase production rate (q_B), specific oxygen consumption rate (q_{O_2}), specific carbon dioxide production rate (q_{CO_2}), specific nitrogen consumption rate (q_N), specific by-product formation rate (q_{byp}) and the carbon recovery (C_r).

Considering all the conditions, the analysis provided similar values for the specific growth rate (0.05 h^{-1} ±5.7 %), specific carbon consumption rate (0.105 Cmol/mol h ±8.6 %), specific oxygen consumption rate (0.0421 mol/mol h ±13 %), specific carbon dioxide production rate (0.0470 mol/mol h ±12 %), specific nitrogen consumption rate (0.0094 mol/mol h ±1.6 %) and carbon recovery (106 % ±5.6 %). However, the conditions provided large differences for the specific PNPGase production rate (407 U/mol h ±97 %) and specific by-product production rate (0.0151 Cmol/mol h ±36 %). This clearly indicates that the carbon sources used influenced the specific production of PNPGase and by-products. The rates of by-product formation fluctuated from 0.0084 to 0.0229 Cmol/mol h, and these by-products are probably related to the presence of extracellular polysaccharides (Chapter 4 and 5).

Table 3.2 – Specific conversion rates during carbon-limited chemostat cultivations on different carbon sources: 10 g/L glucose (G101 and G102); 20 g/L glucose (G201 and G202); fructose/glucose (FG1 and FG2); and sucrose (S1 and S2). All rates are expressed per mol of cell per hour, whereby one mol of cell is defined as the amount containing one mol of carbon

	G101	G102	G201	G202
Feed (g/L)	10	10	20	20
$\mu_X = D$ (h^{-1})	0.0475	0.0550	0.0538	0.05
q_C (Cmol/mol h)	0.0971	0.111	0.120	0.103
q_B (U/mol h)	414.7	347.9	1064.4	1032.4
q_{O_2} (mol/mol h)	0.039	0.041	0.048	0.038
q_{CO_2} (mol/mol h)	0.043	0.048	0.054	0.043
q_N (mol/mol h)	0.0092	0.0094	0.00955	0.0096
q_{byp} (Cmol/mol h)	0.0105	0.0225	0.0167	0.0084
C_r (%)	103.94	113.08	103.25	98.78
	FG1	FG2	S1	S2
Feed (g/L)	5.26/5.26	5.26/5.26	10	10
$\mu_X = D$ (h^{-1})	0.0475	0.0475	0.0475	0.05
q_C (Cmol/mol h)	0.0936	0.0975	0.104	0.117
q_B (U/mol h)	80.3	267.07	30.5	18.4
q_{O_2} (mol/mol h)	0.036	0.042	0.039	0.054
q_{CO_2} (mol/mol h)	0.040	0.047	0.043	0.058
q_{byp} (Cmol/mol h)	0.00921	0.0176	0.0128	0.0229
C_r (%)	102.92	115.21	99.51	111.99

The presence of cells on the walls of the bioreactor and the production of extracellular polysaccharides (Chapter 4 and 5) could have influenced the carbon balance. The polysaccharides could have been acting as a second carbon source and the cells on the wall could be still producing CO_2. In this project it was tried to use cold water to prevent cell growth on the walls of the bioreactor; however, this method did not work for this process.

Table 3.3 presents the cell yield on substrate ($Y_{X/S}$), CO_2 (Y_{X/CO_2}), O_2 (Y_{X/O_2}), by-product yield on substrate ($Y_{byp/S}$) and respiratory coefficient (RQ) for the experiments using glucose, fructose/glucose and sucrose as carbon sources. Based on the average values, for glucose and fructose/glucose conditions, the cell yield on substrate, O_2 and CO_2 were similar. For the sucrose condition, the cell yield on substrate, O_2 and CO_2 were lower; however, considering their standard errors these differences are not significant. The molar mass considered for the cells was 29.7 g/mol.

Table 3.3 – Yields of cell on substrate ($Y_{X/S}$), CO_2 (Y_{X/CO_2}) and O_2 (Y_{X/O_2}), by-product yield on substrate ($Y_{byp/S}$) and respiratory coefficient (RQ) for the experiments under carbon-limited chemostat cultivations on different carbon sources: 10 g/L glucose (G101 and G102); 20 g/L glucose (G201 and G202); fructose/glucose (FG1 and FG2); and sucrose (S1 and S2), considering a molar mass of cell of 29.7 g/mol

	G101	G102	G201	G202	Average	
$Y_{X/S}$ (mol/Cmol)	0.49	0.50	0.45	0.49	0.48 ±0.01	
Y_{X/CO_2} (mol/mol)	1.10	1.15	1.00	1.16	1.10 ±0.04	
Y_{X/O_2} (mol/mol)	1.22	1.34	1.12	1.32	1.25 ±0.05	
$Y_{byp/S}$ (Cmol/Cmol)	0.11	0.20	0.14	0.08	0.13 ±0.03	
RQ (mol/mol)	1.10	1.17	1.13	1.13	1.13 ±0.01	
	FG1	FG2	Average	S1	S2	Average
$Y_{X/S}$ (mol/Cmol)	0.51	0.49	0.50 ± 0.01	0.46	0.43	0.44 ±0.01
Y_{X/CO_2} (mol/mol)	1.19	1.01	1.10 ±0.09	1.10	0.86	0.98 ±0.12
Y_{X/O_2} (mol/mol)	1.32	1.13	1.23 ±0.09	1.22	0.93	1.07 ±0.15
$Y_{byp/S}$ (Cmol/Cmol)	0.10	0.18	0.14 ±0.04	0.12	0.20	0.16 ±0.04
RQ (mol/mol)	1.11	1.12	1.12 ±0.004	1.10	1.07	1.09 ±0.01

Figure 3.7 highlights the average of specific PNPGase production rates (U/(mol (cells) h)) for all the conditions in ascending order of PNPGase productivity, starting with sucrose, followed by CMC, fructose/glucose, glucose at 10 g/L, CMCG, and the highest, 20 g/L of glucose. Doubling the cell concentration resulted in an increase of 6 fold in PNPGase activity for the experiments using glucose, and this result can be further exploited by working with higher cell concentrations than applied in this project.
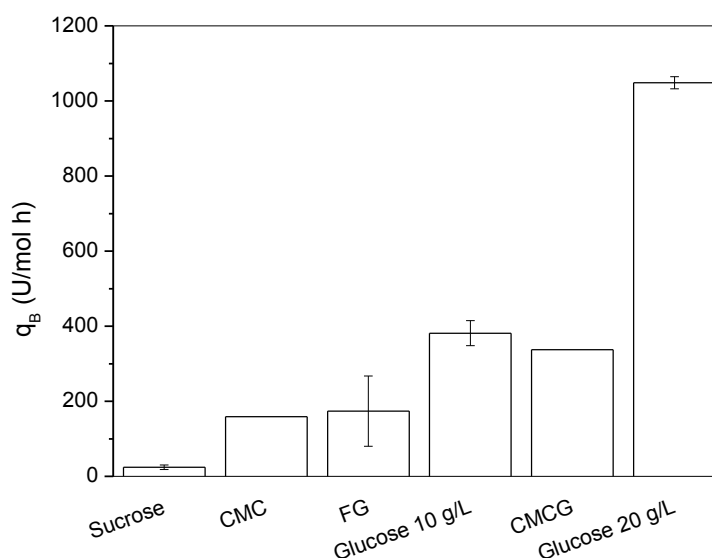
Figure 3.7 – Average of the specific PNPGase production rates, CMC – carboxymethyl cellulose, FG – fructose/glucose, CMCG – carboxymethyl cellulose/glucose

3.3.4   Sugar analysis

Samples were taken for quantification of the residual concentrations of fructose, glucose and sucrose during the last days of the continuous cultures. All the conditions presented low concentrations of the sugars analysed. Due to low concentrations, oscillations for the same conditions were observed. Fructose concentration was lower than 25 mg/L. The highest concentration of glucose remaining in the bioreactor was for the condition using CMC (16-19 mg/L). For the other conditions, the concentration was lower than 7 mg/L. The highest sucrose concentrations were observed for the sucrose experiments. In the first culture with sucrose (S1) the residual concentration was 17 mg/L and in the second sucrose condition (S2) the concentration of this sugar dropped from 465 to 77 mg/L. From the residual sugar analysis, it seems that the low sugar concentrations in the glucose cultures could have prevented carbon catabolite repression, which indicates that another mechanism could be controlling extracellular enzyme synthesis.

Carbon-limited continuous cultures were achieved due to the low concentration of sugars and the excess of nitrogen and phosphorus present in the effluent (data not presented) for the experiments using glucose, sucrose and fructose/glucose.

3.4   Conclusions

Continuous production of PNPGase was investigated in carbon-limited chemostat cultures. Glucose was the carbon source on which the highest productivity was obtained. Sucrose and fructose seem to inhibit PNPGase synthesis. Extracellular polysaccharides could be involved in the production of the enzymes evaluated in this chapter and this is discussed in Chapter 4. PNPGase production under glucose-limited conditions has the potential to be improved through optimization of the operating conditions as well as through genetic engineering. The PNPGase produced in this project needs to be evaluated regarding the hydrolysis of cellobiose and other disaccharides, and then could be used as a supplement for enzymatic cocktails to generate simple sugars from lignocellulosic materials.

Chapter 4

Analysis of the production of enzymes under carbon-limited conditions – secretome and metabolome

In this chapter, the extracellular enzymes produced under carbon-limited conditions were analysed through shotgun proteomics and SDS-page analysis. Intracellular metabolite levels were quantified for cells grown in glucose-limited chemostat cultures. A mechanism was proposed for continuous PNPGase production under glucose-limited conditions.
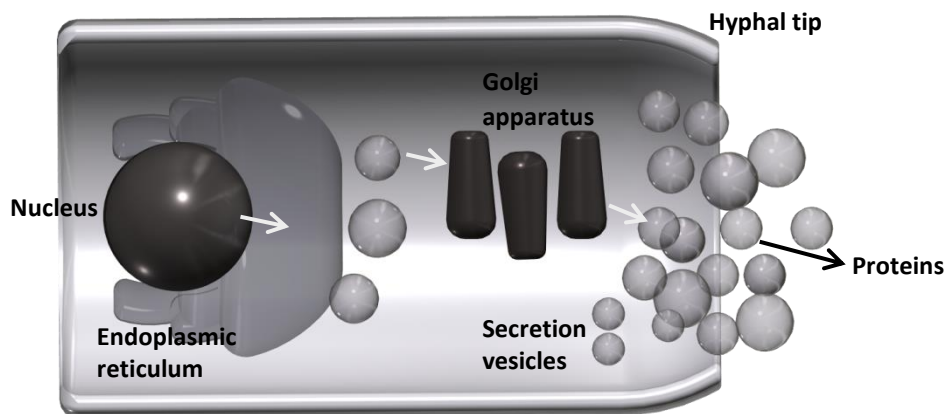
Abstract

The wild type strain of *Trichoderma harzianum* was able to synthesize PNPGase in carbon-limited chemostat cultures. Shotgun proteomics and SDS-PAGE analysis of the proteins present in the supernatant of three different chemostat cultures performed under carbon-limited conditions were analysed to evaluate the possible enzymatic cocktail secreted. The shotgun proteomics analysis suggests the presence of beta-glucosidase and the intensities of the analysis correlate with the enzymatic activity (PNPGase). PNPGase production was also analysed for two continuous cultures using 20 g/L of glucose in the feed under carbon-limited conditions. The first continuous culture was analysed during the PNPGase production phase and its steady-state, and due to the interesting result, the condition was repeated to analyse the beginning of the process: the batch phase; transition phase (phase preceding the steady-state of cells and CO_2); and the start of the PNPGase production phase. The presence of extracellular polysaccharides was confirmed by FT-IR and NMR analysis. In addition, sugar analysis showed the presence of sugar with the same retention time as gentiobiose in the supernatant of the glucose-limited chemostat, which could be a fragment of polymers released from the cell wall. Gentiobiose could be acting as an inducer of enzymes. Based on this information, a mechanism was proposed for continuous PNPGase production under glucose-limited conditions assuming that PNPGase includes beta-glucosidase. Intracellular metabolites were quantified during PNPGase production for the condition using 20 g/L of glucose in the feed and differences were observed, indicating that intracellular glucose could be inhibiting PNPGase production.

4.1   Introduction

Proteins are a diverse group of molecules containing different properties such as catalytic activity, molecular weight and solubility (McDonald and Yates, 2002). Proteins are also a biotechnological product and their identification and characterization are important for understanding their functionalities and possible applications. In proteomics, a method called shotgun analysis can be used to identify proteins (Nesvizhskii and Aebersold, 2005). Proteolytic enzymes, such as trypsin, are used to digest the proteins, and due to the specificity of this enzyme, it generates peptides of a size that is more readily analysed in the mass spectrometer and facilitates the identification of the protein (McDonald and Yates, 2002). Liquid chromatography can be used to separate the peptides, and then peptide sequencing can be performed by tandem mass spectrometry (MS/MS) (McDonald and Yates, 2002). In this method, peptides are ionized and selected peptides ions are subjected to sequencing, which is determined by MS/MS spectra using a database search approach (Nesvizhskii and Aebersold, 2005) (Figure 4.1).
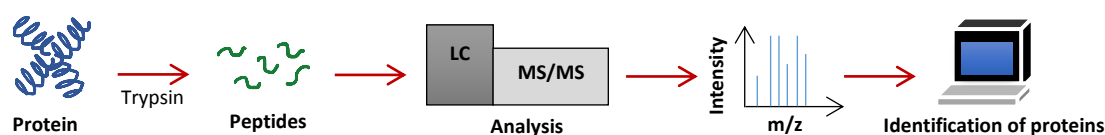
Figure 4.1 – Shotgun proteomics analysis

It has been reported that beta-glucosidase can be produced by filamentous fungi using glucose as the sole carbon source (Jäger et al., 2001; Ximenes et al., 1996). However, glucose can be imported from the extracellular medium through facilitated diffusion (Lehninger et al., 2005) or via specific glucose transporters by active transport. Glucose monomers, therefore, do not require the presence of extracellular enzymes to be taken up by the cells. Thus, the presence of beta-glucosidase during growth on glucose as the sole carbon source must be due to a constitutive production or stimulation by inducers.

Rau (1999) investigated the production of an extracellular polysaccharide, schizophyllan, by *Schizophyllum commune* using glucose as the carbon source, and observed that prolonged cultivation under carbon-limited conditions leads to the release of beta-glucanase, followed by a sharp drop in the viscosity of the supernatant. The reason for this behaviour was that small fragments of the extracellular polysaccharide served as a carbon source for the fungus. Thus, in a process using glucose as the growth limiting carbon source, the presence of extracellular polysaccharides could act as a source of inducers for the production of beta-glucanase.

Gentiobiose, a disaccharide that can be produced by transglycosylation by beta-glucosidase (Seiboth et al., 2011) can also act as an inducer for the synthesis of this group of enzymes (Eberhart and Beck, 1973). This disaccharide could also be released as a fragment from extracellular polysaccharides, such as beta-glucans, as a result of shear stress in bioreactors and stimulate beta-glucosidase synthesis. Hence, in the presence of glucose, beta-glucosidase could be produced as a result of the presence of these fragments.

Carbon catabolite repression (CCR) is one of the mechanisms that prevent the unnecessary synthesis of cellulase and beta-glucosidase. Thus, the presence of an easily assimilated substrate activates the repression of the production of enzymes responsible for

the degradation of complex substrates (Suto and Tomita, 2001). During growth under glucose-limited conditions, it is expected that CCR does not occur due to low substrate concentration. Xiong et al. (2014) reported that a transcription factor (*vib-1*) could repress CCR under carbon-limited conditions in *Neurospora crassa.* Apart from CCR, other mechanisms can be responsible for controlling the production of those enzymes. Catabolite inhibition is also a mechanism reported to control cellulase production and acts through preventing enzyme synthesis by inhibiting the transport of the inducer (Strobel and Russell, 1987). The latter mechanism could be more active under carbon-limited conditions.

It was found that *T. harzianum* is able to synthesize extracellular enzymes that can catalyse the hydrolysis of p-nitrophenyl-β-D-glucopyranoside (PNPGase) during steady-state under carbon-limited chemostat cultivations (Chapter 3), especially when using glucose as the carbon source. When sucrose or equimolar mixtures of fructose and glucose were used, low levels of PNPGase activity were observed. To investigate whether under these conditions other enzymes were produced, a shotgun proteomics analysis of their supernatants was performed and it is presented in this chapter.

In addition, analysis of PNPGase production was evaluated according to the results from two continuous cultures using 20 g/L of glucose in the feed under carbon-limited conditions. The first culture was analysed during the PNPGase production phase and its steady-state, and due to the interesting result, a second experiment was performed to analyse the production during the batch phase, the transition phase (phase preceding the steady-state of cells and CO_2) and the start of the PNPGase production phase. Extracellular polysaccharides were present in the supernatant of the samples as well as gentiobiose, a possible fragment of the polysaccharides and an inducer of beta-glucosidase. Based on this, a mechanism is proposed for continuous PNPGase production under glucose-limited conditions thereby assuming that PNPGase activity is a measure for the presence of beta-glucosidase, to be verified by the shotgun proteomics analysis. Finally, intracellular metabolites were analysed to verify the possible influence of their concentrations on PNPGase production.

4.2   Materials and Methods

4.2.1   Microorganism

The wild type strain *Trichoderma harzianum* P49P11 was used in this study. The strain was isolated from the Amazon forest (Delabona et al., 2013). It was grown on potato dextrose agar at 29 $^{\circ}$C and then harvested after 5-7 days with sterilized water. The spore solutions were kept in stock at -80 $^{\circ}$C.

4.2.2   Samples for the analysis

For shotgun proteomics and SDS-PAGE analysis, samples from the steady-state of the experiments using glucose (G101), fructose/glucose (FG1) and sucrose (S1) were used (Chapter 3). For the analysis of the PNPGase production phase, samples from the experiment with 20 g/L of glucose (G201) were used (Chapter 3), which were named points D and E (Table 4.2). These samples were at steady-state of cells and CO_2. For the analysis of PNPGase production during the batch phase, transition phase (phase preceding the steady-state of cells and CO_2) and the start of PNPGase production phase, a new experiment was performed and corresponds to the points A, B and C, respectively (Table 4.2). The samples for point C were

taken at steady-state of cell and CO_2. The operating conditions for this new experiment were the same as presented in Chapter 3 for the condition G201.

4.2.3 Enzymatic activity

The enzymatic activity was performed according to Gelain et al. (2015). Cellulase activity was determined using the filter paper activity (FPA) assay (Ghose, 1987). The method was downscaled with a factor 10 to minimize time and reagents. The filter paper activity was assayed by incubating the diluted enzymes (50 μL) with 100 μL of 50 mM sodium citrate buffer (pH 4.8) containing the filter paper Whatman No. 1 (5 mg). The reaction mixture was incubated at 50 °C for 60 min and stopped by adding 300 μL of the DNS reagent. Reducing sugars were measured by the DNS method (Miller, 1959). The solution was placed in a water bath at 95 °C for 5 min and, after cooling, 2 mL of water was added and the measurement was performed at 540 nm in a spectrophotometer.

The activity of PNPGase was measured according to Zhang et al. (2009) using p-nitrophenyl-β-D-glucopyranoside (PNPG) as the substrate. The reaction mixture was composed of 80 μL of 1 mM substrate diluted in 50 mM citrate buffer (pH 4.8), and 20 μL of the diluted enzyme extract. After 10 min at 50 °C, the reaction was stopped by adding 100 μL of 1 M sodium carbonate. The measurement was performed at 400 nm.

4.2.4 Sugar and dry cell weight analysis

For sugar analysis, the samples were diluted with 1 M NaOH to precipitate the proteins that could interfere with the analysis. Subsequently, the precipitate was removed by centrifugation (2000x g, 10 min). The samples were analysed using high-performance anion exchange (HPAE) Dionex ICS-5000 with PAD detector (Rohrer et al., 2013).

For the quantification of dry cell weight, 5 mL of sample was withdrawn from the bioreactor. The weight of the samples was measured and then they were poured on a 0.45 μm filter of known mass (Pall membrane filter, Supor). Subsequently, the cells were filtered and washed with Milli-Q water. The filter was placed in an oven at 70 °C for one day and cooled down in a desiccator before the measurement of the weight.

4.2.5 Qualitative analysis of polysaccharides

From supernatant samples filtered through 0.45 μm pore size membrane filters (Millex-HV durapore PVDF membrane), qualitative analysis of polysaccharides was performed using ethanol precipitation whereby 1 mL of sample was mixed with 3 mL of pure ethanol. Then, after centrifuging at 2000x g for 5 min, the precipitate was solubilized with water (1 mL) and precipitated again with ethanol (3 mL), followed by a second centrifugation step, whereafter the precipitate was freeze dried. Fourier-transform infrared spectroscopy (FT-IR) was performed placing 2-5 mg of precipitate on a universal attenuated total reflectance accessory (Perkin Elmer spectrum 100).

Reagent for proton NMR analysis was prepared by using 0.2 g of LiCl in 1.0 mL D_2O, followed by 9 mL of DMSO and a few grains of deuterated (3-(trimethylsilyl)-2,2,3,3-tetradeutero propionic acid or TMSP-d4) were added. Subsequently, 0.5 ml of this solution was transferred to the vials containing the samples (5-15 mg). Then, they were heated in a thermo-shaker at 100 °C for 12 hours. The cooled solutions were then transferred to an NMR tube and

all measurements were carried out at 25 $^{\circ}$C using an Agilent 400-MR DD2 (5 mm OneNMR probe). The data for proton NMR spectra were collected with 1024 scans, d1 = 1s (399.7 MHz).

4.2.6   Quantification of intracellular metabolites

For samples named C and E (Table 4.2), intracellular metabolites from the tricarboxylic acid cycle, glycolysis and nucleotides were quantified. The estimation of the metabolites for samples C and E was performed in duplicate using different samples withdrawn at the same time (10 seconds difference). Intracellular metabolites were extracted and analysed according to Lameiras et al. (2015). Broth (approx. 1.3 mL) was rapidly withdrawn into 10 mL of pre-cooled 40 % (v/v) aqueous methanol solution (-20 $^{\circ}$C) and after, the samples were weighted for the estimation of cell mass and kept at -20 $^{\circ}$C until extraction of the metabolites. Methanol was removed by filtration and the samples were washed thrice with cold methanol solution (-20 $^{\circ}$C). Then, boiling ethanol extraction was performed to disrupt the cell and inactivate the enzymes. 25 mL of ethanol solution (75 % v/v) was first pre-heated at 75 $^{\circ}$C, and after the filtration and washing of the samples, they were placed into the ethanol solution along with 100 µL of U-^{13}C-labeled cell extract of *S. cerevisiae* as the internal standard and moved to a water bath at 95 $^{\circ}$C for 3 min. After the extraction, the samples were first placed on ice and then stored at -80 $^{\circ}$C.

Before the quantification of the metabolites, ethanol was evaporated until almost dryness in a Rapid-Vap under vacuum for 240 min. After evaporation, the residues were suspended in 500 µL of Milli-Q water, and centrifuged at 1000x g for 5 min in a tube coupled with a filter (0.22 µm) to remove cell debris. The supernatants were stored at -80 $^{\circ}$C until analysis. The concentrations of the intracellular metabolites were measured by isotope dilution mass spectrometry (LCIDMS/ MS and GC-IDMS) according to the protocols of Dam et al. (2002), Jonge et al. (2011) and Cipollina et al. (2009).

4.2.7   SDS-PAGE

The samples were concentrated using Amicon 10 kDa cut-off Eppendorf tube concentrators. Then, they were mixed with NuPAGE LDS sample buffer (4x) (Thermo Fischer Scientific, NP0007) at a ratio of 1 to 4 and heated at 70 $^{\circ}$C for 15 min. For the SDS page analysis, a mini-protean polyacrylamide gel was prepared (10 % resolving gel) (BIO-RAD, 1610182), 1 µg protein was loaded from each sample. SDS-PAGE was run using a MES buffer (Thermo Fischer Scientific, NP0002) at constant voltage (200 V) for 25 minutes. Following a short fixation, the gel was stained using Coomassie Brilliant Blue for 15 minutes and destained in 10 % acetic acid over-night. The gel image was taken using a XY camera and the image was processed using the Microsoft Office Picture Manager, 2010.

4.2.8   Shotgun proteomics and label-free quantification

Protein was precipitated from the supernatant using 4 volumes of ice-cold acetone at -20 $^{\circ}$C for 20 minutes, centrifuged at 14.000 rpm for 10 minutes, and the pellet was washed twice using ice-cold acetone. The protein pellet was reconstituted in 200 mM ammonium bicarbonate containing 6 M urea. The protein solution was further reduced using DTT and then alkylated using iodoacetamide according to the protocol by Herbert et al. (2014). The protein solution was diluted using 200 mM ammonium bicarbonate buffer to approximately 1 M urea and further digested using trypsin in a ratio of protein to trypsin of approximately 50 to 1, at 37 $^{\circ}$C over-night (Hebert et al., 2014).

The proteolytic digest was purified using an Oasis HLB solid-phase extraction plate (Waters) and approximately 250 ng of the proteolytic digest was then analysed by a one-dimensional reverse-phase gradient (Acclaim PepMap RSLC 50 μm x 15 cm, 2 μm, 100 A, Thermo) using an EASY-nLC 1200 coupled to a QE plus Orbitrap mass spectrometer operating in top 10 DDA mode. Further details regarding one-dimensional shotgun proteomics approaches are described in Köcher et al. (2012). Tandem-MS data were analysed using PEAKS Studio 8.5 against the TrEMBL *Trichoderma harzianum* protein database (un-reviewed, taxon 5544 http://www.uniprot.org/), and results were filtered for <1 % FDR for both, peptide and protein identification. 3 replicate injections for each condition were finally analysed using the label-free quantification option provided by PEAKS Studio 8.5 (Zhang et al., 2012).

4.3   Results and Discussion

4.3.1   Secretome analysis

SDS-PAGE analysis was performed in the supernatant of the samples from carbon-limited chemostat cultivations with glucose (G101), sucrose (S1), and fructose/glucose (FG1) as growth limiting substrates (Figure 4.2). For the glucose and fructose/glucose-limited chemostat cultures, more intense bands were observed than for the sucrose-limited culture, indicating higher protein concentrations. The molecular weights of the majority of the proteins were between 70.3 and 92 kDa for the glucose and fructose/glucose-limited cultures. For the sucrose-limited culture, the molecular weight of the majority of the proteins was between 54 and 70.3 kDa.
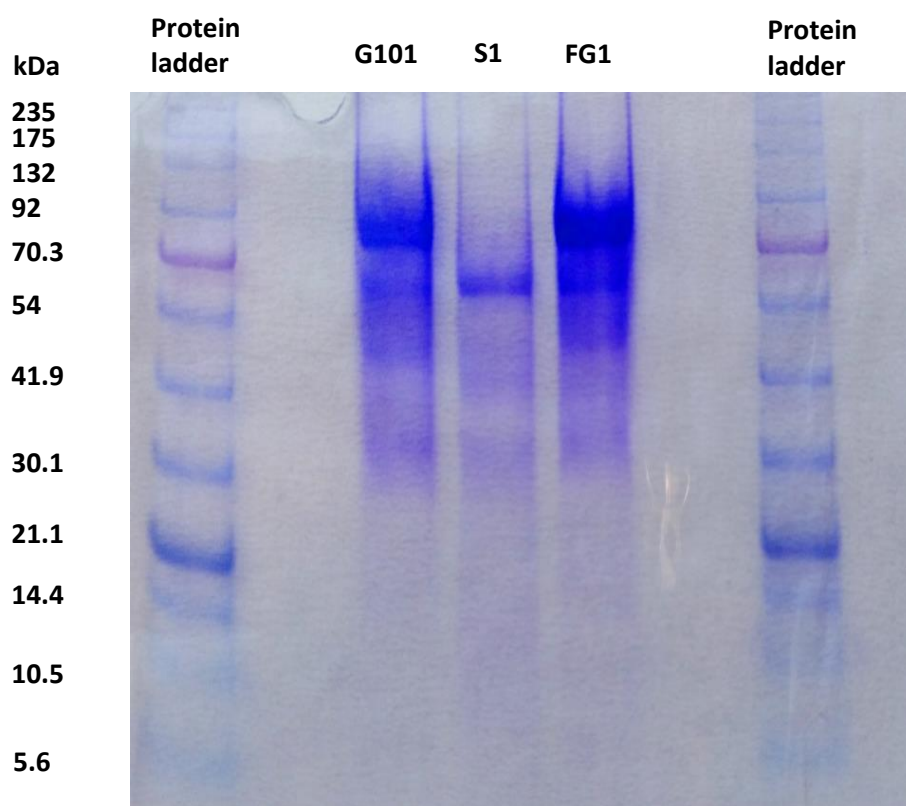
Figure 4.2 – SDS-PAGE for the conditions using glucose at 10 g/L (G101), sucrose (S1) and fructose/glucose (FG1)

Shotgun proteomics analysis was performed and indicates the presence of 207 proteins (92 enzymes and 115 other proteins of which 99 are uncharacterized). Figure 4.3 highlights spectrum intensity, indicating the relative abundance for specific groups of enzymes. For the glucose-limited condition, higher intensities were observed for most of the proteins, indicating higher protein levels. According to Owen et al. (2014), ionized peptides generate an ion spectrum; whereby the relative intensity of each spectrum peak is proportional to the peptide concentration. This allows a relative quantification across different experimental conditions. Table 4.1 shows the result of some enzymes related to Figure 4.3. Several enzymes were found including four 1,3-beta-glucanosyltransferase, two alpha-1,2-mannosidase, two alpha-galactosidase, two beta-glucosidase, two glucan 1,3-beta-glucosidase, two glucan endo-1,3-beta-glucosidase, thirteen glycosyl hydrolase and three mutanase.

The complete table is presented in the supplementary material (Table S4.1). It presents the coverage, the number of peptides and unique peptides identified, and intensities of the samples for each protein. Coverage is the fraction of the protein sequence covered by the identified peptides (number of identified peptides per protein) (Nesvizhskii and Aebersold, 2005). The number of peptides corresponds to the number of peptides identified for a specific protein group. Unique peptides are those that are not present in other proteins regarding the protein database (Fonslow et al., 2014). Beta-glucosidase is highlighted in Table 4.1, the first one had coverage of 37 %, 26 peptides, 24 unique peptides, 93 kDa and the second one, coverage of 8 %, 8 peptides, 7 unique peptides and 95 kDa. The intensities correlate with the measured PNPGase activities (approx. 1 (G101), 0.24 (FG1) and 0.1 (S1) U/mL, Chapter 3), the highest intensity was found for the glucose-limited condition, followed by fructose/glucose and sucrose.

Vale et al. (2012) reported a secretome analysis of *T. harzianum* using batch cultivation on cellulose performed in Erlenmeyer flasks with a liquid volume of 20 mL. They identified 56 proteins based on at least 2 unique peptides. In this project, the proteins with at least 1 unique peptide are presented in order to visualize the possible enzymatic cocktail secreted. Nevertheless, there are 114 proteins identified based on at least 2 peptides and 93 with only 1 unique peptide. According to Vale et al. (2012), nowadays, high MS accuracy, low ppm mass errors, and rich MS/MS data, provided by mass spectrometers, offer excellent identification even based on single peptides.

Figure 4.4 indicates through a heat map, the presence of proteins in the supernatant of the three samples analysed (G101, S1 and FG1). The B sample corresponds to the blank (no protein present, bright green colour). The samples came from continuous cultures with a dilution rate of 0.05 h^{-1} and the differences observed are mainly due to the carbon source used since no other variables were changed. The presence of beta-glucosidase is indicated by yellow frames. The heat map shows a higher concentration for the glucose-limited condition, followed by fructose/glucose and sucrose, which correlates with the measured PNPGase activities (Chapter 3). Clear differences in protein abundances were observed between the three experimental conditions. If they would have been similar, this would indicate the constitutive expression of these enzymes/proteins; however, the observed difference indicates that their production was possibly influenced by different inducers (possible fragments of extracellular polysaccharides, section 4.3.2 and 4.3.3).

1,3-beta-glucanosyltransferase

■ Glucose ■ Sucrose ■ Fructose/glucose

27%
4%
69%

Alpha-1,2-mannosidase

■ Glucose ■ Sucrose ■ Fructose/glucose

43%
54%
3%

Beta-glucosidase

■ Glucose ■ Sucrose ■ Fructose/glucose

24%
1%
75%

Alpha-galactosidase

■ Glucose ■ Sucrose ■ Fructose/glucose

25%
0%
75%

Glycosyl hydrolase

■ Glucose ■ Sucrose ■ Fructose/glucose

45%
53%
2%

Murein transglycosylase

■ Glucose ■ Sucrose ■ Fructose/glucose

19%
14%
67%

Tyrosinase

■ Glucose ■ Sucrose ■ Fructose/glucose

38%
23%
39%

Mutanase

■ Glucose ■ Sucrose ■ Fructose/glucose

24%
31%
45%

Figure 4.3 – Spectrum intensity (%), indicating the relative abundance for some groups of enzymes suggested by the shotgun proteomics analysis

Gómez-Mendoza et al. (2014) evaluated the *T. harzianum* secretome using glucose, carboxymethyl cellulose, xylan and an agricultural by-product (sugarcane bagasse) as carbon sources. The experiments were performed in shake flasks containing 1 % of the carbon source with a liquid volume of 30 mL. Glucose was used as the promoter of catabolite repression of enzymes and the condition resulted in the secretion of 107 groups of proteins of which 40

were exclusively identified in this carbon source. The secretion of cellobiohydrolase and beta-glucosidase were detected for this condition and their presence was attributed to the consequence of low constitutive enzyme expression. In this project, however, the relative abundance of proteins indicated by different colour intensities in Figure 4.4 suggests that glucose condition was capable of inducing the expression of proteins in different levels.

The difference between the conditions G101 and FG1 is the lack of fructose in the G101 sample. This change resulted in different protein expressions as indicated in Figure 4.4. It seems that the presence of fructose inhibited/induced the expression of different proteins, but the samples also share common ones. Sucrose-limited conditions resulted in the lowest protein levels in the culture supernatant. The use of monosaccharides (fructose and glucose – FG1) had a positive influence on the diversity of the expressed proteins/enzymes than the disaccharide used. The glucose-limited condition showed the highest diversity of expressed proteins. It seems that each condition provided a distinct enzymatic cocktail, which could be related to the different carbon sources used. However, more research is needed to identify the uncharacterized proteins suggested by shotgun proteomics analysis. According to the analysis, PNPGase could be including the activity of beta-glucosidase.

Table 4.1 – Description of some enzymes from shotgun proteomics analysis, beta-glucosidase is highlighted in grey frames

Accession	Coverage (%)	Peptides	Unique Peptides	Blank Intensity	G101 Intensity	S1 Intensity	FG1 Intensity	Avg. Mass	Description, GN – gene name, PE – protein existence, SV – sequence version
A0A0G0A6L8|A0A0G0A6L8_TRIHA	43	30	29	5.00E+06	5.51E+08	2.98E+07	6.51E+08	83322	Glycosyl hydrolase, GN=THAR02_00025, PE=4, SV=1
A0A0F9ZTK2|A0A0F9ZTK2_TRIHA	24	17	17	4.13E+05	4.52E+07	0	2.94E+07	104391	Glycosyl hydrolase family 3 N terminal domain-containing protein, GN=THAR02_04349, PE=4, SV=1
A0A0G0AG54|A0A0G0AG54_TRIHA	29	23	23	2.43E+06	3.96E+08	6.78E+06	2.00E+08	104855	Glycosyl hydrolase family 31, GN=THAR02_03951, PE=3, SV=1
A0A0G0A0B1|A0A0G0A0B1_TRIHA	13	9	9	0	7.50E+07	0	3.03E+07	92668	Glycosyl hydrolase family 3 N terminal domain-containing protein, GN=THAR02_02181, PE=4, SV=1
A0A0F9Y0X0|A0A0F9Y0X0_TRIHA	37	26	24	2.35E+06	8.65E+08	1.23E+07	2.77E+08	92791	Beta-glucosidase, GN=THAR02_02132, PE=3, SV=1
A0A0F9X7W2|A0A0F9X7W2_TRIHA	8	8	7	0	1.38E+07	0	5.74E+06	95013	Beta-glucosidase, GN=THAR02_07292, PE=4, SV=1
A0A0F9ZUH3|A0A0F9ZUH3_TRIHA	14	6	6	1.36E+05	5.93E+07	1.03E+07	4.71E+07	52933	1,3-beta-glucanosyltransferase, GN=THAR02_04021, PE=3, SV=1
A0A0F9ZGV2|A0A0F9ZGV2_TRIHA	11	5	5	6.70E+05	5.52E+07	9.15E+07	8.96E+07	60083	Tyrosinase, GN=THAR02_08385, PE=4, SV=1
A0A0F9ZZ00|A0A0F9ZZ00_TRIHA	13	5	5	1.74E+05	5.71E+07	2.73E+08	7.89E+07	46519	Mutanase, GN=THAR02_09460, PE=4, SV=1
A0A0F9ZTK0|A0A0F9ZTK0_TRIHA	12	5	5	4.37E+05	4.45E+07	1.86E+07	1.19E+07	63234	Murein transglycosylase, GN=THAR02_04344, PE=4, SV=1
A0A0F9XN15|A0A0F9XN15_TRIHA	16	7	7	3.21E+05	7.52E+07	0	2.40E+07	48188	Alpha-galactosidase, GN=THAR02_01852, PE=3, SV=1
A0A0F9WYR7|A0A0F9WYR7_TRIHA	13	4	4	6.56E+04	5.74E+07	0	1.69E+07	55601	Alpha-1,2-Mannosidase, GN=THAR02_10337, PE=3, SV=1
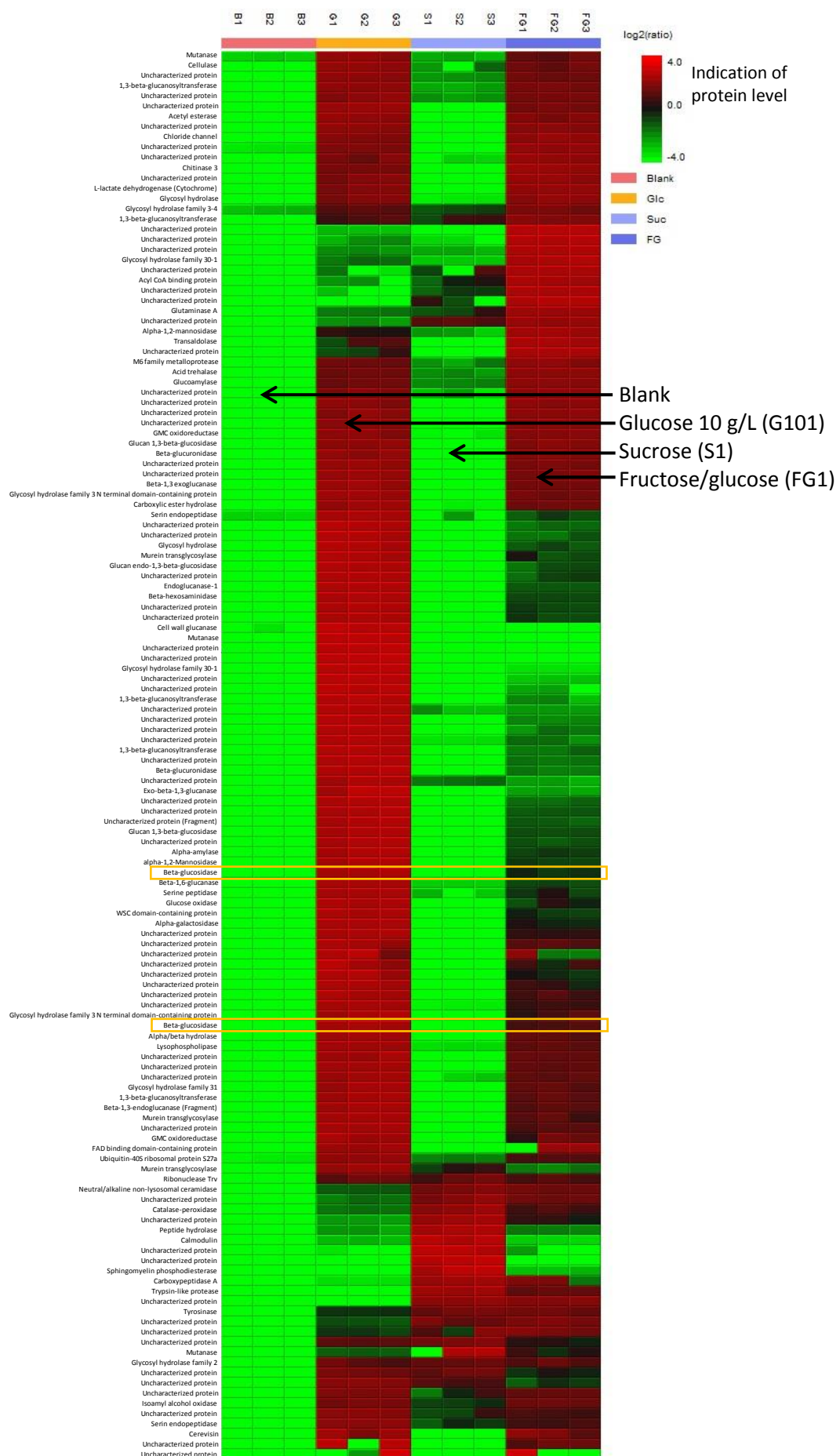
Figure 4.4 - Heat map from the shotgun proteomics analysis (triplicate), indicating the possible enzymes present in the supernatant of samples at steady-state

4.3.2 Analysis of PNPGase production under glucose-limited conditions

Carbon-limited chemostat cultivations on glucose as the carbon source provided the highest PNPGase production compared to similar chemostat cultivations using other sugars as growth limiting carbon source (Chapter 3). Although the cells do not require the presence of these enzymes when grown on glucose as the sole carbon source, their production could be related to the presence of extracellular polysaccharides, which could act as inducers. In this section, some features of enzyme production under glucose-limited conditions are discussed based on two experiments with 20 g/L glucose in the chemostat feed. The experiment named G (Table 4.2) was concerned with the beginning of the PNPGase production and the experiment G201 (Table 4.2) was concerned with the PNPGase production and its steady-state. Table 4.2 shows the results of the analysis of samples during the pre-steady state phase, from the end of the batch phase (A) to the achievement of the steady-state with respect to PNPGase production (E). The PNPGase activity, cell concentration and glucose concentration were quantified. The batch was performed using a medium containing 10 g/L glucose. The presence of glucose during the batch cultivation did not result in PNPGase production. At the end of the batch (A), the glucose concentration was 36 mg/L, but after 24 h of chemostat cultivation (B), the concentration had increased to 2500 mg/L. This accumulation of glucose in the chemostat indicates that during this transition phase, the glucose supply via the chemostat feed was faster than glucose consumption by the cells. At this point, no PNPGase activity was detected, most probably due to the high residual glucose concentration.

At point C, after the steady-state with respect to cell concentration and CO_2 concentration in the off-gas, the residual glucose concentration had decreased to a value below 1 mg/L and some enzyme activity was detected (1.1 U/mL). At time point D, the enzymatic activity was 4.1 U/mL and increased further to 6.2 U/mL (E). Both times points, D and E, were within the steady-state with respect to cell dry weight and CO_2 (after at least 6 residence times). The increase in PNPGase activity between time points C and E suggests the presence of inducers, while the low residual glucose concentration could have minimized the influence of carbon catabolite repression (CCR). Considering that CCR was not the mechanism controlling the production, perhaps catabolite inhibition could have had more influence, and the concentrations of the inducer could have been controlling PNPGase synthesis.

Table 4.2 – Analysis of PNPGase production under glucose-limited conditions

Experiment	Point	Time (h)	Phase description	PNPGase (U/mL)	Glucose (mg/L)	Cells (g/L)
G[a]	A	24	End of the batch	0	36 ±3.12	4.6 ±0.61
	B	48	Transition phase	0	2500 ±20.5	8 ±0.55
	C	200	Beginning of PNPGase production	1.1 ±0.02	0.7 ±0.10	8.3 ±0.30
G201[b]	D	500	Increasing point of the production	4.1 ±0.63	2.95 ±0.31	8.6 ±0.03
	E	550	Steady-state of PNPGase production	6.2 ±0.41	2.62 ±0.65	9.47 ±0.72

a – Experiment performed to evaluate the beginning of enzyme production. b – Experiment G201 from Chapter 3, evaluation of enzyme production at steady-state.

Microscopic analysis of the culture morphology (Figure 4.5) revealed that at the end of the batch (A), the mycelium had shorter hyphae than at the starting point of the production phase (C). During the transition phase (B) the shortest hyphae were observed, which could have been caused by damage provoked on the hyphae by shear stress due to stirring. During the batch phase, the stirrer speed was dependent on the dissolved oxygen percentage and was allowed changing from 200 to 400 rpm. On the other hand, during the chemostat phase, the

stirrer was set to a constant speed of 600 rpm. After the transition phase, the mycelia became healthier (C), with long and thin hyphae and the medium seemed more viscous. Apparently, the mycelia recovered from the damage imposed by shear stress, and this could have happened due to the presence of extracellular polysaccharides, which could have acted as a shock absorber, thus protecting the hyphae. According to Arroyo et al. (2016), hyphal cell walls can appear relatively static; however, fungi are able to change their polysaccharide composition and distribution to adapt to the environmental conditions.
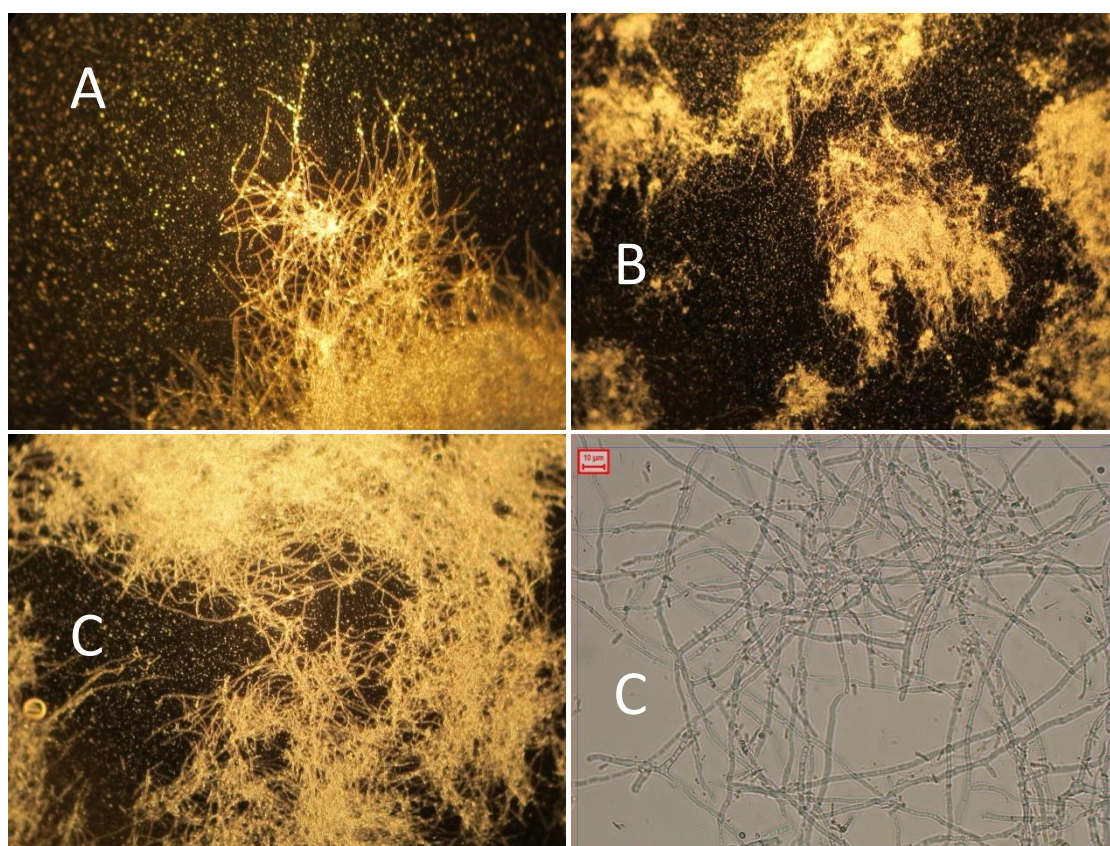
Figure 4.5 – *Trichoderma harzianum* morphology during continuous PNPGase production. A – at the end of the batch, 100x magnification, B – first day of continuous condition (transition phase), 100x magnification, C – starting point of PNPGase production, 100x magnification (left), 400x magnification (right)

Extracellular polysaccharides were qualitatively analysed by ethanol precipitation and their presence was confirmed in the supernatant of all samples, including the ones taken at the batch (A) and during the transition phase (B) (Table 4.2). Although there were extracellular polysaccharides in sample B, only after the transition phase the mycelia seemed healthier. This suggests that the polysaccharides surrounding the cells could have changed due to the shear stress influence.

The results of the FT-IR analysis of the extracellular polysaccharides for the samples A, B, C and E (Table 4.2), are presented in Figure 4.6 and show a clear peak for all the samples in the region of polysaccharides (1200-900 cm^{-1}) (Thumanu et al., 2015). It seems that no proteins were present in the polysaccharide samples as no peaks were observed in the corresponding region (1700–1580 cm^{-1}) (Thumanu et al., 2015).
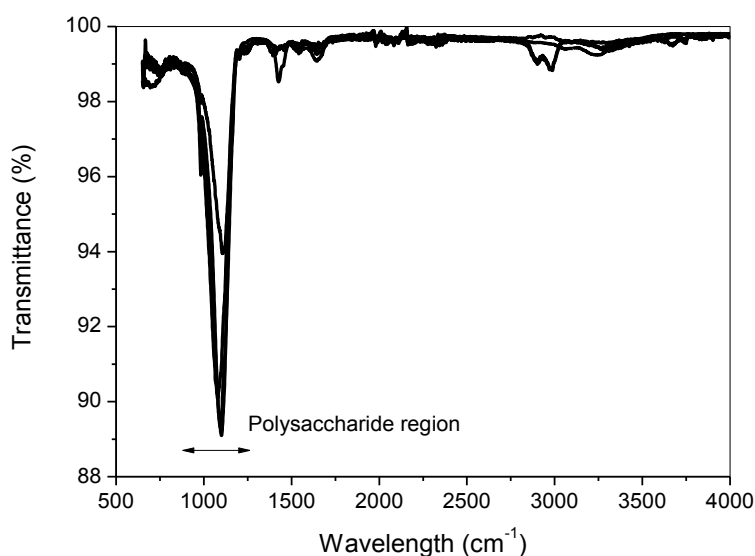
Figure 4.6 – FT-IR analysis for samples A, B, C, and E (Table 4.2)

The presence of gentiobiose was suggested by sugar analysis for all the samples (sugar chromatograms are not presented) presented in Table 4.2. This disaccharide could have been released as a fragment from the hyphal cell walls or from extracellular polysaccharides and could have acted as an inducer of PNPGase production, likely including beta-glucosidase (according to the shotgun proteomics analysis).

Qualitative analysis of polysaccharides was accessed using proton NMR analysis for samples A, B, C and E (Table 4.2). The spectra are presented in Figures 4.7 to 4.10. The region between 3.1 and 4.5 ppm corresponds to the ring proton region from sugar residues, the region between 4.5 and 5.5 ppm is the anomeric proton region and the region from 1.2 to 2.3 ppm is the alkyl region (Elnahas et al., 2017). The region between approximately 7 and 8 ppm could indicate the presence of aromatic compounds (Kuplich et al., 2012). The highest signal is from the DMSO reagent. The spectra of the samples are very similar, mainly for the samples A, C and E. Sample B provided different signals in the aromatic region (7 and 8 ppm).

Based on the analysis of the polysaccharides presented here, they have similar characteristics, indicating that during the different phases of the cultivation (Table 4.2) the composition of the polysaccharides present in the culture supernatant was not much different. However, the polysaccharide matrices surrounding the cells were not analysed and their structure could have changed.
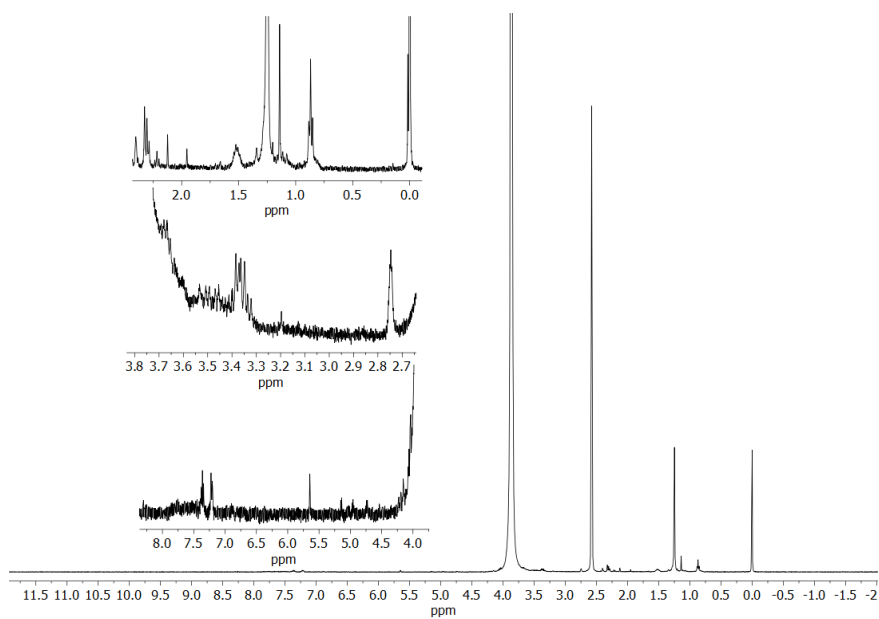
Figure 4.7 – Proton NMR, precipitate from the end of the batch (A)
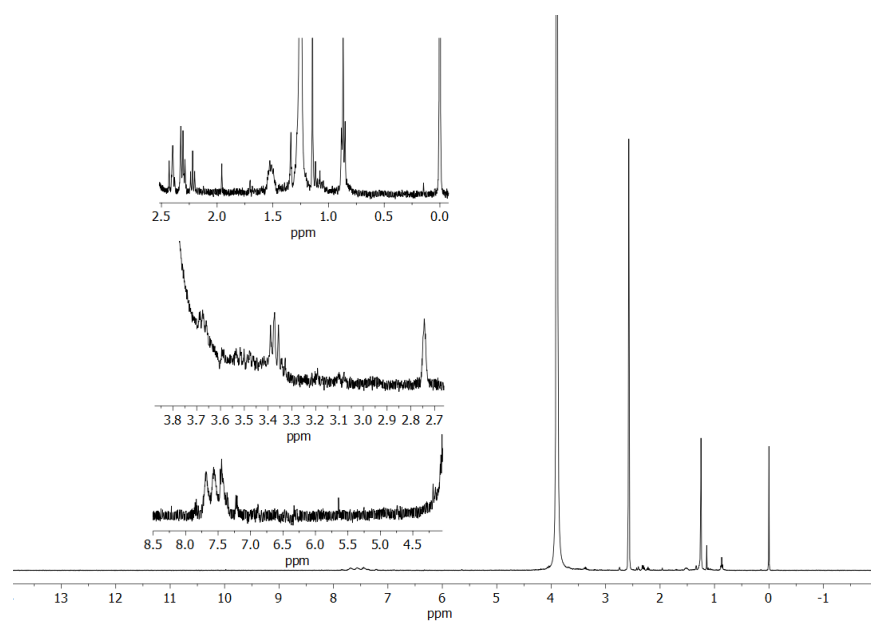
Figure 4.8 – Proton NMR, precipitate from the first day of the continuous condition (transition phase) (B)
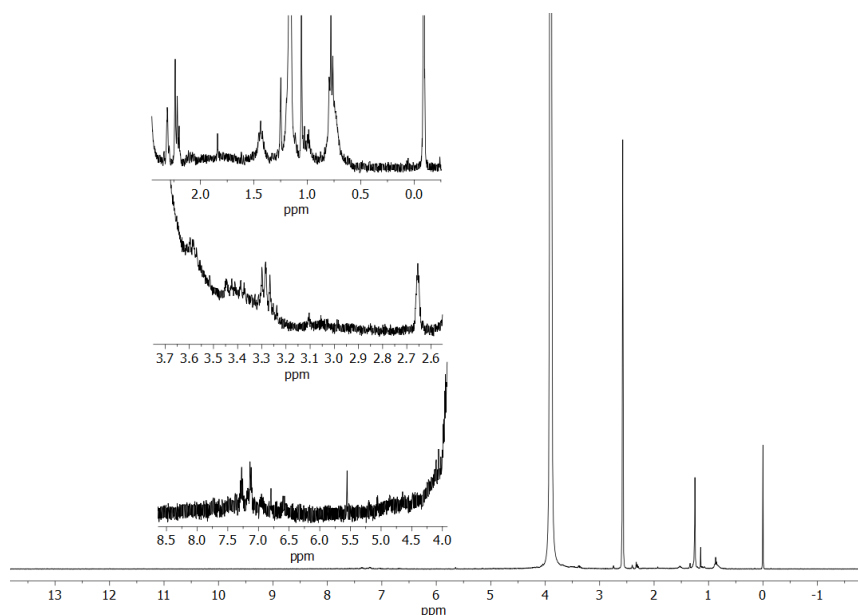
Figure 4.9 – Proton NMR, precipitate from the starting point of PNPGase production (C)
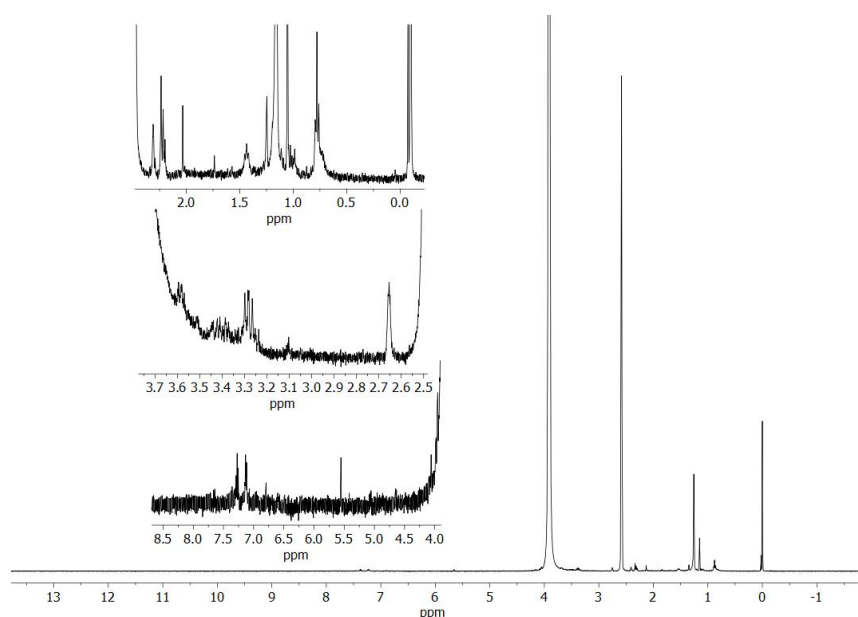
Figure 4.10 – Proton NMR, precipitate from the steady-state of PNPGase production (E)

Based on the observations and the data described above, a hypothetical mechanism for PNPGase production under glucose-limited conditions is proposed (Figure 4.11). Hereby it is considered that the measured PNPGase activity includes beta-glucosidase (assumed from the shotgun proteomics analysis). The presence of shear stress and a particular carbon source supplied may have a great influence on extracellular polysaccharide production and composition, and consequently on the production of enzymes through induction, if the polymers and enzymes are related. Extracellular polysaccharides can be loosely attached to the cell wall and fragments can be released due to shear stress (Rau, 1999). The concentration of these fragments could be influencing enzyme induction (Figure 4.11 – 1). According to Kubicek et al. (1993), a beta-diglucoside permease is able to transport cellobiose for *T. reesei* and can compete with beta-glucosidase. Analysis of the beta-diglucoside permease kinetics

provided a higher cellobiose specificity but a lower activity than the beta-glucosidase (Kubicek et al., 1993). Thus, at low concentrations of cellobiose, uptake by beta-diglucoside permease is preferable than hydrolysis by beta-glucosidase.

Therefore, at low concentrations of gentiobiose, which could also be transported by beta-diglucoside permease (Kubicek et al., 1993), the uptake (2) is preferable than hydrolysis (3), stimulating induction and secretion of PNPGase (5) (Figure 4.11). On the other hand, at high gentiobiose concentrations, hydrolysis would be preferable. Perhaps, at low concentration, gentiobiose could have acted as an inducer of PNPGase, but not as cellulase inducer according to filter paper activity (data not presented). This could indicate that cellulase was repressed to prevent the hydrolysis of extracellular polysaccharides, which might be produced to protect the cells.
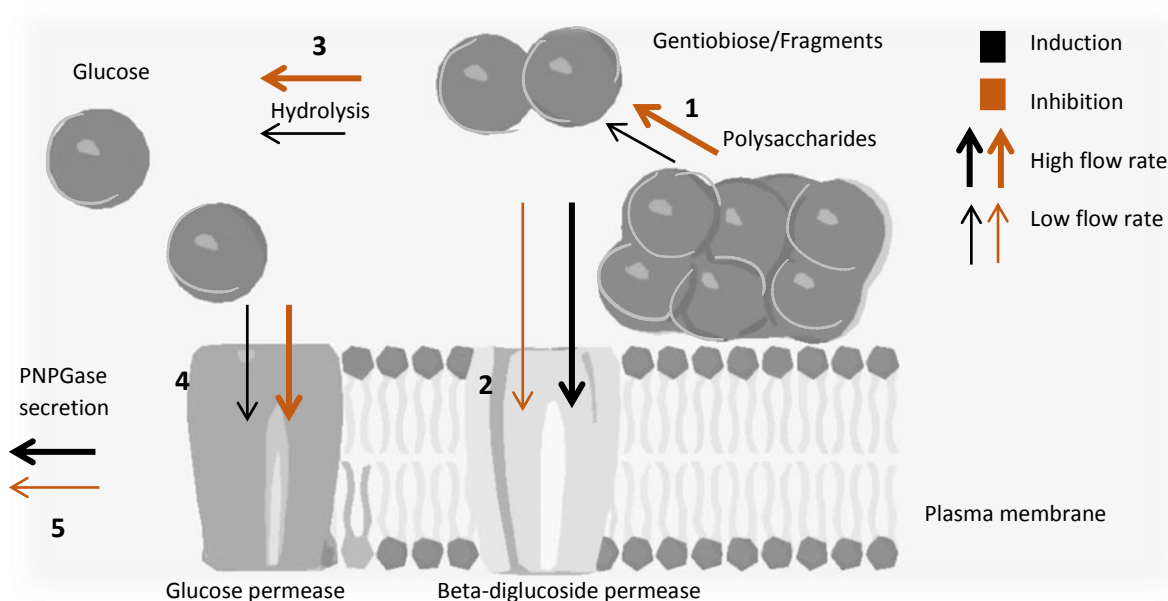
Figure 4.11 – Hypothetical induction mechanism for PNPGase production under glucose-limited conditions: 1 – releasing of fragments from extracellular polysaccharides due to shear stress; 2 – uptake of gentiobiose or fragments, which can require an active ATP gradient coupled to H^+ (Kubicek et al., 1993); 3 – hydrolysis of gentiobiose or fragments; 4 – uptake of glucose from hydrolysis through facilitated diffusion; 5 – PNPGase secretion

4.3.3 Analysis of intracellular metabolites during PNPGase production under glucose-limited conditions

The intracellular metabolites from the tricarboxylic acid cycle, glycolysis and pentose phosphate pathway, as well as nucleotides, were quantified for samples C and E (Table 4.2). Both samples (C and E) came from the same condition at steady-state of cells and CO_2 but at different sampling times. The difference between them is that point C was not at steady-state of PNPGase production. The Tukey test with 95 % confidence interval (OriginPro 8 software) was applied to analyse the average values for each metabolite. Significant differences among metabolite levels could indicate metabolites that might be directly or indirectly related to PNPGase production. Statistically significant differences in concentrations of the metabolites are highlighted in blue (Table 4.3).

The high experimental errors observed for some metabolites could be attributed to the sample processing and/or analytical errors. Another explanation considered is a possible heterogeneity of cells inside the bioreactor caused by the consumption of fragments of the polysaccharides under carbon-limited conditions. Considering that the highest shear rates in a mixing vessel are close to the blades of the impeller (Albright, 2008), there are regions with different shear rates inside the bioreactor. Fragments of polysaccharides from the cell wall can be released due to this shear stress (Rau, 1999), and because of different shear rate regions inside the bioreactor, it could also be expected that there exist regions with different concentrations of fragments. Since the cells can consume these fragments, the cells closer to the regions with a higher concentration of fragments could present different concentrations of some intracellular metabolites than the cells farther from that region.

Sugar chromatograms indicate the presence of several peaks, based on the retention times, these peaks could indicate the presence of disaccharides or oligosaccharides, which might come from polysaccharide fragments (Figure 4.12). Figure 4.12 shows, for example, the sugar chromatogram for the condition using 20 g/L of glucose at steady-state (G201), in which lower retention times correspond to sugars with lower molecular weights (e.g. the monosaccharides glucose and fructose), higher retention times could correspond to disaccharides and oligosaccharides. The peak at a retention time of 32.6 minutes corresponds to the retention time of gentiobiose (Figure 4.13). Sugar chromatograms for samples A, B and C (Table 4.2) are presented in the supplementary material. Although samples C and E were at steady-state of cell concentration and CO_2 production, it seems that there was another parameter, perhaps polysaccharide fragments, influencing the intracellular metabolite concentrations and the changes highlighted in Table 4.3 are not considered as resulting from sample processing and/or analytical errors due to the low standard experimental errors.

Table 4.3 shows a significant difference regarding intracellular glucose concentration that decreases from sample C to E and its concentration is inversely proportional to PNPGase activity (C = 1.1 U/mL, E = 6.2 U/mL). The higher glucose concentration for sample C could explain the lower enzymatic activity. Perhaps at this stage (C), the process was still unstable and glucose was inhibiting the inducer uptake. In addition, 1.6 µmol/g (E) seems to be an intracellular glucose concentration that could prevent CCR. Changes in the specific concentration of metabolites could be more related to the consumption of polysaccharide fragments than the production of PNPGase due to the low concentration of the proteins secreted (20 – 200 mg/L).

Based on PNPGase activity and intracellular glucose concentration, it can be considered that sample C provides information on an inhibition-state and sample E provides information of an inducer-state for PNPGase synthesis. For the sample E, the uptake rate of inducer fragments (e.g. gentiobiose) of PNPGase synthesis was probably higher than for sample C, meanwhile, the uptake rate of hydrolysed fragments (e.g. glucose) was higher for sample C, provoking inhibition. Therefore, significant differences observed between some metabolite levels indicate changes in the metabolic pathway when there is a higher consumption of inducers (sample E) or inhibitors (sample C) of PNPGase production. The higher uptake of inducers resulted in higher concentrations of metabolites from the tricarboxylic acid cycle, part of glycolysis (from glyceraldehyde-3-phosphate to phosphoenolpyruvate) and lower values for metabolites from the pentose phosphate pathway.
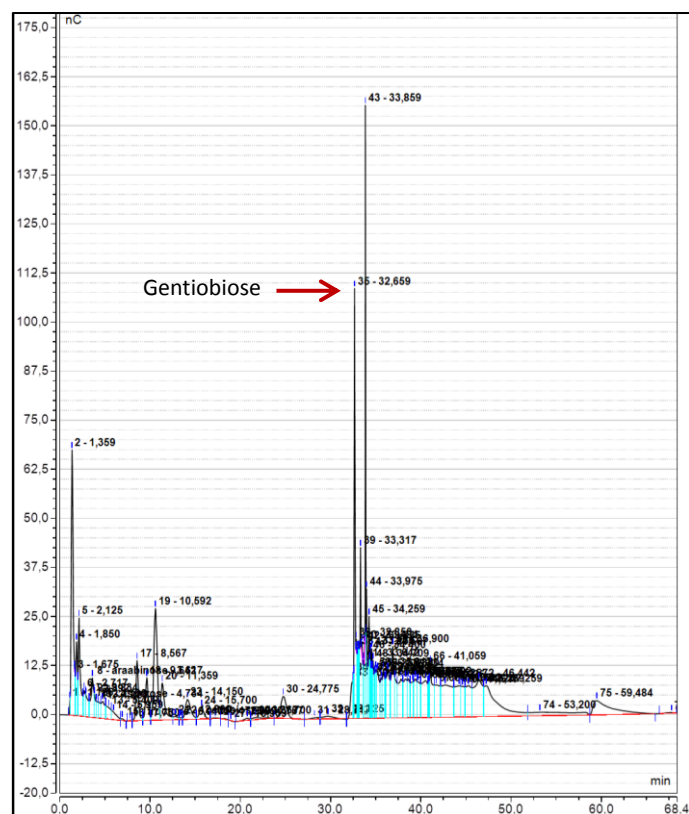
Figure 4.12 – Sugar chromatogram for the condition using 20 g/L of glucose (G201) at steady-state of PNPGase production
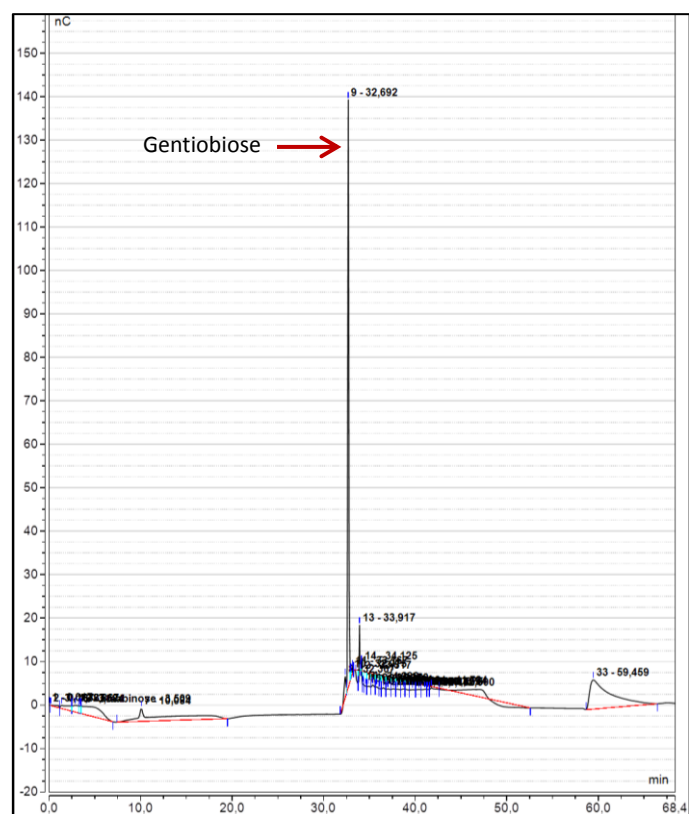
Figure 4.13 – Sugar chromatogram for a gentiobiose solution

Table 4.3 – Intracellular metabolite levels analysed for points C and E, metabolites with significantly different levels are indicated in blue (Tukey test with 95 % confidence interval)

	C (µmol/g)			E (µmol/g)				C (µmol/g)			E (µmol/g)		
Gluc	31.789	±	2.978	1.559	±	0.375	Fum	1.104	±	0.016	0.970	±	0.093
G6P	0.937	±	0.442	1.417	±	0.023	G3P	0.226	±	0.060	1.783	±	0.112
F6P	0.227	±	0.105	0.298	±	0.019	G1P	0.030	±	0.012	0.063	±	0.011
FBP	0.381	±	0.139	0.410	±	0.008	UDPG	1.256	±	0.049	1.231	±	0.003
GAP	0.015	±	0.001	0.026	±	0.002	T6P	0.025	±	0.006	0.051	±	0.007
DHAP	0.108	±	0.021	0.153	±	0.014	Tre	112.059	±	16.836	49.693	±	4.970
3PG	0.396	±	0.001	0.497	±	0.020	M6P	0.388	±	0.146	0.478	±	0.020
2PG	0.041	±	0.001	0.054	±	0.004	AMP	0.296	±	0.006	0.533	±	0.042
PEP	0.011	±	0.001	0.017	±	0.0001	ADP	1.484	±	0.055	0.993	±	0.129
M1P	0.087	±	0.001	0.097	±	0.014	ATP	2.726	±	0.083	2.871	±	0.476
6PG	0.745	±	0.273	0.618	±	0.044	cAMP	0.018	±	0.00005	0.021	±	0.004
Ribu5P	0.283	±	0.006	0.222	±	0.038	UMP	0.053	±	0.008	0.065	±	0.007
Rib5P	0.615	±	0.033	0.386	±	0.030	UDP	0.129	±	0.015	0.110	±	0.010
Xyl5P	0.382	±	0.004	0.357	±	0.057	UTP	0.715	±	0.002	0.511	±	0.096
S7P	0.786	±	0.021	0.443	±	0.025	GMP	0.213	±	0.021	0.152	±	0.012
E4P	0.0046	±	0.0003	0.0049	±	0.0004	GDP	0.149	±	0.009	0.222	±	0.035
Cit	6.656	±	0.039	13.080	±	1.005	GTP	0.766	±	0.018	0.679	±	0.089
iCit	0.098	±	0.001	0.278	±	0.014	CMP	0.031	±	0.003	0.058	±	0.006
αKG	0.525	±	0.004	0.649	±	0.043	CDP	0.066	±	0.007	0.061	±	0.008
Suc	0.590	±	0.027	1.143	±	0.242	CTP	0.353	±	0.016	0.180	±	0.029
Mal	2.441	±	0.155	3.034	±	0.223							

2PG 2-phosphoglycerate, **3PG** 3-phosphoglycerate, **6PG** 6-phosphogluconate, **ADP** Adenosine diphosphate, **αKG** α-Ketoglutarate, **AMP** Adenosine monophosphate, **ATP** Adenosine triphosphate, **cAMP** Cyclic AMP, **CDP** Cytidine diphosphate, **Cit** Citrate, **CMP** Cytidine monophosphate, **CTP** Cytidine triphosphate, **DHAP** Dihydroxyacetone phosphate, **E4P** Erythrose-4-phosphate, **F6P** Fructose-6-phosphate, **FBP** Fructose-1,6-bisphosphate, **Fum** Fumarate, **G1P** Glucose-1-phosphate, **G3P** Glycerol-3-phosphate, **G6P** Glucose-6-phosphate, **GAP** Glyceraldehyde-3-phosphate, **GDP** Guanosine diphosphate, **Gluc** Glucose, **GMP** Guanosine monophosphate, **GTP** Guanosine triphosphate, **iCit** Isocitrate, **M1P** Mannitol-1-phosphate, **M6P** Mannose-6-phosphate, **Mal** Malate, **PEP** Phosphoenolpyruvate, **Rib5P** Ribose-5-phosphate, **Ribu5P** Ribulose-5-phosphate, **S7P** Sedoheptulose-7-phosphate, **Suc** Succinate, **T6P** Trehalose-6-phosphate, **Tre** Trehalose, **UDP** Uridine diphosphate, **UDPG** Uridine-5-diphosphoglucose, **UMP** Uridine monophosphate, **UTP** Uridine triphosphate, and **Xyl5P** Xylulose-5-phosphate.

Table 4.4 presents the mass-action ratios for some reactions based on the average values between C and E (Table 4.3). Mass-action ration (Q) is the ratio between the concentrations of products and reagents for a specific reaction and can be used to identify near-equilibrium reactions by comparing their values with equilibrium constants (K_{eq}) (Lehninger et al., 2005). Mass-action ratios indicated that the average of the majority of the reactions analysed was close to the equilibrium, except for the [PEP]/[2PG], which was 14 times far from the equilibrium. [ATP]/[ADP] ratio provided a value much far from the equilibrium due to the cell growth reactions. [G6P][ADP]/[Gluc][ATP] ratio was also far from the equilibrium, and this makes the reaction practically irreversible providing the driving force that moves the metabolites through the glycolytic pathway (Karp, 2009). The mass-action value for C ([G6P][ADP]/[Gluc][ATP] = 0.016) was farther from the equilibrium than sample E ([G6P][ADP]/[Gluc][ATP] = 0.31) due to the higher glucose concentration.

Although the average values between the samples C and E were close to the equilibrium, standard error (SE) with a high value was observed for the ratio $[ATP][AMP]/[ADP]^2$ (SE = 62 %). Sample C provided a similar concentration of ATP, but a higher concentration for ADP and a lower concentration for AMP than sample E. This resulted in a mass-action value for C ($[ATP][AMP]/[ADP]^2$ = 0.37) farther from the equilibrium than sample E ($[ATP][AMP]/[ADP]^2$ = 1.56).

According to De la Fuente et al. (2014), the ratio of ATP, ADP and AMP is functionally more important than the absolute concentration of ATP. They also discussed that a simple index to measure the energy status of the cell was proposed by Atkinson in 1967 and was defined as: ([ATP] + 0.5[ADP])/([ATP] + [ADP] + [AMP]). This test results in a value ranging between 0 and 1, when there is only AMP, the energy charge is zero, with only ADP, the energy charge is 0.5 and when there is only ATP, the energy charge is 1 (De la Fuente et al., 2014). The energy charge average observed was 0.77 ±0.002 (Table 4.4). This value is inside the range (0.7 and 0.95) considered normal for many organisms growing under optimal conditions (De la Fuente et al., 2014).

Table 4.4 – Average of mass-action ratios between sample C and E for some intracellular metabolites presented in Tables 4.3

Mass-action ratio (Q)	EC number	Enzyme	Q			K_{eq} literature[a]
$[G6P][ADP]/[Gluc][ATP]$	2.7.1.1	Hexokinase	0.17	±	0.15	$4.7 ±0.8x10^3$
$[F6P]/[G6P]$	5.3.1.9	Phosphohexose isomerase	0.23	±	0.02	0.32 ±0.08
$[G1P]/[G6P]$	5.4.2.2	Phosphoglucomutase	0.04	±	0.01	0.058 ±0.0003
$[2PG]/[3PG]$	5.4.2.1	Phosphoglycerate mutase	0.11	±	0.003	0.092 ±0.004
$[PEP]/[2PG]$	4.2.1.11	Enolase	0.29	±	0.02	4.1 ±0.7
$[Rib5P]/[Ribu5P]$	5.3.1.6	Ribose 5-phosphate isomerase	1.96	±	0.22	3 ±1
$[Mal]/[Fum]$	4.2.1.2	Fumarate hydratase	2.67	±	0.46	4.3 ±0.7
$[Xyl5P]/[Ribu5P]$	5.1.3.1	Ribose 5-phosphate epimerase	1.48	±	0.13	1.7 ±0.8
$[M6P]/[F6P]$	5.3.1.8	Phosphomannose isomerase	1.66	±	0.05	0.8 ±0.2
$[iCit]/[Cit]$	4.2.1.3	Aconitate hydratase	0.02	±	0.003	0.06 ±0.02
$[ATP][AMP]/[ADP]^2$	2.7.4.3	Adenylate kinase	0.96	±	0.59	1.2 ±0.3
$[ATP]/[ADP]$			2.36	±	0.53	10^{-5}
Energy charge			**Value**			**Literature[b]**
([ATP]+0.5[ADP])/([ATP]+[AMP]+[ADP])			0.77	±	0.002	0.7 - 0.95

a – Equilibrium constants (K_{eq}) reported by Canelas et al. (2011), [ATP]/[ADP] reported by Meyrat and Ballmoos (2018), and [G6P][ADP]/[Gluc][ATP] reported by Kubota and Ashihara (1990). b – Energy charge range reported by De la Fuente et al. (2014).

4.4 Conclusions

Shotgun proteomics and SDS-PAGE analysis were performed for the proteins present in the supernatant of carbon-limited chemostat cultures using glucose, fructose/glucose and sucrose as carbon sources. The shotgun proteomics analysis has indicated that the different carbon sources used greatly influenced the amounts of secreted proteins, of which many of them are enzymes. The presence of beta-glucosidase was confirmed and the measured amounts correlated with the measured enzymatic activities (PNPGase). The possible differences regarding the enzymes secreted could be related to the presence of different inducers. This brings the possibility of creating a hypothesis that different carbon sources

easily assimilated by the cells under carbon-limited conditions could lead to the synthesis of different inducers and thus different enzymes. Most of the measured proteins are uncharacterized, which makes it difficult to correlate them with the conditions. Microscope observations of mycelia during PNPGase production have shown that there were changes in the morphology of the cells from the batch to the transition phase. After the transition phase, the mycelia became healthier and started producing PNPGase. A mechanism for continuous PNPGase production at glucose-limited conditions was proposed based on the influence of extracellular polysaccharides and a possible gentiobiose permease (beta-diglucoside permease). Analysis of the intracellular metabolites has suggested that high intracellular glucose concentrations can inhibit the production of enzymes.

Chapter 5

Metabolome evaluation during extracellular polysaccharide production – an interesting by-product synthesized by *T. harzianum* P49P11

Intracellular metabolites from glycolysis, citric acid cycle, pentose phosphate pathway, as well as nucleotides were analysed during the continuous production of extracellular polysaccharides. Different limiting carbon sources were used in duplicate (glucose, sucrose and fructose/glucose).
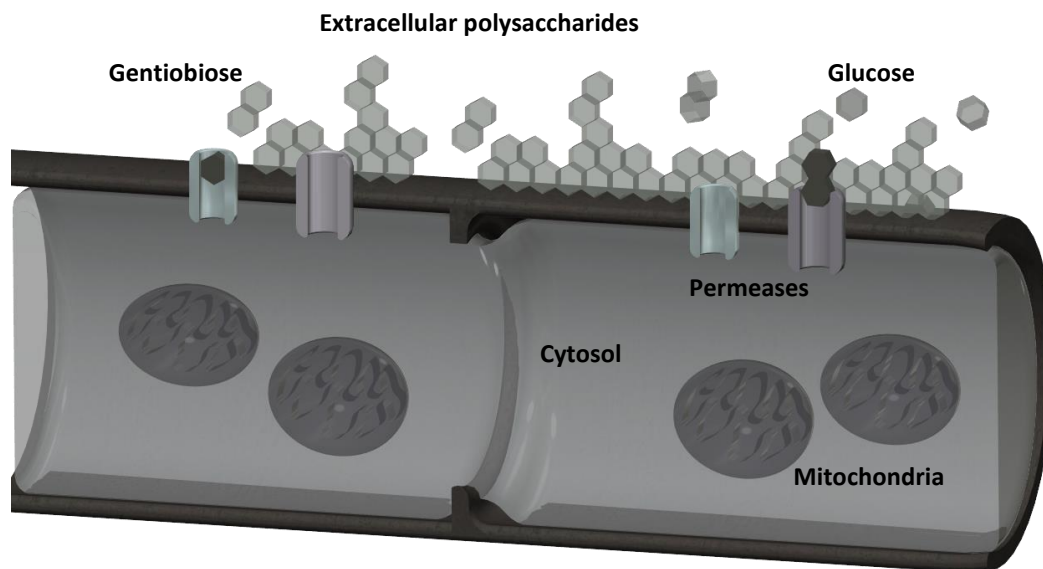
Abstract

Intracellular metabolites were evaluated under four different conditions in duplicate (10 and 20 g/L of glucose, 5.26/5.26 g/L of fructose/glucose and 10 g/L of sucrose) during the production of extracellular polysaccharides by *Trichoderma harzianum* under carbon-limited conditions. The average values of each duplicate were compared. Two groups of the conditions evaluated were also compared, the first group using glucose as the carbon source and the second using fructose/glucose and sucrose as the carbon sources. Differences in the values of some specific concentrations of the intracellular metabolites were observed for the duplicates and in the comparison of the conditions from each group. Considering that the carbon sources used do not interfere with the specific concentrations of the metabolites analysed, the differences observed were mainly attributed to the consumption of fragments from extracellular polysaccharides.

Keywords

5.1 Introduction

Extracellular polysaccharides have several applications in industries, in different product areas such as pharmaceuticals, medicine and foods. Despite their importance, information about fungal polysaccharide synthesis is scarce and an extensive search for new fungal species that can produce novel extracellular polysaccharides is still needed (Mahapatra and Banerjee, 2013). According to Mahapatra and Banerjee (2013), the nature of the carbon source used for the growth of the fungus has, in most cases, little influence on the composition of the fungal extracellular polysaccharides; however, the intensity of the production is dependent on the carbon source and its concentration. They also mentioned that only a few pathways for fungal synthesis of extracellular polysaccharides have been studied. Most researchers have studied the optimization of the culture medium and operating conditions for polysaccharide production using different fungal strains.

For polysaccharides produced by yeasts, the factors that affect the production include the medium composition, pH, temperature, oxygenation, stirring, inoculum quantity, and time of the culture (Gientka et al., 2015). According to Gientka et al. (2015), industrial polysaccharide production by yeast is mainly limited by the low yield. Some extracellular polysaccharides of yeasts show antitumor, immunostimulatory and antioxidant activity (Gientka et al., 2015).

Trichoderma species are recognized for their high extracellular enzyme production but there are limited reports on the production of polysaccharides (Li et al., 2016). Li et al. (2016) evaluated *in vitro* the anti-tumour properties of an extracellular polysaccharide from *Trichoderma* sp. KK19L1 on human cervical carcinoma cells (HeLa) and human breast carcinoma cells (MCF-7). MTT assay (colorimetric assay) to assess cell viability was used to determine the inhibition effect of polysaccharides on cancer cells. The inhibition rate was calculated and the authors reported that for a polysaccharide concentration of 400 μg/mL, the inhibition rate was about 50 % on HeLa cells at 48 h. For MCF-7 cells, the inhibition rate was lower than 20 % for all the polysaccharide concentrations used. These data show the potential of extracellular polysaccharides from *Trichoderma* sp.

In Chapter 3 (section 4.3.3), it is discussed the possibility of heterogeneity of cells inside the bioreactor caused by the consumption of fragments from polysaccharides under carbon-limited conditions. Assuming that these fragments can be released from the cell wall due to shear stress and that there are regions inside the bioreactor with different concentrations of fragments caused by different shear rate regions, these conditions could create an environment heterogeneous enough to affect the estimation of intracellular metabolites. To date, no studies have been found in the literature on the analysis of intracellular metabolites under carbon-limited conditions using filamentous fungi during the production of extracellular polysaccharides. Based on this, the aim of this chapter is to analyse the specific concentrations of intracellular metabolites from the tricarboxylic acid cycle, glycolysis and pentose phosphate pathway, as well as nucleotides during the continuous synthesis of extracellular polysaccharides by *T. harzianum* under carbon-limited conditions.

5.2   Materials and Methods

5.2.1   Samples for the analysis

Mycelium and supernatant samples were withdrawn from carbon-limited chemostat cultures carried out under the four different conditions addressed in Chapter 3 to measure and characterize the extracellular polysaccharides as well as the intracellular metabolite levels (µmol/g of cells). The conditions were divided into two groups, the first group of chemostat experiments used glucose as the sole carbon source with concentrations in the chemostat feed medium of 10 g/L (G101 and G102) and 20 g/L (G201 and G202), and the second group used fructose/glucose (FG1 and FG2) and sucrose (S1 and S2) as carbon sources, at concentrations in the chemostat feed of 10 g/L. All chemostat experiments were performed at a dilution rate of 0.05 ±0.003 h^{-1}. A steady-state was assumed to be achieved when the CO_2 production rate and cell concentration were stable during a period of at least 6 residence times.

5.2.2   Qualitative analysis of polysaccharides

Culture supernatant was obtained by filtration of chemostat culture broth through 0.45 µm pore size filters (Millex-HV durapore PVDF membrane). Ethanol precipitation was performed by mixing 1 mL of the sample with 3 mL of pure ethanol. After centrifugation at 2000x g for 5 min, the precipitate was solubilized with 1 mL of water and precipitated again with 3 mL of pure ethanol. After a second centrifugation, the precipitate (approximately 2 mg) was freeze dried and subsequently hydrolysed with 400 µL of trifluoroacetic acid (2 M) for 1 h at 100 ^{o}C. The acid was removed by airflow. The sugars released were analysed using high-performance anion exchange chromatography (HPAE) as described below. Enzymatic hydrolysis was also performed; to this end the precipitate (2-3 mg) was hydrolysed with beta-glucanase (2 mg) from *Trichoderma longibrachiatum* (Sigma-Aldrich) in 1 mL of 50 mM citrate buffer (pH 4.8) for 1 h at 37 ^{o}C in a water bath. The sugars released were analysed using high-performance anion exchange chromatography (HPAE). Fourier-transform infrared spectroscopy (FT-IR) was performed placing 2-5 mg of polysaccharides on a universal attenuated total reflectance accessory (Perkin Elmer spectrum 100).

Samples for proton NMR analysis were prepared by using 0.2 g of LiCl in 1.0 mL D_2O, followed by 9 mL of DMSO and a few grains of deuterated (3-(trimethylsilyl)-2,2,3,3-tetradeutero propionic acid or TMSP-d4) were added. 0.5 ml of this solution was transferred to the vials containing the samples (5-15 mg). Then, they were heated in a thermo-shaker at 100 ^{o}C for 12 hours. The cooled solutions were then transferred to an NMR tube and all measurements were carried out at 25 ^{o}C using an Agilent 400-MR DD2 equipped with a 5 mm OneNMR probe. The data for proton NMR spectra were collected with 1024 scans, d1 = 1s (399.7 MHz).

5.2.3   Extracellular glucose analysis

For the analysis of extracellular glucose, the samples were diluted with 1 M NaOH to precipitate proteins that could interfere with the analysis. Precipitated proteins were removed by centrifugation (2000x g, 10 min). The samples were analysed using high-performance anion exchange chromatography (HPAE), Dionex ICS-5000 with PAD detector (Rohrer et al., 2013). The analysis was performed in triplicate.

5.2.4 Total organic carbon (TOC)

For the determination of the TOC, 3 mL of the supernatant was analysed with a Shimadzu TOC-L CSH analyser using the differential method where the TOC is measured as the difference between the total carbon and the inorganic carbon values. The analysis was performed in triplicate.

5.2.5 Analysis of intracellular metabolites

The samples for the analysis of the intracellular metabolites of each condition came from 3 different days during the steady-state. The cells on the walls of the bioreactor were not considered to influence the specific concentrations of the metabolites since the system was very stable during the steady-state. Intracellular metabolites were extracted and analysed according to Lameiras et al. (2015). Broth (approx. 1.3 mL) was rapidly withdrawn into 10 mL of pre-cooled 40 % (v/v) aqueous methanol solution (-20 ^{o}C) and after, the samples were weighted for estimation of the cell mass and kept at -20 ^{o}C until extraction of the metabolites. Methanol was removed by filtration and the samples were washed thrice with a cold methanol solution (-20 ^{o}C). Then, boiling ethanol extraction was performed to disrupt the cells and inactivate the enzymes. To this end, 25 mL of ethanol solution (75 % v/v) was first pre-heated at 75 ^{o}C, whereafter the quenched and washed cell samples were added to the ethanol solution together with 100 µL of U-^{13}C-labeled cell extract of *S. cerevisiae* as the internal standard and incubated in a water bath at 95 ^{o}C for 3 min. After the extraction, the samples were first placed on ice and then stored at -80 ^{o}C.

Before the quantification of the metabolites, ethanol was evaporated until almost dryness in a Rapid-Vap under vacuum for 240 min. After evaporation, the residues were suspended in 500 µL of Milli-Q water, and centrifuged at 1000x g for 5 min in a tube coupled with a filter (0.22 µm) to remove cell debris. The supernatants were stored at -80 ^{o}C until analysis. The concentrations of the intracellular metabolites were measured by isotope dilution mass spectrometry (LCIDMS/ MS and GC-IDMS) according to the protocols of Dam et al. (2002), Jonge et al. (2011) and Cipollina et al. (2009).

5.3 Results and Discussion

5.3.1 Extracellular polysaccharides

The presence of polysaccharides in the culture supernatant was confirmed through ethanol precipitation, followed by enzymatic and acid hydrolysis for the experiments with glucose at 10 g/L (G101), sucrose (S1) and fructose/glucose (FG1). Ethanol precipitation provided a white coloured substance (Figure 5.1) that was hydrolysed by beta-glucanase only generating glucose. For the enzymatic hydrolysis, a control only containing enzymes and buffer was also analysed since there was the presence of glucose in the enzymes used. The release of glucose after hydrolysis of the polysaccharides suggests the presence of beta-glucans. Acid hydrolysis resulted in a solution containing at least glucose, mannose and galactose for all the samples.

Figure 5.1 shows a precipitate solution under the microscope. In picture A, the hyphae are surrounded by the precipitate. This picture could indicate how the polysaccharides surround the hyphae.
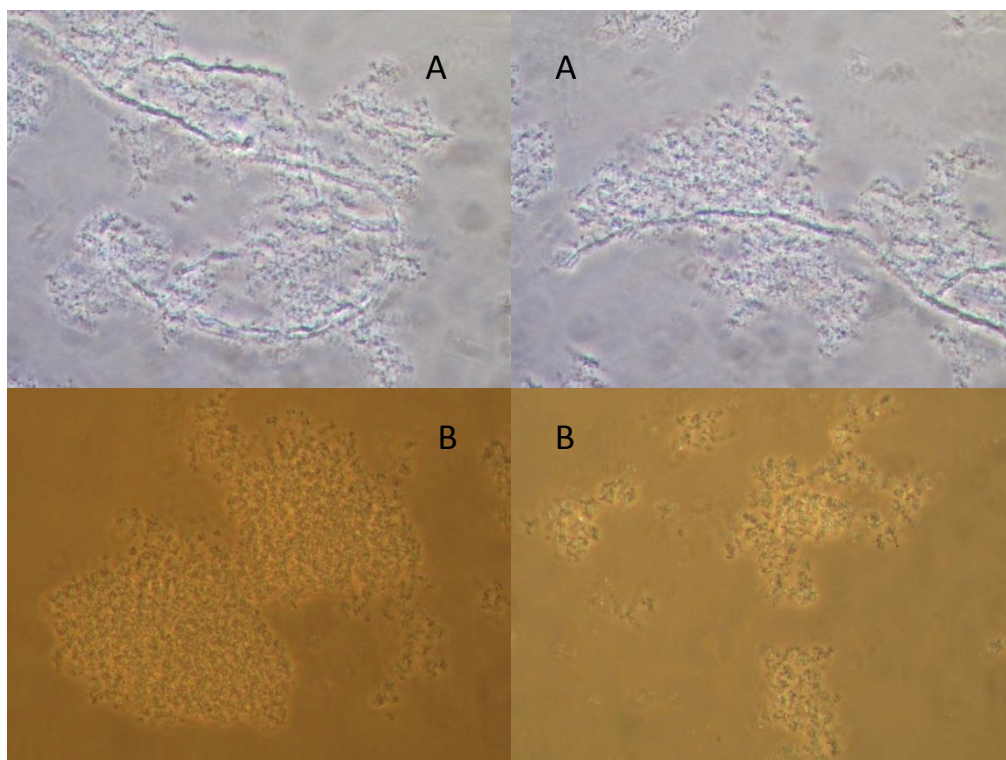
Figure 5.1 – Precipitate solution 400x magnification, A – hyphae are surrounded by the precipitate, B – precipitate in the solution

Figure 5.2 shows the concentrations of the precipitate for the different cultivation conditions applied. For the conditions using 10 g/L in the feed medium (G101, G102, FG1, FG2, S1 and S2) the average concentration was 2.8 g/L of the precipitate. On the other hand, for the conditions using twice the amount of sugar in the chemostat feed (G201 and G202), the precipitate concentration practically increased twice.

Table 5.1 presents the measured carbon concentrations in the supernatants (total organic carbon, TOC), which partly represents the carbon present in the form of polysaccharides. For the conditions using 10 g/L in the feed media (G101, G102, FG1, FG2, S1 and S2) the average concentration was 610 mg/L of carbon, thus it was expected a value twice higher for the conditions using 20 g/L (G201 and G202). However, only the conditions G201 provided a value close to the concentration expected (1220 mg/L), but with a high experimental error. Due to the high experimental errors of TOC values, it is difficult to make a correlation with the concentrations of the precipitate.

For the cultivations presented in Table 5.1, the standard errors of the values obtained were large and the duplicates also provided different values, which show that the extracellular carbon concentration was not very stable during steady-state conditions. Because all experiments were performed under carbon-limited conditions, the instability of carbon concentration could be related to changes in polysaccharide production and/or sudden changes in the amounts of cell lysis products, e.g. due to clumps of dead mycelia falling from the bioreactor wall into the liquid. TOC analysis was also used to estimate the concentrations of carbon in the chemostat feed medium (Table 5.1) to show the accuracy of the analysis (the feed concentration of carbon for the conditions G101, G102, FG1, FG2, S1 and S2 was 4 g/L and for the conditions G201 and G202 was 8 g/L).
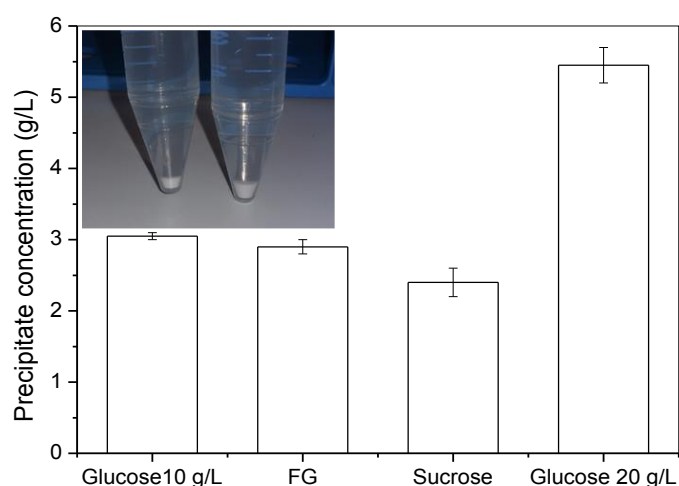
Figure 5.2 – Precipitate concentrations for the conditions at steady-state (duplicate)

Table 5.1 – TOC analysis for the conditions at steady-state, 10 g/L of glucose (G101 and G102), 5.26/5.26 g/L of fructose/glucose (FG1 and FG2), 10 g/L of sucrose (S1 and S2), 20 g/L of glucose (G201 and G202), and estimation of carbon concentration in the feed

Condition	Samples (mg/L)	Concentration in the feed (g/L)
G101	417 ±12	3.90
G102	788 ± 71	3.96
FG1	400 ±5	4.08
FG2	737 ±36	4.12
S1	502 ±43	4.14
S2	814 ±72	4.20
G201	1149 ±209	8.52
G202	639 ±106	8.04

FT-IR analysis of the precipitates (Figure 5.3) shows a clear peak in the region of polysaccharides (1200-900 cm^{-1}) (Thumanu et al., 2015). The samples analysed were the conditions with glucose at 10 and 20 g/L, fructose/glucose and sucrose in duplicate.
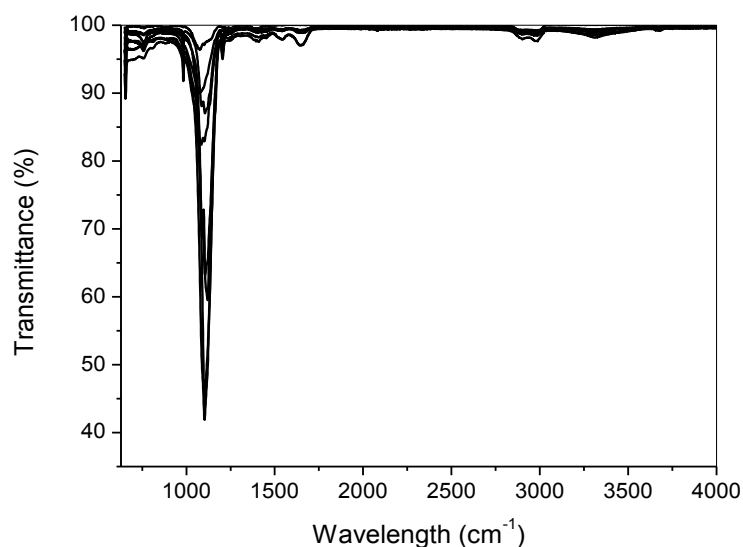
Figure 5.3 – FT-IR analysis, glucose at 10 and 20 g/L, fructose/glucose and sucrose conditions in duplicate

Proton NMR analysis was applied in order to obtain more information about the properties of the extracellular polysaccharides. The samples analysed were the conditions with glucose at 10 (G101) and 20 g/L (G201), fructose/glucose (FG1) and sucrose (S1). The proton NMR spectrum of polysaccharides is mainly composed of three regions: ring proton region of sugar residues (3.1-4.5 ppm); anomeric proton region (4.5-5.5 ppm); and alkyl region (1.2-2.3 ppm) (Elnahas et al., 2017). The region between approximately 7 and 8 ppm could indicate the presence of aromatic compounds (Kuplich et al., 2012). Although proton NMR spectra are very informative, the results of samples with fully protonated molecules, high-molecular weights, and with a certain degree of heterogeneity are complex to interpret (Pomin, 2012). This can be seen in spectra with the presence of crowded signals from polysaccharides with no clear pattern (Pomin, 2012). Figures 5.4 – 5.7 show the proton NMR spectra for four samples. The highest peak is from the DMSO reagent. Similar spectra were obtained for all the samples. Peaks corresponding to the region of sugar residues and one peak at the anomeric proton region can be observed. This indicates that the structures of the extracellular polysaccharides produced were not dependent on the carbon sources used.
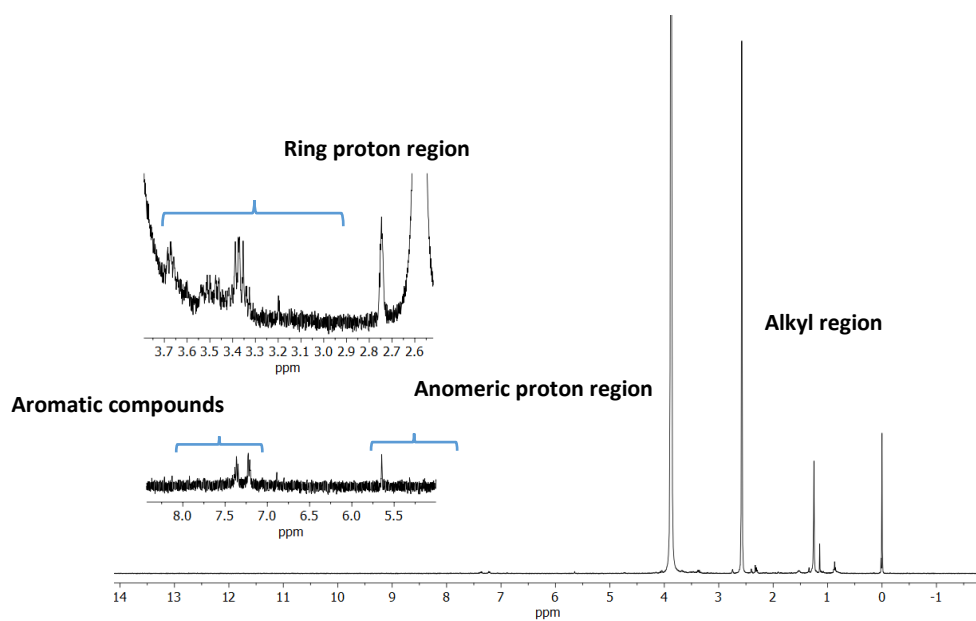
Figure 5.4 – Proton NMR, fructose/glucose condition (FG1)
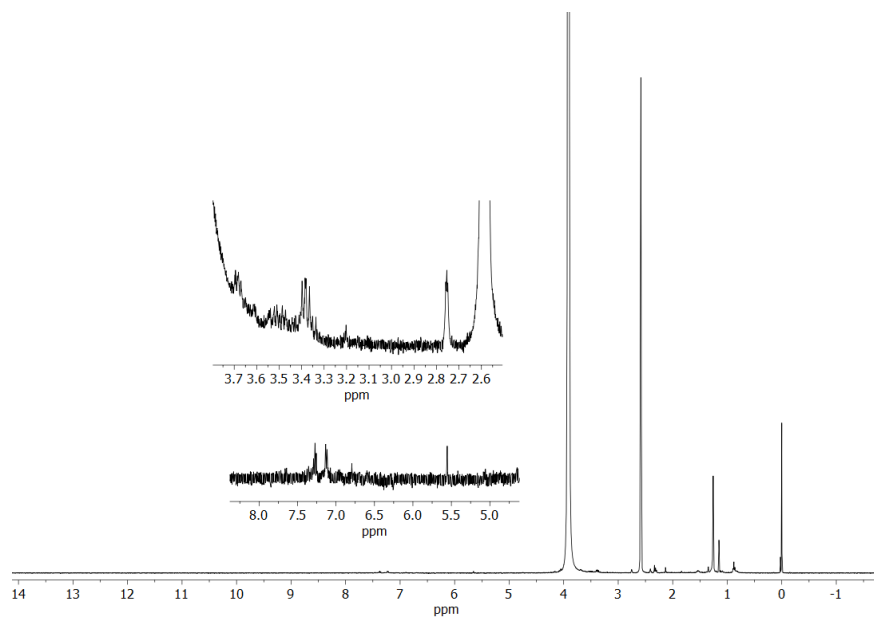
Figure 5.5 – Proton NMR, glucose at 20 g/L condition (G201)
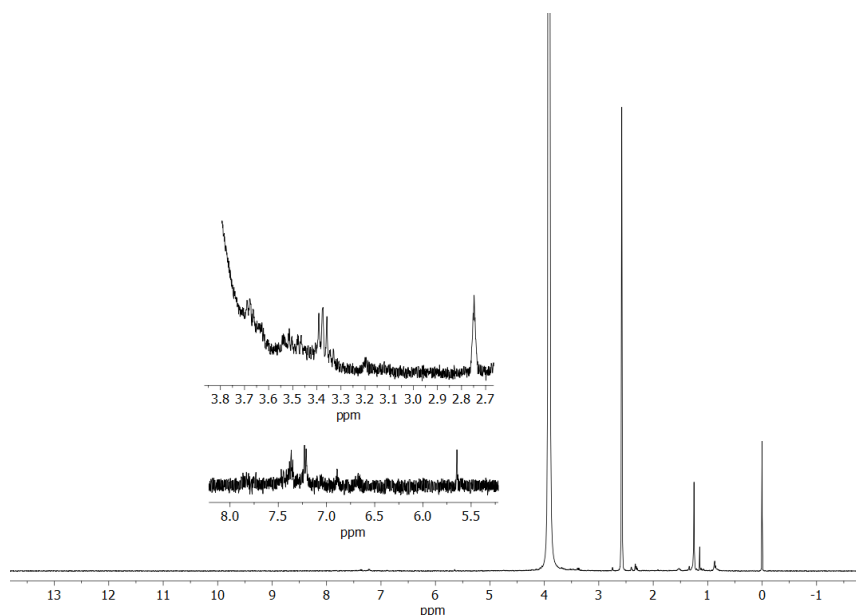
Figure 5.6 – Proton NMR, glucose at 10 g/L condition (G101)
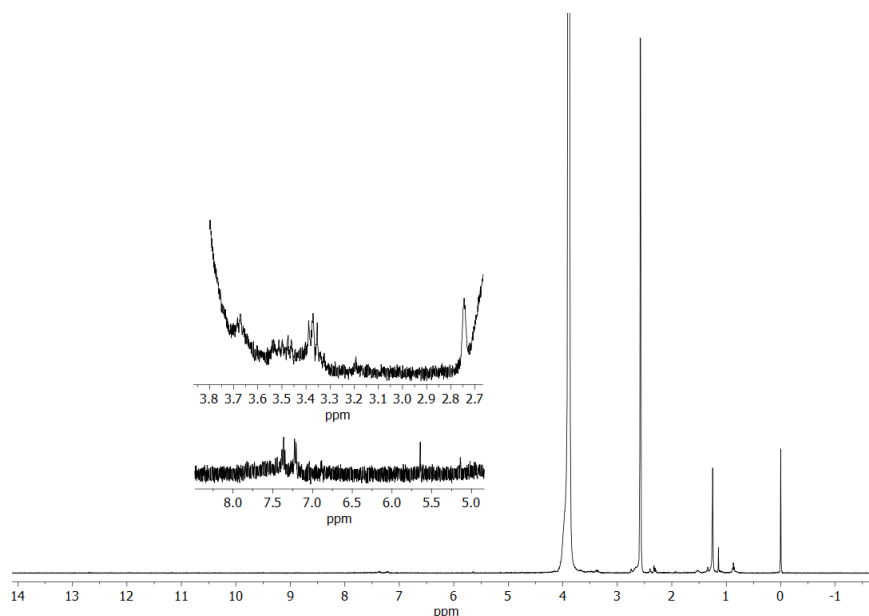
Figure 5.7 – Proton NMR, sucrose condition (S1)

5.3.2   Analysis of intracellular metabolites

Intracellular metabolites from the tricarboxylic acid cycle, glycolysis and pentose phosphate pathway, as well as nucleotides were quantified. Tables 5.2 – 5.5 show the specific concentrations of the intracellular metabolites and the concentrations of extracellular glucose at steady-state for all the conditions. The high experimental errors observed for some metabolites could be attributed to the sample processing and/or analytical errors. Another explanation considered and already presented in Chapter 4 (section 4.3.3), is a possible heterogeneity of cells inside the bioreactor caused by the consumption of fragments of the polysaccharides, which can be released from the cell wall due to the shear stress. The bioreactor present regions with different shear levels and consequently, could also present regions with different concentrations of fragments. Thus, the cells would be in the presence of

a concentration gradient of these fragments. Sugar analysis suggested the presence of fragments of polysaccharides and gentiobiose (Chapter 3).

The Tukey test with 95 % confidence interval (OriginPro 8 software) was applied to analyse the average values for the replicates. The test was applied between the conditions G101 and G102, G201 and G202, FG1 and FG2, S1 and S2. Statistically significant differences in concentrations of metabolites are highlighted in blue (Tables 5.2 – 5.5). All the conditions were at steady-state of cell concentration and CO_2, and differences observed can be due to the consumption of fragments from extracellular polysaccharides and the products from their hydrolysis. In addition, TOC (Table 5.1) analysis indicates the instability of carbon concentration in the supernatant and could be related to the presence of these fragments.

The conditions evaluated can be divided into two groups, first group composed of the conditions using glucose as the sole carbon source (G101, G102, G201 and G202) and the second group composed of the conditions using fructose/glucose and sucrose (FG1, FG2, S1 and S2). It is assumed that the first group of chemostat experiments would result in similar intracellular metabolite levels during steady-state, as well as the conditions of the second group using fructose/glucose and sucrose as carbon sources. First of all, because the sugars used as substrates were highly similar (glucose, fructose and sucrose) and all enter the central metabolism via glycolysis. Second, because the cell growth rate was the same in all experiments. To verify the similarity of the values of the intracellular metabolites for each group, it was calculated how far each specific concentration of the metabolite analysed for each condition was from the average of all the conditions (Equation 5.1). If all the metabolites from each group are close to the average, which would be expected, the D_m value is close to zero percent.

$$D_m(\%) = \frac{\sqrt{\frac{(m-\bar{x})^2+(Av-\bar{x})^2}{2}}}{Av} 100 \tag{5.1}$$

Where D_m is the difference in the specific concentration of the metabolite analysed regarding the average of the conditions for each group, m is the value of the specific concentration of the metabolite analysed (Tables 5.2 – 5.5), Av is the average of all the specific concentrations of the metabolite analysed for each group, $\bar{x}$ is the average between m and Av. The values of D_m are presented in Tables 5.2 – 5.5.

The high values of D_m observed for several metabolites analysed including glycerol-3-phosphate, trehalose-6-phosphate, ribulose-5-phosphate and succinate indicate instability of their concentrations among the conditions of each group. Assuming that the fragments of polysaccharides contributed to the increase in experimental errors, they could also have contributed to the instability observed for the concentrations of some metabolites.

Table 5.2 – Intracellular metabolites of glycolysis and extracellular glucose (m, µmol/g), experimental errors (e, %) and the difference in the specific concentration of the metabolite regarding the average of the group (D_m, %), metabolites with significantly different levels for the duplicates are indicated in blue (Tukey test with 95 % confidence interval)

Conditions	Extracellular glucose			Glucose			Glucose-6-phosphate		
	m	e	D_m	m	e	D_m	m	e	D_m
G101	1.220	±19.3	9.6	2.029	±21.4	12.8	1.737	±15.3	1.4
G102	2.392	±17.4	29.2	5.018	±19.9	41.9	1.737	±12.9	1.4
G201	1.742	±15.7	7.7	1.184	±31.7	28.3	1.393	±1.7	8.8
G202	0.683	±3.8	27.4	2.689	±54.5	0.8	1.895	±5.4	6.0
FG1	0.790	±31.8	26	1.655	±22.9	31.2	1.100	±5.1	20.2
FG2	0.583	±41.3	32.3	9.460	±64.3	57.5	1.820	±10.9	0.7
S1	1.469	±7.0	5.4	4.030	±28.3	4.2	1.753	±0.3	2.6
S2	3.746	±21.5	63.7	2.456	±5.9	22.1	2.716	±8.1	23.5

Conditions	Fructose-6-phosphate			Fructose-1,6-bisphosphate			Glyceraldehyde-3-phosphate		
	m	e	D_m	m	e	D_m	m	e	D_m
G101	0.323	±15.5	2.4	0.351	±7.7	0.9	0.017	±19.9	4.5
G102	0.388	±12.9	7.1	0.407	±26.2	6.9	0.024	±19.8	14.7
G201	0.279	±7.0	8.9	0.403	±1.9	6.3	0.024	±8.5	15.1
G202	0.368	±2.0	4.2	0.269	±16.4	12.4	0.009	±4.3	25.3
FG1	0.265	±2.8	19.2	0.338	±6.4	14.5	0.017	±4.0	7.8
FG2	0.511	±11.6	9.5	0.343	±3.3	14.0	0.014	±7.5	15.2
S1	0.310	±16.0	13.9	0.416	±17.0	6.3	0.016	±35.5	9.4
S2	0.633	±6.6	23.6	0.807	±4.1	34.8	0.033	±18.4	32.4

Conditions	Dihydroxyacetone phosphate			3-Phosphoglycerate			2-Phosphoglycerate		
	m	e	D_m	m	e	D_m	m	e	D_m
G101	0.123	±5.9	6.3	0.449	±18.1	5.1	0.041	±18.8	7.2
G102	0.184	±16.0	15.1	0.442	±3.7	5.8	0.044	±4.5	4.9
G201	0.139	±10.4	0.8	0.476	±4.2	2.3	0.050	±8.3	1.9
G202	0.119	±1.5	8.0	0.632	±17.9	13.2	0.058	±17.5	10.1
FG1	0.132	±4.0	12.1	0.487	±6.5	12.5	0.044	±8.5	15.0
FG2	0.160	±1.1	4.0	0.477	±8.2	13.2	0.050	±7.1	9.8
S1	0.121	±6.9	15.2	0.938	±31.1	22.3	0.086	±32.6	18.3
S2	0.283	±12.2	31.3	0.692	±7.9	3.4	0.071	±9.1	6.6

Conditions	Phosphoenolpyruvate		
	m	e	D_m
G101	0.030	±20.1	10.5
G102	0.011	±6.2	27.9
G201	0.017	±0.8	16.2
G202	0.042	±68.9	33.6
FG1	0.043	±25.0	11.3
FG2	0.030	±30.6	23.3
S1	0.078	±41.2	19.8
S2	0.073	±6.9	14.8

Table 5.3 – Nucleotides (m, µmol/g), experimental errors (e, %) and the difference in the specific concentration of the nucleotide regarding the average of the group (D_m, %), nucleotides with significantly different levels for the duplicates are indicated in blue (Tukey test with 95 % confidence interval)

Conditions	Adenosine monophosphate			Adenosine diphosphate			Adenosine triphosphate		
	m	e	D_m	m	e	D_m	m	e	D_m
G101	0.163	±10.1	25.7	0.980	±5.2	6.3	3.386	±5.6	9.8
G102	0.294	±24.4	6.1	0.879	±1.1	10.8	2.737	±5.9	1.7
G201	0.411	±20.2	11.4	0.879	±8.7	10.8	2.642	±14.0	3.4
G202	0.470	±11.9	20.3	1.745	±8.4	27.8	2.560	±15.6	4.8
FG1	0.160	±43.6	26.3	0.825	±7.8	12.8	2.573	±9.8	8.5
FG2	0.361	±9.6	3.5	1.345	±8.8	10.6	3.353	±0.1	8.4
S1	0.355	±3.9	2.6	1.225	±5.1	5.2	2.925	±4.0	1.5
S2	0.473	±6.2	20.1	1.044	±10.9	3.0	3.539	±0.9	11.4
Conditions	Uridine monophosphate			Uridine diphosphate			Uridine triphosphate		
	m	e	D_m	m	e	D_m	m	e	D_m
G101	0.058	±11.3	8.5	0.146	±4.3	10.8	0.658	±3.5	11.0
G102	0.065	±14.6	3.4	0.097	±6.2	9.6	0.440	±12.7	9.3
G201	0.069	±7.1	0.6	0.099	±6.0	9.0	0.464	±16.0	7.0
G202	0.087	±26.2	12.5	0.139	±16.0	7.7	0.596	±24.4	5.3
FG1	0.117	±65.4	19.7	0.126	±8.7	4.1	0.520	±5.0	11.8
FG2	0.105	±41.5	12.9	0.144	±45.7	2.5	0.965	±30.4	21.0
S1	0.083	±26.1	0.4	0.148	±12.8	4.0	0.601	±11.6	5.8
S2	0.030	±49.6	32.2	0.130	±7.6	2.4	0.632	±2.9	3.5
Conditions	Guanosine monophosphate			Guanosine diphosphate			Guanosine triphosphate		
	m	e	D_m	m	e	D_m	m	e	D_m
G101	0.152	±9.7	0.4	0.233	±7.3	7.2	0.872	±7.7	9.4
G102	0.094	±30.8	19.5	0.221	±5.2	4.2	0.679	±7.0	3.8
G201	0.111	±25.9	13.7	0.191	±10.6	3.1	0.607	±8.9	8.7
G202	0.257	±34.2	33.6	0.170	±19.9	8.2	0.780	±26.7	3.1
FG1	0.336	±74.1	22.7	0.207	±6.6	0.4	0.689	±1.9	11.6
FG2	0.140	±36.6	19.8	0.183	±40.5	6.1	1.248	±27.0	19.6
S1	0.314	±64.3	17.9	0.218	±13.7	2.1	0.800	±3.4	5.4
S2	0.135	±13.5	20.8	0.227	±4.1	4.3	0.847	±5.5	2.7

Table 5.4 – Intracellular metabolites of pentose phosphate pathway and citric acid cycle (m, µmol/g), experimental errors (e, %) and the difference in the specific concentration of the metabolite regarding the average of the group (D_m, %), metabolites with significantly different levels for the duplicates are indicated in blue (Tukey test with 95 % confidence interval)

Conditions	6-Phosphogluconate			Ribulose-5-phosphate			Ribose-5-phosphate		
	m	e	D_m	m	e	D_m	m	e	D_m
G101	1.053	±29.9	19.8	0.080	±18.8	15.7	0.323	±8.3	1.2
G102	0.680	±11.3	4.9	0.164	±37.6	20.5	0.378	±21.6	10.0
G201	0.662	±6.6	6.1	0.183	±20.9	28.6	0.356	±8.4	6.5
G202	0.622	±18.4	8.8	0.038	±15.9	33.5	0.204	±1.3	17.7
FG1	1.075	±8.3	9.4	0.079	±21.3	19.6	0.246	±0.8	13.3
FG2	1.325	±3.4	0.1	0.123	±7.7	2.8	0.339	±4.7	0.6
S1	0.820	±14.8	19.0	0.096	±38.7	13.0	0.331	±31.7	0.6
S2	2.075	±2.4	28.4	0.222	±17.3	35.4	0.423	±12.7	13.2

Conditions	Xylulose-5-phosphate			Sedoheptulose-7-phosphate			Erythrose-4-phosphate		
	m	e	D_m	m	e	D_m	m	e	D_m
G101	0.154	±17.0	13.0	0.467	±20.6	1.1	0.0037	±9.2	1.9
G102	0.297	±47.0	21.3	0.536	±17.6	6.2	0.0045	±23.5	12.5
G201	0.300	±18.9	22.1	0.418	±6.0	6.2	0.0045	±8.8	12.8
G202	0.081	±0.5	30.5	0.488	±6.9	1.1	0.0016	±24.7	27.2
FG1	0.138	±16.6	19.5	0.358	±5.6	18.6	0.0028	±10.5	16.8
FG2	0.229	±9.8	0.7	0.580	±5.8	0.9	0.0036	±2.3	7.2
S1	0.172	±12.3	11.8	0.579	±6.3	0.8	0.0046	±34.7	4.5
S2	0.364	±12.3	30.6	0.763	±4.9	16.9	0.0059	±4.4	19.5

Conditions	Citrate			Isocitrate			α-Ketoglutarate		
	m	e	D_m	m	e	D_m	m	e	D_m
G101	12.49	±16.6	5.2	0.237	±34.0	2.1	0.424	±21.4	12.3
G102	14.41	±7.4	1.7	0.201	±8.2	5.7	0.514	±11.0	4.2
G201	12.08	±8.3	6.7	0.265	±5.1	8.3	0.606	±7.2	3.9
G202	16.79	±3.4	10.2	0.205	±21.6	4.8	0.703	±18.2	12.6
FG1	18.75	±3.0	17.5	0.355	±3.0	38.8	0.523	±1.6	11.0
FG2	10.31	±6.6	12.9	0.158	±6.7	10.3	0.920	±10.7	18.7
S1	15.24	±3.4	4.9	0.119	±35.7	20.3	0.443	±6.5	17.0
S2	11.26	±11.2	9.5	0.167	±2.8	8.2	0.793	±6.9	9.2

Conditions	Succinate			Fumarate			Malate		
	m	e	D_m	m	e	D_m	m	e	D_m
G101	1.804	±9.6	34.6	1.021	±9.4	4.0	1.810	±15.1	13.4
G102	0.845	±42.5	10.4	1.110	±12.3	8.7	2.339	±16.5	2.7
G201	0.901	±26.9	7.7	0.877	±10.6	3.6	2.811	±7.9	6.8
G202	0.714	±18.8	16.5	0.771	±7.6	9.2	2.937	±13.3	9.4
FG1	2.408	±9.0	26.1	0.950	±1.5	6.7	2.578	±4.6	8.1
FG2	0.586	±19.1	31.5	0.984	±5.2	5.2	3.014	±2.5	1.0
S1	2.647	±22.4	33.7	1.053	±8.0	2.0	2.938	±13.6	2.3
S2	0.687	±9.2	28.3	1.402	±16.5	13.9	3.782	±7.6	11.4

Table 5.5 – Intracellular metabolites for trehalose synthesis, glycerol-3-phosphate and mannose-6-phosphate (m, µmol/g), experimental errors (e, %) and the difference in the specific concentration of the metabolite regarding the average of the group (D_m, %), metabolites with significantly different levels for the duplicates are indicated in blue (Tukey test with 95 % confidence interval)

Conditions	Glycerol-3-phosphate			Glucose-1-phosphate			Uridine-5-diphosphoglucose		
	m	e	D_m	m	e	D_m	m	e	D_m
G101	1.985	±28.7	10.9	0.079	±15.7	7.3	1.774	±7.9	5.6
G102	2.400	±36.0	23.6	0.085	±6.2	11.6	1.481	±3.9	3.6
G201	1.671	±6.7	1.3	0.052	±20.6	12.0	1.227	±0.3	11.6
G202	0.463	±15.4	35.8	0.059	±2.4	6.9	1.905	±4.3	9.6
FG1	1.516	±45.8	3.9	0.060	±15.3	8.3	1.366	±3.3	10.2
FG2	0.720	±30.5	24.4	0.058	±15.3	9.6	1.607	±2.8	3.1
S1	1.452	±62.3	1.6	0.061	±20.5	7.4	2.098	±18.3	11.2
S2	1.937	±2.1	18.9	0.107	±9.6	25.3	1.784	±13.5	2.1
Conditions	Trehalose-6-phosphate			Trehalose			Mannose-6-phosphate		
	m	e	D_m	m	e	D_m	m	e	D_m
G101	0.096	±19.3	7.3	79.97	±18.3	7.8	0.561	±16.1	4.1
G102	0.063	±18.3	12.1	74.38	±14.4	10.7	0.495	±18.1	2.2
G201	0.044	±15.8	23.5	44.72	±11.1	26.4	0.458	±4.4	5.9
G202	0.131	±2.3	28.3	179.58	±0.9	44.9	0.561	±3.0	4.1
FG1	0.033	±1.6	19.9	29.02	±1.7	2.8	0.417	±6.1	16.1
FG2	0.027	±12.7	25.5	35.06	±3.4	7.0	0.585	±8.1	2.4
S1	0.101	±19.8	41.7	35.82	±1.5	8.3	0.542	±3.3	5.9
S2	0.059	±9.3	3.8	23.08	±27.1	12.5	0.913	±5.5	24.3

The average of the intracellular metabolites was compared with the results presented by Lameiras et al. (2015) in Table 5.6. These authors optimized the method used in this project for quantitative analysis of metabolites from continuous culture. Lameiras et al. (2015) presented continuous cultures using *Aspergillus niger,* glucose as the carbon source and dilution rate close to the one used here, 0.043 h^{-1}. Interestingly, the concentrations of the majority of the metabolites (Table 5.6) are similar to those obtained by Lameiras et al. (2015).

Table 5.6 – Comparison of the metabolites using the average of the concentrations presented in Tables 5.2 – 5.5

	Lameiras et al. (2015)			This work (average values)						
	μmol/g			μmol/g				μmol/g		
G6P	3.482	±	0.131	1.769	±	0.164	Gluc	3.565	±	0.952
F6P	0.843	±	0.04	0.385	±	0.045	M6P	0.566	±	0.054
FBP	0.212	±	0.023	0.417	±	0.058	UDPG	1.655	±	0.103
GAP	0.018	±	0.003	0.019	±	0.003	AMP	0.336	±	0.044
DHAP	0.238	±	0.025	0.158	±	0.020	ADP	1.115	±	0.110
3PG	0.542	±	0.043	0.574	±	0.061	ATP	2.964	±	0.142
2PG	0.049	±	0.003	0.056	±	0.005	UMP	0.077	±	0.010
PEP	0.054	±	0.007	0.041	±	0.009	UDP	0.128	±	0.007
6PG	0.283	±	0.015	1.039	±	0.172	UTP	0.609	±	0.058
Ribu5P	0.144	±	0.003	0.123	±	0.022	GMP	0.192	±	0.034
Rib5P	0.329	±	0.01	0.325	±	0.025	GDP	0.206	±	0.008
Xyl5P	0.252	±	0.009	0.217	±	0.034	GTP	0.815	±	0.070
S7P	1.102	±	0.041	0.524	±	0.044				
E4P	0.008	±	0	0.004	±	0.0005				
Cit	15.982	±	0.723	13.915	±	1.027				
iCit	0.215	±	0.01	0.213	±	0.026				
αKG	0.906	±	0.087	0.616	±	0.062				
Suc	0.649	±	0.025	1.324	±	0.295				
Fum	0.844	±	0.034	1.021	±	0.066				
Mal	3.203	±	0.131	2.776	±	0.202				
Tre	66.73	±	3.377	62.703	±	18.229				
T6P	0.061	±	0.007	0.069	±	0.013				
G1P	0.07	±	0.004	0.070	±	0.007				
G3P	0.147	±	0.005	1.518	±	0.229				

2PG 2-phosphoglycerate, **3PG** 3-phosphoglycerate, **6PG** 6-phosphogluconate, **ADP** Adenosine diphosphate, **αKG** α-Ketoglutarate, **AMP** Adenosine monophosphate, **ATP** Adenosine triphosphate, **Cit** Citrate, **DHAP** Dihydroxyacetone phosphate, **E4P** Erythrose-4-phosphate, **F6P** Fructose-6-phosphate, **FBP** Fructose-1,6-bisphosphate, **Fum** Fumarate, **G1P** Glucose-1-phosphate, **G3P** Glycerol-3-phosphate, **G6P** Glucose-6-phosphate, **GAP** Glyceraldehyde-3-phosphate, **GDP** Guanosine diphosphate, **Gluc** Glucose, **GMP** Guanosine monophosphate, **GTP** Guanosine triphosphate, **iCit** Isocitrate, **M6P** Mannose-6-phosphate, **Mal** Malate, **PEP** Phosphoenolpyruvate, **Rib5P** Ribose-5-phosphate, **Ribu5P** Ribulose-5-phosphate, **S7P** Sedoheptulose-7-phosphate, **Suc** Succinate, **T6P** Trehalose-6-phosphate, **Tre** Trehalose, **UDP** Uridine diphosphate, **UDPG** Uridine-5-diphosphoglucose, **UMP** Uridine monophosphate, **UTP** Uridine triphosphate, and **Xyl5P** Xylulose-5-phosphate.

In order to evaluate the results of the intracellular metabolites presented in Tables 5.2 – 5.5, it was performed analysis of the mass-action ratios for some reactions considering the average ratios of all the conditions (G101, G102, G201, G202, FG1, FG2, S1 and S2). Table 5.7 presents the results of mass-action ratios and indicates that the majority of the reactions analysed was close to the equilibrium, except for the [PEP]/[2PG] ratio, which was almost 6 times lower than the equilibrium. As already mentioned in Chapter 4 for the analysis of the intracellular metabolites (section 4.3.3), [ATP]/[ADP] ratio provides a value much far from the equilibrium due to the cell growth reactions and [G6P][ADP]/[Gluc][ATP] ratio is also far from

the equilibrium providing the driving force that moves the metabolites through the glycolytic pathway (Karp, 2009). The average energy charge observed was 0.80 ±0.01, which is considered normal for many organisms growing under optimal conditions (De la Fuente et al., 2014). Despite the high experimental errors displayed in Tables 5.2 – 5.5, the average values of the mass-action ratios provided small errors.

Table 5.7 – Average of mass-action ratios considering all the conditions for some intracellular metabolites presented in Tables 5.2 – 5.5

Mass-action ratio (Q)	EC number	Enzyme	Q	K_{eq} literature[a]
[G6P][ADP]/[Gluc][ATP]	2.7.1.1	Hexokinase	0.25 ± 0.05	$4.7 ±0.8x10^3$
[F6P]/[G6P]	5.3.1.9	Phosphohexose isomerase	0.22 ± 0.01	0.32 ±0.08
[G1P]/[G6P]	5.4.2.2	Phosphoglucomutase	0.04 ± 0.003	0.058 ±0.0003
[2PG]/[3PG]	5.4.2.1	Phosphoglycerate mutase	0.09 ± 0.01	0.092 ±0.004
[PEP]/[2PG]	4.2.1.11	Enolase	0.72 ± 0.09	4.1 ±0.7
[Rib5P]/[Ribu5P]	5.3.1.6	Ribose 5-phosphate isomerase	3.11 ± 0.42	3 ±1
[Mal]/[Fum]	4.2.1.2	Fumarate hydratase	2.77 ± 0.22	4.3 ±0.7
[Xyl5P]/[Ribu5P]	5.1.3.1	Ribose 5-phosphate epimerase	1.82 ± 0.06	1.7 ±0.8
[M6P]/[F6P]	5.3.1.8	Phosphomannose isomerase	1.51 ± 0.08	0.8 ±0.2
[iCit]/[Cit]	4.2.1.3	Aconitate hydratase	0.02 ± 0.002	0.06 ±0.02
$[ATP][AMP]/[ADP]^2$	2.7.4.3	Adenylate kinase	0.86 ± 0.15	1.2 ±0.3
[ATP]/[ADP]			2.80 ± 0.23	10^{-5}
Energy charge			**Value**	**Literature[b]**
([ATP]+0.5[ADP])/([ATP]+[AMP]+[ADP])			0.80 ± 0.01	0.7 - 0.95

a – Equilibrium constants (K_{eq}) reported by Canelas et al. (2011), [ATP]/[ADP] reported by Meyrat and Ballmoos (2018), and [G6P][ADP]/[Gluc][ATP] reported by Kubota and Ashihara (1990). b – Energy charge range reported by De la Fuente et al. (2014).

5.3.3 Strategy for the production of extracellular polysaccharides and enzymes

Strategies for the production of not only extracellular polysaccharides but also extracellular enzymes can be proposed. For example, Figure 5.8 illustrates a strategy for the production of extracellular enzymes and polysaccharides. First, optimal conditions could be studied to maximize a continuous production of extracellular polysaccharides (Figure 5.8A), for example, using glycerol and sugars in the feed aiming at the control of extracellular polysaccharide production. Glycerol can be used to maintain a high cell density, followed by sugar-limited conditions. The shear stress is also an interesting parameter to be studied and optimized for the production of extracellular polysaccharides.

Fragments of extracellular polysaccharides from bioreactor A could also be applied as inducers of extracellular enzymes. For bioreactor B, conditions for the production of the target enzymes in fed-batch mode could be optimized since *T. harzianum* does not seem to produce many enzymes to hydrolyse polymers in continuous culture (for example, cellulase, Chapter 3). Several other bioreactors in fed-batch mode could be connected to bioreactor A to increase productivity. A filter could be used to block the cells from the continuous production of extracellular polysaccharides (A) into the bioreactor for enzyme production (B). Glycerol could also be used as a carbon supplement in bioreactor B to keep a high cell density.
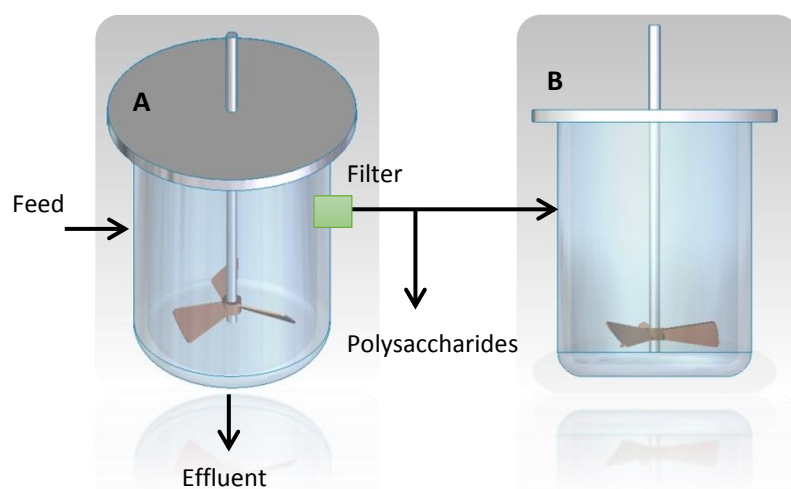
Figure 5.8 – Illustration of continuous production of extracellular polysaccharides (A) and production of extracellular enzymes in fed-batch mode (B)

5.4 Conclusions

Intracellular metabolites were analysed during the production of extracellular polysaccharides using different limiting carbon sources. Some specific concentrations of the intracellular metabolites analysed were different regarding their duplicates and the analysis provided high experimental errors. In order to explain the differences observed and high experimental errors, two hypotheses were considered. First, sample processing and analysis errors affected the results and the methods used need to be optimized for the strain employed in this project. Second, the consumption of fragments from extracellular polysaccharides under carbon-limited conditions could have influenced the estimation of intracellular concentrations of the metabolites due to the possible heterogeneity of the cells inside the bioreactor. Considering that the second hypothesis has a higher influence on the analysis, an average based on several conditions could be more suitable for representing the intracellular behaviour under those conditions. Extracellular polysaccharides are interesting products and their production should be more exploited employing *T. harzianum*. This chapter has provided the first step for the optimization of extracellular polysaccharide production and the information about the behaviour of intracellular metabolites using this wild type strain is essential to the development of optimal strains.

Chapter 6

Conclusions and Outlook

A mathematical model describing cell growth using glycerol as well as cell growth and cellulase production using cellulose was developed and presented a good fit for the majority of the experimental data (**Chapter 2**). Simulations of strategies were presented as possibilities that can be exploited in future works. The model and strategies were developed as tools to be used for cellulase maximization and to be adapted for strains less repressed. Fed-batch analysis has indicated the potential of the model to predict the profiles of cellulase production first using glycerol, followed by cellulose. However, more experiments in fed-batch mode are needed to validate the model under this condition and to find the best set of parameters to describe the inhibition influence. Nevertheless, these new experiments, including the validation, should be performed by employing the optimized strain since the wild strain imposes limitations regarding the increase in cellulase synthesis.

This is the first time that *T. harzianum* P49P11 has been used in continuous culture under carbon-limited conditions (**Chapter 3**). This microorganism has shown an interesting potential to produce enzymes that can catalyse the hydrolysis of glycosidic bonds using glucose as the carbon source. In this project, the hydrolysis of p-nitrophenyl-β-D-glucopyranoside was analysed to verify the efficiency of the enzymes produced. The enzymes hydrolyse the beta-glycosidic bond releasing p-nitrophenol. The enzymatic activity using this substrate indicates the potential of these enzymes to hydrolyse disaccharides like cellobiose, and could be used as a supplement for enzymatic cocktails to generate simple sugars from lignocellulosic materials. Although the enzymes produced in this project still need to be evaluated regarding the hydrolysis of cellobiose. This enzyme production process has the potential to be maximized through the optimization of operating conditions and strain.

The production of PNPGase could be related to the presence of extracellular polysaccharides and fragments could be inducing the synthesis of these enzymes under carbon-limited conditions (**Chapter 4**). A mathematical model can be developed aiming at the optimization of this new enzyme production process. For example, below, it is proposed an equation trying to explain the higher productivity for the condition using 20 g/L of glucose than the condition at 10 g/L (**Chapter 3**); this idea could also be used to create strategies to maximize the production. The equation describes the production of PNPGase under glucose-limited conditions (Equation 6.1) and is dependent on cell concentration and inducer concentration. It does not take into account the glucose concentration since under carbon-limited conditions, the carbon catabolite repression is considered to be minimized.

$$R_B = q_{Bm} \, g(C_I) C_X M_l \tag{6.1}$$

Where, $g(C_I)$ is the function that represents the influence of the inducers present in the supernatant and it is dependent on their concentrations, C_I (mol/kg), q_{Bm} is the maximum specific rate for PNPGase production (U/mol h), M_l is the mass of liquid (kg) and C_X is the cell concentration (mol/kg). Equation 6.1 can be used to evaluate the PNPGase production rate between the conditions using 10 ($R_B|_{10}$) and 20 g/L of glucose ($R_B|_{20}$) (Equation 6.2). Based on the average values of the conditions in duplicate, it seems that the induction was 2.79 times more potent for the condition using 20 g/L than at 10 g/L (Equation 6.3), which can indicate a higher concentration of inducers, but not an inhibiting concentration.

$$\frac{R_B|_{20}}{R_B|_{10}} = \frac{g(C_I)|_{20}\, C_X|_{20}}{g(C_I)|_{10}\, C_X|_{10}} \tag{6.2}$$

$$\frac{1307}{242} = \frac{g(C_I)|_{20}\, 0.31}{g(C_I)|_{10}\, 0.16}$$

$$\frac{g(C_I)|_{20}}{g(C_I)|_{10}} = 2.79 \tag{6.3}$$

Equation 6.4 is an example of a mathematical structure that could represent the influence of the concentration of inducers on the synthesis of enzymes but needs to be tested. The equation shows a high inhibition effect at high concentrations of inducers. A high concentration of inducers could lead to a high concentration of glucose (for example) due to hydrolysis, thus inhibiting enzyme synthesis.

$$g(C_I) = \left(\frac{k_1 C_I}{\frac{C_I^{\,n}}{k_2} + 1} \right) \tag{6.4}$$

Where, k_1 is a proportional constant (kg/mol) and k_2 is an inhibition constant ($(\text{mol/kg})^n$). The optimal C_I concentration ($C_{I,op}$) will provide the highest value for the function $g(C_I)$, which is proportional to PNPGase production rate (Equation 6.5). The optimal value of C_I can be found by the derivative of the function $g(C_I)$ equal to zero:

$$\frac{d\big(g(C_I)\big)}{dC_I} = \left(\frac{k_1}{\frac{C_I^{\,n}}{k_2} + 1} \right) - \left(\frac{k_1 n C_I^{\,n}}{k_2 \left(\frac{C_I^{\,n}}{k_2} + 1 \right)^2} \right) = 0$$

$$C_{I,op} = \sqrt[n]{\frac{k_2}{(n-1)}} \tag{6.5}$$

Considering $n = 2$ and $g(C_{I,op}) = 1$:

$$k_1 = \frac{2}{C_{I,op}}$$

$$k_2 = C_{I,op}^{\,2}$$

$$R_B = q_{Bm} \left(\frac{2 C_{I,op}\, C_I}{C_I^{\,2} + C_{I,op}^{\,2}} \right) C_X M_l \tag{6.6}$$

The C_I concentration could be closer to the optimal value for the condition using 20 g/L of glucose than for the conditions at 10 g/L, which could explain the higher productivity. Another explanation could be that the relation between the number of the enzymes secreted and the enzymatic activity is not linear. Figure 6.1 shows a possible profile generated by the function $g(C_I)$ as a function of C_I, indicating that at low inducer concentrations, the function achieves high values. The delay in PNPGase production observed in the condition G202 (Figure 3.4, Chapter 3) could be related to a high concentration of inducers at the transition phase, which are converted into glucose (for example), thus inhibiting the synthesis of the enzymes.
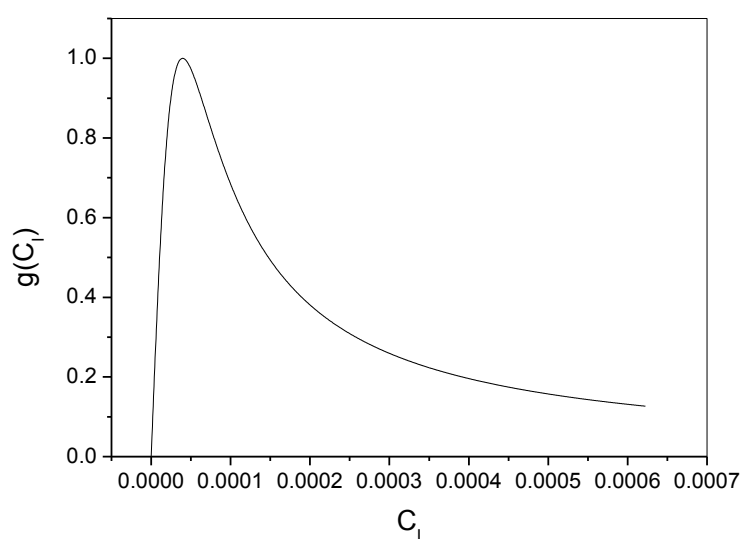
Figure 6.1 – A possible profile generated by the function $g(C_I)$ as a function of inducer concentration (C_I)

The concentration of the possible inducers is difficult to estimate due to their low concentrations and hydrolysis of them, thus equations are important to have an idea about their influence based on interpretations and available data. The addition of a feed of inducers could be an interesting strategy to manipulate their concentrations inside the bioreactor to evaluate the best concentrations that can lead to optimal PNPGase productivity.

Proteomics analysis has suggested that the use of different carbon sources can lead to the production of different enzymes (**Chapter 4**). This interesting result can be more exploited in future works employing different conditions and carbon sources to increase productivity. Several uncharacterized proteins were also suggested by the analysis and methods to identify them and their functions could reveal new promising products. A mechanism for continuous PNPGase production at glucose-limited conditions was proposed based on the influence of extracellular polysaccharides. This mechanism can be useful for proposing strategies aiming at the maximization of the production of enzymes using continuous culture.

This is the first time that the production of extracellular polysaccharides by *T. harzianum* P49P11 has been observed and investigated (**Chapter 5**). These are interesting by-products discovered in this project and they have the potential to become a new product synthesized by this strain. New studies to maximize their production and evaluate their commercial value need to be performed. Based on the analysis of the polysaccharides, their structures seem to be independent of the carbon sources used; however, the soluble fragments from these polysaccharides were not analysed, and only the solid structures from ethanol precipitation were analysed. The presence of different fragments could explain the induction of different enzymes observed by the shotgun proteomics analysis.

Finally, this project provides a new mathematical model and simulation platforms to be used for cellulase maximization by filamentous fungi. A new enzymatic production process was exploited under carbon-limited conditions and raise interesting possibilities of synthesizing the inducer substrate and the induced enzymes in a single step. A hypothesis raised from this project is that different carbon sources easily assimilated by the cells could

lead to the synthesis of different inducers (fragments of extracellular polysaccharides), which could induce the synthesis of different enzymes under carbon-limited conditions (Figure 6.2). In addition, a new product synthesized by this strain was identified, extracellular polysaccharides. Since the characteristics of extracellular polysaccharides depend not only on the microorganism but also on the operating conditions, the polysaccharides produced in this project can be unique.
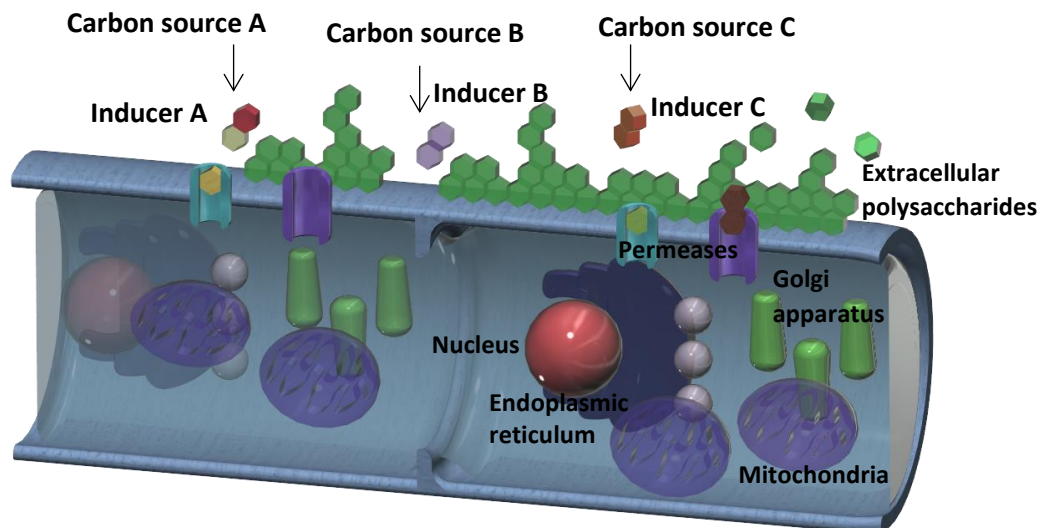
Figure 6.2 – Illustration of a hypha (sectional view), indicating the possibility that different carbon sources can lead to the synthesis of different inducers (fragments of extracellular polysaccharides), which can induce the production of different extracellular enzymes under carbon-limited conditions

Supplementary material

Chapter 2

It is presented the complete code (Matlab) used for parameter estimation for the experiments in batch mode using different initial concentrations of cellulose (Chapter 2). The same code structure was used for parameter estimation of the batch mode experiments using glycerol. The main program, *Master*, the function to be minimized, *M8*, and the simulation platform, *slim29* (Simulink), are described below. These programs are presented as examples that can be adapted to solving other parameter estimation problems.

```matlab
%Master

global X1 S1 F1 B1 Xy1 t1
global X2 S2 F2 B2 Xy2 t2
global X3 S3 F3 B3 Xy3 t3

global exp1 texp1 exp2 texp2 exp3 texp3 Soma1 Soma2 Soma3

%_____
% Experiment 1, t = time, F = cellulase, B = beta-glucosidase, X = cells, S  =
cellulose

t1 = xlsread('20gL.xlsx','A1:A10');
F1 = xlsread('20gL.xlsx','B1:B10');
B1 = xlsread('20gL.xlsx','C1:C10');
X1 = xlsread('20gL.xlsx','E1:E10');
S1 = xlsread('20gL.xlsx','F1:F10');

%_____
% Experiment 2

t2 = xlsread('10gL.xlsx','A1:A10');
F2 = xlsread('10gL.xlsx','B1:B10');
B2 = xlsread('10gL.xlsx','C1:C10');
X2 = xlsread('10gL.xlsx','E1:E10');
S2 = xlsread('10gL.xlsx','F1:F10');

%_____
% Experiment 3

t3 = xlsread('30gL.xlsx','A1:A10');
F3 = xlsread('30gL.xlsx','B1:B10');
B3 = xlsread('30gL.xlsx','C1:C10');
X3 = xlsread('30gL.xlsx','E1:E10');
S3 = xlsread('30gL.xlsx','F1:F10');

%_____
Tfinal = 96;
h = 1;
N = Tfinal/h;
options = optimset('Algorithm','interior-point','MaxFunEvals',8000);
%_____
% Parameters

b = xlsread('par8.xlsx','A1:A22');
lb = xlsread('par8.xlsx','B1:B22');
ub = xlsread('par8.xlsx','C1:C22');
```

```matlab
[Bmi,fval,flag] = fmincon(@M8,b,[],[],[],[],lb,ub,[],options,h,Tfinal,N);

%_____

% Outputs

disp(fval)
disp (flag)
disp (Soma1)
disp (Soma2)
disp (Soma3)

d = texp1;
e = exp1;
f = texp2;
g = exp2;
h = texp3;
n = exp3;
m = Bmi;


warning('off','MATLAB:xlswrite:AddSheet');
xlswrite('data.xlsx', d, 'Ensaio 20 gL', 'A1');
xlswrite('data.xlsx', e, 'Ensaio 20 gL', 'B1');
xlswrite('data.xlsx', f, 'Ensaio 10 gL', 'A1');
xlswrite('data.xlsx', g, 'Ensaio 10 gL', 'B1');
xlswrite('data.xlsx', h, 'Ensaio 30 gL', 'A1');
xlswrite('data.xlsx', n, 'Ensaio 30 gL', 'B1');
xlswrite('data.xlsx', m, 'parâmetros', 'A1');
```

Function *M8* contains the objective function to be minimized and calls the simulation platform.

```matlab
function M=M8 (b,h,Tfinal,N)
global exp1 texp1 exp2 texp2 exp3 texp3 Soma1 Soma2 Soma3 Soma4

opt = simset('solver', 'ode8','FixedStep',h);

%Parameters

T = [0:h:Tfinal-h]';
b1 = b(1)*ones(N,1);
Tb1 = [T b1];
b2 = b(2)*ones(N,1);
Tb2 = [T b2];

b3 = b(3)*ones(N,1);
Tb3 = [T b3];
b4 = b(4)*ones(N,1);
Tb4 = [T b4];

b5 = b(5)*ones(N,1);
Tb5 = [T b5];
b6 = b(6)*ones(N,1);
Tb6 = [T b6];

b7 = b(7)*ones(N,1);
Tb7 = [T b7];
b8 = b(8)*ones(N,1);
Tb8 = [T b8];

b9 = b(9)*ones(N,1);
Tb9 = [T b9];
b10 = b(10)*ones(N,1);
Tb10 = [T b10];

b11 = b(11)*ones(N,1);
```

```matlab
Tb11 = [T b11];
b12 = b(12)*ones(N,1);
Tb12 = [T b12];

b13 = b(13)*ones(N,1);
Tb13 = [T b13];
b14 = b(14)*ones(N,1);
Tb14 = [T b14];

b15 = b(15)*ones(N,1);
Tb15 = [T b15];
b16 = b(16)*ones(N,1);
Tb16 = [T b16];

b17 = b(17)*ones(N,1);
Tb17 = [T b17];
b18 = b(18)*ones(N,1);
Tb18 = [T b18];
b19 = b(19)*ones(N,1);
Tb19 = [T b19];

b20 = b(20)*ones(N,1);
Tb20 = [T b20];
b21 = b(21)*ones(N,1);
Tb21 = [T b21];

%_____
%Experiment 1

b22 = 0.4*ones(N,1);
Tb22 = [T b22];
b23= 20*ones(N,1);
Tb23 = [T b23];


[tout,xout,yout] = sim('slim29',[0
Tfinal],opt,Tb1,Tb2,Tb3,Tb4,Tb5,Tb6,Tb7,Tb8,Tb9,Tb10,Tb11,Tb12,Tb13,Tb14,Tb15,
Tb16,Tb17,Tb18,Tb19,Tb20,Tb21,Tb22,Tb23);


global X1 S1 F1 B1 t1

exp1 = yout;
texp1 = tout;


%Interpolate

Xpred1 = interp1(tout,yout (:,1),t1);
Spred1 = interp1(tout,yout (:,2),t1);
Fpred1 = interp1(tout,yout (:,3),t1);
Bpred1 = interp1(tout,yout (:,4),t1);


% Minimize objective function

S = 0;

for i = 1:length(t1)


  S = S +((((Spred1(i)- S1(i)))^2)/(20^2))+(((Xpred1(i)- X1(i)))^2)/...
  (9^2) + (((Fpred1(i)-F1(i)))^2)/(900^2)+ (((Bpred1(i)-B1(i)))^2)/(2000^2);

end

Soma1 = real(S);
%_____
```

```matlab
%Experiment 2


b22 = 0.4*ones(N,1);
Tb22 = [T b22];
b23= 10*ones(N,1);
Tb23 = [T b23];



[tout,xout,yout] = sim('slim29',[0
Tfinal],opt,Tb1,Tb2,Tb3,Tb4,Tb5,Tb6,Tb7,Tb8,Tb9,Tb10,Tb11,Tb12,Tb13,Tb14,Tb15,
Tb16,Tb17,Tb18,Tb19,Tb20,Tb21,Tb22,Tb23);


global X2 S2 F2 B2 t2

exp2 = yout;
texp2 = tout;

% Interpolate

Xpred2 = interp1(tout,yout (:,1),t2);
Spred2 = interp1(tout,yout (:,2),t2);
Fpred2 = interp1(tout,yout (:,3),t2);
Bpred2 = interp1(tout,yout (:,4),t2);


% Minimize

S = 0;

for i = 1:length(t2)


  S = S +((((Spred2(i)- S2(i)))^2)/(10^2))+(((Xpred2(i)- X2(i)))^2)/...
 (6^2) + (((Fpred2(i)-F2(i)))^2)/(900^2)+ (((Bpred2(i)-B2(i)))^2)/(2000^2);

end

Soma2 = real(S);

%_____
%Experiment 3


b22 = 0.4*ones(N,1);
Tb22 = [T b22];
b23= 30*ones(N,1);
Tb23 = [T b23];



[tout,xout,yout] = sim('slim29',[0
Tfinal],opt,Tb1,Tb2,Tb3,Tb4,Tb5,Tb6,Tb7,Tb8,Tb9,Tb10,Tb11,Tb12,Tb13,Tb14,Tb15,
Tb16,Tb17,Tb18,Tb19,Tb20,Tb21,Tb22,Tb23);

global X3 S3 F3 B3 t3

exp3 = yout;
texp3 = tout;

% Interpolate

Xpred3 = interp1(tout,yout (:,1),t3);
Spred3 = interp1(tout,yout (:,2),t3);
Fpred3 = interp1(tout,yout (:,3),t3);
Bpred3 = interp1(tout,yout (:,4),t3);
```

```matlab
% Minimize

S = 0;

for i = 1:length(t3)


  S = S +(((((Spred3(i)- S3(i)))^2)/(30^2))+((((Xpred3(i)-
X3(i)))^2)/(10^2)))...
      +((((Fpred3(i)- F3(i)))^2)/(800^2))+ (((Bpred3(i)-B3(i)))^2)/(2000^2);

end

Soma3 = real(S);
%_____


M = Soma1+Soma2+Soma3;

end
```

The simulation of the mathematical model was performed in the simulation platform of Simulink (*slim29*):
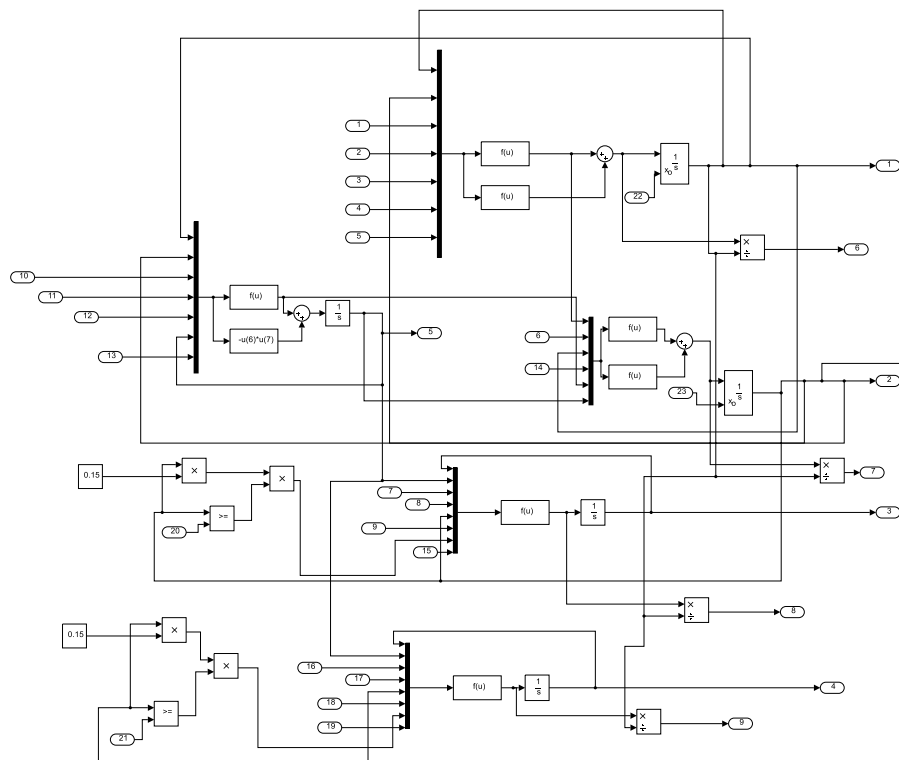
The Matlab code used for the maximization of cellulase production is presented below. It is based on Becerra (2004). It contains the main program, the objective function to be maximized (cellulase activity) and a function with the constraints. The example has a constant feed of glycerol (simulation platform) and a periodic feed of cellulose, which is optimized. The algorithm finds a set of optimal concentrations of cellulose in the feed that maximizes the cellulase activity at the final time (96 h). The feed is periodic and it is added with an interval of 8 h. Every concentration of the feed is individually optimized.

```matlab
%Based on Becerra (2004), the main program

%Time and integration step

Tfinal = 96;
h = 1;
N = Tfinal/h;

Xmax = 10;
Xmin = 0;

options = optimset('Algorithm','interior-point','MaxFunEvals',2000);
% Vector of the manipulated variable
u = zeros(N,1);
aa = zeros(2,1);
%Initial substrate concentration
u(1) = 10;
%Finding the best feeding concentration for every 8 h
test = 2;

while(test > 1)
for j=1:2
for i=8:8:Tfinal-8

 x0 = 0;

[bb,f,fig] =
fmincon(@obj_fun2,x0,[],[],[],[],Xmin,Xmax,@con_fun2,options,h,Tfinal,u,i,N);

u(i) = bb;

end
aa(j) = f;
end
test = abs(aa(2)-aa(1));

end


T = [0:h:Tfinal-h]';
TU = [T u];

opt = simset('solver', 'ode8', 'SrcWorkspace', 'Current', 'FixedStep',h);
[tout,xout,yout] = sim('otimo',[0 Tfinal],opt,TU);

plot(T,u);
disp(f)
disp(fig);


d = tout;
e = yout;
f = T;
g = u;
warning('off','MATLAB:xlswrite:AddSheet');
xlswrite('data.xlsx', d, 'otimo', 'A1');
xlswrite('data.xlsx', e, 'otimo', 'B1');
xlswrite('data.xlsx', f, 'feed', 'A1');
xlswrite('data.xlsx', g, 'feed', 'B1');
```

The objective function to be maximized (cellulase activity) at the final time.

```matlab
%Objective function

function f = obj_fun2(uot,h,Tfinal,u,i,N)
```

```
opt = simset('solver', 'ode8', 'SrcWorkspace', 'Current', 'FixedStep',h);
u(i) = uot;
T = [0:h:Tfinal-h]';
TU = [T u];
[tout,xout,yout] = sim('otimo',[0 Tfinal],opt,TU);

f = -yout(Tfinal,2);


end
```

The function containing the constraints is presented below. Substrate concentration inside the bioreactor is not allowed to be higher than 10 g/L.

```
%Constraints
function [g,psi] = con_fun2(uot,h,Tfinal,u,i,N)
u(i) = uot;
opt = simset('solver', 'ode8', 'SrcWorkspace', 'Current', 'FixedStep',h);
T = [0:h:Tfinal-h]';
TU = [T u];
[tout,xout,yout] = sim('otimo',[0 Tfinal],opt,TU);
g = [yout(:,1)-10];
psi= [];

end
```

The simulation of the equations was performed in the simulation platform (*otimo*):
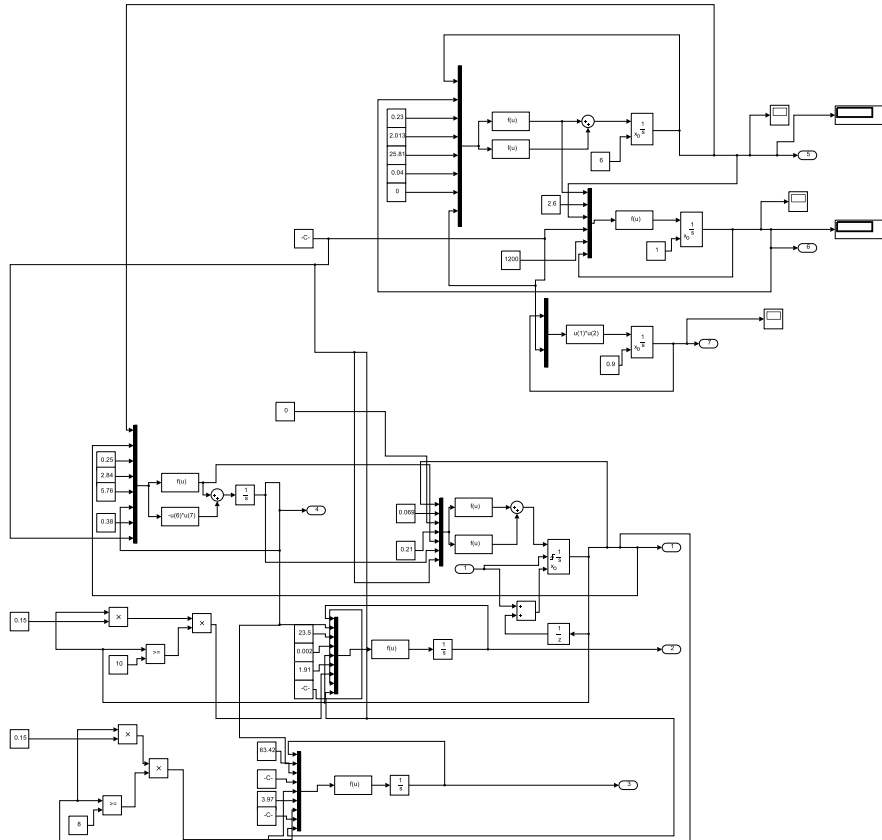
Chapter 3

The equations and considerations for the material balance presented in Chapter 3 were based on Figure S3.8.
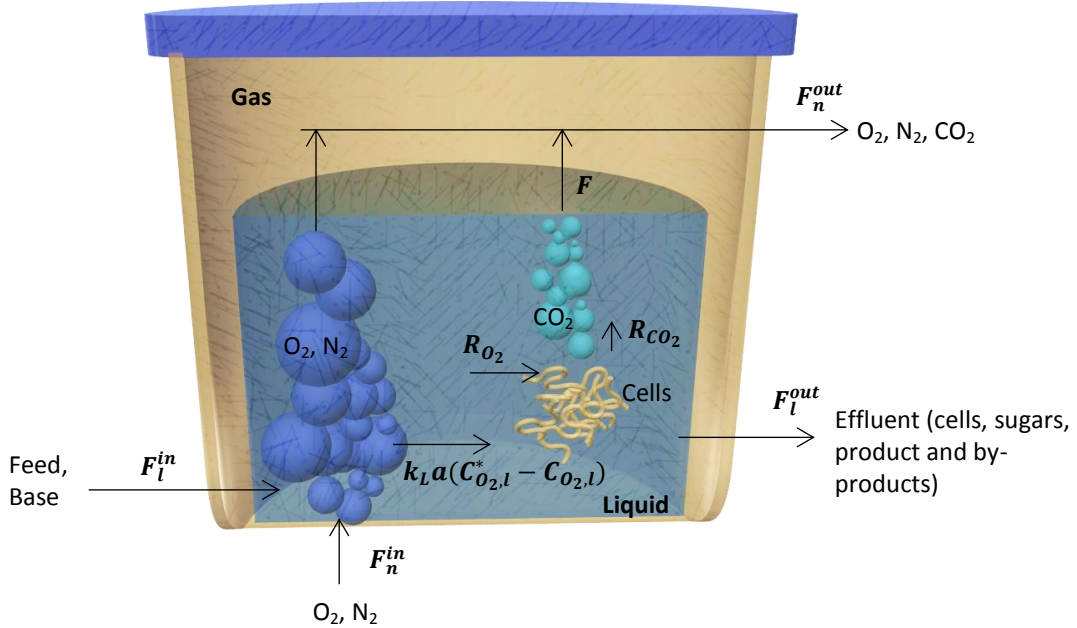
Figure S3.8 – Control volume for the material balance

Equation S3.5 describes the total material balance for the inflow and outflow of liquid and gas considering the bioreactor as the system of control.

$$\frac{dM_T}{dt} = \left(F_l^{in} - F_l^{out}\right) + \left(F_n^{in} - F_n^{out}\right) \tag{S3.5}$$

Where, M_T is the total mass (kg), F_l^{in} is the inflow rate of liquid (kg/h), F_l^{out} is the outflow rate of liquid (kg/h), F_n^{in} is the inflow rate of gas (kg/h), F_n^{out} is the outflow rate of gas (kg/h). The inflow of gas was considered composed of oxygen and nitrogen and the outflow composed of oxygen, carbon dioxide and nitrogen. Since nitrogen is neutral, it was not included in the material balance. Equation S3.6 considers oxygen consumption and carbon dioxide production rates.

$$\frac{dM_T}{dt} = \left(F_l^{in} - F_l^{out}\right) + R_{O_2} M_{O_2} - R_{CO_2} M_{CO_2} \tag{S3.6}$$

Where, M_{O_2} is the oxygen molar mass (kg/mol), M_{CO_2} is the carbon dioxide molar mass (kg/mol), R_{O_2} is the oxygen consumption rate (mol/h), R_{CO_2} is the carbon dioxide production rate (mol/h). The inflow rate of liquid considers the addition of the feed and base (Equation S3.7).

$$F_l^{in} = F_m^{in} + F_b^{in} \tag{S3.7}$$

Where, F_m^{in} is the inflow rate of medium (kg/h), F_b^{in} is the inflow rate of base (kg/h). The inflow rate of the medium is calculated according to Equation S3.6 considering steady-state:

$$F_m^{in} = -F_b^{in} + F_l^{out} - R_{O_2} M_{O_2} + R_{CO_2} M_{CO_2} \tag{S3.8}$$

Equation S3.9 describes the material balance for cell growth.

$$R_X = F_l^{out} C_X \tag{S3.9}$$

The specific cell growth rate was considered the same as the dilution rate (Equation 3.10).

$$q_X = \mu_X = D = \frac{F_l^{out}}{M_l} \tag{S3.10}$$

Where, M_l is the mass of liquid (kg), C_X is the cell concentration in the liquid (mol/kg), R_X is the cell production rate (mol/h), q_X and μ_X are the specific cell growth rate (h⁻¹), D is the dilution rate (h⁻¹). The PNPGase material balance was based on the enzymatic activity (Equation S3.11 and S3.12).

$$R_B = F_l^{out} C_B \tag{S3.11}$$

$$q_B = \frac{R_B}{C_X M_l} \tag{S3.12}$$

Where, C_B is the PNPGase activity in the liquid phase (U/kg), R_B is the PNPGase production rate (U/h), q_B is the specific PNPGase production rate (U/mol h). The oxygen material balance is described below. For the liquid phase:

$$\frac{d(M_l C_{O_2,l})}{dt} = F_l^{in} C_{O_2,l}^{in} - F_l^{out} C_{O_2,l} - R_{O_2} + M_l k_L a (C_{O_2,l}^* - C_{O_2,l})$$

Where, $C_{O_2,l}$ is the oxygen concentration in the liquid phase (mol/kg), $C_{O_2,l}^{in}$ is the oxygen concentration in the liquid phase from the inflow rate (mol/kg), $k_L a$ is the mass transfer coefficient for oxygen (h⁻¹), $C_{O_2,l}^*$ is the equilibrium concentration of oxygen in the liquid (mol/kg). For the gas phase:

$$\frac{d(N_g x_{O_2}^{out})}{dt} = F_g^{in} x_{O_2}^{in} - F_g^{out} x_{O_2}^{out} - M_l k_L a (C_{O_2,l}^* - C_{O_2,l})$$

Where, N_g is the amount of gas in the headspace and bubbles of the bioreactor (mol), F_g^{in} is the inflow rate of gas (mol/h), F_g^{out} is the outflow rate of gas (mol/h), $x_{O_2}^{in}$ is the inflow of oxygen fraction in the gas phase (mol/mol), $x_{O_2}^{out}$ is the outflow of oxygen fraction in the gas phase (mol/mol). At steady-state and neglecting the oxygen dissolved in the inflow and outflow of liquid, the combination of gas with liquid phase is:

$$R_{O_2} = F_g^{in} x_{O_2}^{in} - F_g^{out} x_{O_2}^{out} \tag{S3.13}$$

$$q_{O_2} = \frac{R_{O_2}}{C_X M_l} \tag{S3.14}$$

Where, q_{O_2} is the specific oxygen consumption rate (mol/mol h). The carbon dioxide material balance is described below. For the liquid phase:

$$\frac{d(M_l C_{CO_2,l})}{dt} = F_l^{in} C_{CO_2,l}^{in} - F_l^{out} C_{CO_2,l} + R_{CO_2} - F$$

Where, $C_{CO_2,l}$ is the carbon dioxide concentration in the liquid phase (mol/kg), $C_{CO_2,l}^{in}$ is the carbon dioxide concentration in the liquid phase from the inflow rate (mol/kg), F is the

carbon dioxide flow rate produced by the cells and transferred from the liquid to the gas phase (mol/h). For the gas phase:

$$\frac{d(N_g x_{CO_2}^{out})}{dt} = F_g^{in} x_{CO_2}^{in} - F_g^{out} x_{CO_2}^{out} + F$$

Where, $x_{CO_2}^{in}$ is the inflow of carbon dioxide fraction in the gas phase (mol/mol), $x_{CO_2}^{out}$ is the outflow of carbon dioxide fraction in the gas phase (mol/mol). At steady-state and neglecting the carbon dioxide dissolved in the liquid and from the inlet of gas, the combination of gas with liquid phase is:

$$R_{CO_2} = F_g^{out} x_{CO_2}^{out} \tag{S3.15}$$

$$q_{CO_2} = \frac{R_{CO_2}}{C_X M_l} \tag{S3.16}$$

Where, q_{CO_2} is the specific carbon dioxide production rate (mol/mol h). Equation S3.17 describes the material balance for carbon.

$$R_C = F_m^{in} C_{C,l}^{in} - F_l^{out} C_{C,l} \tag{S3.17}$$

$$q_C = \frac{R_C}{C_X M_l} \tag{S3.18}$$

Where, $C_{C,l}$ is the carbon concentration in the liquid phase (Cmol/kg), R_C is the carbon consumption rate (Cmol/h), $C_{C,l}^{in}$ is the carbon concentration in the liquid phase from the inflow rate (Cmol/kg), q_C is the specific carbon consumption rate (Cmol/mol h).

Equation S3.19 describes the material balance for carbon dioxide (R_{CO_2}) considering the exponential phase of cell growth. The maximum specific carbon dioxide production rate ($q_{CO_2 m}$) was considered constant.

$$R_{CO_2} = F_g^{out} x_{CO_2}^{out} = q_{CO_2 m} C_X M_l$$

$$C_X = C_{X,0} e^{\mu_{Xm} t}$$

$$x_{CO_2}^{out} = \frac{q_{CO_2 m} M_l C_{X,0}}{F_g^{out}} (e^{\mu_{Xm} t})$$

$$\frac{q_{CO_2 m} M_l C_{X,0}}{F_g^{out}} = \theta$$

$$x_{CO_2}^{out} = \theta (e^{\mu_{Xm} t}) \tag{S3.19}$$

Where, μ_{Xm} is the maximum specific cell growth rate (h^{-1}), $q_{CO_2 m}$ is the maximum specific carbon dioxide production rate (mol/mol h), $C_{X,0}$ is the initial cell concentration (mol/kg).

For the standard deviation (σ), Equation S3.20 was used and Equation S3.21 was used for the standard error (σ_x).

$$\sigma = \sqrt{\frac{\sum_{i=1}^n (x_i - \bar{x})^2}{n - 1}} \tag{S3.20}$$

$$\sigma_x = \frac{\sigma}{\sqrt{n}}$$

(S3.21)

Where, x_i is the experimental value, $\bar{x}$ is the average, n is the number of samples.

Chapter 4

Sugar chromatograms for the samples of Table 4.2 are presented below.

At the end of the batch phase (A) (left) and transition phase (B) (right)

The starting point of PNPGase production (C)
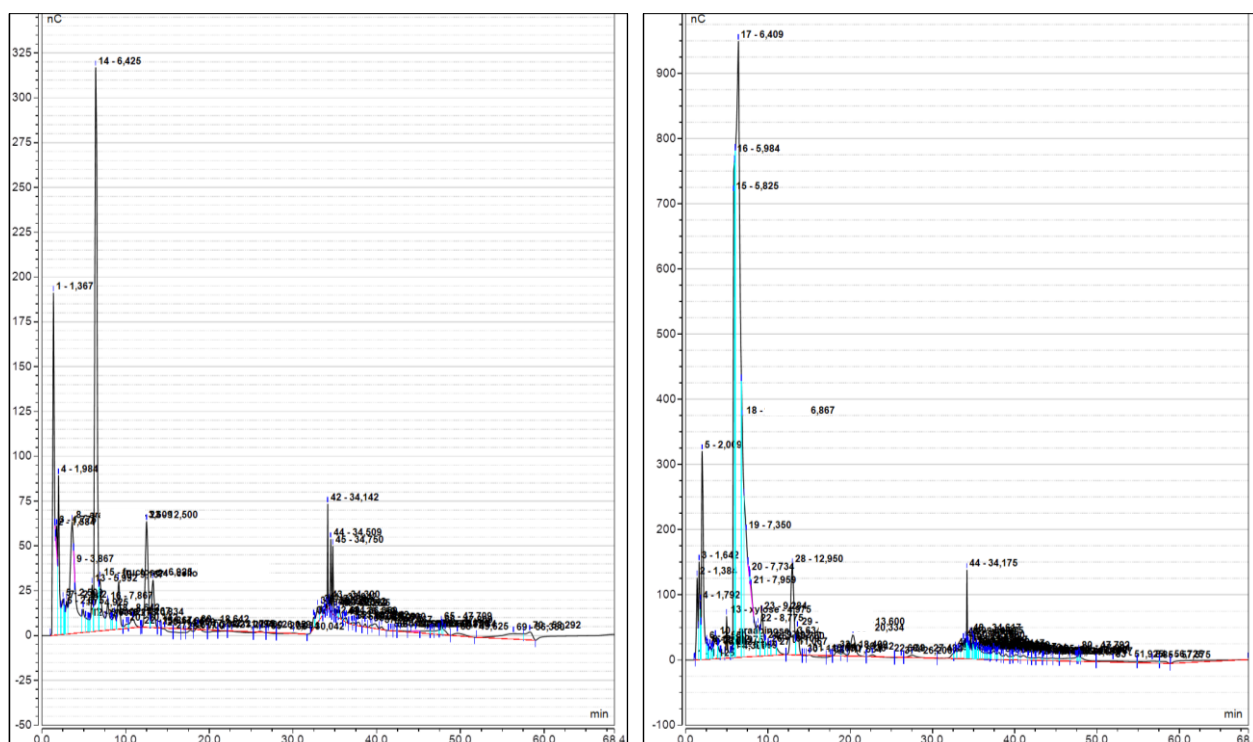
Table S4.1 – Description of enzymes and uncharacterized proteins from shotgun proteomics analysis (Chapter 4), gene name (GN), sequence version (SV) and protein existence number (PE)

Accession	Coverage (%)	Peptides	Unique Peptides	PTM	Blank Intensity	G101 Intensity	S1 Intensity	FG1 Intensity	Avg. Mass	Description
A0A0G0A6L8| A0A0G0A6L8_ TRIHA	43	30	29	Carbamidomethylation; Oxidation (M)	5,00E+06	5,51E+08	2,98E+07	6,51E+08	83322	Glycosyl hydrolase OS=*Trichoderma harzianum* GN=THAR02_00025 PE=4 SV=1
A0A0F9XGV0| A0A0F9XGV0_ TRIHA	44	26	26	Carbamidomethylation; Oxidation (M)	3,34E+06	1,16E+09	3,95E+06	3,79E+08	84899	Uncharacterized protein OS=*Trichoderma harzianum* GN=THAR02_04148 PE=4 SV=1
A0A0F9Y0X0| A0A0F9Y0X0_T RIHA	37	26	24	Carbamidomethylation; Oxidation (M)	2,35E+06	8,65E+08	1,23E+07	2,77E+08	92791	Beta-glucosidase OS=*Trichoderma harzianum* GN=THAR02_02132 PE=3 SV=1
A0A0G0AG54| A0A0G0AG54_ TRIHA	29	23	23	Carbamidomethylation; Oxidation (M)	2,43E+06	3,96E+08	6,78E+06	2,00E+08	104855	Glycosyl hydrolase family 31 OS=*Trichoderma harzianum* GN=THAR02_03951 PE=3 SV=1
A0A0F9XTX0| A0A0F9XTX0_T RIHA	30	23	23	Carbamidomethylation; Oxidation (M)	3,44E+06	7,76E+08	1,14E+07	3,88E+08	92201	Uncharacterized protein OS=*Trichoderma harzianum* GN=THAR02_04381 PE=4 SV=1
A0A0F9XC99| A0A0F9XC99_T RIHA	21	11	11	Oxidation (M)	5,73E+06	1,20E+09	7,29E+08	1,09E+09	61993	Isoamyl alcohol oxidase OS=*Trichoderma harzianum* GN=THAR02_05677 PE=3 SV=1
Q599K8|Q599 K8_TRIHA	18	12	12		3,91E+06	5,03E+08	1,88E+08	6,90E+08	66255	Glucoamylase OS=*Trichoderma harzianum* GN=gla66 PE=2 SV=1
A0A0F9XF89|A 0A0F9XF89_TR IHA	35	18	18	Carbamidomethylation; Oxidation (M)	1,42E+06	7,08E+08	4,98E+06	1,93E+08	83087	Uncharacterized protein OS=*Trichoderma harzianum* GN=THAR02_04684 PE=4 SV=1
A0A0F9ZTK2|A 0A0F9ZTK2_TR IHA	24	17	17	Carbamidomethylation; Oxidation (M)	4,13E+05	4,52E+07	0	2,94E+07	104391	Glycosyl hydrolase family 3 N terminal domain-containing protein OS=*Trichoderma harzianum* GN=THAR02_04349 PE=4 SV=1
A0A0F9ZY32|A 0A0F9ZY32_TR IHA	10	10	8	Carbamidomethylation; Oxidation (M)	6,42E+05	1,35E+08	4,11E+05	3,62E+07	107210	Glucan 1,3-beta-glucosidase OS=*Trichoderma harzianum* GN=THAR02_03008 PE=4 SV=1
A0A0F9X6Z0|A 0A0F9X6Z0_TR IHA	21	3	3	Carbamidomethylation	7,62E+06	1,34E+09	1,05E+07	6,07E+08	18452	Uncharacterized protein OS=*Trichoderma harzianum* GN=THAR02_07588 PE=4 SV=1
A0A0F9XCM0| A0A0F9XCM0_ TRIHA	37	9	9	Carbamidomethylation; Oxidation (M)	2,06E+06	5,02E+08	3,69E+05	1,57E+08	35814	WSC domain-containing protein OS=*Trichoderma harzianum* GN=THAR02_05022 PE=4 SV=1
A0A0G0ARJ7| A0A0G0ARJ7_ TRIHA	28	11	11	Carbamidomethylation	1,18E+06	1,91E+08	4,13E+07	1,35E+08	40277	Uncharacterized protein OS=*Trichoderma harzianum* GN=THAR02_00769 PE=4 SV=1
A0A0F9Y3W7| A0A0F9Y3W7_ TRIHA	26	11	11	Carbamidomethylation	4,51E+05	9,12E+07	2,04E+06	7,28E+07	41830	Uncharacterized protein OS=*Trichoderma harzianum* GN=THAR02_01090 PE=4 SV=1
F2YBR1|F2YBR 1_TRIHA	20	9	3	Oxidation (M)	1,07E+07	1,32E+08	1,89E+07	8,45E+07	67638	Mutanase OS=*Trichoderma harzianum* GN=mutAW PE=4 SV=1

Continuation of Table S4.1

Accession	Coverage (%)	Peptides	Unique Peptides	PTM	Blank Intensity	G101 Intensity	S1 Intensity	FG1 Intensity	Avg. Mass	Description
A0A0F9XS42|A0A0F9XS42_TRIHA	29	10	10	Carbamidomethylation	3,43E+06	2,07E+08	2,34E+06	1,73E+08	37342	Acetyl esterase OS=*Trichoderma harzianum* GN=THAR02_00584 PE=4 SV=1
A0A0G0A2A5|A0A0G0A2A5_TRIHA	16	12	12	Carbamidomethylation; Oxidation (M)	0	6,37E+07	1,91E+06	2,40E+07	82543	Uncharacterized protein OS=*Trichoderma harzianum* GN=THAR02_08461 PE=4 SV=1
A0A0F9ZJ74|A0A0F9ZJ74_TRIHA	21	11	11	Carbamidomethylation	3,22E+05	1,33E+08	0	3,78E+07	64163	Beta-hexosaminidase OS=*Trichoderma harzianum* GN=THAR02_07531 PE=3 SV=1
A0A0F9ZS41|A0A0F9ZS41_TRIHA	8	8	8		1,93E+05	5,30E+07	1,65E+07	7,61E+07	116867	Acid trehalase OS=*Trichoderma harzianum* GN=THAR02_04798 PE=4 SV=1
A0A0F9XQW3|A0A0F9XQW3_TRIHA	15	14	13	Carbamidomethylation; Oxidation (M)	1,93E+05	7,13E+07	3,16E+06	3,61E+07	87301	Uncharacterized protein OS=*Trichoderma harzianum* GN=THAR02_00986 PE=4 SV=1
A0A0G0A0B1|A0A0G0A0B1_TRIHA	13	9	9	Carbamidomethylation; Oxidation (M)	0	7,50E+07	0	3,03E+07	92668	Glycosyl hydrolase family 3 N terminal domain-containing protein OS=*Trichoderma harzianum* GN=THAR02_02181 PE=4 SV=1
A0A0G0A3D5|A0A0G0A3D5_TRIHA	35	5	5		1,52E+06	4,07E+07	1,37E+07	2,33E+07	17578	Ubiquitin-40S ribosomal protein S27a OS=*Trichoderma harzianum* GN=THAR02_08131 PE=4 SV=1
B9VQ16|B9VQ16_TRIHA	28	10	9	Oxidation (M)	7,57E+04	1,07E+08	6,32E+06	3,19E+07	47995	Beta-1,6-glucanase BG16.1 OS=*Trichoderma harzianum* PE=2 SV=1
A0A0F9ZUH3|A0A0F9ZUH3_TRIHA	14	6	6	Carbamidomethylation	1,36E+05	5,93E+07	1,03E+07	4,71E+07	52933	1,3-beta-glucanosyltransferase OS=*Trichoderma harzianum* GN=THAR02_04021 PE=3 SV=1
A0A0F9XQD6|A0A0F9XQD6_TRIHA	14	10	10	Carbamidomethylation; Oxidation (M)	1,87E+06	3,23E+07	0	4,17E+07	85548	Uncharacterized protein OS=*Trichoderma harzianum* GN=THAR02_01038 PE=4 SV=1
A0A0F9X3Z8|A0A0F9X3Z8_TRIHA	9	7	7	Carbamidomethylation	1,84E+05	2,29E+07	8,10E+07	4,05E+07	88742	Catalase-peroxidase OS=*Trichoderma harzianum* GN=katG PE=3 SV=1
A0A0F9XQT4|A0A0F9XQT4_TRIHA	13	9	8		3,04E+06	1,50E+07	1,04E+07	2,08E+07	77141	Glycosyl hydrolase family 3-4 OS=*Trichoderma harzianum* GN=THAR02_00890 PE=4 SV=1
A0A0F9XT87|A0A0F9XT87_TRIHA	14	8	7	Carbamidomethylation; Oxidation (M)	6,73E+04	2,88E+07	0	7,41E+06	87418	Glycosyl hydrolase OS=*Trichoderma harzianum* GN=THAR02_04626 PE=4 SV=1
A0A0G0A3L0|A0A0G0A3L0_TRIHA	26	6	6	Carbamidomethylation	1,26E+06	5,39E+08	1,97E+06	1,02E+08	46598	Uncharacterized protein OS=*Trichoderma harzianum* GN=THAR02_01069 PE=4 SV=1
A0A0F9XAS9|A0A0F9XAS9_TRIHA	12	8	8	Carbamidomethylation	3,20E+05	1,23E+07	2,68E+07	2,34E+07	83040	Neutral/alkaline non-lysosomal ceramidase OS=*Trichoderma harzianum* GN=THAR02_05625 PE=4 SV=1

Continuation of Table S4.1

Accession	Coverage (%)	Peptides	Unique Peptides	PTM	Blank Intensity	G101 Intensity	S1 Intensity	FG1 Intensity	Avg. Mass	Description
A0A0F9XDX5|A0A0F9XDX5_TRIHA	13	7	7		0	2,04E+07	7,08E+05	4,14E+06	58222	Uncharacterized protein OS=*Trichoderma harzianum* GN=THAR02_05108 PE=4 SV=1
A0A0F9ZGV2|A0A0F9ZGV2_TRIHA	11	5	5	Carbamidomethylation; Oxidation (M)	6,70E+05	5,52E+07	9,15E+07	8,96E+07	60083	Tyrosinase OS=*Trichoderma harzianum* GN=THAR02_08385 PE=4 SV=1
A0A0F9X7K0|A0A0F9X7K0_TRIHA	19	7	7	Carbamidomethylation	1,45E+05	4,90E+07	9,13E+06	3,60E+07	34302	Uncharacterized protein OS=*Trichoderma harzianum* GN=THAR02_07387 PE=4 SV=1
A0A0F9X224|A0A0F9X224_TRIHA	15	8	7		7,80E+04	2,77E+07	1,28E+07	1,70E+07	62637	Uncharacterized protein OS=*Trichoderma harzianum* GN=THAR02_09150 PE=4 SV=1
A0A0G0A8Y0|A0A0G0A8Y0_TRIHA	17	6	6	Carbamidomethylation	2,48E+06	1,46E+08	0	9,81E+07	44174	Uncharacterized protein OS=*Trichoderma harzianum* GN=THAR02_06379 PE=4 SV=1
O14402|O14402_TRIHA	4	3	1	Carbamidomethylation	3,12E+05	1,33E+08	0	8,63E+07	107912	Beta-1,3 exoglucanase OS=*Trichoderma harzianum* PE=4 SV=2
A0A0F9XIJ9|A0A0F9XIJ9_TRIHA	14	7	6	Carbamidomethylation	7,56E+04	4,92E+07	2,54E+06	2,51E+07	69828	Lysophospholipase OS=*Trichoderma harzianum* GN=THAR02_07581 PE=3 SV=1
A0A0G0ABI7|A0A0G0ABI7_TRIHA	14	7	7	Oxidation (M)	7,97E+04	3,25E+07	9,44E+05	2,01E+07	58397	Carboxylic ester hydrolase OS=*Trichoderma harzianum* GN=THAR02_05496 PE=3 SV=1
A0A0F9Y245|A0A0F9Y245_TRIHA	14	4	4	Carbamidomethylation	1,10E+06	1,67E+08	0	8,30E+07	37299	Alpha/beta hydrolase OS=*Trichoderma harzianum* GN=THAR02_01664 PE=4 SV=1
A0A0F9XP75|A0A0F9XP75_TRIHA	13	6	6		1,92E+05	1,78E+08	0	9,59E+06	31531	Uncharacterized protein OS=*Trichoderma harzianum* GN=THAR02_01434 PE=4 SV=1
A0A0F9XN15|A0A0F9XN15_TRIHA	16	7	7	Carbamidomethylation	3,21E+05	7,52E+07	0	2,40E+07	48188	Alpha-galactosidase OS=*Trichoderma harzianum* GN=THAR02_01852 PE=3 SV=1
A0A0F9X8K8|A0A0F9X8K8_TRIHA	15	4	4		7,56E+05	6,72E+07	0	1,33E+07	31758	Uncharacterized protein OS=*Trichoderma harzianum* GN=THAR02_10795 PE=4 SV=1
A0A0G0AB16|A0A0G0AB16_TRIHA	24	4	4	Carbamidomethylation	3,39E+05	2,27E+07	1,60E+08	6,25E+07	19185	Uncharacterized protein OS=*Trichoderma harzianum* GN=THAR02_05676 PE=4 SV=1
A0A0F9ZXS2|A0A0F9ZXS2_TRIHA	7	4	4		0	3,69E+07	1,03E+06	4,40E+07	55073	L-lactate dehydrogenase (Cytochrome) OS=*Trichoderma harzianum* GN=THAR02_09939 PE=3 SV=1
A0A0F9X2D5|A0A0F9X2D5_TRIHA	7	5	4	Carbamidomethylation	0	2,95E+07	1,31E+07	9,19E+06	58893	Serine peptidase OS=*Trichoderma harzianum* GN=THAR02_09052 PE=4 SV=1

Continuation of Table S4.1

Accession	Coverage (%)	Peptides	Unique Peptides	PTM	Blank Intensity	G101 Intensity	S1 Intensity	FG1 Intensity	Avg. Mass	Description
A0A0F9ZZN6|A0A0F9ZZN6_TRIHA	10	4	4	Carbamidomethylation; Oxidation (M)	3,79E+05	1,12E+08	0	1,65E+07	57215	1,3-beta-glucanosyltransferase OS=*Trichoderma harzianum* GN=THAR02_09247 PE=3 SV=1
A0A0F9X7W2|A0A0F9X7W2_TRIHA	8	8	7	Carbamidomethylation	0	1,38E+07	0	5,74E+06	95013	Beta-glucosidase OS=*Trichoderma harzianum* GN=THAR02_07292 PE=4 SV=1
A0A0F9Y225|A0A0F9Y225_TRIHA	17	7	6		1,32E+05	3,15E+07	3,45E+05	2,13E+07	38330	Uncharacterized protein OS=*Trichoderma harzianum* GN=THAR02_01721 PE=4 SV=1
A0A0F9X6H8|A0A0F9X6H8_TRIHA	11	7	7		2,02E+05	5,99E+06	8,88E+06	2,51E+07	76515	Glutaminase A OS=*Trichoderma harzianum* GN=THAR02_07728 PE=4 SV=1
A0A0F9XN01|A0A0F9XN01_TRIHA	14	3	3	Carbamidomethylation; Oxidation (M)	1,58E+05	1,01E+08	0	3,54E+07	30715	Uncharacterized protein OS=*Trichoderma harzianum* GN=THAR02_06242 PE=4 SV=1
A0A0F9ZZ00|A0A0F9ZZ00_TRIHA	13	5	5	Carbamidomethylation	1,74E+05	5,71E+07	2,73E+08	7,89E+07	46519	Mutanase OS=*Trichoderma harzianum* GN=THAR02_09460 PE=4 SV=1
A0A0F9WYR7|A0A0F9WYR7_TRIHA	13	4	4		6,56E+04	5,74E+07	0	1,69E+07	55601	alpha-1,2-Mannosidase OS=*Trichoderma harzianum* GN=THAR02_10337 PE=3 SV=1
Q8WZM5|Q8WZM5_TRIHA	7	3	3		2,59E+05	1,67E+06	6,48E+07	3,39E+07	25801	Trypsin-like protease OS=*Trichoderma harzianum* GN=PRA1 PE=2 SV=2
A0A0F9XMS0|A0A0F9XMS0_TRIHA	10	8	8	Oxidation (M)	0	2,82E+07	0	3,98E+06	89834	Exo-beta-1,3-glucanase OS=*Trichoderma harzianum* GN=THAR02_06360 PE=4 SV=1
A0A0F9XIN0|A0A0F9XIN0_TRIHA	14	8	7		1,18E+05	1,41E+07	6,87E+05	1,33E+07	59195	GMC oxidoreductase OS=*Trichoderma harzianum* GN=THAR02_07559 PE=3 SV=1
A0A0F9XTJ0|A0A0F9XTJ0_TRIHA	8	5	5	Carbamidomethylation; Oxidation (M)	2,32E+05	7,58E+07	0	1,89E+07	79720	Glucan endo-1,3-beta-glucosidase OS=*Trichoderma harzianum* GN=THAR02_00043 PE=4 SV=1
A0A0F9ZQX2|A0A0F9ZQX2_TRIHA	10	4	4	Carbamidomethylation	0	1,05E+07	0	3,24E+06	50690	1,3-beta-glucanosyltransferase OS=*Trichoderma harzianum* GN=THAR02_05189 PE=3 SV=1
A0A0F9Y0U3|A0A0F9Y0U3_TRIHA	6	4	4		2,52E+05	3,76E+07	3,82E+06	5,09E+07	51658	Uncharacterized protein OS=*Trichoderma harzianum* GN=THAR02_02182 PE=4 SV=1
A0A0F9XKJ8|A0A0F9XKJ8_TRIHA	6	5	5	Carbamidomethylation; Oxidation (M)	0	2,22E+07	2,85E+06	2,47E+06	112154	Uncharacterized protein OS=*Trichoderma harzianum* GN=THAR02_02560 PE=4 SV=1
A0A0G0ACS4|A0A0G0ACS4_TRIHA	9	2	2	Carbamidomethylation	3,53E+05	3,66E+07	3,12E+07	2,88E+07	42506	Ribonuclease Trv OS=*Trichoderma harzianum* GN=THAR02_05011 PE=3 SV=1

Continuation of Table S4.1

Accession	Coverage (%)	Peptides	Unique Peptides	PTM	Blank Intensity	G101 Intensity	S1 Intensity	FG1 Intensity	Avg. Mass	Description
A0A0F9XK33|A0A0F9XK33_TRIHA	4	3	3		0	2,47E+07	0	2,15E+07	58238	Beta-glucuronidase OS=*Trichoderma harzianum* GN=THAR02_03122 PE=4 SV=1
A0A0F9ZHK4|A0A0F9ZHK4_TRIHA	19	7	7		0	3,81E+06	0	7,30E+06	35344	Transaldolase OS=*Trichoderma harzianum* GN=THAR02_08121 PE=4 SV=1
A0A0G0ABI9|A0A0G0ABI9_TRIHA	8	7	6		3,39E+05	1,77E+07	5,23E+06	4,28E+07	89553	Alpha-1,2-mannosidase OS=*Trichoderma harzianum* GN=THAR02_05501 PE=4 SV=1
A0A0F9ZWU1|A0A0F9ZWU1_TRIHA	8	4	4		2,86E+05	5,38E+06	1,15E+08	7,90E+07	46933	Carboxypeptidase A OS=*Trichoderma harzianum* GN=THAR02_10248 PE=4 SV=1
A0A0F9ZCK3|A0A0F9ZCK3_TRIHA	22	5	5		0	2,79E+07	0	8,94E+06	50627	Alpha-amylase OS=*Trichoderma harzianum* GN=THAR02_09676 PE=3 SV=1
A0A0F9ZTK0|A0A0F9ZTK0_TRIHA	12	5	5		4,37E+05	4,45E+07	1,86E+07	1,19E+07	63234	Murein transglycosylase OS=*Trichoderma harzianum* GN=THAR02_04344 PE=4 SV=1
A0A0F9ZYY1|A0A0F9ZYY1_TRIHA	10	4	4		6,13E+04	1,84E+07	6,83E+05	6,25E+06	41056	Uncharacterized protein OS=*Trichoderma harzianum* GN=THAR02_09486 PE=4 SV=1
A0A0F9ZIR5|A0A0F9ZIR5_TRIHA	10	3	3	Oxidation (M)	0	3,12E+06	1,77E+06	3,70E+06	36652	Glucanase B OS=*Trichoderma harzianum* GN=THAR02_07716 PE=4 SV=1
A0A0F9WVU4|A0A0F9WVU4_TRIHA	8	1	1		1,22E+06	6,96E+07	3,47E+05	6,38E+07	29926	Uncharacterized protein OS=*Trichoderma harzianum* GN=THAR02_11305 PE=4 SV=1
A4V8W1|A4V8W1_TRIHA	5	3	3	Carbamidomethylation	0	1,16E+07	4,48E+06	5,54E+06	74277	Serin endopeptidase OS=*Trichoderma harzianum* GN=p5216 PE=2 SV=1
A0A0G0API0|A0A0G0API0_TRIHA	16	6	6	Oxidation (M)	2,78E+05	1,99E+06	4,29E+06	1,58E+07	49453	Uncharacterized protein OS=*Trichoderma harzianum* GN=THAR02_01480 PE=4 SV=1
A0A0G0A4N5|A0A0G0A4N5_TRIHA	4	4	4		0	1,03E+07	4,45E+06	7,46E+06	105976	Uncharacterized protein OS=*Trichoderma harzianum* GN=THAR02_07754 PE=4 SV=1
A0A0F9XR87|A0A0F9XR87_TRIHA	10	5	5	Carbamidomethylation	0	6,74E+07	8,28E+05	2,08E+07	42748	Uncharacterized protein OS=*Trichoderma harzianum* GN=THAR02_05127 PE=4 SV=1
A0A0F9X1Z0|A0A0F9X1Z0_TRIHA	11	2	2	Oxidation (M)	0	5,10E+06	6,74E+07	3,15E+06	16983	Calmodulin OS=*Trichoderma harzianum* GN=THAR02_08645 PE=4 SV=1
A0A0F9XQK6|A0A0F9XQK6_TRIHA	6	3	3		0	4,90E+06	9,64E+05	1,66E+07	51685	Glycosyl hydrolase family 30-1 OS=*Trichoderma harzianum* GN=THAR02_00972 PE=3 SV=1

Continuation of Table S4.1

Accession	Coverage (%)	Peptides	Unique Peptides	PTM	Blank Intensity	G101 Intensity	S1 Intensity	FG1 Intensity	Avg. Mass	Description
A0A0F9XNA4|A0A0F9XNA4_TRIHA	21	6	6	Carbamidomethylation	3,84E+05	2,53E+07	0	2,28E+07	42767	Glucan 1 3-beta-glucosidase OS=*Trichoderma harzianum* GN=THAR02_06159 PE=4 SV=1
A4V8W2|A4V8W2_TRIHA	4	2	2		0	1,04E+07	0	5,38E+06	57467	Cerevisin OS=*Trichoderma harzianum* GN=p5431 PE=2 SV=1
A0A0F9XNX7|A0A0F9XNX7_TRIHA	13	2	2	Oxidation (M)	0	1,13E+07	1,53E+07	1,74E+07	26529	Uncharacterized protein OS=*Trichoderma harzianum* GN=THAR02_05966 PE=4 SV=1
A0A0F9XLQ0|A0A0F9XLQ0_TRIHA	13	4	4	Carbamidomethylation	6,04E+04	3,07E+07	0	4,65E+06	43816	Uncharacterized protein OS=*Trichoderma harzianum* GN=THAR02_02170 PE=4 SV=1
A0A0F9XCM6|A0A0F9XCM6_TRIHA	2	2	2		0	0	1,74E+06	8,01E+06	106898	Uncharacterized protein OS=*Trichoderma harzianum* GN=THAR02_05570 PE=4 SV=1
A0A0F9ZXC9|A0A0F9ZXC9_TRIHA	2	3	3		0	2,51E+06	3,58E+06	4,42E+06	117541	WSC domain-containing protein OS=*Trichoderma harzianum* GN=THAR02_03210 PE=4 SV=1
A0A0F9XGZ8|A0A0F9XGZ8_TRIHA	2	2	2		0	1,89E+06	2,07E+05	1,67E+06	97767	Heterokaryon incompatibility protein OS=*Trichoderma harzianum* GN=THAR02_03627 PE=4 SV=1
A0A0F9ZTP8|A0A0F9ZTP8_TRIHA	2	2	2		0	4,55E+06	4,94E+06	2,92E+06	91177	Uncharacterized protein OS=*Trichoderma harzianum* GN=THAR02_11396 PE=4 SV=1
A0A0F9ZMY4|A0A0F9ZMY4_TRIHA	14	2	2	Oxidation (M)	0	3,92E+06	5,16E+06	5,27E+06	18351	Uncharacterized protein OS=*Trichoderma harzianum* GN=THAR02_06264 PE=4 SV=1
A0A0F9XL67|A0A0F9XL67_TRIHA	11	3	3		0	9,80E+06	2,74E+06	2,84E+06	47504	Uncharacterized protein OS=*Trichoderma harzianum* GN=THAR02_02338 PE=4 SV=1
A0A0G0AN43|A0A0G0AN43_TRIHA	6	3	3	Carbamidomethylation	0	1,49E+07	0	5,42E+06	51955	Murein transglycosylase OS=*Trichoderma harzianum* GN=THAR02_01871 PE=4 SV=1
A0A0F9WY34|A0A0F9WY34_TRIHA	6	5	4	Carbamidomethylation	1,05E+05	3,45E+07	7,10E+06	3,72E+06	66204	Uncharacterized protein OS=*Trichoderma harzianum* GN=THAR02_09868 PE=4 SV=1
A0A0F9XIK6|A0A0F9XIK6_TRIHA	13	3	3	Oxidation (M)	0	2,10E+07	0	5,12E+05	51822	Glycosyl hydrolase family 30-1 OS=*Trichoderma harzianum* GN=THAR02_07549 PE=3 SV=1
A0A0F9ZKA8|A0A0F9ZKA8_TRIHA	5	2	2	Carbamidomethylation	0	2,26E+07	0	9,84E+06	56280	1,3-beta-glucanosyltransferase OS=*Trichoderma harzianum* GN=THAR02_07194 PE=3 SV=1
A0A0F9ZP62|A0A0F9ZP62_TRIHA	13	2	2		1,35E+05	4,04E+06	1,07E+07	1,97E+07	17128	Uncharacterized protein OS=*Trichoderma harzianum* GN=THAR02_05837 PE=4 SV=1

Continuation of Table S4.1

Accession	Coverage (%)	Peptides	Unique Peptides	PTM	Blank Intensity	G101 Intensity	S1 Intensity	FG1 Intensity	Avg. Mass	Description
A0A0F9WZJ0|A0A0F9WZJ0_TRIHA	7	4	4	Oxidation (M)	0	2,49E+06	7,17E+06	3,91E+06	56332	Peptide hydrolase OS=*Trichoderma harzianum* GN=THAR02_10053 PE=3 SV=1
A0A0G0APA7|A0A0G0APA7_TRIHA	5	3	3		1,77E+05	9,82E+06	3,02E+06	1,37E+07	73700	M6 family metalloprotease OS=*Trichoderma harzianum* GN=THAR02_01512 PE=4 SV=1
A0A0F9XPH0|A0A0F9XPH0_TRIHA	10	4	4	Carbamidomethylation	0	1,42E+07	0	0	51988	Mutanase OS=*Trichoderma harzianum* GN=THAR02_01461 PE=4 SV=1
A0A0G0A0W2|A0A0G0A0W2_TRIHA	22	3	3	Carbamidomethylation	0	8,92E+06	0	1,20E+07	13898	Uncharacterized protein OS=*Trichoderma harzianum* GN=THAR02_08901 PE=4 SV=1
A0A0G0ALT6|A0A0G0ALT6_TRIHA	6	3	3		0	3,46E+06	3,58E+05	3,00E+06	50522	Exo-rhamnogalacturonase B OS=*Trichoderma harzianum* GN=THAR02_02325 PE=3 SV=1
A0A0G0A527|A0A0G0A527_TRIHA	15	3	3	Carbamidomethylation	0	3,02E+06	5,65E+05	2,31E+06	26496	Uncharacterized protein OS=*Trichoderma harzianum* GN=THAR02_00636 PE=4 SV=1
A0A0F9XKM3|A0A0F9XKM3_TRIHA	17	4	4		0	3,20E+06	6,38E+05	1,77E+07	32615	Uncharacterized protein OS=*Trichoderma harzianum* GN=THAR02_02511 PE=4 SV=1
A0A0F9XQN9|A0A0F9XQN9_TRIHA	11	3	3	Carbamidomethylation	0	1,18E+07	3,22E+05	3,79E+06	25494	Uncharacterized protein OS=*Trichoderma harzianum* GN=THAR02_05380 PE=4 SV=1
A0A0F9ZKV9|A0A0F9ZKV9_TRIHA	6	4	4		0	1,84E+07	0	6,33E+06	64437	Glucose oxidase OS=*Trichoderma harzianum* GN=THAR02_06980 PE=3 SV=1
A0A0F9X8U2|A0A0F9X8U2_TRIHA	2	2	2		0	1,85E+07	0	7,49E+06	92095	Uncharacterized protein OS=*Trichoderma harzianum* GN=THAR02_10702 PE=4 SV=1
A0A0F9WVH5|A0A0F9WVH5_TRIHA	3	2	2	Carbamidomethylation	0	2,86E+06	4,85E+05	3,92E+05	51342	Uncharacterized protein OS=*Trichoderma harzianum* GN=THAR02_10761 PE=4 SV=1
A0A0F9XFJ7|A0A0F9XFJ7_TRIHA	3	2	2		4,81E+04	1,48E+07	0	8,79E+06	63621	Uncharacterized protein OS=*Trichoderma harzianum* GN=THAR02_08493 PE=4 SV=1
A0A0F9ZMW7|A0A0F9ZMW7_TRIHA	7	2	2	Carbamidomethylation; Oxidation (M)	1,04E+05	7,06E+06	0	0	48710	Cell wall glucanase OS=*Trichoderma harzianum* GN=THAR02_06347 PE=4 SV=1
A0A0F9ZEF1|A0A0F9ZEF1_TRIHA	22	4	4		0	5,03E+06	0	1,31E+07	20586	Uncharacterized protein OS=*Trichoderma harzianum* GN=THAR02_09129 PE=4 SV=1

Continuation of Table S4.1

Accession	Coverage (%)	Peptides	Unique Peptides	PTM	Blank Intensity	G101 Intensity	S1 Intensity	FG1 Intensity	Avg. Mass	Description
A0A0F9XRY7|A0A0F9XRY7_TRIHA	1	1	1		2,02E+05	3,98E+07	0	1,40E+07	190020	Uncharacterized protein OS=*Trichoderma harzianum* GN=THAR02_00513 PE=4 SV=1
A0A0F9X8Y8|A0A0F9X8Y8_TRIHA	4	2	2		0	4,08E+06	7,97E+05	2,04E+06	47133	Cellulase OS=*Trichoderma harzianum* GN=THAR02_10655 PE=3 SV=1
A0A0F9X834|A0A0F9X834_TRIHA	3	2	2	Carbamidomethylation	0	1,46E+07	0	3,46E+06	45175	Uncharacterized protein (Fragment) OS=*Trichoderma harzianum* GN=THAR02_07204 PE=4 SV=1
A0A0F9X441|A0A0F9X441_TRIHA	5	1	1	Carbamidomethylation	2,46E+05	8,79E+06	1,88E+06	1,02E+07	49675	Uncharacterized protein OS=*Trichoderma harzianum* GN=THAR02_07909 PE=4 SV=1
A0A0G0A2Q6|A0A0G0A2Q6_TRIHA	3	1	1	Carbamidomethylation	0	2,49E+06	2,92E+07	1,10E+07	25953	Complex I intermediate-associated protein 30 OS=*Trichoderma harzianum* GN=THAR02_01275 PE=4 SV=1
A0A0G0A4C2|A0A0G0A4C2_TRIHA	9	1	1		0	0	4,67E+06	4,27E+05	10492	Uncharacterized protein OS=*Trichoderma harzianum* GN=THAR02_00841 PE=4 SV=1
A0A0F9X6D2|A0A0F9X6D2_TRIHA	3	2	2		0	1,00E+06	7,83E+05	0	41291	Glycosylhydrolase family 18-1 OS=*Trichoderma harzianum* GN=THAR02_07777 PE=3 SV=1
A0A0F9XRH9|A0A0F9XRH9_TRIHA	10	2	2	Carbamidomethylation	1,30E+05	9,68E+07	3,13E+05	2,40E+07	26332	Uncharacterized protein OS=*Trichoderma harzianum* GN=THAR02_00630 PE=4 SV=1
A0A0F9XM06|A0A0F9XM06_TRIHA	6	1	1		0	1,19E+07	0	4,78E+06	24314	Uncharacterized protein OS=*Trichoderma harzianum* GN=THAR02_02095 PE=4 SV=1
A0A0F9ZYM1|A0A0F9ZYM1_TRIHA	4	2	2		0	2,79E+07	0	8,52E+06	51169	Murein transglycosylase OS=*Trichoderma harzianum* GN=THAR02_02834 PE=4 SV=1
A0A0F9X9K8|A0A0F9X9K8_TRIHA	4	2	2		0	5,92E+06	0	4,72E+06	48200	Uncharacterized protein OS=*Trichoderma harzianum* GN=THAR02_06005 PE=4 SV=1
A0A0F9XQT0|A0A0F9XQT0_TRIHA	5	2	2		0	1,27E+07	0	6,09E+06	65298	GMC oxidoreductase OS=*Trichoderma harzianum* GN=THAR02_05334 PE=4 SV=1
A0A0F9Y713|A0A0F9Y713_TRIHA	6	2	2		0	7,67E+06	0	1,92E+06	52332	Beta-glucuronidase OS=*Trichoderma harzianum* GN=THAR02_00021 PE=4 SV=1
Q8NJQ4|Q8NJQ4_9HYPO	6	2	2	Carbamidomethylation	0	1,54E+06	0	6,30E+05	35538	37 kDa chitinase (Fragment) OS=Trichoderma inhamatum GN=chit37 PE=3 SV=1
A0A0F9X117|A0A0F9X117_TRIHA	4	2	2		0	5,99E+06	0	2,05E+06	47989	Uncharacterized protein OS=*Trichoderma harzianum* GN=THAR02_09509 PE=4 SV=1

Continuation of Table S4.1

Accession	Coverage (%)	Peptides	Unique Peptides	PTM	Blank Intensity	G101 Intensity	S1 Intensity	FG1 Intensity	Avg. Mass	Description
A0A0F9WVK6|A0A0F9WVK6_TRIHA	5	2	2		0	3,77E+06	0	1,32E+06	47387	Carboxylic ester hydrolase OS=*Trichoderma harzianum* GN=THAR02_10725 PE=3 SV=1
A0A0G0A871|A0A0G0A871_TRIHA	3	2	2		0	2,17E+06	0	1,41E+06	75834	Uncharacterized protein OS=*Trichoderma harzianum* GN=THAR02_06594 PE=3 SV=1
A0A0F9Y411|A0A0F9Y411_TRIHA	6	1	1	Carbamidomethylation	0	5,85E+06	0	1,16E+06	22472	Uncharacterized protein OS=*Trichoderma harzianum* GN=THAR02_01025 PE=4 SV=1
A0A0F9XS98|A0A0F9XS98_TRIHA	2	1	1	Carbamidomethylation	0	2,01E+06	0	1,05E+06	53569	Uncharacterized protein OS=*Trichoderma harzianum* GN=THAR02_00522 PE=4 SV=1
A0A0F9XTH3|A0A0F9XTH3_TRIHA	1	1	1		1,02E+05	2,03E+07	0	2,14E+07	72808	Uncharacterized protein OS=*Trichoderma harzianum* GN=THAR02_00178 PE=4 SV=1
A0A0F9ZHA7|A0A0F9ZHA7_TRIHA	2	1	1		0	3,93E+06	0	5,80E+06	39092	Chitinase 3 OS=*Trichoderma harzianum* GN=THAR02_08235 PE=4 SV=1
A0A0F9ZTV9|A0A0F9ZTV9_TRIHA	1	1	1		7,33E+05	2,83E+07	0	3,30E+07	95650	Chloride channel other eukaryote OS=*Trichoderma harzianum* GN=THAR02_04272 PE=4 SV=1
A0A0F9XQN5|A0A0F9XQN5_TRIHA	1	1	1		4,18E+05	1,45E+08	7,06E+07	8,47E+07	145730	CMGC/DYRK/DYRK2 protein kinase OS=*Trichoderma harzianum* GN=THAR02_01097 PE=4 SV=1
A0A0F9ZP48|A0A0F9ZP48_TRIHA	1	1	1		0	4,86E+06	0	6,05E+06	68981	Uncharacterized protein OS=*Trichoderma harzianum* GN=THAR02_05862 PE=4 SV=1
A0A0F9X4X9|A0A0F9X4X9_TRIHA	1	1	1		0	2,81E+06	9,26E+07	8,59E+06	63356	Uncharacterized protein OS=*Trichoderma harzianum* GN=THAR02_07639 PE=4 SV=1
A0A0F9XYZ7|A0A0F9XYZ7_TRIHA	4	1	1		0	2,10E+06	6,17E+06	4,79E+06	20508	Uncharacterized protein OS=*Trichoderma harzianum* GN=THAR02_02717 PE=4 SV=1
A0A0F9XJ35|A0A0F9XJ35_TRIHA	7	1	1		0	8,31E+06	0	0	23952	Uncharacterized protein OS=*Trichoderma harzianum* GN=THAR02_03429 PE=4 SV=1
A0A0G0AFJ7|A0A0G0AFJ7_TRIHA	2	1	1		0	0	3,88E+06	3,43E+06	56939	Uncharacterized protein OS=*Trichoderma harzianum* GN=THAR02_04109 PE=4 SV=1
A0A0G0ATQ4|A0A0G0ATQ4_TRIHA	1	1	1		1,28E+05	1,06E+07	3,40E+06	1,19E+07	44623	Uncharacterized protein OS=*Trichoderma harzianum* GN=THAR02_00022 PE=4 SV=1

Continuation of Table S4.1

Accession	Coverage (%)	Peptides	Unique Peptides	PTM	Blank Intensity	G101 Intensity	S1 Intensity	FG1 Intensity	Avg. Mass	Description
A0A0G0ALQ8|A0A0G0ALQ8_TRIHA	1	1	1		0	6,76E+06	0	6,27E+06	56814	FAD binding domain-containing protein OS=*Trichoderma harzianum* GN=THAR02_02295 PE=4 SV=1
A0A0G0AMT0|A0A0G0AMT0_TRIHA	8	1	1	Carbamidomethylation	0	6,69E+06	0	0	21967	Uncharacterized protein OS=*Trichoderma harzianum* GN=THAR02_01963 PE=4 SV=1
A0A0F9XMT4|A0A0F9XMT4_TRIHA	10	1	1		0	7,21E+05	1,44E+06	4,46E+06	10736	Acyl CoA binding protein OS=*Trichoderma harzianum* GN=THAR02_01997 PE=4 SV=1
A0A0F9X6K7|A0A0F9X6K7_TRIHA	3	1	1		0	0	1,55E+07	4,41E+06	31334	Succinate dehydrogenase [ubiquinone] iron-sulfur subunit mitochondrial OS=*Trichoderma harzianum* GN=THAR02_11427 PE=3 SV=1
A0A0F9WVS7|A0A0F9WVS7_TRIHA	7	1	1		1,67E+05	1,17E+06	7,88E+05	8,07E+06	21034	Uncharacterized protein OS=*Trichoderma harzianum* GN=THAR02_11323 PE=4 SV=1
A0A0G0A377|A0A0G0A377_TRIHA	4	1	1		0	2,13E+06	1,83E+06	3,34E+06	48694	1,3-beta-glucanosyltransferase OS=*Trichoderma harzianum* GN=THAR02_01079 PE=3 SV=1
A0A0F9X3M8|A0A0F9X3M8_TRIHA	4	1	1		0	4,43E+06	0	9,24E+05	25652	Uncharacterized protein OS=*Trichoderma harzianum* GN=THAR02_08091 PE=4 SV=1
A0A0F9ZZV9|A0A0F9ZZV9_TRIHA	3	1	1		0	1,62E+06	0	1,74E+06	41997	Fasciclin domain-containing protein OS=*Trichoderma harzianum* GN=THAR02_02432 PE=4 SV=1
A0A0G0A8E1|A0A0G0A8E1_TRIHA	3	1	1		1,84E+05	8,77E+05	2,56E+05	1,45E+07	36286	Uncharacterized protein OS=*Trichoderma harzianum* GN=THAR02_06499 PE=4 SV=1
A0A0F9XJ80|A0A0F9XJ80_TRIHA	1	1	1		0	3,25E+06	0	1,73E+06	72706	Uncharacterized protein OS=*Trichoderma harzianum* GN=THAR02_02962 PE=4 SV=1
A0A0F9ZI31|A0A0F9ZI31_TRIHA	6	1	1		0	0	7,16E+06	0	19264	Uncharacterized protein OS=*Trichoderma harzianum* GN=THAR02_07952 PE=4 SV=1
A0A0G0ABJ1|A0A0G0ABJ1_TRIHA	2	1	1		0	0	0	1,90E+06	58550	Carboxylic ester hydrolase OS=*Trichoderma harzianum* GN=THAR02_05506 PE=3 SV=1
A0A0F9Z8G0|A0A0F9Z8G0_TRIHA	2	1	1		0	1,36E+06	1,44E+06	1,31E+06	68518	Glycosyl hydrolase family 2 OS=*Trichoderma harzianum* GN=THAR02_11028 PE=4 SV=1
A0A0F9XTF3|A0A0F9XTF3_TRIHA	3	1	1		0	4,25E+06	0	8,57E+05	45317	Uncharacterized protein OS=*Trichoderma harzianum* GN=THAR02_04506 PE=4 SV=1

Continuation of Table S4.1

Accession	Coverage (%)	Peptides	Unique Peptides	PTM	Blank Intensity	G101 Intensity	S1 Intensity	FG1 Intensity	Avg. Mass	Description
A0A0G0A5A5|A0A0G0A5A5_TRIHA	4	1	1	Carbamidomethylation	0	1,25E+07	0	1,84E+06	35396	Uncharacterized protein OS=*Trichoderma harzianum* GN=THAR02_07539 PE=4 SV=1
A0A0F9Y3C1|A0A0F9Y3C1_TRIHA	8	1	1		1,86E+05	2,07E+06	5,85E+06	1,68E+07	12237	Uncharacterized protein OS=*Trichoderma harzianum* GN=THAR02_01245 PE=4 SV=1
A4V8W4|A4V8W4_TRIHA	3	1	1		3,04E+05	6,05E+06	8,55E+05	1,78E+06	25452	Serin endopeptidase OS=*Trichoderma harzianum* GN=p7480 PE=2 SV=1
A0A0F9ZWP3|A0A0F9ZWP3_TRIHA	1	1	1	Carbamidomethylation	0	4,68E+05	1,76E+07	1,79E+06	96970	Uncharacterized protein OS=*Trichoderma harzianum* GN=THAR02_10326 PE=3 SV=1
A0A0F9ZZ66|A0A0F9ZZ66_TRIHA	2	1	1		0	3,05E+06	0	1,40E+06	38702	Beta-1,3-endoglucanase (Fragment) OS=*Trichoderma harzianum* GN=THAR02_09385 PE=4 SV=1
A0A0F9X200|A0A0F9X200_TRIHA	3	1	1		7,27E+04	4,37E+06	3,98E+06	3,28E+06	21704	Uncharacterized protein OS=*Trichoderma harzianum* GN=THAR02_08628 PE=4 SV=1
A0A0F9XDW1|A0A0F9XDW1_TRIHA	2	1	1		0	1,41E+06	0	5,98E+05	30959	UbiA prenyltransferase OS=*Trichoderma harzianum* GN=THAR02_09060 PE=4 SV=1
A0A0F9XRU8|A0A0F9XRU8_TRIHA	1	1	1		0	3,09E+06	0	1,59E+06	165609	Uncharacterized protein OS=*Trichoderma harzianum* GN=THAR02_04962 PE=4 SV=1
A0A0F9X873|A0A0F9X873_TRIHA	2	1	1		0	0	1,18E+07	7,33E+05	70565	Sphingomyelin phosphodiesterase OS=*Trichoderma harzianum* GN=THAR02_06511 PE=3 SV=1
A0A0F9XVE1|A0A0F9XVE1_TRIHA	8	1	1		0	1,93E+06	0	1,74E+06	21099	Uncharacterized protein OS=*Trichoderma harzianum* GN=THAR02_03804 PE=4 SV=1
A0A0G0AJX7|A0A0G0AJX7_TRIHA	3	1	1		0	9,11E+06	0	2,27E+06	26548	Endoglucanase-1 OS=*Trichoderma harzianum* GN=THAR02_02734 PE=3 SV=1
A0A0F9ZAS9|A0A0F9ZAS9_TRIHA	3	1	1		0	2,14E+06	0	6,65E+05	34849	Uncharacterized protein OS=*Trichoderma harzianum* GN=THAR02_10237 PE=4 SV=1
A0SZ74|A0SZ74_TRIHA	4	2	1		0	1,17E+06	0	5,11E+05	49188	Aspartyl proteinase OS=*Trichoderma harzianum* PE=2 SV=1
A0A0F9WTD6|A0A0F9WTD6_TRIHA	4	1	1		0	1,19E+06	0	1,04E+06	41987	Uncharacterized protein OS=*Trichoderma harzianum* GN=THAR02_11448 PE=3 SV=1
A0A0G0ANM4|A0A0G0ANM4_TRIHA	1	1	1		0	0	0	2,14E+06	61721	WSC domain-containing protein OS=*Trichoderma harzianum* GN=THAR02_01780 PE=4 SV=1

Continuation of Table S4.1

Accession	Coverage (%)	Peptides	Unique Peptides	PTM	Blank Intensity	G101 Intensity	S1 Intensity	FG1 Intensity	Avg. Mass	Description
A0A0G0APL4|A0A0G0APL4_TRIHA	2	1	1	Oxidation (M)	0	9,54E+05	1,39E+06	1,76E+06	63300	Uncharacterized protein OS=*Trichoderma harzianum* GN=THAR02_01422 PE=4 SV=1
A0A0F9X231|A0A0F9X231_TRIHA	2	1	1	Carbamidomethylation	0	1,92E+06	0	4,73E+05	66199	Uncharacterized protein OS=*Trichoderma harzianum* GN=THAR02_08601 PE=4 SV=1
A0A0F9XCE1|A0A0F9XCE1_TRIHA	3	1	1		0	6,62E+05	2,03E+06	4,19E+05	35868	Endo-chitosanase OS=*Trichoderma harzianum* GN=THAR02_05160 PE=3 SV=1
A0A0G0A408|A0A0G0A408_TRIHA	1	1	1		0	8,07E+05	0	5,64E+05	86623	Glycosyl hydrolase family 3 N terminal domain-containing protein OS=*Trichoderma harzianum* GN=THAR02_00891 PE=4 SV=1
A0A0F9ZI26|A0A0F9ZI26_TRIHA	2	1	1		0	6,16E+05	2,07E+05	2,69E+05	38520	Uncharacterized protein OS=*Trichoderma harzianum* GN=THAR02_07988 PE=4 SV=1
A0A0F9X1Q3|A0A0F9X1Q3_TRIHA	2	1	1		0	2,57E+07	0	4,69E+07	62039	Uncharacterized protein OS=*Trichoderma harzianum* GN=THAR02_08746 PE=4 SV=1
A0A0F9XIH8|A0A0F9XIH8_TRIHA	2	1	1		0	1,15E+06	1,90E+06	0	40513	Uncharacterized protein OS=*Trichoderma harzianum* GN=THAR02_03587 PE=4 SV=1
A0A0F9X7B7|A0A0F9X7B7_TRIHA	3	1	1	Carbamidomethylation	0	1,60E+06	0	8,42E+05	48221	Uncharacterized protein OS=*Trichoderma harzianum* GN=THAR02_07442 PE=4 SV=1
A0A0F9X8L2|A0A0F9X8L2_TRIHA	9	1	1		0	1,95E+06	0	1,98E+06	14348	Uncharacterized protein OS=*Trichoderma harzianum* GN=THAR02_06353 PE=4 SV=1
A0A0F9X072|A0A0F9X072_TRIHA	1	1	1		0	0	1,64E+06	9,80E+05	59783	FAD binding domain-containing protein OS=*Trichoderma harzianum* GN=THAR02_09219 PE=3 SV=1
A0A0F9X1I6|A0A0F9X1I6_TRIHA	1	1	1		0	1,26E+06	0	0	79459	Glucan endo-1,3-beta-glucosidase OS=*Trichoderma harzianum* GN=THAR02_09359 PE=4 SV=1
Q8WZM8|Q8WZM8_TRIHA	11	1	1		0	1,40E+06	0	0	30972	p4 protein OS=*Trichoderma harzianum* GN=P4 PE=2 SV=1
A0A0F9X7G1|A0A0F9X7G1_TRIHA	17	1	1		0	1,22E+06	0	0	8823	6 7-dimethyl-8-ribityllumazine synthase (Fragment) OS=*Trichoderma harzianum* GN=THAR02_06790 PE=4 SV=1
A0A0G0A1Y3|A0A0G0A1Y3_TRIHA	2	1	1	Carbamidomethylation	0	2,56E+06	0	0	150822	Glycosylhydrolase family 18-6 OS=*Trichoderma harzianum* GN=THAR02_01572 PE=4 SV=1
A0A0F9XRX1|A0A0F9XRX1_TRIHA	0	1	1		0	1,39E+06	0	1,90E+06	688524	Tyrocidine synthetase 1 OS=*Trichoderma harzianum* GN=THAR02_04945 PE=4 SV=1

Continuation of Table S4.1

Accession	Coverage (%)	Peptides	Unique Peptides	PTM	Blank Intensity	G101 Intensity	S1 Intensity	FG1 Intensity	Avg. Mass	Description
A0A0F9XHB1|A0A0F9XHB1_TRIHA	3	1	1		0	3,69E+06	0	9,66E+05	42282	Uncharacterized protein OS=*Trichoderma harzianum* GN=THAR02_07953 PE=4 SV=1
A0A0F9X7M7|A0A0F9X7M7_TRIHA	1	1	1	Carbamidomethylation	0	1,72E+06	0	9,69E+05	140692	Uncharacterized protein OS=*Trichoderma harzianum* GN=THAR02_06722 PE=4 SV=1
A0A0F9XD50|A0A0F9XD50_TRIHA	4	2	1		0	7,00E+05	1,11E+06	1,10E+06	59824	Carboxylic ester hydrolase OS=*Trichoderma harzianum* GN=THAR02_09329 PE=3 SV=1
A0A0F9XXV1|A0A0F9XXV1_TRIHA	2	1	1		0	5,69E+05	1,11E+06	0	48588	Adenosylhomocysteinase OS=*Trichoderma harzianum* GN=THAR02_03091 PE=3 SV=1
A0A0G0AA99|A0A0G0AA99_TRIHA	1	1	1		0	5,04E+05	5,33E+05	4,77E+05	51081	Aspartic proteinase OS=*Trichoderma harzianum* GN=THAR02_05926 PE=3 SV=1
A0A0F9XBN1|A0A0F9XBN1_TRIHA	2	1	1		0	1,17E+06	0	0	38579	Uncharacterized protein OS=*Trichoderma harzianum* GN=THAR02_05332 PE=4 SV=1
A0A0G0AD67|A0A0G0AD67_TRIHA	2	1	1		0	1,56E+06	0	9,84E+05	59756	Uncharacterized protein OS=*Trichoderma harzianum* GN=THAR02_04915 PE=4 SV=1
A0A0F9XRM5|A0A0F9XRM5_TRIHA	3	1	1		0	5,11E+05	6,46E+05	1,37E+06	24146	Lysozyme OS=*Trichoderma harzianum* GN=THAR02_05024 PE=3 SV=1
A0A0F9XJR8|A0A0F9XJR8_TRIHA	2	1	1		0	0	0	1,56E+06	48471	Uncharacterized protein OS=*Trichoderma harzianum* GN=THAR02_02817 PE=4 SV=1
A0A0G0A5Y9|A0A0G0A5Y9_TRIHA	4	1	1		0	2,32E+06	0	3,73E+05	21869	Uncharacterized protein OS=*Trichoderma harzianum* GN=THAR02_07320 PE=4 SV=1
A0A0F9XQU0|A0A0F9XQU0_TRIHA	5	1	1		0	1,01E+06	0	0	42777	Chitin recognition protein OS=*Trichoderma harzianum* GN=THAR02_01057 PE=3 SV=1
A0A0F9ZG19|A0A0F9ZG19_TRIHA	6	1	1		0	1,03E+06	0	3,54E+05	17924	Uncharacterized protein OS=*Trichoderma harzianum* GN=THAR02_08634 PE=4 SV=1
A0A0G0A3Z5|A0A0G0A3Z5_TRIHA	2	1	1		0	0	0	1,44E+06	47873	Lipase OS=*Trichoderma harzianum* GN=THAR02_00876 PE=3 SV=1
A0A0F9XT47|A0A0F9XT47_TRIHA	1	1	1	Carbamidomethylation	0	7,32E+05	0	9,08E+05	81823	Alpha-galactosidase OS=*Trichoderma harzianum* GN=THAR02_04640 PE=3 SV=1

Continuation of Table S4.1

Accession	Coverage (%)	Peptides	Unique Peptides	PTM	Blank Intensity	G101 Intensity	S1 Intensity	FG1 Intensity	Avg. Mass	Description
A0A0F9XM37|A0A0F9XM37_TRIHA	3	1	1		0	3,80E+06	5,78E+05	1,79E+05	32091	Uncharacterized protein OS=*Trichoderma harzianum* GN=THAR02_06513 PE=4 SV=1
A0A0G0AHN3|A0A0G0AHN3_TRIHA	2	1	1		0	1,14E+06	0	2,09E+05	63726	Uncharacterized protein OS=*Trichoderma harzianum* GN=THAR02_03379 PE=4 SV=1
A0A0F9Z9C8|A0A0F9Z9C8_TRIHA	26	1	1	Carbamidomethylation	0	1,55E+06	0	0	11881	Uncharacterized protein OS=*Trichoderma harzianum* GN=THAR02_10690 PE=4 SV=1
A0A0F9XJM3|A0A0F9XJM3_TRIHA	3	1	1		0	9,60E+05	0	3,24E+05	40400	Uncharacterized protein OS=*Trichoderma harzianum* GN=THAR02_03243 PE=3 SV=1
A0A0G0AJF4|A0A0G0AJF4_TRIHA	1	1	1		0	9,48E+05	3,93E+05	8,13E+05	82473	Uncharacterized protein OS=*Trichoderma harzianum* GN=THAR02_02873 PE=4 SV=1
Q8WZM7|Q8WZM7_TRIHA	19	7	1	Carbamidomethylation; Oxidation (M)	0	2,15E+06	0	2,92E+05	67726	Alpha-1,3-glucanase OS=*Trichoderma harzianum* GN=p3 PE=2 SV=1
A0A0G0ADR1|A0A0G0ADR1_TRIHA	6	1	1		0	2,20E+06	0	6,43E+05	22367	Uncharacterized protein OS=*Trichoderma harzianum* GN=THAR02_04792 PE=4 SV=1
A0A0F9XH81|A0A0F9XH81_TRIHA	2	1	1		0	1,82E+06	0	2,17E+06	44433	Uncharacterized protein OS=*Trichoderma harzianum* GN=THAR02_07989 PE=4 SV=1
A0A0F9X9V0|A0A0F9X9V0_TRIHA	3	2	1		0	1,43E+06	0	3,64E+05	65263	Carboxylic ester hydrolase OS=*Trichoderma harzianum* GN=THAR02_10373 PE=3 SV=1
A0A0F9X6X9|A0A0F9X6X9_TRIHA	3	1	1		0	1,03E+06	0	0	45531	Uncharacterized protein OS=*Trichoderma harzianum* GN=THAR02_07578 PE=3 SV=1
A0A0F9XF94|A0A0F9XF94_TRIHA	2	1	1	Oxidation (M)	0	4,16E+05	5,25E+05	8,37E+05	43245	Uncharacterized protein OS=*Trichoderma harzianum* GN=THAR02_04188 PE=3 SV=1
A0A0G0A470|A0A0G0A470_TRIHA	3	1	1		0	0	6,10E+05	0	34016	Uncharacterized protein OS=*Trichoderma harzianum* GN=THAR02_00916 PE=4 SV=1
A0A0F9XQH6|A0A0F9XQH6_TRIHA	5	1	1		0	1,28E+05	0	4,00E+05	32339	Ferulic acid esterase A OS=*Trichoderma harzianum* GN=THAR02_01219 PE=4 SV=1
A0A0F9XRU0|A0A0F9XRU0_TRIHA	1	1	1		0	6,83E+05	0	7,24E+05	121002	Glycosyl hydrolase family 92 OS=*Trichoderma harzianum* GN=THAR02_00770 PE=4 SV=1
A4V8W7|A4V8W7_TRIHA	6	1	1		0	0	4,55E+05	8,66E+05	42479	Serin endopeptidase OS=*Trichoderma harzianum* GN=p10261 PE=2 SV=1
A0A0F9XG87|A0A0F9XG87_TRIHA	5	1	1		0	4,83E+05	0	2,24E+05	19849	Extracellular serine-rich protein OS=*Trichoderma harzianum* GN=THAR02_04347 PE=4 SV=1

References

Ahamed, A., & Vermette, P. (2009). Effect of culture medium composition on *Trichoderma reesei*'s morphology and cellulase production. *Bioresource Technology*, 100(23), 5979-5987.

Ahamed, A., & Vermette, P. (2010). Effect of mechanical agitation on the production of cellulase by *Trichoderma reesei* RUT-C30 in a draft-tube airlift bioreactor. *Biochemical Engineering Journal*, 49(3), 379-387.

Albright, L. F. (2008). Albright's chemical engineering handbook. Boca Raton: CRC Press.

Allen, A. L., & Andreotti, R. L. (1982). Continuous culture of *Aspergillus phoenicis* QM 329 for the production of cellobiase. *Biotechnology and Bioengineering*, 24(12), 2747-2751.

Almquist, J., Cvijovic, M., Hatzimanikatis, V., Nielsen, J., & Jirstrand, M. (2014). Kinetic models in industrial biotechnology – Improving cell factory performance. *Metabolic Engineering*, 24, 38-60.

Andrade, R. R., Filho, F. M., Filho, R. M., & Costa, A. C. (2013). Kinetics of ethanol production from sugarcane bagasse enzymatic hydrolysate concentrated with molasses under cell recycle. *Bioresource Technology*, 130, 351-359.

Aro, N. (2003). Characterization of novel transcription factors ACEI and ACEII involved in regulation of cellulase and xylanase genes in *Trichoderma Reesei*. Retrieved March 27, 2019 from http://www.vtt.fi/inf/pdf/publications/2003/P488.pdf.

Arroyo, J., Farkaš, V., Sanz, A. B., & Cabib, E. (2016). Strengthening the fungal cell wall through chitin-glucan cross-links: effects on morphogenesis and cell integrity. *Cellular microbiology*, 18 9, 1239-50.

Bader, J., Klingspohn, U., Bellgardt, K. H., & Schugerl, K. (1993). Modeling and simulation of the growth and enzyme production of *Trichoderma reesei* Rut C30. *Journal of Biotechnology*, 29, 121-135.

Bailey, M. J., & Poutanen, K. (1989). Production of xylanolytic enzymes by strains of *Aspergillus*. *Applied Microbiology and Biotechnology*, 30, 5-10.

Becerra, V. (2004). Solving optimal control problems with state constraints using nonlinear programming and simulation tools. *IEEE Transactions on Education*, 47(3), 377-384.

Bischof, R. H., Ramoni, J., & Seiboth, B. (2016). Cellulase and beyond: The first 70 years of the enzyme producer *Trichoderma reesei*. *Microbial Cell Factories*, 15(1).

Bolten, C. J., Kiefer, P., Letisse, F., Portais, J. C., & Wittmann, C. (2007). Sampling for metabolome analysis of microorganisms. *Analytical Chemistry*, 79 (10), 3843-3849.

Bradford M. M. (1976). A rapid and sensitive method for the quantitation of microgram quantities of protein utilizing the principle of protein-dye binding. *Analytical Biochemistry* 72, 248-254.

Buchholz, A., Takors, R., & Wandrey, C. (2001). Quantification of intracellular metabolites in *Escherichia coli* K12 using liquid chromatographic-electrospray ionization tandem mass spectrometric techniques. *Analytical Biochemistry*, 295, 129-137.

Canelas, A. B., Ras, C., ten Pierick, A., van Gulik, W. M., & Heijnen, J. J. (2011). An *in vivo* data-driven framework for classification and quantification of enzyme kinetics and determination of apparent thermodynamic data. *Metabolic Engineering*, 13(3), 294-306.

Chen, M., Qin, Y., Cao, Q., Liu, G., Li, J., Li, Z., Zhao, J., & Qu, Y. (2013). Promotion of extracellular lignocellulolytic enzymes production by restraining the intracellular β-glucosidase in *Penicillium decumbens*. *Bioresource Technology*, 137, 33-40.

Cipollina, C., Pierick, A. T., Canelas, A. B., Seifar, R. M., Maris, A. J., Dam, J. C., & Heijnen, J. J. (2009). A comprehensive method for the quantification of the non-oxidative pentose phosphate pathway intermediates in *Saccharomyces cerevisiae* by GC–IDMS. *Journal of Chromatography B*, 877(27), 3231-3236.

Conesa, A., Punt, P. J., Luijk, N. V., & Hondel, C. A. (2001). The secretion pathway in filamentous fungi: a biotechnological view. *Fungal Genetics and Biology*, 33(3), 155-171.

Dam, J. C., Eman, M. R., Frank, J., Lange, H. C., Dedem, G. W., & Heijnen, S. J. (2002). Analysis of glycolytic intermediates in *Saccharomyces cerevisiae* using anion exchange chromatography and electrospray ionization with tandem mass spectrometric detection. *Analytica Chimica Acta*, 460(2), 209-218.

Delabona, P. S., Lima, D. J., Robl, D., Rabelo, S. C., Farinas, C. S., & Pradella, J. G. (2016). Enhanced cellulase production by *Trichoderma harzianum* by cultivation on glycerol followed by induction on cellulosic substrates. *Journal of Industrial Microbiology & Biotechnology*, 43(5), 617-626.

Delabona, P. S., Cota, J., Hoffman, Z. B., Paixão, D. A. A., Farias, C. S., Cairo, J. P. L. F., Lima, D. J., Squina, F. M., Ruller, R., & Pradella, J. G. (2013). Understanding the cellulolytic system of *Trichoderma harzianum* P49P11 and enhancing saccharification of pretreated sugarcane bagasse by supplementation with pectinase and α-arabinofuranosidase. *Bioresource Technology*, 131, 500-507.

De la Fuente, I. M., Cortés, J. M., Valero, E., Desroches, M., Rodrigues, S., Malaina, I., & Martínez L. (2014). On the dynamics of the adenylate energy system: homeorhesis vs homeostasis. *PLoS One*, 9.

Dias, M., Junqueira, T., Jesus, C., Rossell, C., Filho, R. M., & Bonomi, A. (2012). Improving bioethanol production – Comparison between extractive and low temperature fermentation. *Applied Energy*, 98, 548-555.

Doran, P. M. (1995). *Bioprocess engineering principles*. Elsevier/Academic Press.

Dyk, J. V., & Pletschke, B. (2012). A review of lignocellulose bioconversion using enzymatic hydrolysis and synergistic cooperation between enzymes – Factors affecting enzymes, conversion and synergy. *Biotechnology Advances*, 30(6), 1458-1480.

Eberhart, B. M., & Beck, R. S. (1973). Induction of β-Glucosidases in *Neurospora crassa*. *Journal of Bacteriology,* 116(1):295-303.

Edwards, J. B., & Munkvold, G. (2014). Process for producing cellulase mixtures from *Myceliophthora* and related organisms. United States patent US 2014/0363846A1.

El-Enshasy, H. A. (2007). Chapter 9 - Filamentous fungal cultures – Process characteristics, products, and applications. In Shang-Tian Yang (Ed), *Bioprocessing for value-added products from renewable resources* (225-261). Amsterdam: Elsevier.

Elnahas, M., Amin, M., Hussein, M., Shanbhag, V., Ali, A., & Wall, J. (2017). Isolation, characterization and bioactivities of an extracellular polysaccharide produced from *Streptomyces* sp. MOE6. *Molecules*, 22(9), 1396.

Fiehn, O. (2002). Metabolomics - the link between genotypes and phenotypes. *Plant Molecular Biology*, 48(1/2), 155-171.

Fonslow, B. R. et al. (2014). Mass spectrometry-based shotgun proteomic analysis of *C. elegans* protein complexes. *WormBook*, 1-18.

Fujikawa, H., Kai, A., & Morozumi, S. (2004). A new logistic model *for Escherichia coli* growth at constant and dynamic temperatures. *Food Microbiology*, 21 (5), 501-509.

Gao, Z., Hop, D. V., Yen, L. T., Ando, K., Hiyamuta, S., & Kondo, R. (2012). The production of β-glucosidases by *Fusarium proliferatum* NBRC109045 isolated from Vietnamese forest. *AMB Express*, 2(1), 49.

Gelain, L., Pradella, J. G. C., & Costa, A. C. (2015). Mathematical modeling of enzyme production using *Trichoderma harzianum* P49P11 and sugarcane bagasse as carbon source. *Bioresource Technology*, 198, 101-107.

Ghose, T. K. (1987). Measurement of cellulase activities. *Pure and Applied Chemistry*, 59, 257-268.

Gientka, I., Błażejak, S., Stasiak-Różańska, L., & Chlebowska-Śmigiel, A. (2015). Exopolysaccharides from yeast: Insight into optimal conditions for biosynthesis, chemical composition and functional properties – review. *Acta Scientiarum Polonorum Technologia Alimentaria*, 14(4), 283-292.

Gonzalez, B., François, J., & Renaud, M. (1997). A rapid and reliable method for metabolite extraction in yeast using boiling buffered ethanol. *Yeast,* 13, 1347-1355.

Gómez-Mendoza, D. P, Junqueira, M., Do Vale, L. H. F., Domont, G. B., Filho, E. X. F., Sousa, M. V. D., & Ricart, C. A. O. (2014). Secretomic survey of *Trichoderma harzianum* grown on plant biomass substrates. *Journal of Proteome Research*, 13(4):1810-1822.

Hebert, A. S., Richards, A. L., Bailey, D. J., Ulbrich, A., Coughlin, E. E., Westphall, M. S., & Coon, J. J. (2014). The one hour yeast proteome. *Molecular & Cellular Proteomics*, 13(1), 339-347.

Hofsetz, K., & Silva, M. A. (2012). Brazilian sugarcane bagasse: Energy and non-energy consumption. *Biomass and Bioenergy*, 46, 564-573.

Ilmén, M., Saloheimo, A., Onnela, M. L., & Penttilä, M. E. (1997). Regulation of cellulase gene expression in the filamentous fungus *Trichoderma reesei*. *Applied and Environmental Microbiology,* 63, 1298-1306.

Jäger, S., Brumbauer, A., Fehér, E., Réczey, K., & Kiss, L. (2001). Production and characterization of β-glucosidases from different *Aspergillus* strains. *World Journal of Microbiology and Biotechnology*, 17(5), 455-461.

Jonge, L. P., Buijs, N. A., Pierick, A. T., Deshmukh, A., Zhao, Z., Kiel, J. A., Heijnen, J. J., & van Gulik, W. M. (2011). Scale-down of penicillin production in *Penicillium chrysogenum*. *Biotechnology Journal*,6(8), 944-958.

Jonge, L. P., Douma, R. D., Heijnen, J. J., & van Gulik, W. M. (2012). Optimization of cold methanol quenching for quantitative metabolomics of *Penicillium chrysogenum*. *Metabolomics*, 8(4), 727-735.

Karp, G. (2009). *Cell and molecular biology: Concepts and experiments*. 6 ed. New York: J. Wiley.

Kapoore, R. V., & Vaidyanathan, S. (2018). Quenching for microalgal metabolomics: a case study on the unicellular eukaryotic green alga *Chlamydomonas reinhardtii*. *Metabolites*, 8(4), 72.

Karaffa, L., Fekete, E., Gamauf, C., Szentirmai, A., Kubicek, C. P., & Seiboth, B. (2006). D-Galactose induces cellulase gene expression in *Hypocrea jecorina* at low growth rates. *Microbiology*, 152(5), 1507-1514.

Köcher, T., Pichler, P., Swart, R., & Mechtler, K. (2012). Analysis of protein mixtures from whole-cell extracts by single-run nano LC-MS/MS using ultralong gradients. *Nature Protocols*, 7(5), 882-890.

Koning, W., & Van Dam, K. (1992). A method for the determination of changes of glycolytic metabolites in yeast on a subsecond time scale using extraction at neutral pH. *Analytical Biochemistry*, 204, 118-123.

Kubicek, C. P. (2013). Systems biological approaches towards understanding cellulase production by *Trichoderma reesei*. *Journal of Biotechnology*, 163(2), 133-142.

Kubicek, C. P., Mikus, M., Schuster, A., Schmoll, M., & Seiboth, B. (2009). Metabolic engineering strategies for the improvement of cellulase production by *Hypocrea jecorina*. *Biotechnology for Biofuels*, 2(1), 19.

Kubicek, C. P., Messner, R., Gruber, F., Mandels, M., & Kubicek-Pranz, E. M. (1993). Triggering of cellulase biosynthesis by cellulose in *Trichoderma reesei*. Involvement of a constitutive, sophorose-inducible, glucose-inhibited beta-diglucoside permease. *The Journal of Biology Chemestry*, 268(26), 19364-19368.

Kubota, K., & Ashihara, H. (1990). Identification of non-equilibrium glycolytic reactions in suspension-cultured plant cells. *Biochimica et Biophysica Acta,* 1036: 138-142.

Kuplich, M. D., Grasel, F. S., Campo, L. F., Rodembusch, F. S., & Stefani, V. (2012). Synthesis, characterization and photophysical properties of ESIPT reactive triazine derivatives. *Journal of the Brazilian Chemical Society*.

Lago, A. C., Bonomi, A., Cavalett, O., Cunha, M. P., & Lima, M. A. (2012). Sugarcane as a carbon source: The Brazilian case. *Biomass and Bioenergy*, 46, 5-12.

Lameiras, F., Heijnen, J. J., & van Gulik, W. M. (2015). Development of tools for quantitative intracellular metabolomics of *Aspergillus niger* chemostat cultures. *Metabolomics*, 11(5), 1253-1264.

Lamichhane, S., Sen, P., Dickens, A. M., Hyötyläinen, T., & Orešič, M. (2018). An overview of metabolomics data analysis: current tools and future perspectives. *Comprehensive analytical chemistry*, 82, 387-413.

Lehninger, A. L., Nelson, D. L., & Cox, M. M. (2005). *Principles of biochemistry*. New York, NY: W. H. Freeman.

Li, H., Yu, H., & Zhu, H. (2016). Structure studies of the extracellular polysaccharide from *Trichoderma* sp. KK19L1 and its antitumor effect via cell cycle arrest and apoptosis. *Applied Biochemistry and Biotechnology*, 182(1), 128-141.

Ma, L., Li, C., Yang, Z., Jia, W., Zhang, D., & Chen, S. (2013). Kinetic studies on batch cultivation of *Trichoderma reesei* and application to enhance cellulase production by fed-batch fermentation. *Journal of Biotechnology*, 166, 192-197.

Mahapatra, S., & Banerjee, D. (2013). Fungal exopolysaccharide: production, composition and applications. *Microbiology Insights*, 6.

Mandels, M., & Reese, E. T. (1957). Induction of cellulase in *Trichoderma viride* as influenced by carbon sources and metals. *Journal of Bacteriology*,73(2), 269-278.

Mcdonald, W. H., & Yates, J. R. (2002). Shotgun proteomics and biomarker discovery. *Disease Markers*, 18(2), 99-105.

Meyrat, A., & von Ballmoos, C. (2019). ATP synthesis at physiological nucleotide concentrations. *Scientific reports*, 9(1), 3070.

Miller, G. L. (1959). Use of dinitrosalicylic acid reagent for determination of reducing sugar. *Analytical Chemistry*, 31(3), 426-428.

Mussatto, S.I, & Teixeira, J. A. (2010). Lignocellulose as raw material in fermentation processes. Retrieved March 27, 2019 from http://www.formatex.info/microbiology2/897-907.pdf.

Nesvizhskii, A. I., & Aebersold, R. (2005). Interpretation of shotgun proteomic data. *Molecular & Cellular Proteomics*, 4(10), 1419-1440.

Neto, J. M., Reis Garcia, D., Rueda, S. M. G., & Costa, A. C. (2013). Study of kinetic parameters in a mechanistic model for enzymatic hydrolysis of sugarcane bagasse subjected to different pretreatments. *Bioprocess and Biosystems Engineering*, 36, 1579-1590.

Nitta, M., Furukawa, T., Shida, Y., Mori, K., Kuhara, S., Morikawa, Y., & Ogasawara, W. (2012). A new Zn(II)2Cys6-type transcription factor BglR regulates β-glucosidase expression in *Trichoderma reesei*. *Fungal Genetics and Biology*, 49(5), 388-397.

Owen, C. B., Hughes, D. J., Baquero-Perez, B., Berndt, A., Schumann, S., Jackson, B. R., & Whitehouse, A. (2014). Utilising proteomic approaches to understand oncogenic human herpesviruses (Review). *Molecular and Clinical Oncology*, 2(6), 891-903.

Pessoni, R. A., Tersarotto, C. C., Mateus, C. A., Zerlin, J. K., Simões, K., Figueiredo-Ribeiro, R. D., & Braga, M. R. (2015). Fructose affecting morphology and inducing β-fructofuranosidases in *Penicillium janczewskii*. *SpringerPlus*, 4(1).

Pinu, F. R., Villas-Boas, S. G., & Aggio, R. (2017). Analysis of intracellular metabolites from microorganisms: quenching and extraction protocols. *Metabolites,* 7(4), 53.

Pomin, V. H. (2012). *Unravelling glycobiology by NMR spectroscopy*. INTECH Open Access Publisher.

Portnoy, T., Margeot, A., Seidl-Seiboth, V., Crom, S. L., Chaabane, F. B., Linke, R., Seiboth, B., & Kubicek, C. P. (2011). Differential regulation of the cellulase transcription factors XYR1, ACE2, and ACE1 in *Trichoderma reesei* strains producing high and low levels of cellulase. *Eukaryotic Cell*, 10(2), 262-271.

Rau, Udo. (1999). Chapter 4 – Production of Schizophyllan. In Christopher Bucke (Ed), *Carbohydrate Biotechnology Protocols*. Humana Press Inc.

Reis, L., Fontana, R. C., Delabona P. S., Lima, D. J. S., Camassola, M., Pradella J. G. C., & Dillon, A. J. P. (2013). Increased production of cellulases and xylanases by *Penicillium echinulatum* S1M29 in batch and fed-batch culture. *Bioresource Technology*, 146, 597-603.

Rohrer, J. S., Basumallick, L., & Hurum, D. (2013). High-performance anion-exchange chromatography with pulsed amperometric detection for carbohydrate analysis of glycoproteins. *Biochemistry* (Moscow), 78(7), 697-709.

Ross, A., Schfigerl, K., & Scheiding, W. (1983). Cellulase production by *Trichoderma reesei*. *European Journal of Applied Microbiology and Biotechnology*, 18(1), 29-37.

Seiboth, B., Ivanova, C., & Seidl-Seiboth, V. (2011). *Trichoderma reesei*: a fungal enzyme producer for cellulosic biofuels. *Biofuel Production-Recent Developments and Prospects*.

Shida, Y., Furukawa, T., & Ogasawara, W. (2016). Deciphering the molecular mechanisms behind cellulase production in *Trichoderma reesei*, the hyper-cellulolytic filamentous fungus. *Bioscience, Biotechnology, and Biochemistry*, 80(9), 1712-1729.

Sørensen, A., Lübeck, M., Lübeck, P., & Ahring, B. (2013). Fungal beta-glucosidase: a bottleneck in industrial use of lignocellulosic materials. *Biomolecules*, 3(4), 612-631.

Strakowska, J., Błaszczyk, L., & Chełkowski, J. (2014). The significance of cellulolytic enzymes produced by *Trichoderma* in opportunistic lifestyle of this fungus. *Journal of Basic Microbiology*, 54(S1).

Strobel, H. J., & Russell, J. B. (1987). Regulation of beta-glucosidase in *Bacteroides ruminicola* by a different mechanism: growth rate-dependent derepression. *Applied and Environmental Microbiology*, 53(10), 2505-2510.

Suto, M., & Tomita, F. (2001). Induction and catabolite repression mechanisms of cellulase in fungi. *Journal of Bioscience and Bioengineering*, 92(4), 305-311.

Taher, I. B., Fickers, P., Chniti, S., & Hassouna, M. (2017). Optimization of enzymatic hydrolysis and fermentation conditions for improved bioethanol production from potato peel residues. *Biotechnology Progress*, 33(2), 397-406.

Thilakavathi, M., Basak, T., & Panda, T. (2006). Modeling of enzyme production kinetics. *Applied Microbiology and Biotechnology*, 73(5), 991-1007.

Thumanu, K., Sompong, M., Phansak, P., Nontapot, K., & Buensanteai, N. (2015). Use of infrared microspectroscopy to determine leaf biochemical composition of cassava in response *to Bacillus subtilis* CaSUT007. *Journal of Plant Interactions*, 10(1), 270-279.

Tiwari, P., Misra, B. N., & Sangwan, N. S. (2013). β-Glucosidases from the fungus *Trichoderma*: an efficient cellulase machinery in biotechnological applications. *BioMed Research International*, 1-10.

Uniprot. Retrieved March 27, 2019 from https://www.uniprot.org/help/protein_existence.

Vale, L. H., Gómez-Mendoza, D. P., Kim, M., Pandey, A., Ricart, C. A., Edivaldo, X. F., & Sousa, M. V. (2012). Secretome analysis of the fungus *Trichoderma harzianum* grown on cellulose*. Proteomics*, 12(17), 2716-2728.

Velkovska, S., Marten, M. R., Ollis, & David, F. (1997). Kinetic model for batch cellulase production by *Trichoderma reesei* RUT C30. *Journal of Biotechnology,* 54(2), 83-94.

Verardi, A., De, I., Ricca, E., & Calabr, V. (2012). Hydrolysis of lignocellulosic biomass: current status of processes and technologies and future perspectives. *Bioethanol*.

Ximenes, E., Felix, C. & Ulhoa, C. (1996). Production of cellulase by *Aspergillus fumigatus* and characterization of one β-Glucosidase. *Current Microbiology*, 32, 119.

Xiong, Y., Sun, J., & Glass, N. L. (2014). VIB1, a link between glucose signaling and carbon catabolite repression, is essential for plant cell wall degradation by *Neurospora crassa*. *PLoS Genetics*, 10(8).

Zhang, J., Xin, L., Shan, B., Chen, W., Xie, M., Yuen, D., Zhang, W., Zhang, Z., Lajoie, G. A. & Ma, B. (2012). PEAKS DB: de novo sequencing assisted database search for sensitive and accurate peptide identification. *Molecular and Cell Proteomics*, 11.

Zhang, Y. H., Hong, J., & Ye, X. (2009). Cellulase assays. *Methods in Molecular Biology Biofuels*, 213-231.

Zhang, Y., Tang, B., & Du, G. (2017). Self-induction system for cellulase production by cellobiose produced from glucose in *Rhizopus stolonifer*. *Scientific Reports*, 7(1).

Acknowledgements

First, I would like to thank my family for all the support, education and the freedom I had to choose my path. This thesis is dedicated to my parents, Ari Gelain and Mairi Parenti Gelain, and my brother, Rafael Gelain.

I would like to thank my supervisors. Aline Carvalho da Costa always helped me to improve the quality of our works. I always had interesting discussions with José Geraldo da Cruz Pradella about fermentation process and strategies. Walter M. van Gulik taught me how to use the chemostat and helped me to design interesting experiments. Luuk van der Wielen and Patricia Osseweijer provided the opportunity to realize the dual degree PhD between Unicamp and TU Delft, a great opportunity that I hope it will continue forever.

I would like to thank the experimental support I had in the Netherlands, I thank Cor Ras, Johan Knoll, Martin Pabst, Patricia van Dam, and Stephen Eustace for the accurate analysis. I thank Apilena Sapioper, Astrid van Uijen and Jannie Kempff-Gruwel for the help in the laboratory. I thank Dirk Geerts and Rob Kerste for the technical support.

And I would also like to thank the support I had in Brazil, I thank Deise Juliana da Silva Lima for the ideas and assistance in the preparation of the experiments. I thank Letícia Zanphorlin and Reginaldo Guirardello for the advice about the organization of the thesis.

I want to thank Francisca Lameiras for the experimental protocols for continuous cultures and analysis of intracellular metabolites.

I want to thank Esther Kingma for her help with the experiments using continuous cultures, the first student I provided assistance in the final bachelor project, it was very fun.

I would like to thank the groups I had the pleasure to work with, LNBR and CSE.

This is a PhD thesis in the dual degree program as agreed between UNICAMP and TU Delft.
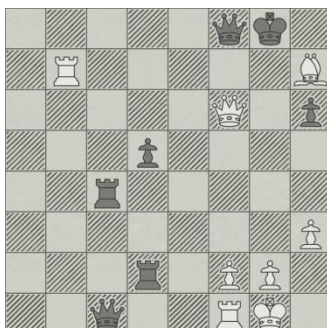
Curriculum vitae

Lucas Gelain was born on the 26th of January of 1988 in Caxias do Sul, Brazil. He also has Italian nationality by the city of Livorno Ferraris (VC), Italy.

He is a Chemical Engineer graduated from the University of Caxias do Sul. He started working as a volunteer at the Biotechnological Institute during his bachelor and became very interested in the complexity, diversity and capacity of microorganisms.

After his graduation, he went to Campinas to perform his master degree working with mathematical modelling of the fermentation process at the University of Campinas.

He started his PhD about enzyme production at the University of Campinas and after one year, he was admitted for the Dual Degree Program between the University of Campinas and TU Delft.

Publication list

GELAIN, **L**.; PRADELLA, J. G. C.; COSTA, A. C. Mathematical modeling of enzyme production using *Trichoderma harzianum* P49P11 and sugarcane bagasse as carbon source. **Bioresource Technology**, 198, 101-107, 2015.

GELAIN, **L**.; ANTUNES, M.; CRESPO, J. S.; GIOVANELA, M. Removal of zinc (II) from aqueous solutions using an eco-friendly biosorbent originating from the winery industry. **Separation Science and Technology** (Print), 49, 2212 - 2220, 2014.

Future publications from PhD thesis

GELAIN, **L.**; KINGMA, E.; PRADELLA, J. G. C.; COSTA, A. C.; WIELEN, L. VAN DER; GULIK, W. M. VAN. Enzyme production by *Trichoderma harzianum* P49P11 under carbon-limited conditions.

GELAIN, **L.**; PRADELLA, J. G. C.; COSTA, A. C.; WIELEN, L. VAN DER; GULIK, W. M. VAN. Analysis of the production of enzymes by *Trichoderma harzianum* P49P11 under carbon-limited conditions – secretome and metabolome.

GELAIN, **L.**; PRADELLA, J. G. C.; COSTA, A. C.; WIELEN, L. VAN DER; GULIK, W. M. VAN. Metabolome evaluation during the production of extracellular polysaccharides by *Trichoderma harzianum* P49P11.

GELAIN, **L.**; WIELEN, L. VAN DER; GULIK, W. M. VAN; PRADELLA, J. G. C.; COSTA, A. C. Mathematical modelling for the optimization of cellulase production using glycerol for cell growth and cellulose as the inducer substrate.

Brazilian Patents

POLIDORO, T. A.; SILVEIRA, M. M.; **GELAIN, L**. Rotating drum device, 2009. Financial Institution: the University of Caxias do Sul. MU 8901075-2.

https://www.ucs.br/site/midia/arquivos/carta-patente-tambor-rotativo.pdf

GELAIN, **L.**; COSTA, A. C. Antifoam system, 2016. Financial Institution: University of Campinas. BR 10 2016 030412 1.

http://patentes.inova.unicamp.br/item/1129_espuma/